SECTION T

DEFENSE RESEARCH LABORATORY
THE UNIVERSITY OF TEXAS
AUSTIN TEXAS

Operating Under Contract NOrd 9195
With the Bureau of Ordnance, U. S. Navy

DIELECTRIC WAVEGUIDES AND RADIATORS

by

Chester M. McKinney, Jr.

Bumblebee Series
Report No. 138
Copy No. 276

September 1950

SEPTEMBER 1950 BUMBLEBEE REPORT No. 138

DIELECTRIC WAVEGUIDES AND RADIATORS

by Chester M. McKinney, Jr.

A Dissertation presented to the Faculty
of the Graduate School of The University of Texas
in partial fulfillment of the requirements
for the Degree of Doctor of Philosophy

Defense Research Laboratory
The University of Texas Austin, Texas

PREFACE

This dissertation is a report on a rather extensive experimental investigation of the dielectric waveguide and radiator and the associated generating and measuring equipment.

The writer wishes to express his sincere appreciation to Dr. C. W. Horton, who suggested this subject for research and has supervised all of the work. This opportunity is taken to thank Dr. C. P. Boner, Director of Defense Research Laboratory, The University of Texas, for making the project possible. The Navy Department, Bureau of Ordnance, has supplied financial support for the work through Contract NOrd-9195, Task II, with Defense Research Laboratory. Thanks are due also to the entire Electronics Staff of Defense Research Laboratory, and especially to Dr. O. J. Baltzer, Dr. R. B. Watson, Mr. Walter Kuehne, Mr. H. C. Martin, and Mr. F. C. Karal for many helpful suggestions.

Chester M. McKinney

Austin, Texas
June, 1950

TABLE OF CONTENTS

CHAPTER		PAGE
	INTRODUCTION	1
	PART ONE	
	MODE EXCITERS AND TRANSDUCERS FOR ELECTROMAGNETIC WAVES	
I.	General Formulas and Notation for Metallic Waveguides	3
II.	Mode Exciters and Transducers	13
	PART TWO	
	DIELECTRIC WAVEGUIDES OF CIRCULAR CROSS SECTION	
I.	Historical Survey	37
II.	Purposes of Further Experimental Investigations of Dielectric Waveguides	43
III.	Brief Theory of the Dielectric Waveguide	45
IV.	Experimental Procedure and Equipment	61
V.	Experimental Data and Discussion	70
VI.	Practical Aspect of the Dielectric Waveguide	105
	PART THREE	
	DIELECTRIC RADIATORS	
I.	Historical Summary of the Work on the Dielectric Rod Radiator	107
II.	Purposes of the Present Investigation of the Dielectric Rod Radiator	114
III.	Brief Theory of the Dielectric Radiator	116
IV.	Measurement of Antenna Characteristics	134
V.	Data and Discussion of Measurements	154

TABLE OF CONTENTS
(Continued)

PAGE

APPENDIX I. MEASUREMENT OF THE COMPLEX DIELECTRIC CONSTANT . . . 255

APPENDIX II. GLOSSARY OF SYMBOLS 263

BIBLIOGRAPHY 269

INTRODUCTION

The use of a dielectric rod as a waveguide for electromagnetic energy was investigated as early as 1910. Occasional contributions to the theory of these guides and additions to the experimental data were made by several workers before 1936. With the availability of microwave equipment, interest increased and considerable work has been done in recent years. It is one of the characteristics of the dielectric waveguide that some radiation takes place if the waveguide is of finite length. The property of radiation loss, undesirable from the transmission standpoint, has been made use of in the form of the dielectric rod antenna. This type of antenna was first used about 1939 and was developed to the extent that both the Allies and the Axis made use of it in military radar equipment during the last war.

The work which is described in this dissertation consisted of an experimental investigation of the properties of the dielectric waveguide and radiator of circular cross section. The over-all aims were twofold. The first was the use of a wider range of parameters, such as physical size of the guides and radiators, and modes of transmission, than have been used previously, in order to obtain a more complete understanding of the operation of these types of guides and radiators. The second purpose was the obtaining of a large amount of accurate experimental data which could be used to verify present and future theoretical work. The dissertation is divided into three major parts.

Part One is a description and discussion of the metal waveguides and mode exciters used in this project. While this equipment is not peculiar to dielectric waveguide applications, a description is included for the sake of completeness. The designs of three new types of mode exciters are described. These exciters are for the TM_{01} and TM_{11} modes in metal waveguides of circular cross section and for the TE_{20} mode in waveguides of rectangular cross section.

Part Two covers measurements made on dielectric rods used as waveguides and is principally a collection of data that were obtained in order to check existing theoretical calculations. In particular, measurements were made on dielectric rods of sufficiently large diameter to support the second order radial modes of propagation. Attenuation measurements were made as a function of the diameter of the rods and also as a function of a bending of the rods.

Part Three constitutes the major part of the work and consists of measurements made on dielectric radiators. The range of diameters of the radiators used in this project was considerably greater than that of any previous work. It is believed that this is the first investigation of dielectric rod antennas excited in the TM_{01}, TE_{01}, and EH_{11} modes. Some of the conclusions from the antenna work are not in agreement with those of previous workers.

Appendix I is a brief description of equipment and procedures used in the determination of the dielectric constant and loss factor of the dielectrics used in this work.

Appendix II is a glossary of symbols used in this thesis.

The figures, footnotes, and equations are numbered consecutively within each of the major parts.

PART ONE

MODE EXCITERS AND TRANSDUCERS FOR ELECTROMAGNETIC WAVES

BLANK PAGE

CHAPTER I

GENERAL FORMULAS AND NOTATION FOR METALLIC WAVEGUIDES

The electromagnetic waves used to feed the dielectric waveguides and radiators in the experimental work were in all cases generated in metallic waveguides and then transmitted to the dielectric materials. It is not feasible to generate the waves originally in the dielectric materials because of increased spurious radiation (and hence high loss and interference), generation of undesirable modes, and difficulty in arranging the boundary conditions such that the desired mode will be generated. Hence it is in order to discuss briefly some of the pertinent modes in metallic guides and methods of generating them.

The use of hollow metal pipes as guides for electromagnetic waves began in 1936,[1,2,3] and then became exceedingly common during World War II with the development of the microwave (centimeter) equipment. Due to their extended use, a vast amount of material on them appears in the literature and hence it is not necessary to go into detail here. Barrow,[4] Schelkunoff,[5] Southworth,[6] and others, who did the pioneering in the field, showed that an infinite number of configurations of

---

[1]Barrow, W. L., "Transmission of Electromagnetic Waves in Hollow Tubes of Metal," Proc. I.R.E., 24, 1298, October 1936.

[2]Carson, J. R., Mead, S. P., and Schelkunoff, S. A., "Hyperfrequency Wave Guides - Mathematical Theory," B.S.T.J., 15, 310, April 1936.

[3]Southworth, G. C., "Hyperfrequency Wave Guides - General Considerations and Experimental Results," B.S.T.J., 15, 284, April 1936.

[4]Barrow, op. cit.

[5]Schelkunoff, op. cit.

[6]Southworth, op. cit.

electromagnetic fields are possible in metallic pipes of rectangular and circular cross-sections. They also suggested methods for exciting these modes and performed experimental work on some of them. The notation used to specify these modes has become fairly well standardized. These are known as modes of transmission and are divided into two classes: transverse electric (TE or H) and transverse magnetic (TM or E). The principle or TEM wave, in which the electric and magnetic fields are entirely transverse to the direction of propagation, cannot exist with a single conductor. Each mode represents a solution of Maxwell's field equations. However, for a given size hollow conductor there is a lower limit to the frequency of oscillation that it will transmit and this lower limit or "cut off" frequency depends on the particular mode. TE modes or H modes have an electric component transverse to the guide and only magnetic components along the axis of the guide and conversely for the TM or E modes. The coordinate system and notation applied to rectangular guides is shown in Figure 1.01-A. The mode (TE or H, or TM or E) is given two subscripts. The two subscripts are integers that indicate the number of half period variations or loops in transverse field intensity along the x and y axes of the guide, respectively. For any guide, the mode of transmission that has the lowest cutoff frequency is called the dominant mode. For the rectangular guide it is the TE_{10}* or H_{10}. The electric and magnetic field configurations for this mode are shown in Figure 1.02. The TE_{10} is the only mode in rectangular guides that is of concern in this work.

*In many books the x, y, subscript order is reversed and the dominant mode is the TE_{01}. However, the notation of MIT Radiation Laboratory and other recent work is used here.

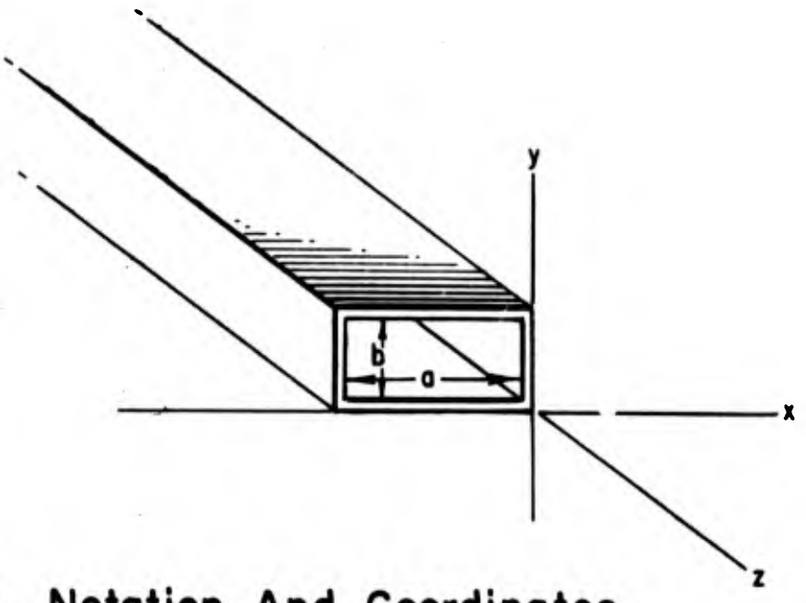

A. Notation And Coordinates
For Rectangular Waveguides.

Fig. 1.01

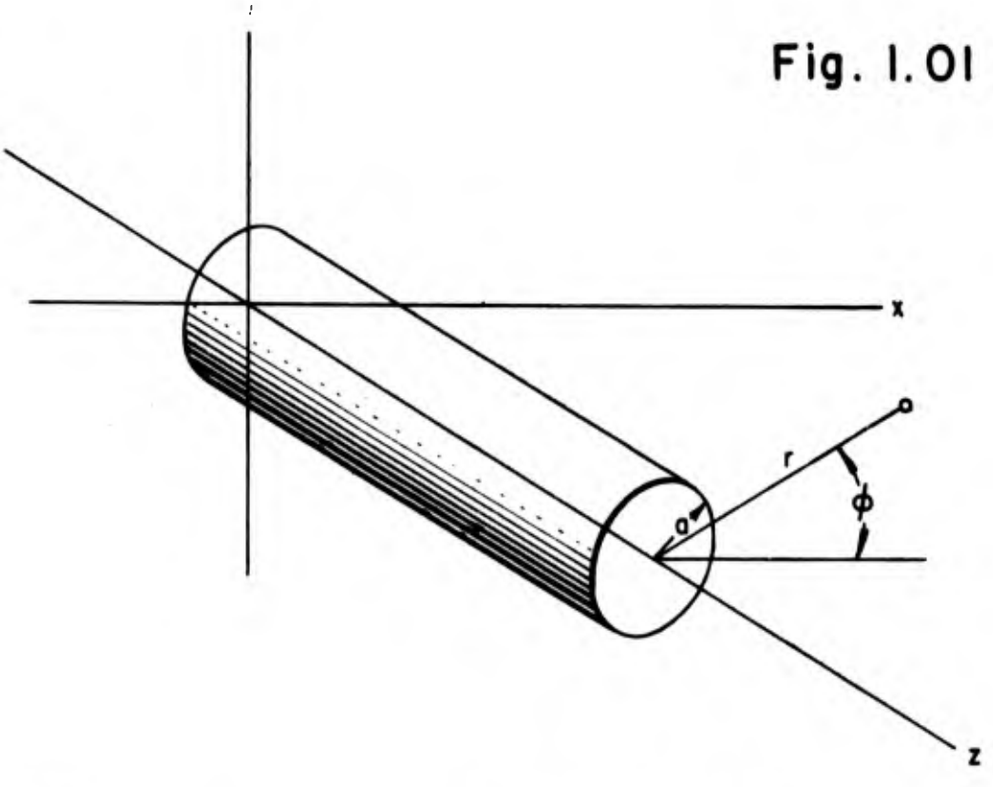

B. Notation And Coordinate System
For Circular Waveguides.

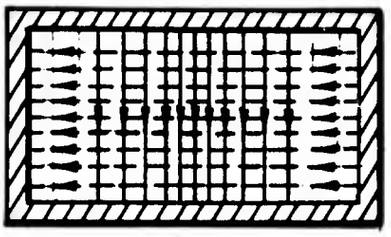

End View

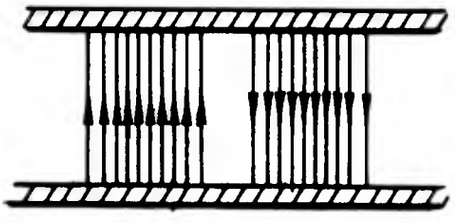

Side View

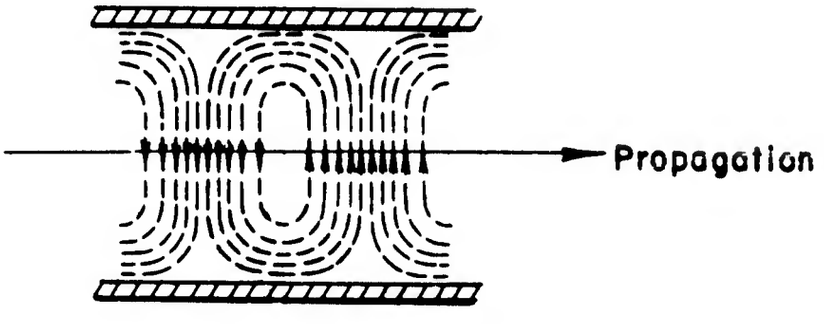

Top View

——— Electric Field
---- Magnetic Field

Electric And Magnetic Field Of TE_{10} Mode.

Fig. 1.02

The notation applied to circular waveguides is shown in Figure 1.01-B. For any mode of transmission in a circular waveguide, the transverse field may be resolved into angular and radial components. These components vary periodically along a circular path concentric with the wall and vary in a manner related to a Bessel Function of order $\underline{m}$ along a radius. Any particular mode is identified by the notation TE_{mn} or TM_{mn}, where $\underline{m}$ is the total number of full period variations of either component of field along a circular path concentric with the wall and $\underline{n}$ is one more than the total number of reversals of signs of either component of field along a radial path. The mode subscripts may also be associated with the nth root of J_m (U).

The four modes that are of particular interest are the TE_{11}, TM_{01}, TE_{01}, and TM_{11}. Field configurations for these modes are shown in Figure 1.03. The TE_{11} is the dominant mode and corresponds to the TE_{10} in rectangular guides.

As was mentioned earlier, there is a cutoff wavelength for each mode for a given size waveguide. For rectangular guides this cutoff wavelength (λ_c) is the same for TM or TE modes and is given by[7]

$$\lambda_c = \frac{2}{\sqrt{\left(\frac{m}{a}\right)^2 + \left(\frac{n}{b}\right)^2}} \qquad (1.01)$$

For the dominant mode, TE_{10}, $m = 1$, $n = 0$, and $\lambda_c = 2a$; i.e., the guide must be at least a half wavelength wide and is independent of

[7]Moreno, Theodore, Microwave Transmission Design Data, McGraw-Hill Book Co., New York, p. 210, 1948.

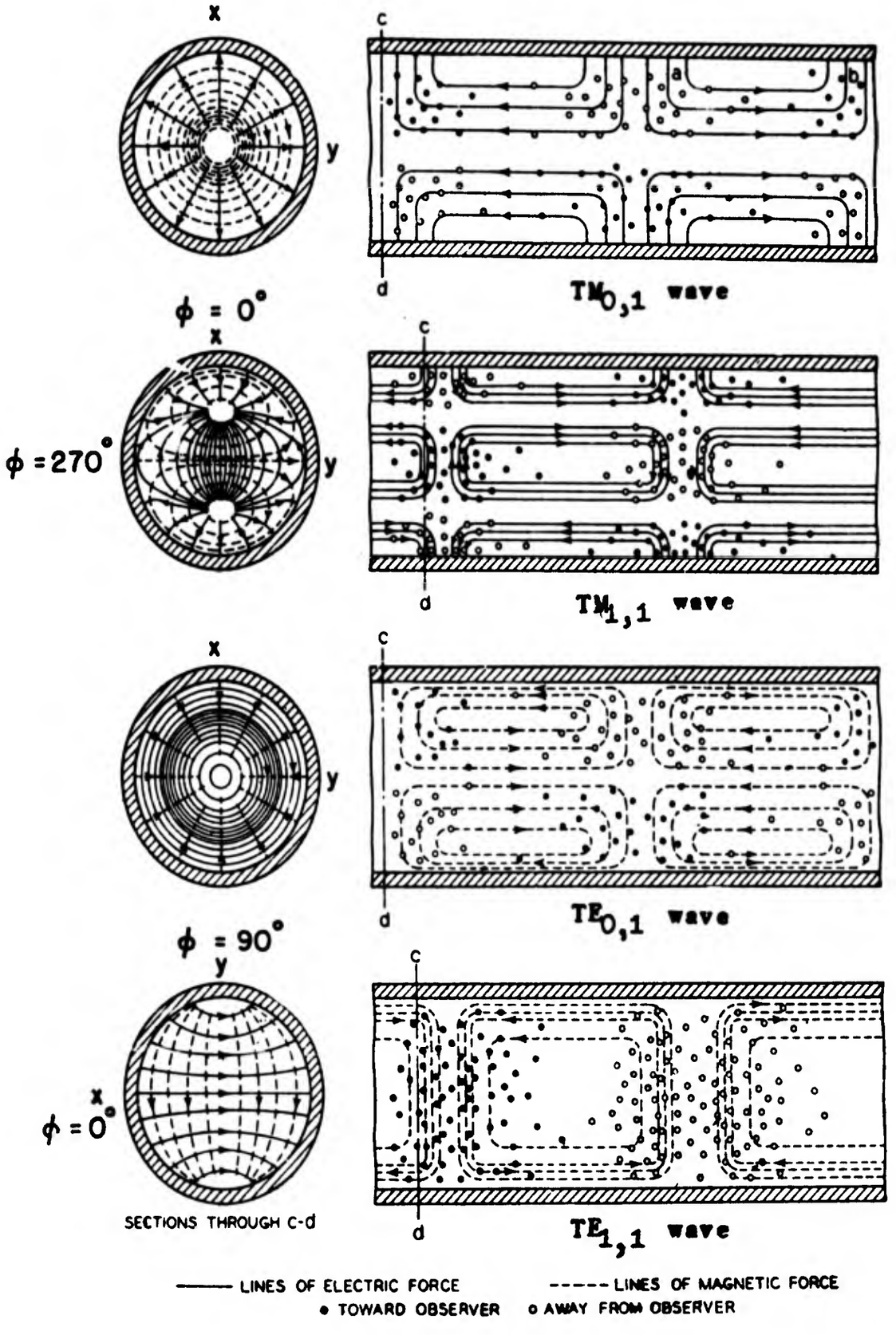

Figure 1.03

Electrical And Magnetic Lines Of Force In A Hollow Circular Cross Section

(From Southworth, Proc. IRE, July, 1937)

the height. Thus it can be seen why waveguides, because of practical considerations, are restricted to use at very short wavelengths.

For circular waveguides, the cutoff wavelength for TE_{mn} waves is given by[8]

$$\lambda_c = \frac{2\pi a}{U'_{mn}} \tag{1.02}$$

U'_{mn} is the nth root of the equation $J'_m(U) = 0$.

For the modes mentioned these are:

TE_{11}	$U'_{11} = 1.841$
TE_{01}	$U'_{01} = 3.832$

For TM_{mn} modes the cutoff wavelength is given by

$$\lambda_c = \frac{2\pi a}{U_{mn}} \tag{1.03}$$

where U_{mn} is the nth root of $J_m(U) = 0$.

For

TM_{01}	$U_{01} = 2.405$
TM_{11}	$U_{11} = 3.832$

Thus it can be seen that for a given wavelength the TE_{11} mode requires the smallest size pipe while the TE_{01} and TM_{11} require a considerably larger one. Thus one of the reasons for using the dominant mode is that a smaller size pipe is allowable. Also, by using as small a waveguide as is practical, all but the dominant mode are suppressed and only a single mode is transmitted. This characteristic

---

[8] ibid., p. 120.

is exceedingly important. However, it should be noted that attenuation increases as $\lambda_o \rightarrow \lambda_c$. Therefore one should not use a waveguide that is just above "cut-off".

The wavelength of waves in an air-filled metallic waveguide is larger than the corresponding free space wavelength. This indicates that the phase velocity, v_p, in the guide is greater than c, the velocity of propagation in free space since

$$v_p = f\lambda_g \tag{1.04}$$

where f is the frequency.

And since

$$v_g v_p = c^2 \tag{1.05}$$

where v_g is the group velocity, the energy is transmitted with velocity v_g, which is less than c. In an air-filled hollow waveguide the λ_g is given by[9]

$$\lambda_g = \frac{\lambda_o}{\sqrt{1 - \frac{\lambda_o}{\lambda_c}^2}} \tag{1.06}$$

Thus, for $\lambda_o = \lambda_c$, $\lambda_g \rightarrow \infty$, $V_p \rightarrow \infty$, and $V_g \rightarrow 0$, and no energy is transmitted through the waveguide.

Table I gives the size of waveguides which were used in this work for the various modes together with λ_c and λ_g. The size of the waveguides was chosen such that only the lowest order branch of a particular mode could propagate.

---

[9] ibid., p. 123.

TABLE I

λ_g AND λ_c FOR CIRCULAR METALLIC WAVEGUIDES. λ_o = 3.20 cm.

Inside Diameter of Guide			λ_c (in cm.)				λ_g (in cm.)			
inches	inches	cm.	TE_{11}	TM_{01}	TE_{01}	TM_{11}	TE_{11}	TM_{01}	TE_{01}	TM_{11}
3/4	.750	1.915	3.27	2.50	1.57	1.57	15.18	C.O.	C.C.	C.C.
7/8	.875	2.221	3.79	2.90	1.82	1.82	5.98	C.C.	C.O.	C.C.
1-3/32	1.093	2.780	4.74	3.63	2.28	2.28	4.33	6.79	C.O.	C.O.
2-1/4	2.250	5.705	9.76	7.46	4.69	4.69	3.39	3.54	4.86	4.86

C.O.: Above cutoff wavelength

Field equations, attenuation formulas, impedance formulas, etc., for these and other modes may be found in any of the textbooks listed in the bibliography for this chapter.

CHAPTER II

MODE EXCITERS AND TRANSDUCERS

The dominant mode for rectangular waveguides is used in practically all commercial applications and for this reason it is the only mode for which equipment is readily available. The popularity of this mode is understandable because it requires the smallest waveguide of any of the modes for rectangular guides and thus, by proper choice of dimensions, the guide may be designed to pass the dominant wave while suppressing the higher order waves. It is also important from an economic standpoint since the dominant mode is easy to excite. Furthermore, the waveguide, when terminated in a horn director[10,11] or when used to feed other radiating systems, such as parabolic reflectors, produces a radiation pattern that has maximum radiation (or gain) in the direction of the axis of the guide. The rectangular guide has two advantages over the circular guide. First, due to the shape of the waveguide, there can be no rotation of the plane of polarization, which is not the case with a circular waveguide. Second, it is easier to fabricate equipment in which joints must be made between several sections of waveguide.

Since all commercially available equipment, such as signal generators, etc., are designed for the TE_{10} mode, it is desirable to

---

[10] Barrow, W. L., and Chu, L. J., "Theory of the Electromagnetic Horn," Proc. I.R.E., 27, 51, January 1939.

[11] Southworth, G. C., and King, A. P., "Metal Horns as Directive Receivers of Ultra Short Waves," Proc. I.R.E., 27, 95, February 1939.

begin with this dominant mode and transform or transduce it into other modes. If the output connection of the signal source is of the waveguide type, the TE_{10} mode is already present and methods of generating it are not necessary. However, if the output connection is in the form of a coaxial cable, the mode may be generated as shown in Figure 1.04. This is essentially using a dipole or probe antenna to propagate waves which are directed or guided along the guide. The waveguide is shorted at the opposite end and the probe is shorted also, at the places where the impedance of the exciting probe matches the characteristic impedance of the waveguide. Slater[12] has shown theoretically that a transition of this type can be matched by variation of the end plate and coaxial-plunger positions, dimensions D and S. The coaxial stub constitutes a variable reactance in series with the waveguide antenna, and by means of variation in position of the end plate, the radiation resistance of the antenna may be changed. Thus the reactance of the antenna is zero and its resistance can be made equal to the characteristic impedance of the coaxial line. A variation of this type of transition is the probe type or the type where the antenna protrudes only part way into the guide.[13] This type of transition has the disadvantage of requiring some sort of dielectric support for the probe which introduces loss. These types of transitions may be used to excite the TE_{11} mode in circular guides.[14] However, due to

[12]Slater, J. C., Microwave Transmission, McGraw-Hill Book Co., New York, Chapter VII, 1942.

[13]Slater, J. C., "Properties of the Coaxial-Waveguide Junction in the 725-A and 2J51 Output," BTL Memorandum 44-180-4, November 1944.

[14]Allen, W. D., "The Coaxial to Waveguide Transformer," British Royal Society Report G8/102, January 1942.

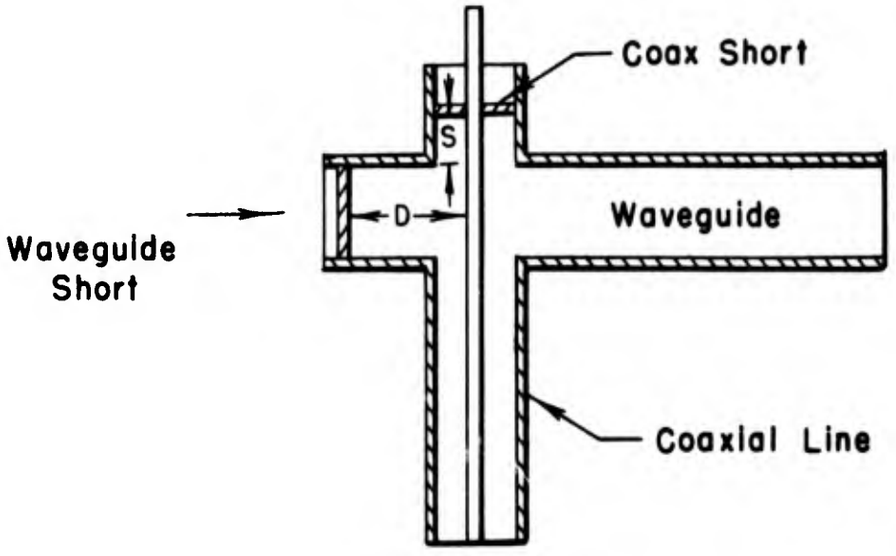

Fig. 1.04
Coaxial Line To Waveguide Transition TE_0

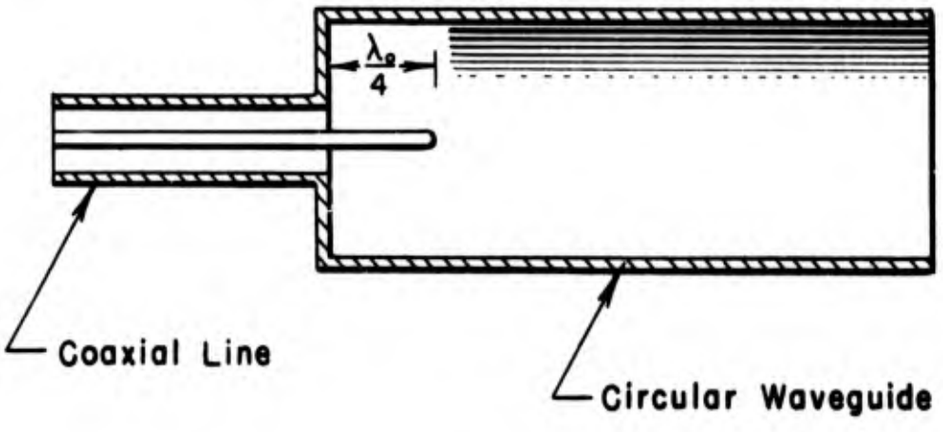

Fig. 1.05
Simple TM_{01} Mode Exciter

the popularity of rectangular guides over circular guides, there has been more development work done on the transitions for the former and ready-made transitions are commercially available for them. It is then a relatively easy job to transform the TE_{10} mode in the rectangular guide to the TE_{11} in the circular guide by means of the transducer shown in Figure 1.06.[15] If the transition is made longer than one wavelength, the impedance match will be quite satisfactory.

Figure 1.08 gives plots of the electric field measured as a function of the radial distance r across the mouth of the TE_{11} exciter shown in Figure 1.06. There was undoubtedly considerable error in these measurements due to the presence of the test probe within the field. The probe used in these measurements is described in detail in Part Two. The curves for both E_φ and E_r indicate the presence of some second harmonic energy. Higher harmonics of the original mode as well as other modes would be generated at the mouth of the exciter due to the impedance mismatch between the exciter and free space. However, if the exciter were used to excite waves in dielectric waveguides, these higher harmonics, in general, would be attenuated very rapidly since they require a larger diameter rod to support propagation. The failure of E_φ to become zero at $r/a = 1$ was due to diffraction at the edge of the waveguide. Inside the waveguide the tangential component undoubtedly did vanish.

---

[15] Ragan, G. L., Microwave Transmission Circuits, MIT Radiation Laboratory Series, 9, McGraw-Hill Book Co., New York, Chapter VI, 1948.

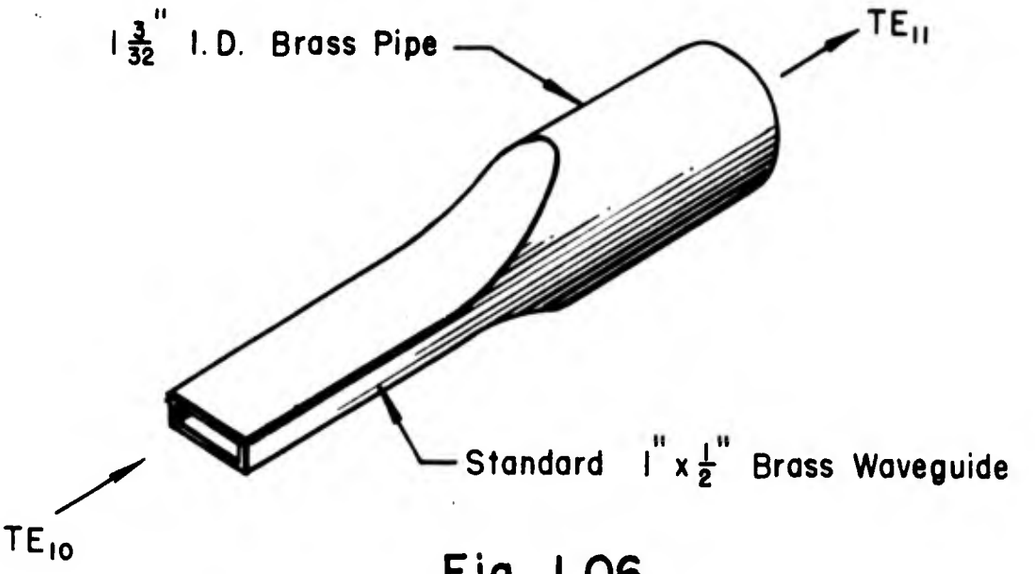

Fig. 1.06
TE_{10} - TE_{11} Mode Transducer

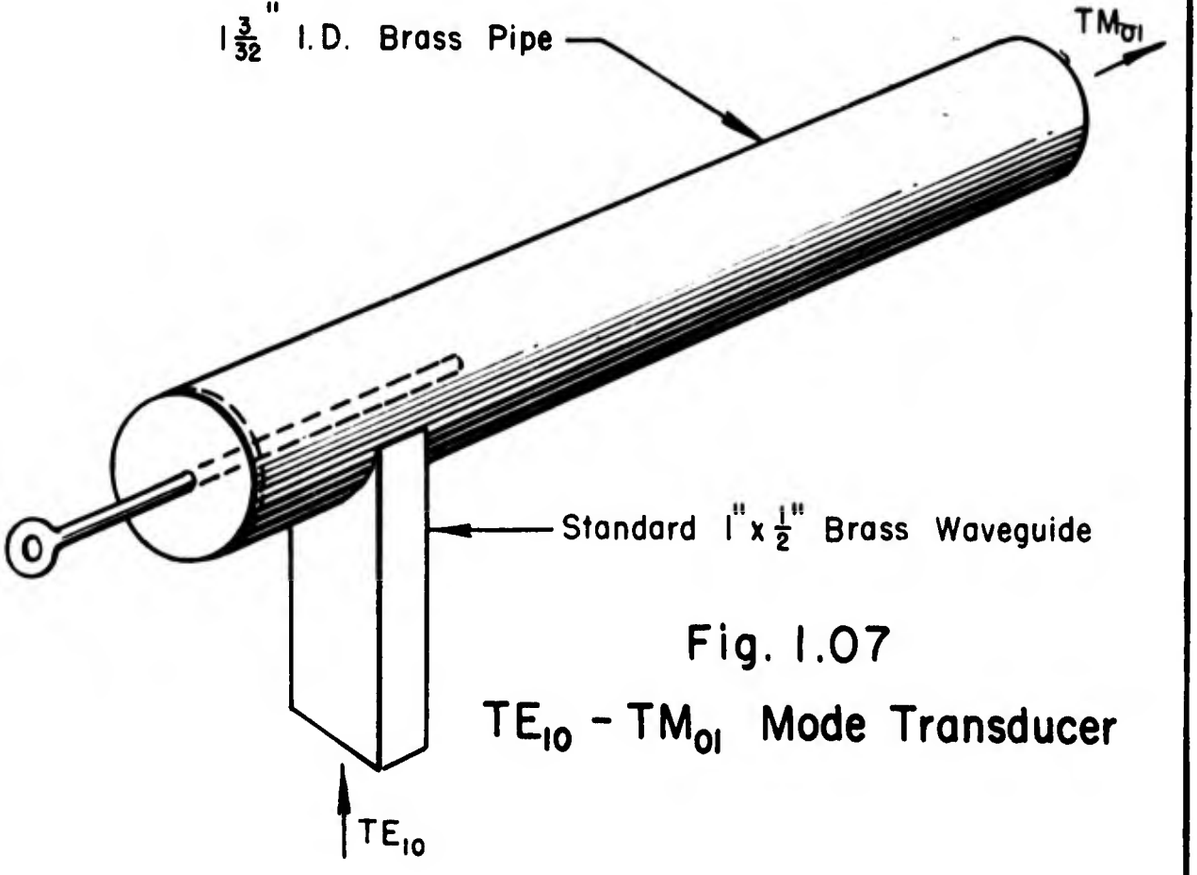

Fig. 1.07
TE_{10} - TM_{01} Mode Transducer

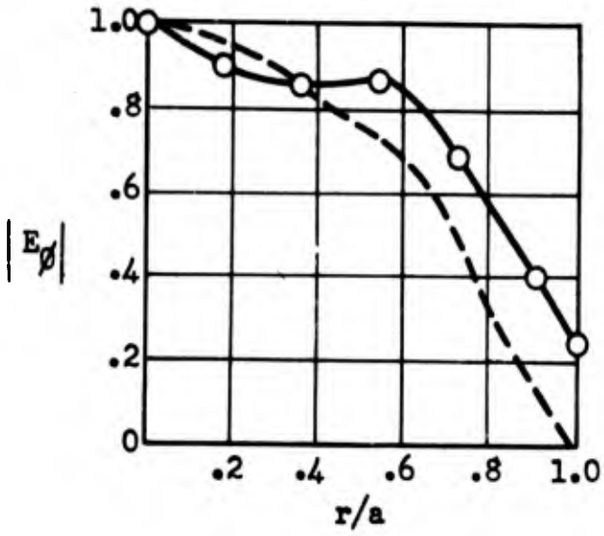

$\phi = 90^\circ$

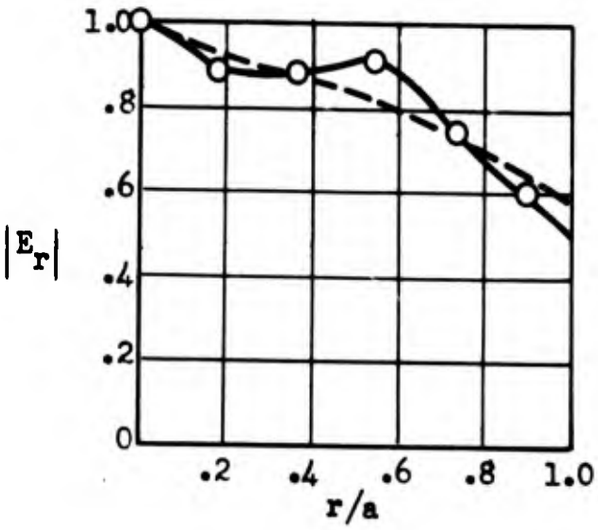

$\phi = 0^\circ$

------ Theoretical ——— Experimental

r: radial distance from origin
a: radius of the waveguide
E_ϕ: angular component of the electric field
E_r: radial component of the electric field

Fig. 1.08

ELECTRIC FIELDS MEASURED ACROSS THE MOUTH OF A TE_{11} MODE EXCITER

There are other methods for transducing from rectangular to circular guides which are smaller physically (of prime importance in many applications) but are more difficult to make and produce a good match.[16]

The TM_{01} mode may be excited in circular waveguides in a number of ways. A very simple method is shown in Figure 1.05.[17,18] The probe is acting as an end fire antenna and the field produced is very similar to that in a coaxial cable. Since in certain military equipment it is often necessary to convert from rectangular to round guides, i.e., TE_{10} - TM_{01} and vice versa, Radiation Laboratory did a vast amount of work on such transducers.[19] The transducer used in the work described here was built before the information in reference 19 was available and is an original design. A sketch of the exciter which was used is shown in Figure 1.07. The TE_{10} mode feeds the circular guide and, due to the metallic center conductor, a transverse electromagnetic wave - (TEM) - is generated which in turn excites the TM_{01}. This center conductor, which is adjustable in length, also acts as a filter to eliminate TE_{11} mode since the electric field lines must terminate on it, and thus the TE_{11} mode cannot be propagated with it present. The center rod is adjusted in length for maximum TM_{01} mode field intensity. The short circuit on the circular guide is set for a compromise between maximum TE_{11} attenuation and TM_{01} minimum

---

[16] ibid., 364.

[17] Sarbacher and Edson, Hyper and Ultra High Frequency Engineering, John Wiley and Sons, Inc., New York, p. 313, 1943.

[18] Southworth, op. cit.

[19] Ragan, op. cit., 379.

attenuation. The bandwidth of the transition has not been measured and may not be too good, but for the nature of this work, wide band width was not necessary, and this method does give good purity of mode.

This exciter has the advantages of having no coaxial lines in it and the tuning element can be easily adjusted, which is not the case with coaxial lines. It is also simple to construct.

In a later phase of this work a TM_{01} exciter was constructed as shown in Figure 1.09, from a design by Radiation Laboratory. The excitation is strictly by means of waveguides and no TEM mode is generated. Filtering of TE_{11} mode is accomplished by means of the different sizes in the inside diameter of the circular tube and positions of the shorting plate.

Figure 1.10 gives the results of field measurements across the end of the TM_{01} exciter shown in Figure 1.09, as a function of radial distance. The sources of error are the same as for the TE_{11} exciters but the field structure is that to be expected. The reason for E_r not being zero at the origin is not entirely evident. Some TE_{11} mode would produce a field at the origin, but if the field were due to this mode, it should be a function of φ, and in this particular case, measurements showed that the field was independent of angular variation.

The TE_{01} mode is of special interest because of the unique property that the attenuation decreases with increasing frequency.*

*It is believed that this characteristic, which is from theoretical considerations, has never been experimentally verified.

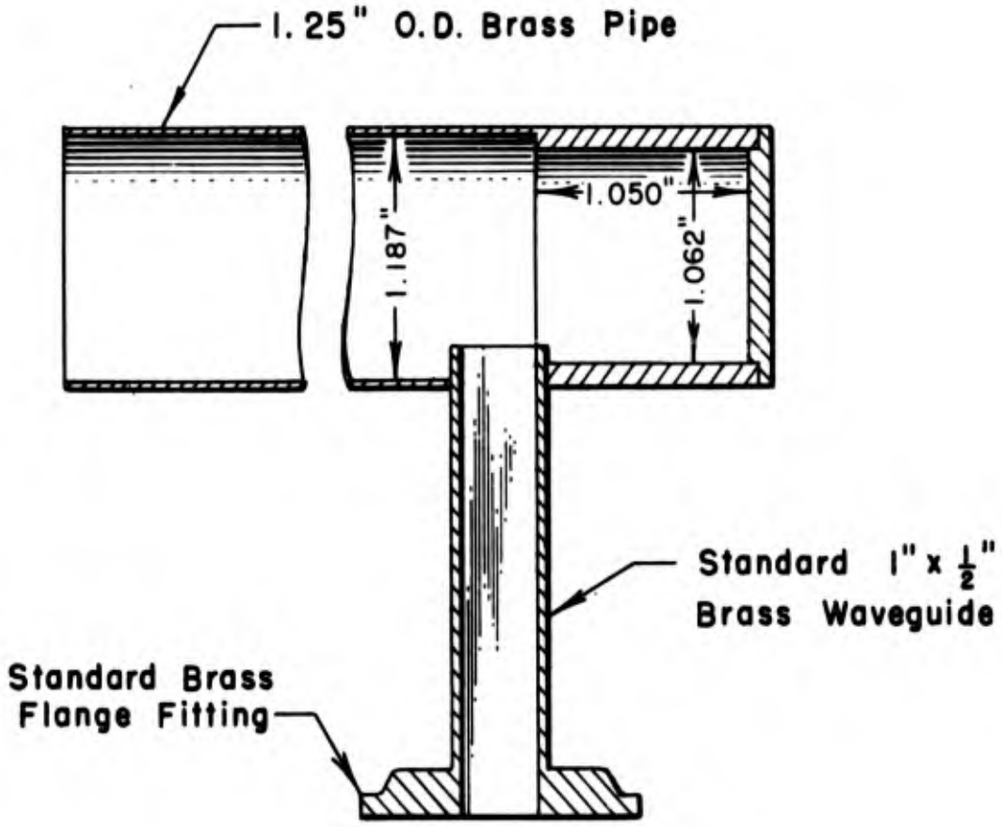

Fig. 1.09

TM_{01} Mode Exciter

(After Radiation Laboratories)

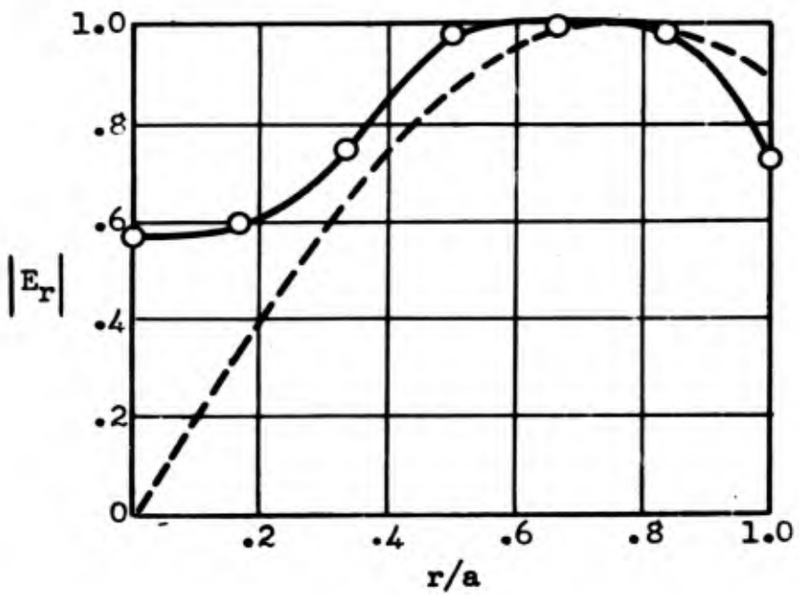

- - - Theoretical ——— Experimental

r: radial distance
a: radius of waveguide

E_r: radial component of the electric field

λ_o = 3.20 cm

Fig. 1.10 RADIAL COMPONENT OF THE ELECTRIC FIELD MEASURED ACROSS THE MOUTH OF A TM_{01} MODE EXCITER.

However, it is not known if the TE_{01} mode has been used in any equipment. This lack of application is probably due to two reasons: first, it requires a considerably larger waveguide than TE_{11} or TM_{01}, and second, it is extremely difficult to excite in pure form. No practical ways of exciting this mode directly in a waveguide by such means as antennas, probes, or current loops are known. Two methods have been suggested for transducing it from other modes.[20,21]

In one of these schemes the TM_{01} mode is transformed into the TE_{01} and suitable filters are used to attenuate the TM_{01} mode. The apparatus for this method is shown in Figure 1.11 and will be described in detail. The TM_{01} mode is excited by means of an axial probe, or other suitable means, and propagates down the guide from left to right. It is scarcely affected by the circular filter, which is composed of thin concentric metallic rings mounted on a thin polystyrene circular disk for support, since the conductors are normal to the radial electric field. But the TM_{01} wave, when striking the transducer unit, which consists of 8 copper wires, shaped as shown and soldered in place on the brass circular waveguide, is partly reflected, partly transmitted, and also induces currents to flow in the radial part of the conductors of the transducer unit. Since these currents will also flow in the circular parts of the conductors, they will excite the TE_{01} mode, which will propagate in both directions of the guide. The TE_{01} wave moving to the right is not affected by the radial filter

---

[20] Sarbacher and Edson, op. cit., 303.

[21] Montgomery, et al, Principles of Microwave Circuits, MIT Radiation Laboratory Series, 8, p. 339, McGraw-Hill Book Co., New York, 1948.

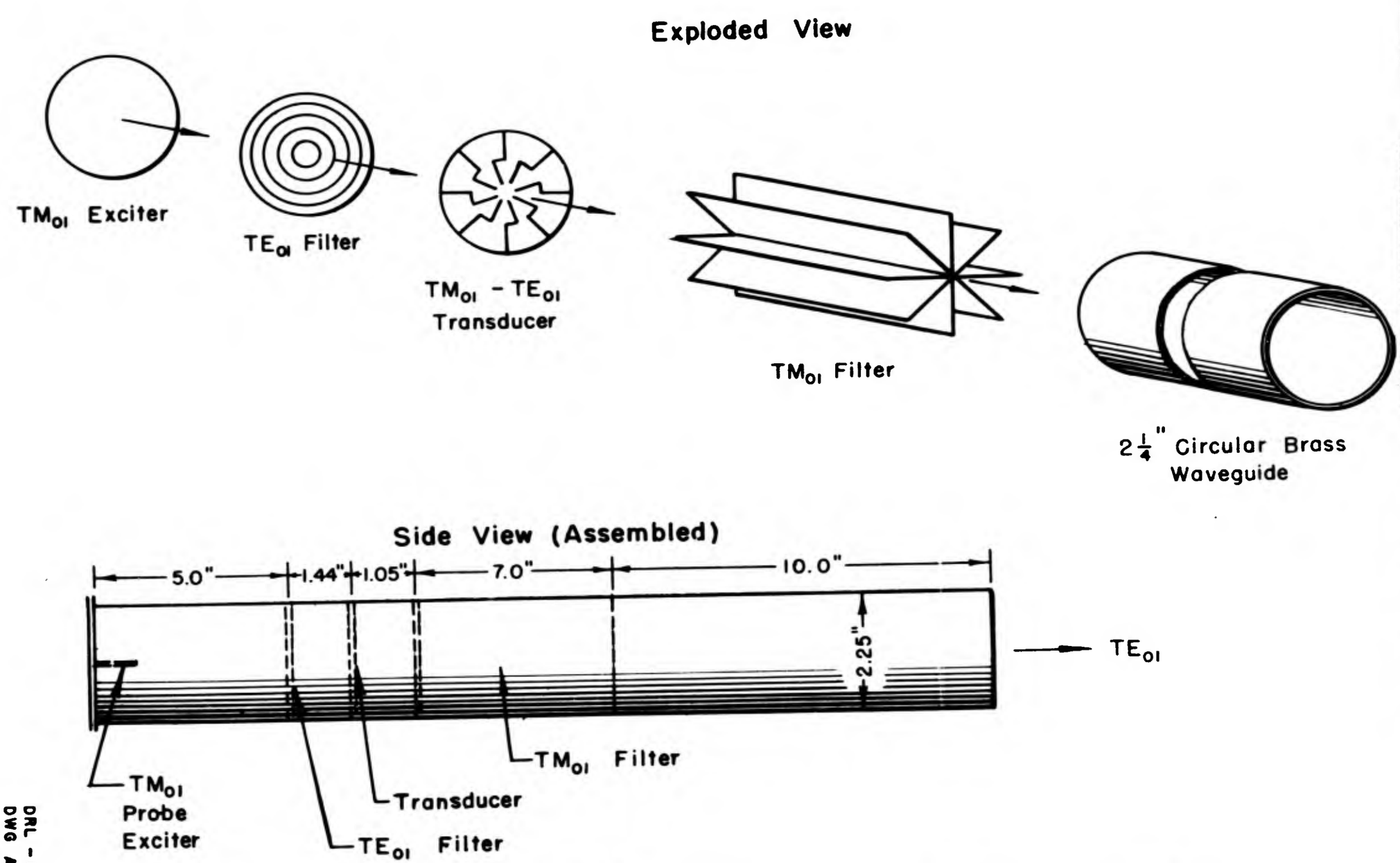

Fig. 1.11 – $TM_{01} - TE_{01}$ Mode Transducer

DRL - UT
DWG AE 661
CMM - CLW
7-9-49

and hence passes down the waveguide. But the TE_{01} wave moving toward the left will be partly absorbed and partly reflected by the circular filter. This filter should be adjusted so that the reflected wave will be in phase with the transduced wave when it arrives there. Since there is 180° phase shift on reflection this spacing between circular filter and transducer should be $\lambda_{ge}/4$ where λ_{ge} is the guide wavelength for the TE_{01} mode. Now consider the TM_{01} wave. The portion of this energy which passes through the transducer is largely reflected or absorbed by the radial filter. This filter should be adjusted so that the reflected wave arriving back at the transducer will be in phase with the incident wave, that is, the spacing should be $\lambda_{gh}/4$ where λ_{gh} is the guide wavelength for the TM_{01}. The portion of the original TM_{01} incident energy which is reflected will return to the exciting axial probe and the end plate is so adjusted that the returning reflected wave is in proper phase for reinforcement. In theory there should be very little loss of energy in this transformation but in practice, due to difficulty in making precise adjustments on the filter elements and due to finite conductivity of the filter elements, the system is not very efficient. However, considerable TE_{01} energy can be obtained in this manner. The principal difficulty is that, due to the large size of waveguide required, other modes propagate readily, such as TE_{11} and TM_{01}, and at each point of discontinuity some of these modes are generated. In order to attenuate the TM_{01} mode more, a radial filter, consisting of radial brass sheets about $6\lambda_o$ long were used, instead of the small wires. The leading edge was adjusted for proper reflection and the rest of the filter served

primarily as an absorber of TM_{01} energy. Unfortunately, the "pie cut" divisions in the filter are large enough to pass TE_{11} mode at this frequency. This type of filter will be discussed in more detail in Part Two.

The exciter just described is the type used in this work although it must be admitted that results were not as good as hoped for. Figure 1.12 gives E_φ as a function of radial distance. Actually the mode purity appears to be quite good. The radial component of E was very, very weak compared to the tangential component and is not plotted. A rough sketch of the field of the TE_{02} mode is included. It can be seen that a combination of pure TE_{01} and TE_{02} could produce the resulting measured field. However, there is some asymmetry of E_φ which is probably due to TE_{11} mode. The TE_{11} mode would reinforce for one half of the pattern and cancel for the other half, giving the resulting asymmetry.

A second type of TE_{01} exciter has been suggested,[22] which transforms the TE_{20} mode in rectangular guides into TE_{01} in the circular guide. It is not known if this type has actually been used. It essentially bends the rectangular guide into a circular guide in a way that the two side walls become the total boundary. Difficulty lies in the construction of the guide and in producing pure TE_{20} in the rectangular guide. Unfortunately, the TE_{10} mode propagates readily in guides that pass TE_{20} and it is difficult to filter out

[22]Montgomery, op. cit., 340.

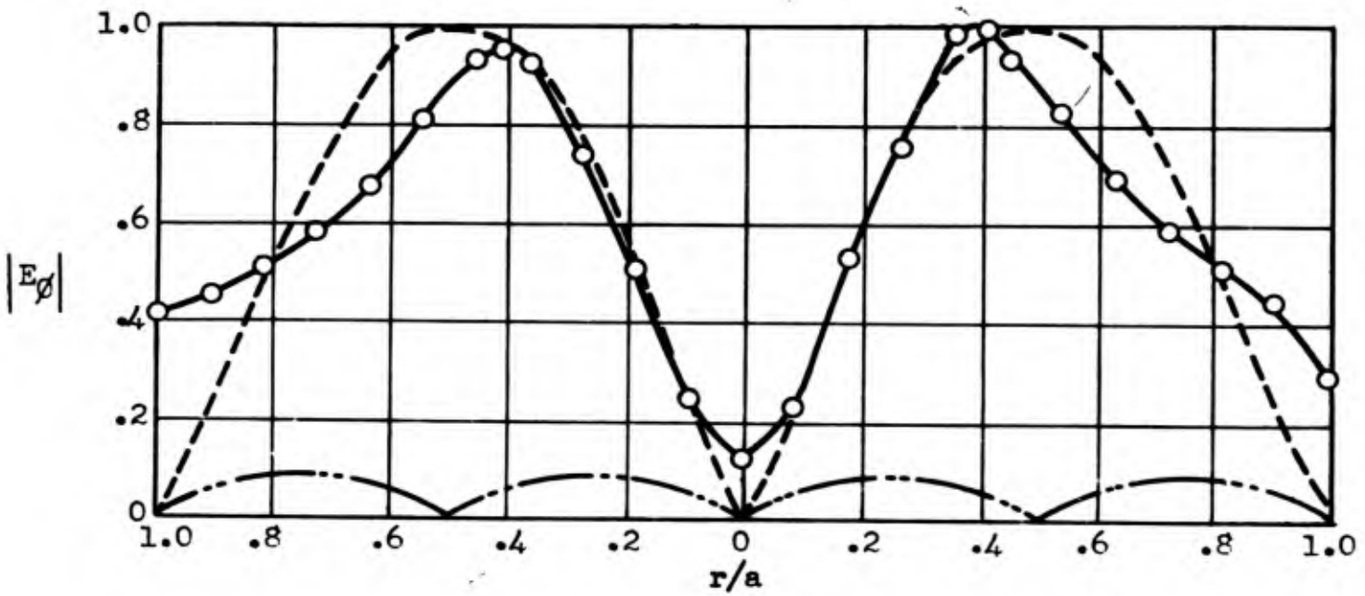

—— Experimental ----- Theoretical •• – •• TE_{02} (Theoretical)

a = radius of waveguide = 1.12 inches r = radial distance

Fig. 1.12

ANGULAR COMPONENT OF THE ELECTRIC FIELD VERSUS RADIAL DISTANCE ACROSS THE MOUTH OF THE TE [illegible]

the TE_{10} without also attenuating the TE_{20} strongly. It is somewhat difficult to generate the TE_{20} mode. Several methods have been suggested.[23] A transverse section of the field structure of the TE_{20} mode for rectangular waveguides is shown in Figure 1.13. One of the first methods suggested for generating the TE_{20} mode was to use two vertical probe antennas fed from coaxial cables one of which was $\lambda_o/2$ longer than the other. This method is satisfactory, but if the frequency changes, the two lines no longer differ in length by $\lambda_o/2$. An alternate method is to feed the probes in phase but have one inserted from the top of the guide at point D and the other at point A, as indicated in Figure 1.13. However, it is desirable to eliminate coaxial cables if possible. Other methods have been given but are of low efficiency or require considerable experimental work to obtain proper transformation.

One method of generating the TE_{20} mode which works well and is not difficult to make is shown in Figure 1.14. This method makes use of the "Magic T". It is believed that this scheme for excitation of the TE_{20} mode is original. Energy coming into the junction from the "E" arm divides into the two arms of symmetry, A and B, and the fields in these arms are out of phase. If there are no reflections from the terminations of these arms, no energy is coupled to the "H" arm. (It should be remarked that if arm H had been used as the input arm, the fields in the arms of symmetry would have been in phase.)

---

[23] Chu, L. J., and Barrow, W. L., "Electromagnetic Waves in Hollow Metal Tubes of Rectangular Cross-section," Proc. I.R.E., 26, 1520, December 1938.

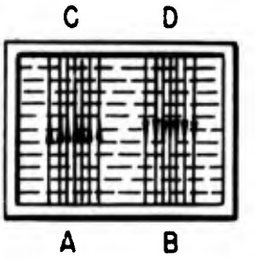

Fig. 1.13

Transverse Fields Of TE_{20} Mode.

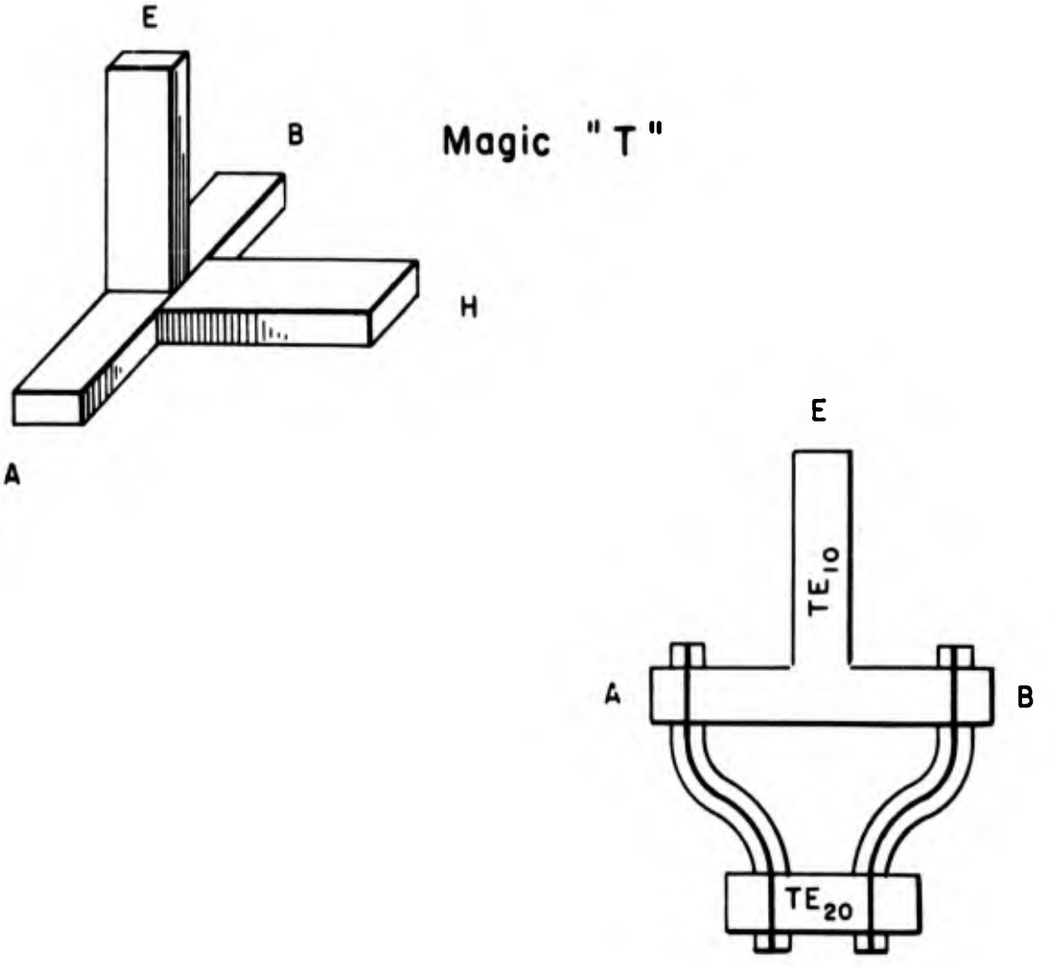

Fig. 1.14 Magic "T" TE_{20} Exciter.

The out of phase fields excite the probes which feed into the TE_{20} waveguide by means of coaxial cables of same length. This device can also be used to excite the TM_{11} mode in circular waveguides as will be described later. Similarly, the TM_{11} described later should also be able to excite TE_{20} mode. This exciter is not dependent on frequency and has good efficiency.

A few measurements were made on an exciter of this type and it was found that some TE_{10} mode was present also. It is obvious that a better design would be to mount the "Magic T" directly on top of the TE_{20} waveguide and omit the coaxial cables. However, there is a minimum spacing for the output probes of a "T", which is greater than the desired spacing of the feeding points of waveguide normally used with TE_{20} mode. However, a tapered section of waveguide could be used.

The symmetry and matching of the system can be checked by terminating the H-arm with a detector. If arms A and B are properly matched there will be no energy in the H-arm.

The TM_{11} mode is the last of the modes which was used in this project. It is not known if there have ever been any uses for it in commercial application. Southworth[24] suggested the first means of exciting this mode and essentially the scheme is the only one known. It consists of feeding two axial probes into the end of a cylindrical waveguide. If the probes are excited 180° out of phase, the TM_{11}

[24]Southworth, G. C., "Some Fundamental Experiments with Waveguides," Proc. I.R.E., 25, July, 1937.

mode will be excited. The spacing, d, is approximately 1/2 diameter (i.e., the radius) as can be determined from the field equation for this mode.

Essentially this mode may be excited by the same methods as described for the TE_{20} in rectangular guides. Figure 1.15 shows an exciter of original design and which works rather well. It is believed that this scheme for mode excitation has not been used before. The conductor across the rectangular guide is excited by the TE_{10} wave. Thus the currents flowing in each arm of the coaxial are 180° out of phase. An adjustable plunger is used in the rectangular guide and is adjusted for maximum output of the TM_{11} mode.

Figure 1.16 illustrates the nature of the measured field across the face of one of these exciters. Evidently, the mode is not pure TM_{11}.

Difficulty was had in obtaining the TM_{11} mode in pure form. A filter was devised for eliminating TM_{01} mode but had certain defects. It consisted merely of a thin sheet of brass, about $6\lambda_o$ long placed diametrically and axially in the circular guide in the y-z plane. (Figure 1.03). This sheet does not disturb TM_{11} waves but does absorb TM_{01} waves. Unfortunately, filters that would eliminate TE_{11} waves will also sharply attenuate TM_{11}. For this reason, a pure TM_{11} mode was not obtainable.

The TE_{11} mode with circular polarization was also generated. The method of obtaining this mode was to use a helical beam antenna as the driving element. Kraus[25] has done much work on this type of

[25] Kraus, J. D., "Helical Beam Antenna," Electronics, 20, 109, April 1947.

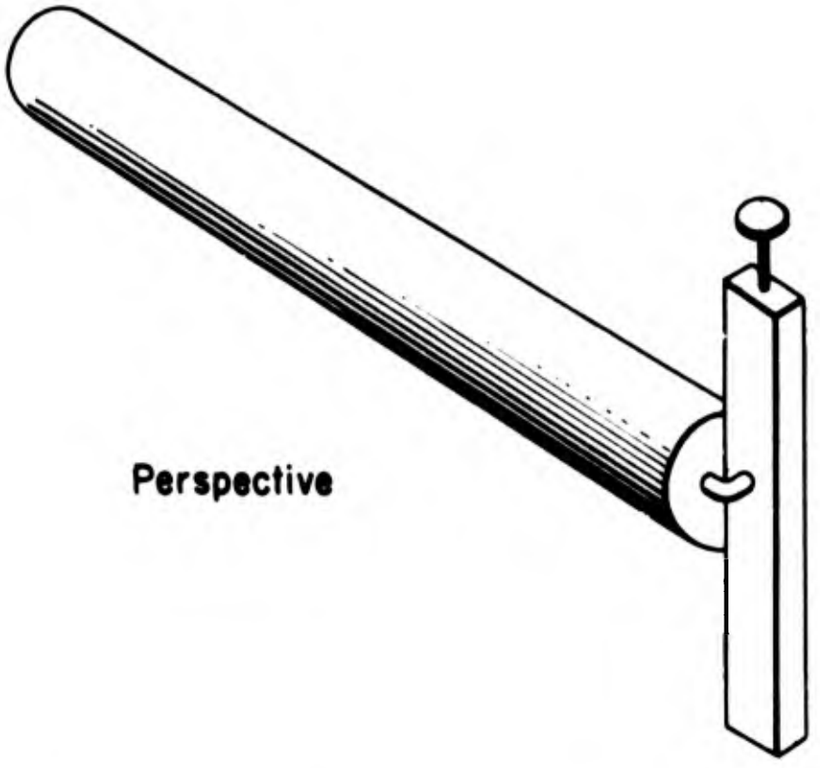

Section A-B

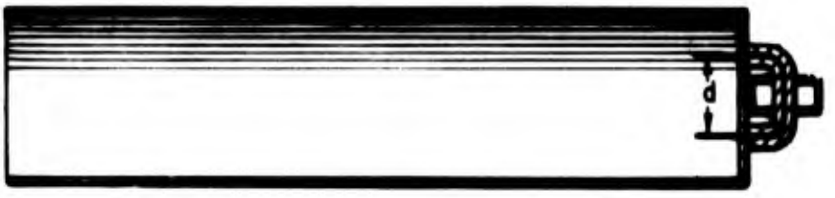

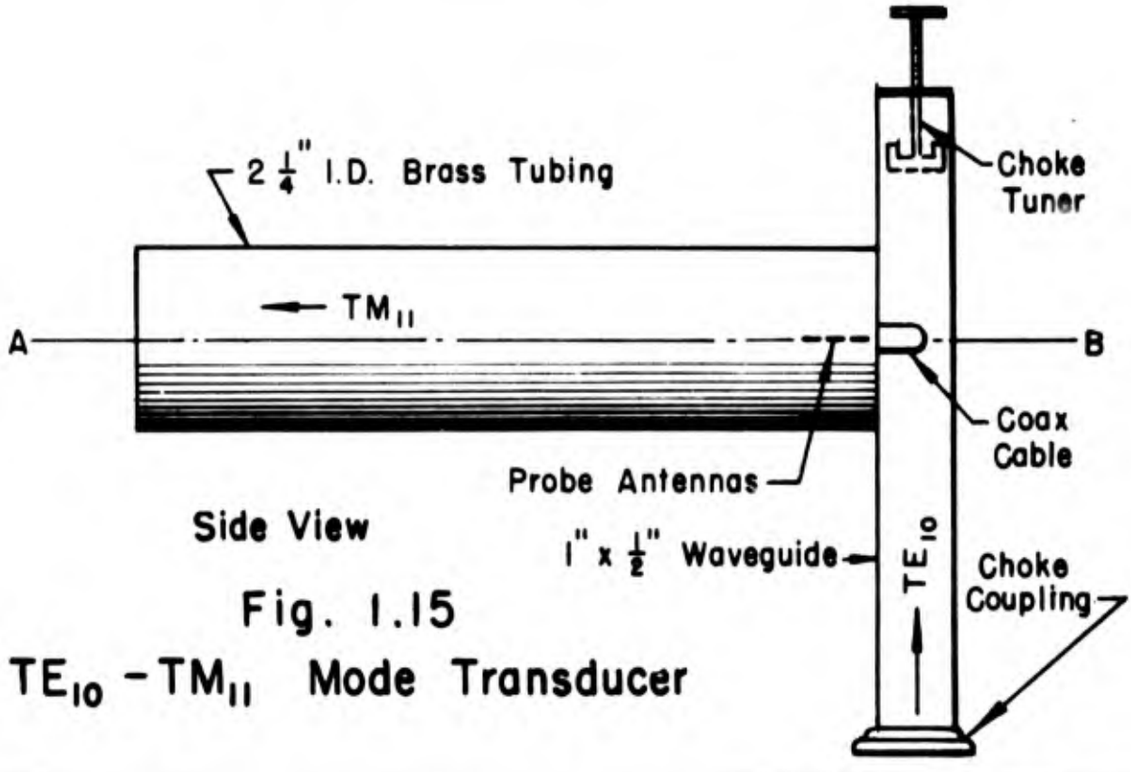

Fig. 1.15

$TE_{10} - TM_{11}$ Mode Transducer

DRL - UT
DWG AE 662
CMM - CLW

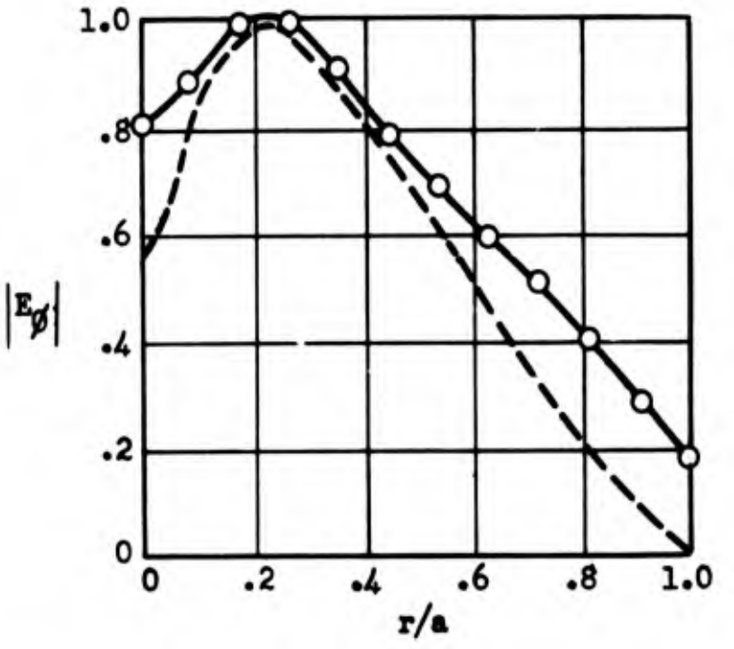

$\phi = 90^\circ$

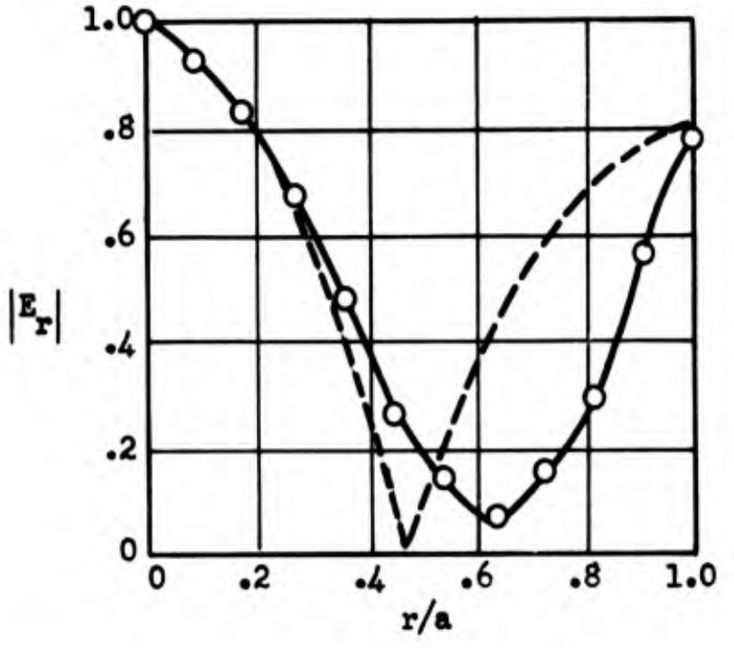

$\phi = 0^\circ$

——— Theoretical

——— Experimental

E_ϕ = angular component

a = radius of waveguide = 1.12 inches

E_r = radial component

r = radial distance

Fig. 1.16

COMPONENTS OF THE ELECTRIC FIELD VERSUS RADIAL DISTANCE ACROSS THE MOUTH OF THE TM_{11} EXCITER

end-fire antenna which gives circular polarization. The antenna consists of a helical coil of wire in which the circumference of one turn is λ_o. Thus between two diametrically opposite points, the currents are 180° out of phase and the field is somewhat as shown in Figure 1.17. The field rotates once per cycle and propagates down the axis of the helix. This type of antenna was used to excite the TE_{11} mode in circular guides and was found to work very satisfactorily. It seemed likely that TE_{M1} modes could be generated where M = circumference in λ_o per turn of helix. However, these higher order modes could not be produced. The TE_{11} was present but other modes were not detected. More work may be done on this type of exciter.

It is not an easy matter to identify different modes in waveguides because of the limitations placed on inserting measuring instruments inside the guide. The slotted line technique is applicable to the TE_{11} and TM_{01} modes. In this method a longitudinal slot is cut in the guide so that it is parallel to the lines of current flow. The radiation through the slot is very slight and the internal field is scarcely disturbed. Then a very small probe antenna is inserted into the guide (not further than 1/32") and moved along the slot to sample the field. Distance between nulls of the standing waves is $\lambda_g/2$. The TE_{01} mode cannot be examined with this type of instrument. Consequently, it was identified and checked by means of radiation patterns from the end of the waveguide and by means of wavelength and field configuration along dielectric waveguides. These measurements are discussed in Parts Two and Three.

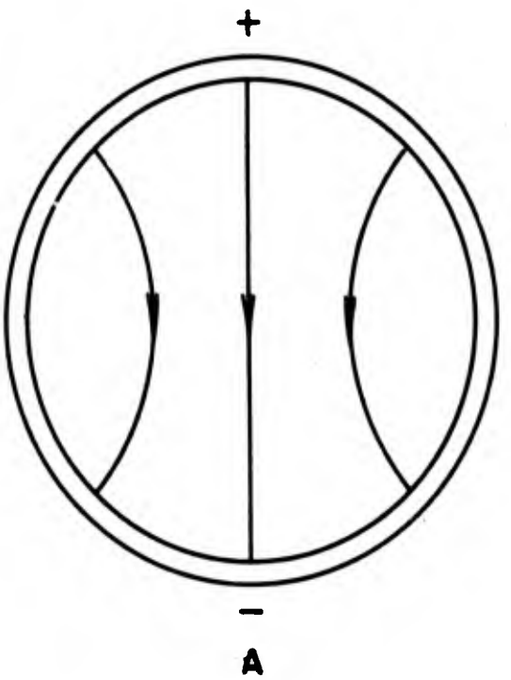

Fig. 1.17

Electric Field For One Turn
Of Helical Antenna.

It is seen that one of the principal difficulties in mode generation is the elimination of undesired modes. The early articles and several current textbooks describe in detail the type of filters used in the TE_{01} exciter that have been described here and state that they are highly effective. However, little experimental work on these filters is available. It was concluded, after considerable experimentation, that these filters were not nearly as effective as desired. Apparently, the filters themselves have certain discontinuities which serve to generate other modes.*

The TE_{01} and TM_{11} were not obtained in pure form and it is believed that good mode purity can not be expected using the type of filters that have been described in this chapter. A resonant type of transmission filter might be more successful. This type of mode filter is described in more detail in Part Two.

It appears that the problem of generating pure modes and designing efficient mode filters for most modes is as yet unsolved.

---

*After the work on mode generators had been completed, a report was obtained on some recent work which The Polytechnic Research and Development Company of Brooklyn, New York, did on a contract for the Signal Corps. This work extended over two years and the problem was to study mode filters for rectangular guides. The primary purpose was to retain the dominant mode and subdue higher order modes. Naturally, this is a much easier problem than the one in this work. However, their general conclusions were that the type of filter which was designed to make the waveguide structure incompatible for certain modes was not satisfactory. The only suitable system they obtained was to generate the dominant mode in a waveguide that was not large enough to support the propagation of the other modes, and then to gradually flare this guide into larger guides. Of course, this solution cannot be applied to the problem of retaining pure higher order modes.

PART TWO

DIELECTRIC WAVEGUIDES OF CIRCULAR CROSS SECTION

BLANK PAGE

CHAPTER I

HISTORICAL SURVEY

Lord Rayleigh[1] was the first person to suggest and consider the use of dielectric rods as a means of guiding electromagnetic waves. However, he considered the case of the dielectric rod enclosed by a metallic conductor. Hondros and Debye,[2] in 1910, made the first theoretical study of the dielectric rod of circular cross section embedded in air, without any metal covering. They applied Maxwell's Field equations in cylindrical coordinates, and obtained field expressions for the waves inside and outside a dielectric rod of circular cross section. They considered rotationally symmetrical waves and obtained graphical solutions for the phase velocity on the rods as a function of diameter for a material of dielectric constant of 81 for the TM_{01} mode. They also calculated the cutoff wavelength for some of the modes.

Zahn,[3] Schriever,[4] and Ruter performed some experimental work in 1914 to check the theoretical work of Hondros and Debye. They used water, methyl alcohol, and acetone in thin-walled glass tubes, terminated by means of a metal reflector. A test probe was used to measure the standing waves. Their measurements were on the lowest order

---

[1]Lord Rayleigh, "On the Passage of Electric Waves Through Tubes," Philosophical Magazine, 43, 125, February 1897.

[2]Hondros, D., and Debye, P., "Elektromagnetische Wellen an dielektrischen Drahten," Ann. d. Phys., 32, 465, (1910).

[3]Zahn, H., "Elektrische Wellen an dielektrischen Drahten," Physikalische Zeitschrift, 16, 414, 1915.

[4]Schriever, O., "Elektromagnetische Wellen an dielektrischen Drahten," Ann d. Phys., 63, 645, (1920).

rotationally symmetrical mode on rods whose diameter was small compared to a wavelength.

In 1936 Carson, Mead, and Schelkunoff[5] published the results of a theoretical investigation of the circular rod waveguide. They took the most general solutions to the wave equation in cylindrical coordinates that represented a wave traveling along the axis. They applied the conditions that the fields be finite, vanish at infinity, and that the tangential components be continuous on the boundary. They obtained a transcendental equation involving Bessel functions of the first and third kind. They showed that in general there are an infinite number of three types of waves, namely TM_{om}, TE_{om} and hybrid waves or HE waves. It was shown that for n not zero, waves could not exist with either the electric or magnetic field components entirely transverse. These waves that have components of both the electric and magnetic field in the direction of propagation are known as HE_{nm} waves. The HE_{11} wave was shown to have no cutoff frequency.

Southworth,[6,7] at Bell Telephone Laboratories, also performed some experimental work on the dielectric waveguide. He considered the TM_{01} wave in a dielectric rod of water, and obtained measurements of phase velocity as a function of diameter. These measurements were made on rods which were considerably less than a wavelength in diameter, but because of the high value of the dielectric constant, the major

---

[5] Carson, J. R., Mead, S. P., and Schelkunoff, S. A., "Hyperfrequency Wave Guides - Mathematical Theory," B.S.T.J., 15, 310, April 1936.

[6] Southworth, G. C., "Hyper-Frequency Wave Guides - General Considerations and Experimental Results," B.S.T.J., 15, 284, April 1936.

[7] Southworth, G. C., "Guided Transmission on Ultra-High Frequency Waves," U. S. Patent No. 2120711, September 13, 1938, Filed March 6, 1933.

position of the energy was in the rod and the rod was therefore "large". He also made calculations of the fields as a function of radial distance for both the internal and external region.

Around 1939 Mallach,[8] in Germany, was working with the dielectric rod antenna. In the course of his work he made some measurements of phase velocity on small diameter polystyrene rods, excited in the HE_{11} mode. These were probably the first measurements using the hybrid asymmetrical mode.

In 1938 Kaspar[9] made some measurements on liquid filled tubes. He varied the experimental arrangement by using a fixed test probe, near the rods, and moving a reflector plate inside the tubes.

The symmetrical mode TM_{01} was used in Kaspar's work. However, he also made some measurements of TM_{02}. He further investigated the attenuation as a function of conductivity for several concentrations of salt solutions. He did not investigate attenuation as a function of diameter of the rods. Kaspar's work was probably the most complete experimental investigation at that time although he considered only the TM_{0m} type of wave.

In 1944 Wegener[10] made a rather exhaustive theoretical investigation of the dielectric waveguide. Using the same approach as previous

---

[8]Mallach, Peter, "Dielectric Directional Antennas for dm. and cm. Waves," Air Materiel Command Report, F-TS-2223-RE, February 1948. (Notes of Mallach and interrogation reports.) Translation by P. L. Harbury, Harvard University, Cambridge, Masaachusetts.

[9]Kaspar, E., "Experimentelle Untersuchung der elektromagnetischer Wellen an dielektrischen Drahten," Ann. d. Phys., 32, 353, (1938).

[10]Wegener, H. J., "Ausbreitungsgeschwindigkeit, Wellenwiderstand, and Daempfung elektromagnetischer Wellen an dielektrischen Zylindern" Vierjahresplan Institut fuer Schwingungsforschung, Berlin, N. W. 87, August 26, 1944.
Air Materiel Command Microfilm ZWB/FB/RL 2018, R. 8117 R831.
Translated by M. M. Astrahan and W. C. Jakes, Northwestern University.

workers, he solved for the various types of possible waves. However, in particular, he stated that the hybrid waves were of two types, HE and EH. The former closely resembles the H type waves in hollow metallic guides and the latter are similar to the E waves in the metal guides. More will be said of the latter. He also considered conduction losses in dielectrics and plotted graphs for attenuation as a function of diameter. A further part of his work was the investigation of the impedance properties of the waves on the dielectric waveguide.

Bondi and Pryce[11] have also considered the dielectric waveguide of circular cross section. They state that the two types of hybrid waves are identical for the lowest order ($n = 1$), but that for $n \geq 2$ the waves are physically different. They also include theoretical plots of the electric fields for the dominant hybrid mode. Curves were computed by them for the phase velocity as a function of diameter for several values of dielectric constants. These curves are for small rods only.

Whitmer,[12,13] Radiation Laboratory, Massachusetts Institute of Technology, made a theoretical investigation of the dielectric rod of circular cross section; also, of an infinite flat dielectric plate. He calculated

---

[11] Bondi, H. and Pryce, M. H. L., "Dielectric Cylinders as Waveguides," ASE Report No. M 434, British - Washington Guided Missile Committee, Admiralty Signal Establishment, August 1942, Lythe Hill House, Haslemere, Surrey.

[12] Whitmer, R., "Fields in Non-Metallic Waveguides," Proc. I.R.E., 36, 1105, 1948.

[13] Whitmer, R., "Waveguides Without Metal Walls," M.I.T. Radiation Laboratory Report No. 726, May 10, 1945.

the transverse attenuation of these guides and was of the opinion that the guides might be of practical importance.

Abele[14] is another of the numerous workers who have published papers on the theory of the dielectric waveguide. He considered the hybrid as well as the transverse modes and also showed that the attenuation tended toward a limit that was independent of the modes and of radius of the rods as the frequency increased.

Horton[15] has obtained some of the roots of the characteristic equation of several modes of waves in dielectric waveguides. These roots are the most accurate ones available. The range of parameters are quite wide and the values for some of the higher modes are also calculated. These solutions are discussed in more detail later.

Astrahan[16] and Jakes[17] have considered the problem of the air-filled dielectric tube as both a waveguide and antenna and have obtained good experimental verification of their theoretical work.

---

[14] Abele, M., "Theoria della propagazione di un campo elettromagnetico lungo una guida dielectrica a sezione circolare," Atti. del Congresso Internazionale della Radio (Rome), 3, Sept. and Oct. 1947.

[15] Horton, C. W., unpublished notes.

[16] Astrahan, M. M., "Guided Waves on Hollow Dielectric Tubes," Ph.D. Dissertation, Dept. of Electrical Engineering, Northwestern University, Evanston, Ill., May 1949.

[17] Jakes, W., "Attenuation and Radiation Characteristics of Dielectric Tube Waveguides," Ph.D. Dissertation, Northwestern University, May 1949.

Chandler, Elsasser, and Iams,[18,19,20] at R. C. A., have also investigated the dielectric rod waveguide. Their work concerned primarily, the attenuation of very small diameter rods, of low loss material excited in the HE_{11} mode. They reasoned that for small diameter rods most of the energy travels external to the rod and hence it is not attenuated by the lossy material. Of primary interest is their experimental arrangement. The dielectric rod passes normally through two small holes in large metal reflecting plates. A maximum of energy transfer occurs when the plates are an integral number of half wave lengths $(\lambda_g/2)$ apart. By this means, the wavelength on the guide may be measured. Also, the cavity formed by the rod and the two plates has a Q which is inversely proportional to the loss in the rod (neglecting metal loss). By comparing the Q of this cavity with a standard cavity, the attenuation can be calculated. Using very small diameter rods, they obtained values of Q as high as 50,000. This method has some defects which will be discussed later. The cavity has the further advantage that it acts as a mode filter.

---

[18] Chandler, C., Elsasser W., Iams, H., "An Investigation of Dielectric Rod as a Waveguide," Digest of paper No. 43 given at USRI-IRE Meeting, Washington, D.C., May 1948.

[19] Chandler, C. H., "An Investigation of Dielectric Rod as Waveguide," Journal of Applied Physics, 20, 1188, December 1949.

[20] Elsasser, W. M., "Attenuation in a Dielectric Circular Rod," Journal of Applied Physics, 20, 1193, December 1949.

CHAPTER II

PURPOSES OF FURTHER EXPERIMENTAL INVESTIGATIONS OF DIELECTRIC WAVEGUIDES

From the previous section it is apparent that considerable work both theoretical and experimental has been done on the problem of the dielectric waveguide of circular cross section. However, the experimental work has been confined to rods with diameters small compared to the wavelength and in most of the work this has limited the possible modes to the lowest order ones. The HE_{11} and TM_{01} modes have been the only ones investigated to any extent. Therefore, it was felt that it was worthwhile to extend the range of these measurements.

Horton[21] has obtained the roots for the characteristic equation for modes HE_{1m}, TM_{0m}, and TE_{0m} for $m = 1$ and 2 and for indices of refraction of 1.50 and 2.00. With the HE_{1m} mode, for $m = 2$, he obtains two branches. It was thought that these two branches might correspond to the HE and EH modes of Wegener's[22] theoretical investigation. As far as is known, the two branches had not been measured experimentally, and therefore, one purpose was to verify their existence. Due to difficulties which are described later, the detection and measurement of higher order modes were not as successful as hoped for, but some measurements were obtained and the two branches of the hybrid wave were measured with some degree of accuracy.

---

[21] Horton, op. cit.

[22] Wegener, op. cit.

A second purpose was to obtain information on the field structure and modes present in order to interpret more fully the information obtained from radiation patterns of dielectric rods used as antennas.

A third purpose was to determine whether the dominant wave in the dielectric rod excited from the TM_{11} mode in the metal guide degenerates to the same mode as that excited from the TE_{11} mode in the metal guide. Over the range of measurements made, the two modes do appear to be the same.

A further reason for making measurements on the dielectric rods was to help in determining the behavior of the mode exciters themselves. By qualitative and quantitative measurements of the fields on the surfaces of the rods, it was possible to obtain some idea of how well the mode exciters were working. This is especially important in the case of modes for which slots cannot be cut in the metal waveguide for measurement.

Very few measurements of the attenuation of the dielectric rod have been made by the previous investigators and those were for small rods and the dominant mode only. While our attenuation measurements were not extensive, they do verify Wegener's[23] theoretical calculation. Attenuation also occurs due to any bends or curves in the dielectric rod. Since this is important from the practical viewpoint, some measurements were made of attenuation caused by a bending of the waveguide.

---

[23] Wegener, op. cit.

CHAPTER III

BRIEF THEORY OF THE DIELECTRIC WAVEGUIDE

The theoretical treatment of the dielectric waveguide is covered rather completely in several papers[24,25,26,27,28,29,30,31] and textbooks and is essentially the same in all of these. The general approach consists of the solution of the boundary value problem of a right circular cylinder of one dielectric constant embedded in a dielectric medium of a lesser dielectric constant. The field expressions are obtained by solving Maxwell's equations in cylindrical coordinates. The orientation of the dielectric waveguide with respect to the coordinate system is the same as that shown in Figure 1.01 of Part One. The wave equation can be solved by the method of separation of variables, giving for the axial components of the fields

---

[24] Hondros and Debye, op. cit.
[25] Carson, Mead, Schelkunoff, op. cit.
[26] Wegener, op. cit.
[27] Bondi and Pryce, op. cit.
[28] Abele, op. cit.
[29] Horton, op. cit.
[30] Schelkunoff, S. A., Electromagnetic Waves, D. Van Nostrand Co., New York, p. 425, 1943.
[31] Stratton, J. A., Electromagnetic Theory, McGraw-Hill Book Co., New York, p. 524, 1941.

$$E_{z1} = A_n J_n(k_1 r) (F_\varphi) e^{j\omega t - \gamma z} \tag{2.01}$$

$$H_{z1} = B_n J_n(k_1 r) (F_\varphi) e^{j\omega t - \gamma z} \tag{2.02}$$

or

$$E_{z2} = C_n H_n^{(1)}(k_2 r) (F_\varphi) e^{j\omega t - \gamma z} \tag{2.03}$$

$$H_{z2} = D_n H_n^{(1)}(k_2 r) (F_\varphi) e^{j\omega t - \gamma z} \tag{2.04}$$

where

A, B, C, D are constants,

$J_n(k_1 r)$ are the Bessel Function of first kind, and

$H_n^{(1)}(k_2 r)$ are Hankel Functions of first kind,

$F_\varphi = e^{jn\varphi}$,

$\omega = 2\pi f$,

$\gamma = \alpha + j\beta = \alpha + j \frac{2\pi}{\lambda}$ = propagation constant,

$k^2 = \gamma^2 + \omega^2 \mu\epsilon = \gamma^2 + \beta^2$,

μ and ϵ are the inductive capacities of the media.

$K = \frac{\epsilon}{\epsilon_o}$ = dielectric constant.

ϵ_o refers to air. It is assumed that $\mu_1 = \mu_2 = \mu_0$.

The Bessel Functions of the first kind have the property of remaining finite for $r \to 0$, while the Hankel Function of first kind vanish for $r \to \infty$. From physical considerations, the electric and magnetic fields must always be finite and vanish at infinitely far distances from the dielectric rod. Therefore the fields inside the cylinder are expressed by equations (2.01) and (2.02) and those outside

the cylinder by equations (2.03) and (2.04). The radial and angular components of the fields may be obtained from the axial components by use of Maxwell's equations. The subscript "1" refers to the medium of the rod while the subscript "2" refers to the surrounding medium.

The boundary conditions require that the tangential components of both E and H be continuous across the boundary. That is, at the boundary, r = a

$$E_{z1} = E_{z2} \tag{2.05}$$

$$H_{z1} = H_{z2} \tag{2.06}$$

$$E_{\varphi 1} = E_{\varphi 2} \tag{2.07}$$

$$H_{\varphi 1} = H_{\varphi 2} \tag{2.08}$$

Therefore for each value of n there are four linear equations. They can be solved to obtain the characteristic equation. This procedure will be briefly outlined. From equations (2.01) through (2.04), the following equations are obtained:

$$E_{\varphi 1} = j\left[- A_n \frac{n\gamma}{k_1^2 r} J_n(k_1 r) + B_n \frac{j\omega\mu}{k_1} J_n'(k_1 r) \right] (F_\varphi)\, e^{j\omega t - \gamma z} \tag{2.09}$$

$$H_{\varphi 1} = + \left[A_n \frac{j\omega\epsilon_1}{k_1} J_n'(k_1 r) + jB_n \frac{n\gamma}{k_1^2 r} J_n'(k_1 r) \right] (F_\varphi)\, e^{j\omega t - \gamma z} \tag{2.10}$$

$$E_{\varphi 2} = - \left[C_n \frac{n\gamma}{k_2^2 r} H_n(k_2 r) - D_n \frac{j\omega\mu_2}{k_2} H_n'(k_2 r) \right] (F_\varphi)\, e^{j\omega t - \gamma z} \tag{2.11}$$

$$H_{\varphi 2} = \left[\frac{C_n j\omega\epsilon_2}{k_2} H_n'(k_2 r) + jD_n \frac{n\gamma}{k_2^2 r} H_n(k_2 r) \right] (F_\varphi)\, e^{j\omega t - \gamma z} \tag{2.12}$$

Apply the boundary conditions at $r = a$

$$A_n J_n(k_1 a) = C_n H_n(k_2 a) \tag{2.13}$$

$$B_n J_n(k_1 a) = D_n H_n(k_2 a) \tag{2.14}$$

$$- A_n \frac{n\gamma}{k_1^2 a} J_n(k_1 a) + B_n \frac{j\omega\mu_1}{k_1} J_n'(k_1 a) = - C_n \frac{n\gamma}{k_2^2 a} H_n(k_2 a) + D_n \frac{j\omega\mu_2}{k_2} H_n'(k_2 a) \tag{2.15}$$

$$A_n \frac{j\omega\epsilon_1}{k_1} J_n'(k_1 a) + B_n \frac{n\gamma}{k_1^2 a} J_n(k_1 a) = + C_n \frac{j\omega\epsilon_2}{k_2} H_n'(k_2 a) + D_n \frac{n\gamma}{k_2^2 a} H_n(k_2 a). \tag{2.16}$$

Let

$$\begin{aligned} A_n &= S H_n(k_2 a), \quad C_n = S J_n(k_1 a) \\ B_n &= T H_n(k_2 a), \quad D_n = T J_n(k_1 a) \end{aligned} \tag{2.17}$$

Substitute into (2.15) and (2.16) and collect terms

$$\frac{n\gamma}{a} J_n(k_1 a) H_n(k_2 a) \left[\frac{1}{k_2^2} - \frac{1}{k_1^2} \right] S = \omega \left[\frac{\mu_2 J_n(k_1 a) H_n'(k_2 a)}{k_2} - \frac{\mu_1 H_n(k_2 a) J_n'(k_1 a)}{k_1} \right] T \tag{2.18}$$

$$\omega - \left[\frac{\epsilon_2 J_n(k_1 a) H_n'(k_2 a)}{k_2} + \frac{\epsilon_1 H_n(k_2 a) J_n'(k_1 a)}{k_1} \right] S =$$

$$\frac{n\gamma}{a} J_n(k_1 a) H_n(k_2 a) \left[\frac{1}{k_2^2} - \frac{1}{k_1^2} \right] T . \tag{2.19}$$

Eliminating S and T from (2.18) and (2.19), one obtains

$$\left[\frac{\mu_2}{k_2}\frac{H_n'}{H_n} - \frac{\mu_1}{k_1}\frac{J_n'}{J_n}\right]\left[\frac{\epsilon_1}{k_1}\frac{J_n'}{J_n} - \frac{\epsilon_2}{k_2}\frac{H_n'}{H_n}\right] = \frac{n^2\gamma^2}{a^2\omega^2}\left[\frac{1}{k_2^2} - \frac{1}{k_1^2}\right]^2$$

where $H_n = H_n(k_2a)$ and $J_n = J_n(k_1a)$.

This may be written as

$$\left[\frac{\mu_2}{q}\frac{H_n'(q)}{H_n(q)} - \frac{\mu_1}{p}\frac{J_n'(p)}{J_n(p)}\right]\left[\frac{\epsilon_1}{p}\frac{J_n'(p)}{J_n(p)} - \frac{\epsilon_2}{q}\frac{H_n'(q)}{H_n(q)}\right] = \frac{n^2\gamma^2}{\omega^2}\left[\frac{1}{p^2} - \frac{1}{q^2}\right]^2 \qquad (2.20)$$

where $k_1a = p$ and $k_2a = q$.

When $n = 0$, the right side of equation (2.20) vanishes and the equation is satisfied when either of the two factors on the left vanish. This yields two equations:

$$\frac{J_0(k_1a)}{J_1(k_1a)} = \frac{\epsilon_1}{\epsilon_2}\frac{k_2}{k_1}\frac{H_0(k_2a)}{H_1(k_2a)} \qquad (2.21)$$

and

$$\frac{J_0(k_1a)}{J_1(k_1a)} = \frac{\mu_1}{\mu_2}\frac{k_2}{k_1}\frac{H_0(k_2a)}{H_1(k_1a)}. \qquad (2.22)$$

The well known relations $J_0'(u) = -J_1(u)$ and $H_0'(u) = -H_1(u)$ have been used.

These last two equations could be obtained by assuming in the first case that the wave had no H component along the axis and in the second case that the wave had no E component in the z direction. Thus they correspond to TM_{0m} and TE_{0m} waves. They have no variation in φ.

The roots of the characteristic equation determine the natural modes of propagation of waves along the dielectric cylinder.

Consider briefly the case of the TM_{0m} waves in order to determine some of the general characteristics of the waves on dielectric rods. For all of the energy to be retained along the dielectric rod and propagated in the z-direction, with no average energy transferred to the surrounding medium, a solution is needed which required an exponential decay of energy in the r-direction. $H_0^{(1)}$ of an imaginary quantity satisfies this requirement. Therefore k_2 should be imaginary and

$$k_2^2 < 0. \tag{2.23}$$

The critical case will be for

$$k_2 = 0. \tag{2.24}$$

Under this condition

$$\gamma^2 = -\omega^2\mu_2\epsilon_2 = \alpha + j\beta. \tag{2.25}$$

If no attenuation is considered,

$$\gamma = j\beta = j\omega\sqrt{\mu_2\epsilon_2}. \tag{2.26}$$

Under this critical condition the wave propagates in the z-direction with a velocity of $1/\sqrt{\mu_2\epsilon_2}$ which is the velocity of light in medium 2.

Also, for $k = 0$ from (2.21)

$$J_0(k_1 a) = 0. \tag{2.27}$$

Thus the critical cases are determined by the roots of the Bessel equation. Call the mth root p_{cm}, then

$$k_1 a = p_{cm}. \tag{2.28}$$

But

$$k = \omega \sqrt{\mu_1 \epsilon_1 - \mu_2 \epsilon_2} \tag{2.29}$$

or where f_c is the critical frequency,

$$f_c = \frac{p_{cm}}{2\pi a \sqrt{\mu_1 \epsilon_1 - \mu_2 \epsilon_2}}. \tag{2.30}$$

For frequencies lower than f_c, the wave no longer propagates in the z-direction but travels transversely.

It can be seen that large negative values of k_2^2 correspond to higher frequencies. The large imaginary value of k_2 requires that the field decay very rapidly in the radial direction, which corresponds to the case of most of the energy traveling inside the rod. As k_2^2 increases negatively the phase velocity approaches that of light in medium 1. As k_2^2 approaches zero, the radial decay is slight and most of the energy travels in the space exterior to the rod.

The actual phase velocity along the rod depends on the free space wavelength, the diameter of the rod, and the indices of refraction of the two media. The characteristic equation can be solved

to obtain pairs of values of p and q which satisfy the equation. Then, ω, the angular frequency, and γ, the propagation constant can be determined in terms of p and q. The phase velocity along the rod is obtained from γ, where

$$\omega = \frac{\sqrt{p^2 + q^2}}{a\sqrt{\mu_1\epsilon_1 - \mu_2\epsilon_2}} \tag{2.31}$$

$$\gamma = j\sqrt{\omega^2\mu_2\epsilon_2 + q^2/a^2} \tag{2.32}$$

or

$$\gamma = j\sqrt{\omega^2\mu_1\epsilon_1 - p^2/a^2}\ . \tag{2.33}$$

Generally, the solutions are plotted in the form of the apparent index of refraction as a function of the ratio of rod diameter, d, to free space wavelength. The apparent index of refraction is defined as

$$n_a = \frac{\lambda_o}{\lambda_g} = \frac{\text{Wavelength in air}}{\text{Wavelength on rod}}\ . \tag{2.34}$$

λ_g is of course obtained from the relation

$$\lambda_g = \frac{v_p}{f} \tag{2.35}$$

where v_p is the phase velocity and f is the frequency.

The waves for $n = 1$ are of special interest.[32] Noting that

$$p^2J_n'^2(p) = -p^2J_{n-1}(p)\,J_{n+1}(p) + n^2J_n^2(p) \tag{2.36}$$

[32] Schelkunoff, op. cit.

and

$$q^2H_n'(q) = q^2H_{n-1}(q)\,H_{n+1}(q) + n^2H_n^2(q) \tag{2.37}$$

the characteristic equation may be expanded and expressed as

$$-\frac{\mu_1\epsilon_1 J_{n-1}(p)\,J_{n+1}(p)}{p^2J_n^2(p)} + \frac{(\mu_1\epsilon_2 + \mu_2\epsilon_1)J_n'(p)\,H_n'(q)}{pqJ_n(p)\,H_n(q)}$$

$$+\frac{\mu_2\epsilon_2 H_{n-1}(q)\,H_{n+1}(q)}{q^2H_n^2(q)} = n^2\,\frac{\mu_1\epsilon_2 + \mu_2\epsilon_2}{p^2q^2}\,. \tag{2.38}$$

For $n = 1$, this becomes

$$\frac{\mu_1\epsilon_2 J_0(p)\,J_2(p)}{p^2J_1^2(p)} + \frac{(\mu_1\epsilon_2 + \mu_2\epsilon_1)J_1'(p)}{pJ_1(p)}\left[\frac{1}{q^2} + \frac{H_0(q)}{qH_1(q)}\right]$$

$$-\frac{\mu_2\epsilon_2 H_0(q)}{H_1^2(q)}\left[\frac{H_0(q)}{q^2} + \frac{2H_1(q)}{q^3}\right] = -\left(\frac{\mu_1\epsilon_1 + \mu_2\epsilon_2}{p^2q^2}\right). \tag{2.39}$$

Multiple by q^2 and let q approach zero. (The critical case is, of course, for $q = 0$.)

$$\frac{(\mu_1\epsilon_2 + \mu_2\epsilon_1)J_1'(p)}{pJ_1(p)} = 2\mu_2\epsilon_2 H_0(q) - \frac{\mu_1\epsilon_1 + \mu_2\epsilon_2}{p^2}\,. \tag{2.40}$$

The value of $H_0(q)$ is given by

$$H_0(q) = -(\log q + C - \log 2.0) \tag{2.41}$$

and hence, as $q \to 0$, $H_0(q)$ becomes infinite. Therefore for equation (2.40) to be satisfied the $J_1(p)$ must approach zero by the same order. This is equivalent to requiring that p approach a root of $J_1(p)$. The lowest root is $p = 0$. Therefore, from equation (2.31), it is seen that the critical frequency is $f_c = 0$.

The critical wavelengths for the modes may be readily calculated. For $n = 0$, the critical or cutoff wavelength for the first several radial modes is given by

$$\frac{d}{\lambda_o} = \frac{0.7655}{\sqrt{K - 1}}, = \frac{1.7571}{\sqrt{K - 1}}, = \frac{2.7554}{\sqrt{K - 1}}, \tag{2.42}$$

where K is the dielectric constant. The critical wavelength, λ_c, is the same for both the TM_{0m} and TE_{0m} modes, but the wavelengths along the rods are different.

For $n = 1$, λ_c is given by

$$J_1\left(\frac{\pi d}{\lambda_o}\sqrt{K - 1}\right) = 0 \tag{2.43}$$

or

$$\frac{d}{\lambda_o} = 0\ ; \quad = \frac{1.2140}{\sqrt{K - 1}}\ ; \quad = \frac{2.2332}{\sqrt{K - 1}} \tag{2.44}$$

for the first, second, and third radial modes.

In a later section, it will be desirable to have theoretical values of the fields as a function of radial distance to compare with measured values. Therefore, explicit expressions for the components of the fields must be available. In order to obtain these expressions,

one must have the relationship between the coefficients A and C and between B and D of equations (2.01) - (2.04). When this is done, the following field expressions are obtained. The propagation factor, $e^{j\omega t-\gamma z}$, is omitted for all of the equations.

The TM_{0m} modes

$$E_{r1} = \left(\frac{\gamma}{\omega\epsilon_1}\right)\left[J_1\left(p\,\frac{r}{a}\right)\right] \tag{2.45}$$

$$E_{r2} = \left(\frac{\gamma}{\omega\epsilon_2}\right)\left[H_1\left(q\,\frac{r}{a}\right)\frac{J_1(p)}{H_1(q)}\right] \tag{2.46}$$

$$E_{\varphi 1} = E_{\varphi 2} = 0 \tag{2.47}$$

$$E_{z1} = \left(\frac{jp}{\omega\epsilon_1 a}\right)J_0\left(p\,\frac{r}{a}\right) \tag{2.48}$$

$$E_{z2} = \left(\frac{jp}{\omega\epsilon_1 a}\right)\left[H_0\left(q\,\frac{r}{a}\right)\frac{J_0(p)}{H(q)}\right] \tag{2.49}$$

$$H_{r1} = H_{r2} = 0 \tag{2.50}$$

$$H_{\varphi 1} = J_1\left(p\,\frac{r}{a}\right) \tag{2.51}$$

$$H_{\varphi 2} = H_1\left(q\,\frac{r}{a}\right)\frac{J_1(p)}{H_1(q)}\,. \tag{2.52}$$

The field expressions for the TE_{0m} modes are found to be

$$E_{r1} = E_{r2} = 0 \tag{2.53}$$

$$E_{\varphi 1} = J_1\left(p\,\frac{r}{a}\right) \tag{2.54}$$

$$E_{\varphi 2} = H_1 \left(q \frac{r}{a}\right) \frac{J_1(p)}{H_1(q)} \tag{2.55}$$

$$E_{z1} = E_{z2} = 0 \tag{2.56}$$

$$H_{r1} = - \frac{\gamma}{\mu_1 \omega} E\varphi 1 \tag{2.57}$$

$$H_{r2} = - \frac{\gamma}{\mu_2 \omega} E\varphi 2 \tag{2.58}$$

$$H_{\varphi 1} = H_{\varphi 2} = 0 \tag{2.59}$$

$$H_{z1} = - \frac{jp}{\mu_1 \omega a} J_0 \left(p \frac{r}{a}\right) \tag{2.60}$$

$$H_{z2} = - \frac{jp}{\mu_1 \omega a} H_0 \left(q \frac{r}{a}\right) \frac{J_0(p)}{H_0(q)} \tag{2.61}$$

The field expressions for the hybrid or HE modes are considerably more complicated due to the angular variation in φ. Since neither the electric nor the magnetic fields are transverse, none of the field components vanish. The following notation is used in order to shorten the expressions for the components:

$$\sigma = p \frac{r}{a} \tag{2.62}$$

$$\rho = q \frac{r}{a} \tag{2.63}$$

$$N = \frac{(n_a^2 - 1)}{(K^2 - n_a^2)} \tag{2.64}$$

$$G = \frac{pJ_1(p)}{qH_1(q)} \tag{2.65}$$

$$M = \frac{\left[K^2 N\left\{\frac{1 - pJ_0(p)}{J_1(p)}\right\} + \left\{\frac{1 + qH_0(q)}{H_1(q)}\right\}\right]}{(1 + N)} \tag{2.66}$$

$$Z_o = \left(\frac{\mu_o}{\epsilon_o}\right)^{\frac{1}{2}} \tag{2.67}$$

$$X = \frac{2\pi a}{\lambda_o} \tag{2.68}$$

In terms of this notation the field components are

$$E_{r1} = \left[J_1'(\sigma) + \left(\frac{\mu_1 M}{\mu_2 n_a^2}\right)\left(\frac{J_1(\sigma)}{\sigma}\right)\right]\sin\varphi \tag{2.69}$$

$$E_{r2} = -G\left[H_1'(\rho) + \left(\frac{M}{n_a}\right)^2 \frac{H_1(\rho)}{\rho}\right]\sin\varphi \tag{2.70}$$

$$E_{\varphi 1} = \left[\frac{J_1(\sigma)}{\sigma} + \frac{\mu_1 M}{\mu_2 n_a^2} J_1'(\sigma)\right]\cos\varphi \tag{2.71}$$

$$E_{\varphi 2} = -G\left[\frac{H_1(\rho)}{\rho} + \frac{M}{n_a^2} H_1'(\rho)\right]\cos\varphi \tag{2.72}$$

$$E_{z1} = \frac{jp}{n_a X} J_1(\sigma)\sin\varphi \tag{2.73}$$

$$E_{z2} = \frac{jpG}{n_a X} H_1(\rho)\sin\varphi \tag{2.74}$$

$$H_{r1} = -\frac{K^2}{n_a Z_o}\left[\frac{\mu_2 J_1(\sigma)}{\mu_1 \sigma} + \frac{M}{K^2} J'(\sigma)\right] \cos\varphi \tag{2.75}$$

$$H_{r2} = \frac{G}{n_a Z_o}\left[\frac{H_1(\rho)}{\rho} + M H_1'(\rho)\right] \cos\varphi \tag{2.76}$$

$$H_{\varphi 1} = \frac{K^2}{n_a Z_o}\left[\frac{\mu_2}{\mu_1} J_1(\sigma) + \frac{M}{K^2 q}\frac{J_1(\sigma)}{\sigma}\right] \sin\varphi \tag{2.77}$$

$$H_{\varphi 2} = -\frac{G}{n_a Z_o}\left[H_1'(\rho) + M\frac{H_1(\rho)}{\rho}\right] \sin\varphi \tag{2.78}$$

$$H_{z1} = \frac{jMp}{n_a^2 Z_o X} J_1(\sigma) \cos\varphi \tag{2.79}$$

$$H_{z2} = \frac{jqGM}{n_a^2 Z_o X} H_1(\rho) \cos\varphi \tag{2.80}$$

Figure 2.01 shows sections of fields for TM_{01}, TE_{01}, and HE_{11} modes. The plots for the HE_{11} mode are from Wegener.

Wegener[33] has considered the case of the dielectric waveguide with attenuation by assuming a complex dielectric constant

$$\epsilon = \epsilon'(1 - j \tan\delta). \tag{2.81}$$

The resulting attenuation is represented by the complex propagation constant

$$\gamma = \alpha + j\beta \tag{2.82}$$

where α is the attenuation constant. The characteristic equation, which was complicated enough before, becomes exceedingly difficult

---

[33] Wegener, op. cit.

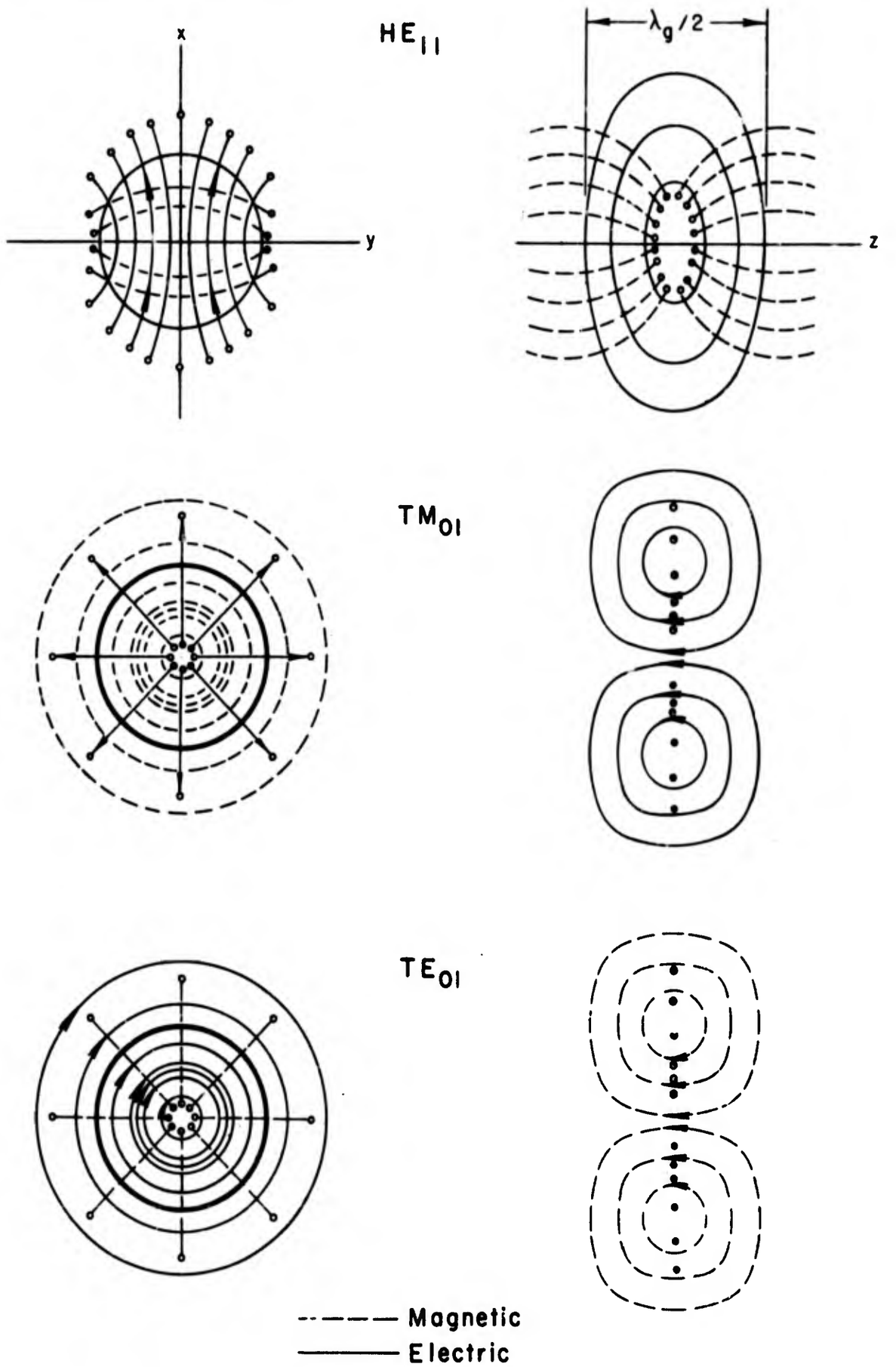

Fig. 2.01 – Electric And Magnetic Field Configurations For Dielectric Rod Waveguides.

to handle when these changes are made. Wegener made the following assumption: (1) only conduction losses are considered; (2) the dielectric is assumed to be sufficiently low loss that only the first power of the imaginary part of the dielectric constant need be considered. He found that the wavelength and phase constants were effectively unchanged by the addition of the attenuation term. He obtained expressions for the attenuation for the TM_{01}, TE_{01}, and HE_{11} waves and plotted α/α_K as a function of rod diameter where α_K is the attenuation of a plane wave in a coaxial cable of the same material. These graphs are included in Chapter V. The attenuation is small for small rods, since most of the energy is external to the rods. However, for large rods, the energy is largely inside the rod and the attenuation approaches that of a metal covered dielectric cable.

CHAPTER IV

EXPERIMENTAL PROCEDURE AND EQUIPMENT

The power source for work on the dielectric waveguide was a type TS-13/AP microwave signal generator. This instrument uses a reflex klystron, type 723 A/B, as a microwave oscillator. The maximum power output is approximately one milliwatt and the frequency range is 8625 mcps to 9625 mcps. In practically all of the work, the equipment operated at 9380 mcps or 3.20 cm wavelength. The signal generator contains a cavity type frequency meter, calibrated in mcps, and a standard attenuator with a 70 decibel range. Energy was coupled to the various mode exciters by means of flexible coaxial cable. The equipment for measuring the fields was built around a Logan Model 200 lathe. Figure 2.02 is a photograph of the equipment and Figure 2.03 shows a block diagram of the apparatus. The supports for the mode exciters were mounted on the lathe bed and so designed that the exciters could be moved in any direction. The section of dielectric waveguide under test was mounted parallel to the lathe bed. Measurements of the electric fields on the surfaces or vicinity of the guides were made by means of a test probe. Several types of probes were constructed and tried but the best one consisted of a section of rigid coaxial cable, 3/16" outside diameter and about eight inches long. One-and-a-half inches from one end the cable was formed into a gradual ninety degree bend. The center conductor protruded about an eighth of an inch. This extension when held parallel to the electric field

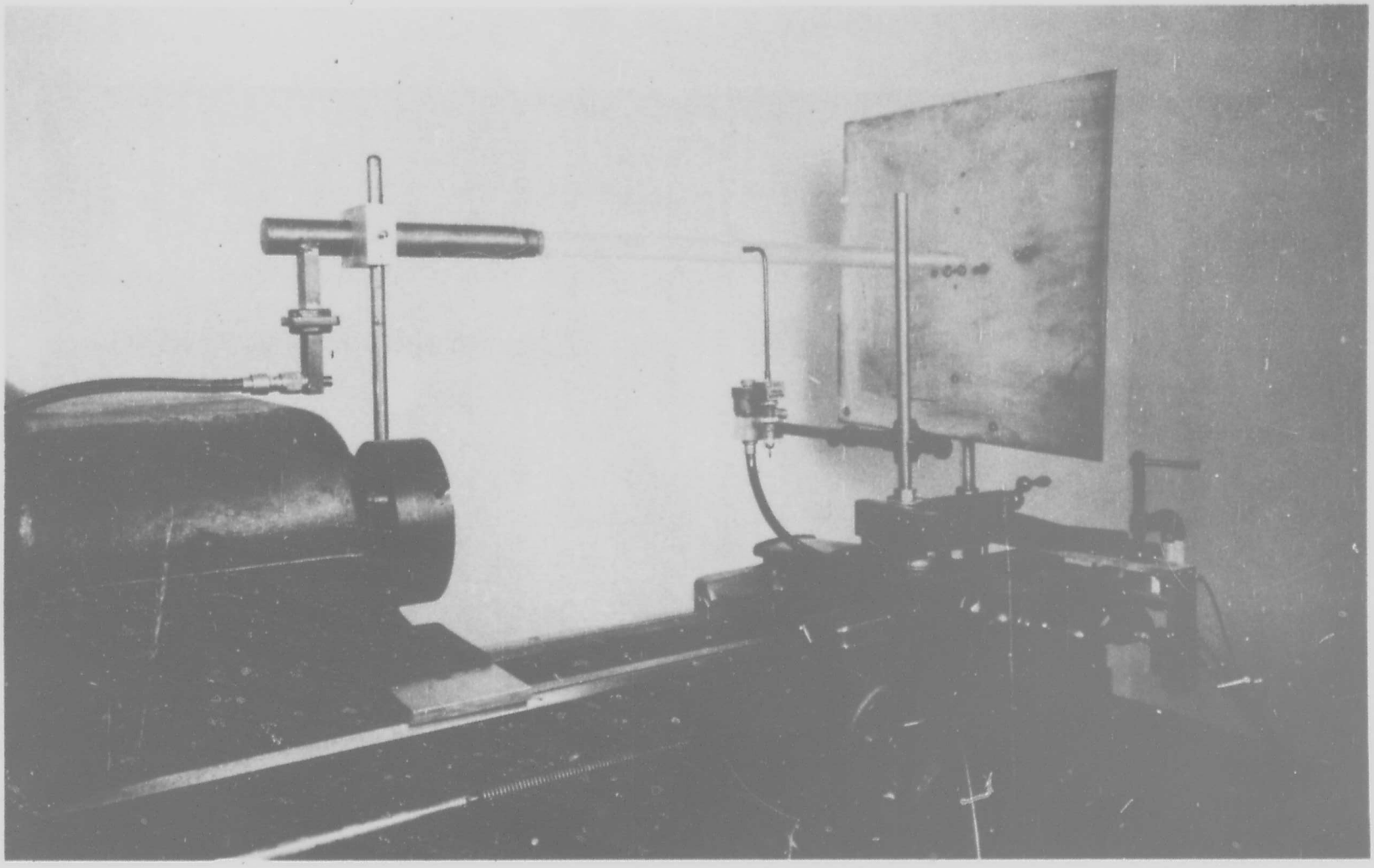

Figure 2.02
Apparatus Used In The Measurement Of The Electric Field On The Surface Of A Dielectric Waveguide

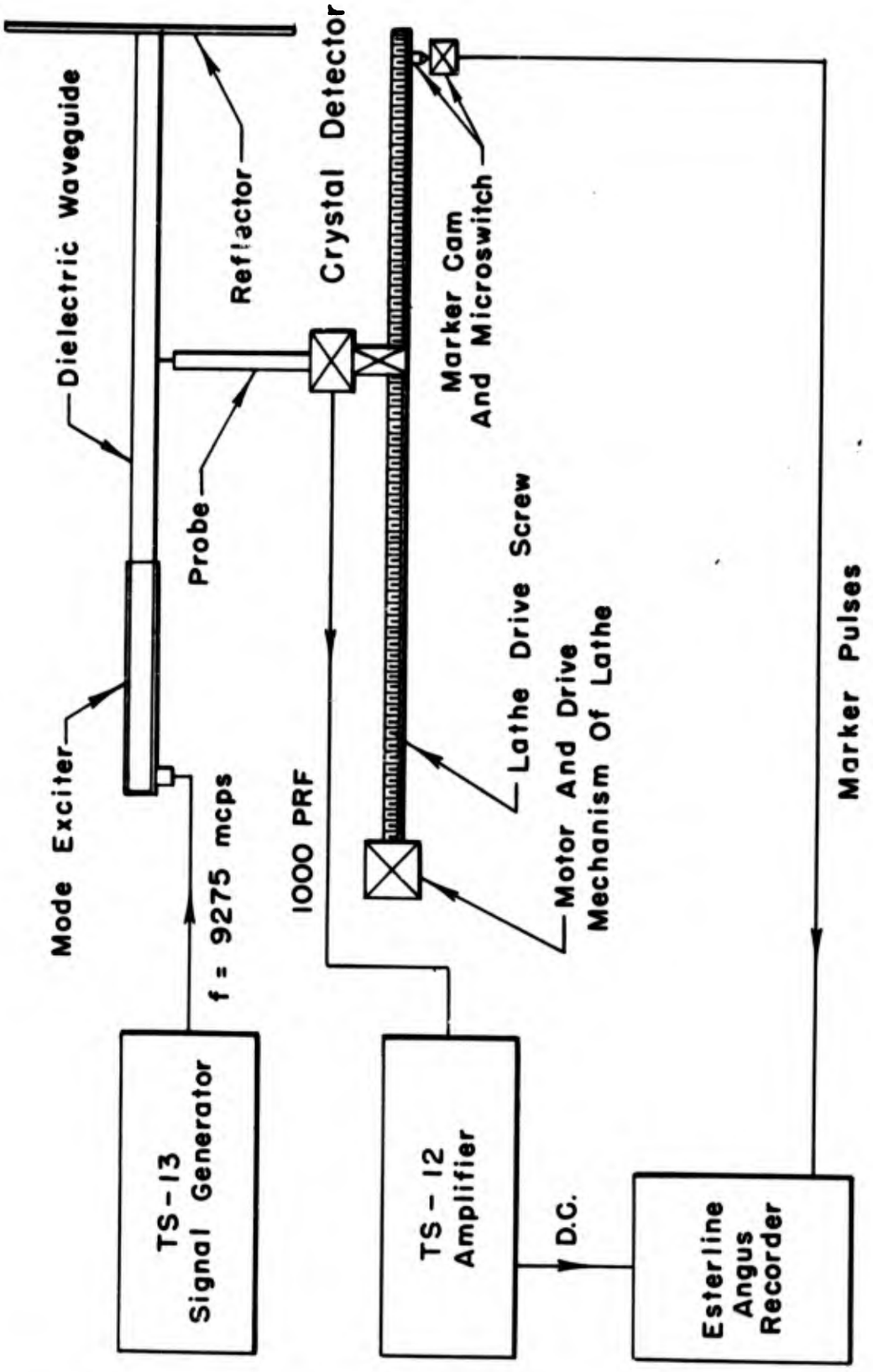

Fig. 2.03 – Block Diagram Of Apparatus Used To Measure Electric Fields On Surfaces Of Dielectric Waveguides.

vector, measures the line integral of the field. The other end of the cable feeds into a section of 1" x 1/2" waveguide which acts as a resonant cavity. A germanium crystal detector is mounted across the cavity and detects the signals. This signal is amplified by a high gain amplifier and then applied to an output indicator. The test probe is in the shape of an L in order to reduce the amount of metal conductors parallel to the electric field. The length of the probe allowed the cavity and detector to be removed several wavelengths from the dielectric rods. The test probe was held in place by suitable supports mounted on the tool carriage of the lathe. The probe could thereby be moved along the surface of the rod by means of the drive mechanism of the lathe. The cross-feed drive allowed for measurement of the fields as a function of radial distance.

Two different amplifiers were used in this work. One was a linear high gain amplifier of the TS-12/AP type. The other was a Hazeltine Model 1052-1 which was tuned for 1000 cps. By synchronizing the signal generator for 1000 cps square wave modulation, a very high gain system was obtained. The crystal detector is approximately a square law device and therefore the recorded signals were essentially power measurements. However, because of non-linearity of the crystal, it was frequently calibrated in terms of the calibrated attenuator of the TS-13 signal generator.

For most purposes, it was desirable to retain a permanent record of the field strength measurements. An Esterline-Angus Recorder, Model AW, was used for this purpose. A cam, mounted on the drive screw

of the lathe operated a microswitch for each eighth of an inch travel of the probe. This microswitch, in series with a six volt transformer operated an indexing solenoid on the recorder.

In order to determine the apparent index of refraction, it is necessary to measure the wavelength along the guide. Two methods were used in this work. The first, and most successful for most purposes, is also the simplest. A rigid brass plate, eighteen inches on each edge was mounted normal to the axis of the dielectric waveguide at the end opposite from the mode exciter. This plate reflects the waves and produces a standing wave pattern which can be measured by the test probe. From the distance between nulls or peaks the wavelength on the guide can be determined.

A second method used is similar to that described in reference 18. Figure 2.04 shows a sketch of this system. The energy is coupled to the rod through a hole in the reflector and the energy is coupled out of the guide through a hole in the second reflector, to a crystal detector. The rod and plates form a transmission cavity with maximum transmission when the distance between the reflector plates is an integral number of half wavelengths along the rod. Using this arrangement, the frequency must be varied to obtain maximum transmission since the length of the rods is fixed. This represents a disadvantage for microwave work because the tuning ranges of the signal sources are narrow and it is rather difficult and tedious to tune a klystron over its full range while maintaining constant amplitude output at all frequencies. However, if the value of λ_g is known rather accurately, the sections of the waveguide may be cut to a value that will at least

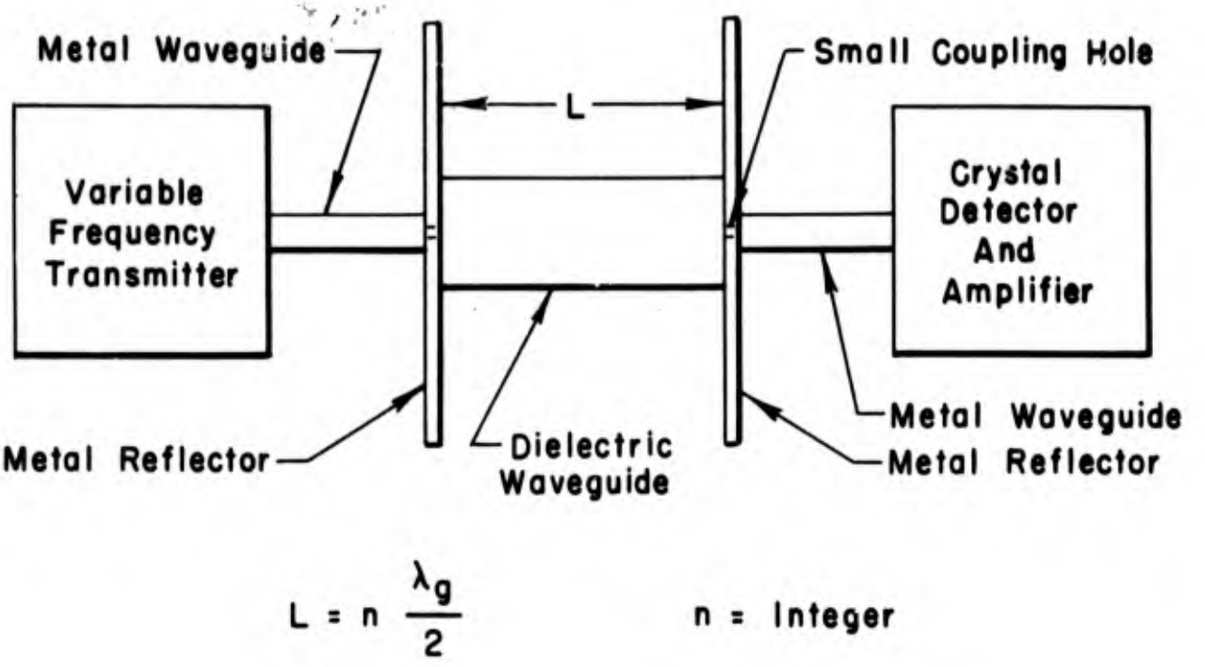

Fig. 2.04 – Variable-Frequency Cavity Method For Measuring λ_g Of Dielectric Waveguides.

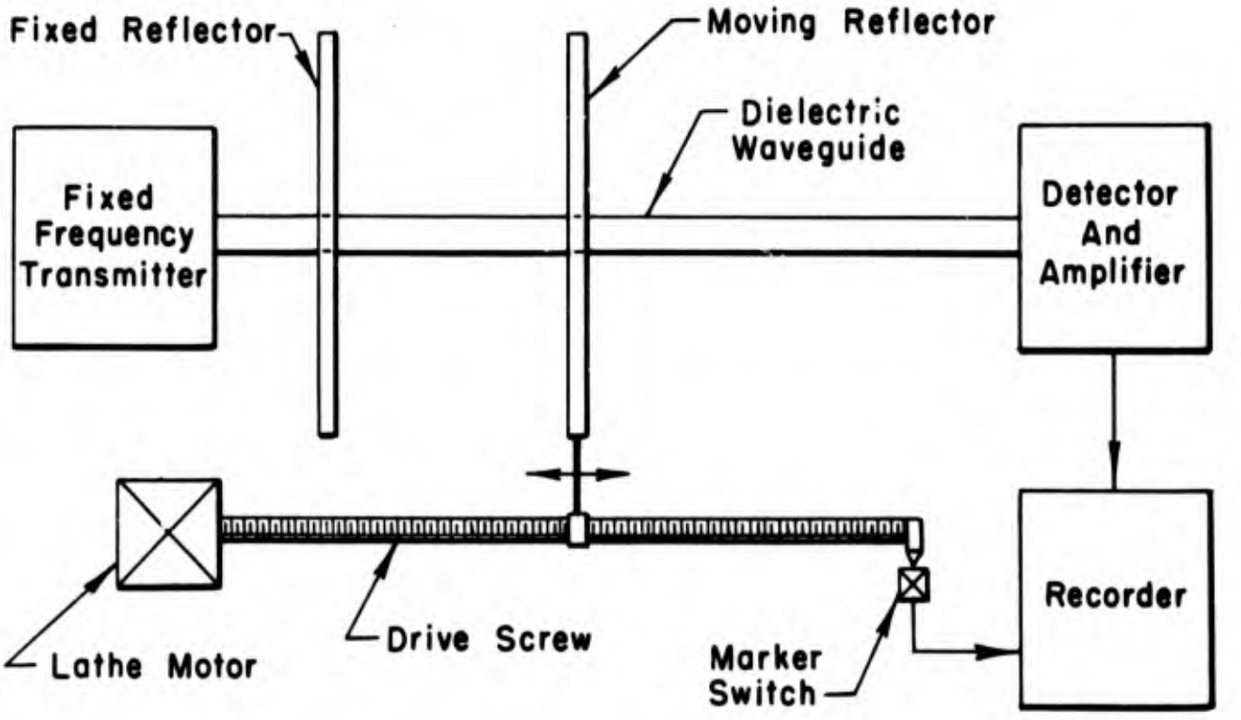

Fig. 2.05 – Fixed-Frequency Cavity Method For Measuring λ_g Of Dielectric Waveguides.

be near an integral number of $\lambda_g/2$ for a given frequency and accurate measurements may be made without difficulty. This method was used to obtain a verification of the two branches of the HE_{12} mode because the branches were very close together.

Figure 2.05 shows a veriation of the above system which was used and which has certain advantages. In this arrangement a longer section of guide was used with one end fitting into the mode exciter and the other end connected to a similar mode detector. The reflector plate at the exciter end was fixed as before but the other reflector had a hole in the center through which the guide passed. This reflector was mounted on the tool carriage of the lathe and moved parallel to the guide. Again, transmission peaks occur as the reflector spacing passes through integral half wavelengths. For small rods $(d < \lambda_o)$, this method works well and has the decided advantage over the former method in that the frequency remains fixed. For $d = \lambda_o/2$, the determination of the distance between transmission peaks is limited only by the accuracy of measuring the spacing between the reflector plates. However, this scheme has a serious disadvantage in that the reflectors actually reflect only the external energy. For large rods, most of the energy is internal to the rods and the reflectors have little effect. Therefore, this method is not well suited for measurements on large diameter rods.

Attenuation was measured by two methods. In the first method the field strength is measured as a function of distance along the rod. From the decrease in field strength, the attenuation constant may be

determined. In these measurements, the waveguide should not be terminated by the reflector plate but should point into an open area. However, the attenuation can be determined with the reflector plate in place, if perfect reflection is assumed, and if the distance from the measuring probe to the reflector is known. This method is simple and is satisfactory for small rods in which the field on the surface is strong. For large rods it was found to be more convenient to measure the attenuation by actual transmission loss. That is, a section of dielectric waveguide was fastened in place between a transmitter and a receiver and the received signal level was measured. Then a section of waveguide of identical shape except in length was substituted for the first piece of waveguide and the transmitted power level was changed to return the received power level to its former value. Thus the attenuation per unit length was determined directly. It should be noted that neither of these two methods is very well suited for dielectrics of extremely low loss because of the difficulty in obtaining dielectric rods sufficiently long to make accurately measurable changes of energy levels.

Figures 2.06 and 2.07 show the arrangement used to measure attenuation due to bends and curves in dielectric rods. The rods used were flexible vinyl tubing filled with Nujol oil. The power level of the TS-13 signal generator was increased, as the bending of the tubes was increased in order to maintain a constant received power level.

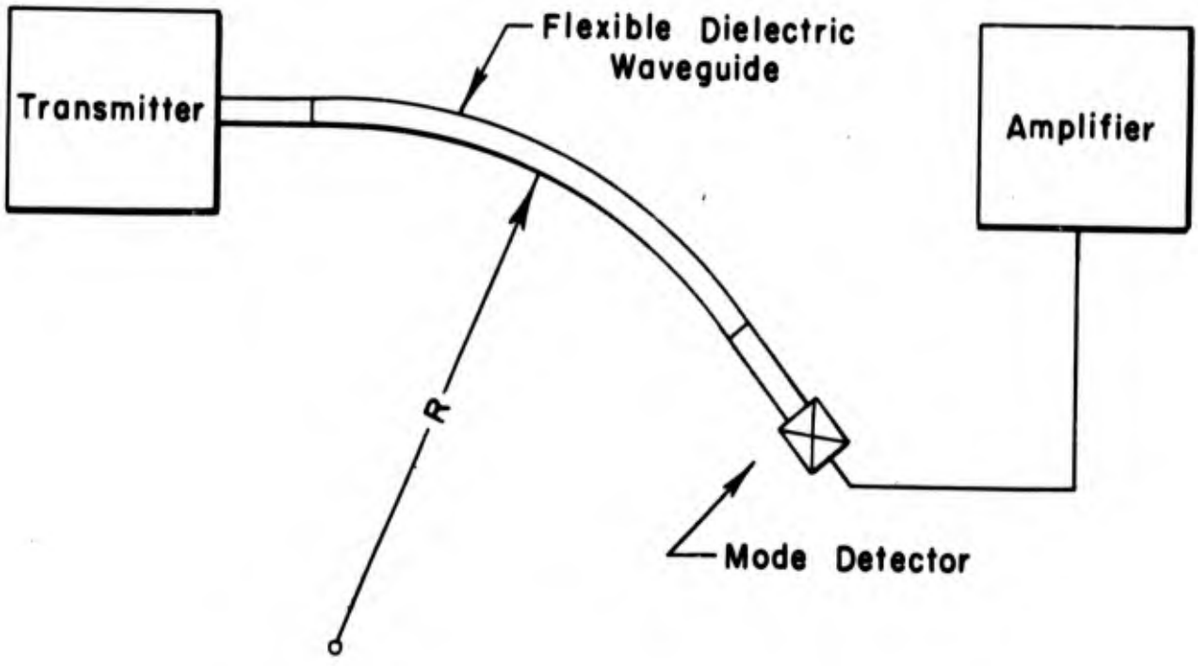

Fig. 2.06 – Apparatus For Measuring Attenuation As A Function Of Curvature Of Waveguide.

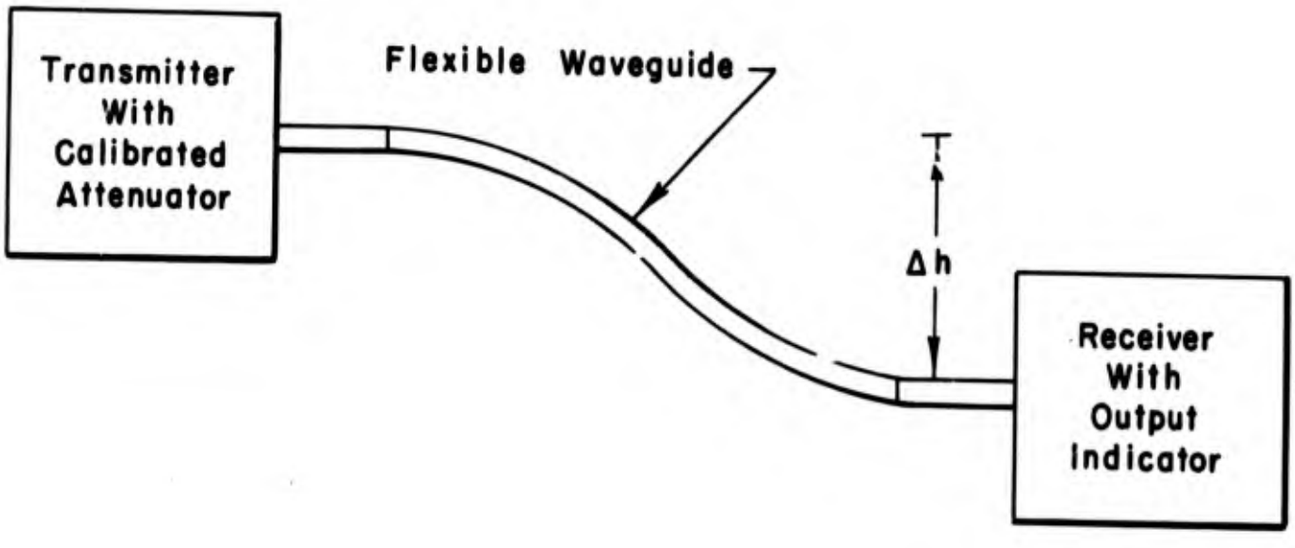

Fig. 2.07 – Apparatus For Measuring Attenuation As A Function Of The Differential Heights Of Transmitter And Receiver.

CHAPTER V

EXPERIMENTAL DATA AND DISCUSSION

1. Apparent Index of Refraction. Measurements have been made of the apparent index of refraction as a function of rod diameter for several materials and several modes. The materials used were Lucite, polystyrene, and Textolite, all with $K \doteq 2.50$ and paraffin and Nujol with $K \doteq 2.25$. Nujol, a mineral oil, is the only liquid known whose loss is sufficiently low to allow it to compete with materials such as polystyrene, etc. A few measurements were made using castor oil and dioxane. The dielectric constant of the latter, an ether, can be varied over a range of $K \doteq 81$ to $K \doteq 2.5$ by mixing it with water. Its loss was found to be tolerable, but unfortunately polystyrene and certain other plastics are soluble in the dioxane and hence, the polystyrene tubes cannot be used as forms. Some attempts were made to use glass tubing but, because the breakage rate was high, it was felt that it was unsafe to use the dioxane.

The range of measurements was not as great as had been hoped. For waveguides propagating only one mode, measurements are relatively simple and satisfactory agreement with the theory was obtained. However, when two or more modes are present, the standing wave pattern on the rods becomes much more complex because the phase velocities for the different modes are different. If only two modes are present, the situation can be handled rather easily.

The wavelength, λ_g, of each mode is different (for a given λ_o) and therefore there will be an effective "modulation" envelope on the standing wave pattern. Consider the two waves

$$E_1 = E_{01} \cos \frac{2\pi z}{\lambda_{g1}} \tag{2.83}$$

$$E_2 = E_{02} \cos \frac{2\pi z}{\lambda_{g2}} \tag{2.84}$$

where E_1 and E_2 are the electric fields of the two modes of the same frequency, E_{01} and E_{02} are the maximum amplitudes of the waves, and λ_{g1} and λ_{g2} are the respective guide wavelengths of the two modes. The time variation and arbitrary phase relation are omitted for simplicity. The resulting field E is given by

$$E = E_1 + E_2 = E_{01} \cos \frac{2\pi z}{\lambda_{g1}} + E_{02} \cos \frac{2\pi z}{\lambda_{g2}} \tag{2.85}$$

or

$$E = E_0 \cos\left(\frac{2\pi z}{\lambda_{g1}} - \alpha \right) \tag{2.86}$$

where

$$E_0^2 = E_{01}^2 + E_{02}^2 + 2E_{01}E_{02} \cos 2\pi z \left(\frac{1}{\lambda_{g1}} - \frac{1}{\lambda_{g2}} \right) \tag{2.87}$$

and

$$\tan \alpha = \frac{E_2 \sin 2\pi z \left(\frac{1}{\lambda_{g1}} - \frac{1}{\lambda_{g2}} \right)}{E_1 + E_2 \cos 2\pi z \left(\frac{1}{\lambda_{g1}} - \frac{1}{\lambda_{g2}} \right)} . \tag{2.88}$$

See Figure 2.08.

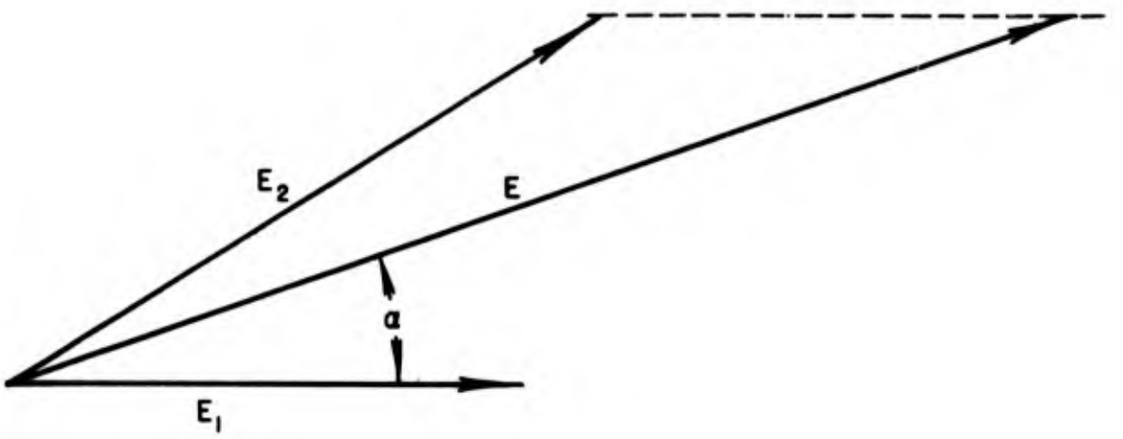

Fig. 2.08

Vector Diagram Of The Radial Components Of The Electric Fields, Of Two Waves, On The Surface Of Dielectric Rod.

$$E_0 = \text{maximum when } \cos 2\pi z \left(\frac{1}{\lambda_{g1}} - \frac{1}{\lambda_{g2}}\right) = 1 \qquad (2.89)$$

which yields

$$E_0 = E_1 + E_2 \,. \qquad (2.90)$$

$$E_0 = \text{minimum when } \cos 2\pi z \left(\frac{1}{\lambda_{g1}} - \frac{1}{\lambda_{g2}}\right) = -1 \qquad (2.91)$$

which gives

$$E_0 = E_1 - E_2 \,. \qquad (2.92)$$

From (2.54) and (2.56)

$$E_1 = \frac{E_0 \text{ max} + E_0 \text{ min}}{2} \qquad (2.93)$$

and

$$E_2 = \frac{E_0 \text{ max} - E_0 \text{ min}}{2} \,. \qquad (2.94)$$

Also

$$\lambda_m = \frac{\lambda_{g1}\,\lambda_{g2}}{\lambda_{g1} - \lambda_{g2}} \qquad (2.95)$$

where λ_m is the "modulation" wavelength, or long period variation.

The phase angle α is a function of distance. α = maximum when $\tan \alpha = E_2/E_1$ and has a minimum value when $\tan \alpha = -E_2/E_1$. Thus it is evident that the short period variation wavelength is not constant but varies from a minimum value of

$$\lambda_{g1} - \frac{\tan^{-1}(E_2/E_1)}{2\pi}\lambda_{g1}$$

to a maximum value of

$$\lambda_{g1} + \frac{\tan^{-1}(E_2/E_1)}{2\pi}\lambda_{g1} .$$

The average value will be λ_{g1}. Therefore by measuring the maximum and minimum values of the "modulation" envelope, the long period variation and the average value of the short period variation, the values of λ_{g1}, λ_{g2}, E_1, and E_2 may be calculated. However, it should be noted that from these measurements E_1 may be the field associated either with λ_{g1} or λ_{g2} and the same is true with E_2. Other considerations must be used to resolve this ambiguity.

However, when three or more modes are present, it is impossible to separate the components when only relatively short lengths of dielectric guide are available. It should be remembered that some of these wavelengths are nearly the same and the modulation envelope is necessarily long. The HE_{1m} mode is especially complicated because of the dual branches of all of the higher order modes. For this mode the situation of the dominant mode plus a single second order mode does not exist. Therefore surface field measurements of the HE_{1m} mode are useful only for rods which are propagating the dominant mode. However, the fixed-plate variable-frequency resonant-cavity method, shown in Figure 2.04 was used with paraffin as the dielectric to verify the HE_{1m} modes.

It should be mentioned that in these measurements, no direct attempt was made to generate the higher order modes. In fact, the metallic waveguides of the exciters were designed to propagate only the lowest order radial modes. However, some discontinuities were present in the system, especially at the junction between exciter and dielectric guide, and these impedance mismatches were evidently sufficient to generate the higher order modes, which were propagated when the rod was of sufficiently large diameter.

One point should be noted and that is for a given rod and free space wavelength, the rod will be "large" for the dominant mode and successively "smaller" for the higher order radial modes. Therefore, the measurements on the surface of the rod do not indicate the relative amounts of the total energy of the different modes present.

Figures 2.09 through 2.18 show graphs of the measured values of n_a as a function of rod diameter for the materials and modes used. For most of the measurements, accuracy of three significant figures was obtained. Most of the error in measurement of λ_g is due to the broadness of the nulls (and peaks) of the standing wave patterns. For a rod supporting the propagation of a single mode, the fluctuation in the measured $\lambda_g/2$ for the individual loops and modes was usually about $\pm$ 0.02 cm. This error was greatly reduced, however, by measuring the length of a large number of $\lambda_g/2$ and calculating the average value. The probable error in measurement was much greater for the case of two modes propagating because the length of the available dielectric waveguides limited the number of cycles of the modulation envelope.

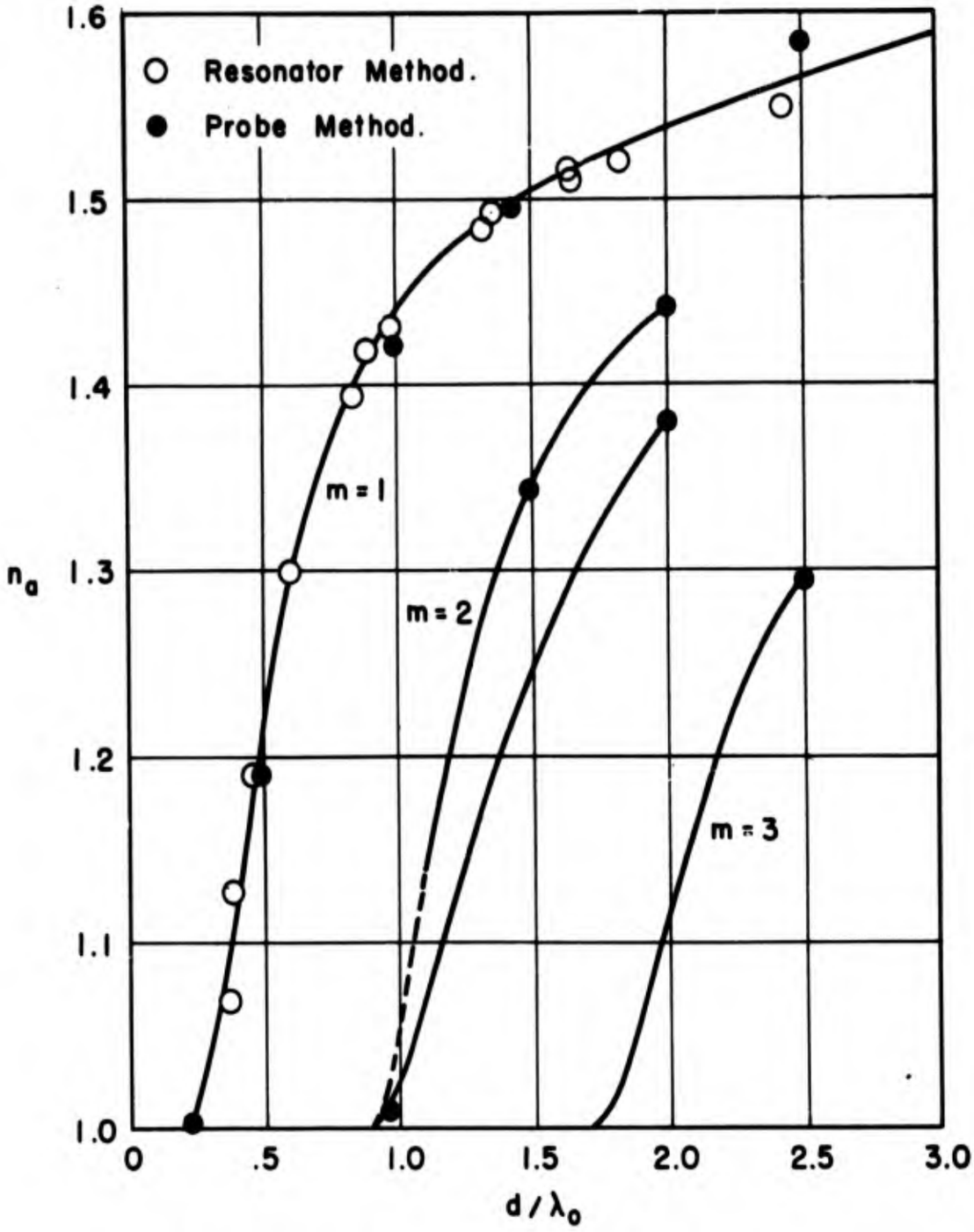

Mode: HE_{1m}. Index Of Refraction = 1.60.

Material: Polystyrene.

$n_a = \lambda_0 / \lambda_g$ = Wavelength In Air / Wavelength On Guide.

(Solid Curves Are Based On Experimental Data Only.)

Fig. 2.09 – The Dependence Of The Apparent Index Of Refraction, n_a, On The Diameter, d, Of The Dielectric Waveguide.

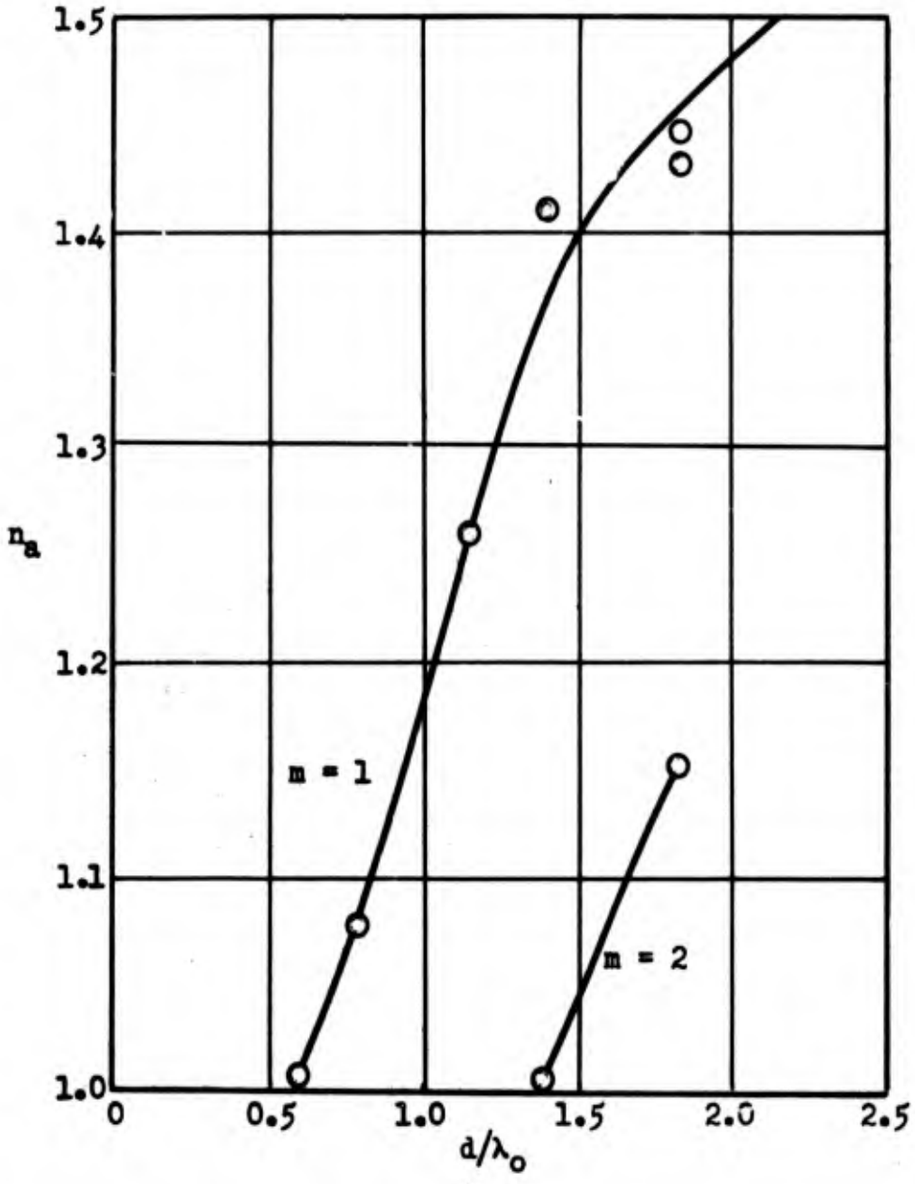

Modes: TM_{0m} Index of Refraction = 1.58

Material: Textolite Method: Resonator (moving plate)

$n_a = \lambda_o/\lambda_g$ = wavelength in air/wavelength on guide

Solid curves are experimental.

Fig. 2.10

THE DEPENDENCE OF THE APPARENT INDEX OF REFRACTION, n_a, ON THE DIAMETER OF THE DIELECTRIC WAVEGUIDE.

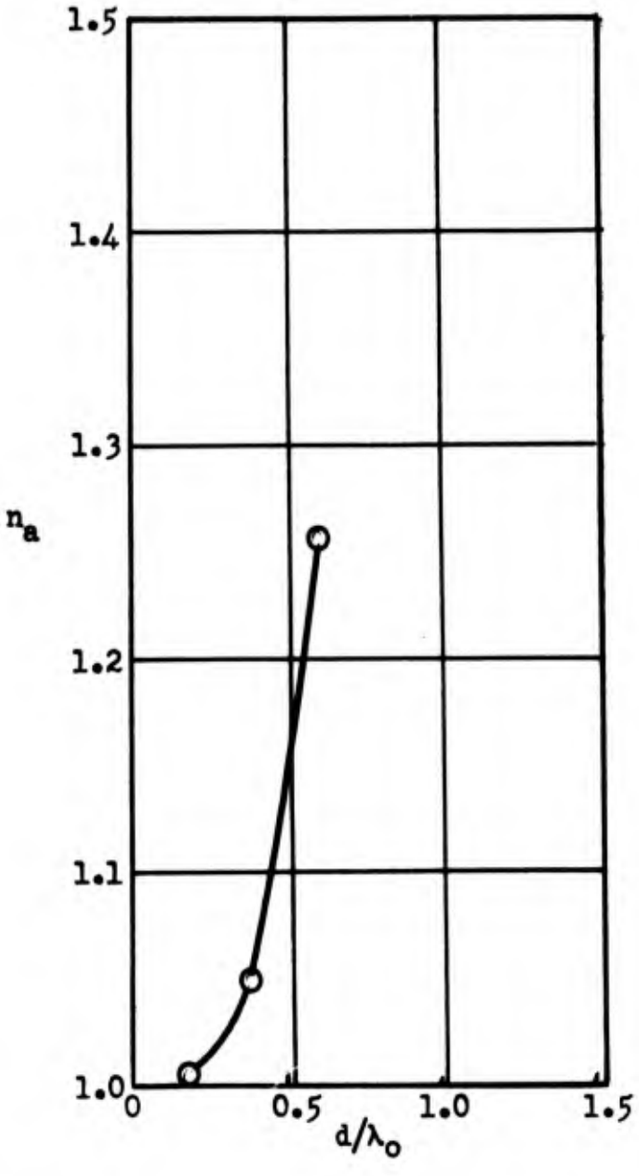

Mode: HE_{11} Index of Refraction = 1.58

Material: Textolite Method: Resonator (moving plate)

Solid curve is experimental.

Fig. 2.11

THE DEPENDENCE OF THE APPARENT INDEX OF REFRACTION, n_a, ON THE DIAMETER OF THE DIELECTRIC WAVEGUIDE.

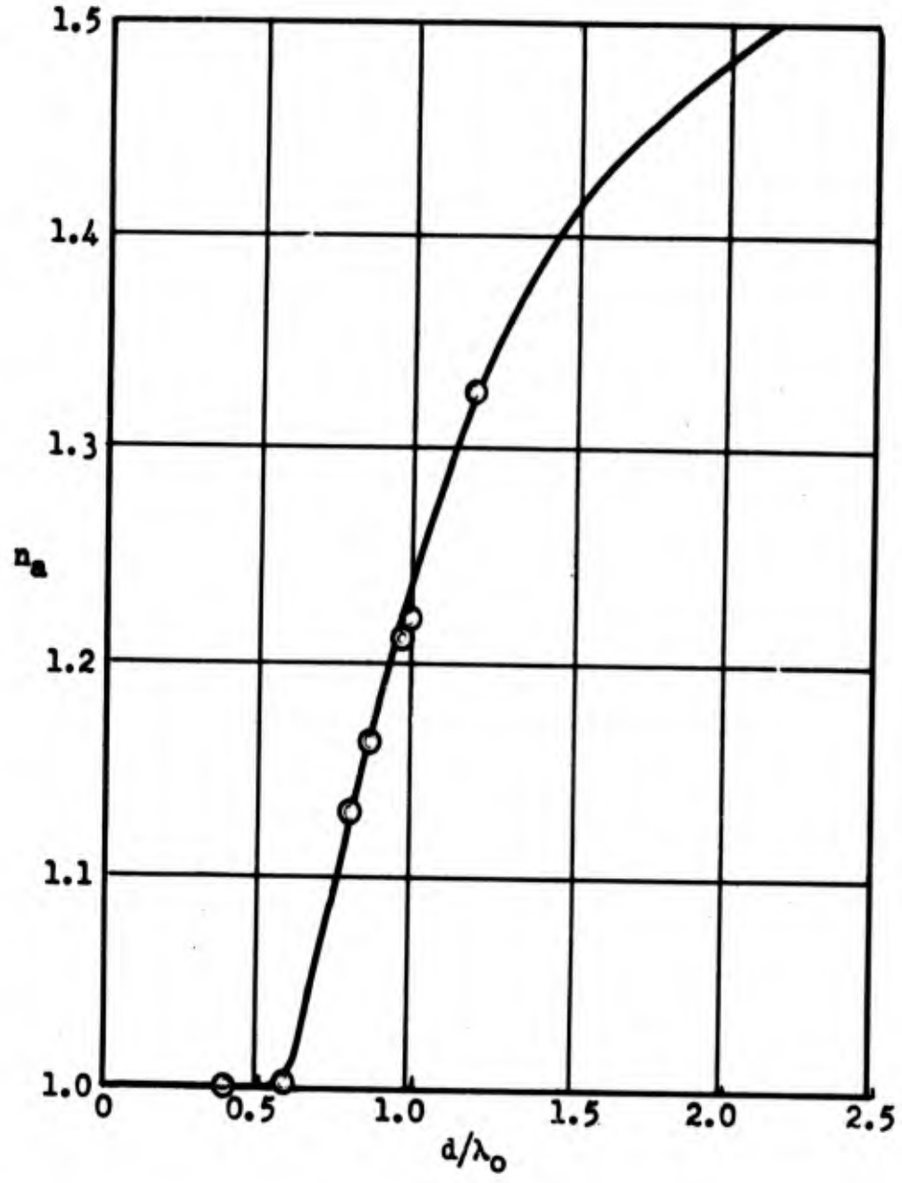

TM_{01} Mode — Index of Refraction = 1.60 ± .01

Probe Method — Apparent Index of Refraction = λ_o/λ_g

Material: Lucite — λ_g = Wavelength on the guide

d: diameter — λ_o = Wavelength in air

Solid curve is experimental.

Fig. 2.12

THE DEPENDENCE OF THE APPARENT INDEX OF REFRACTION ON THE DIAMETER OF A DIELECTRIC WAVEGUIDE.

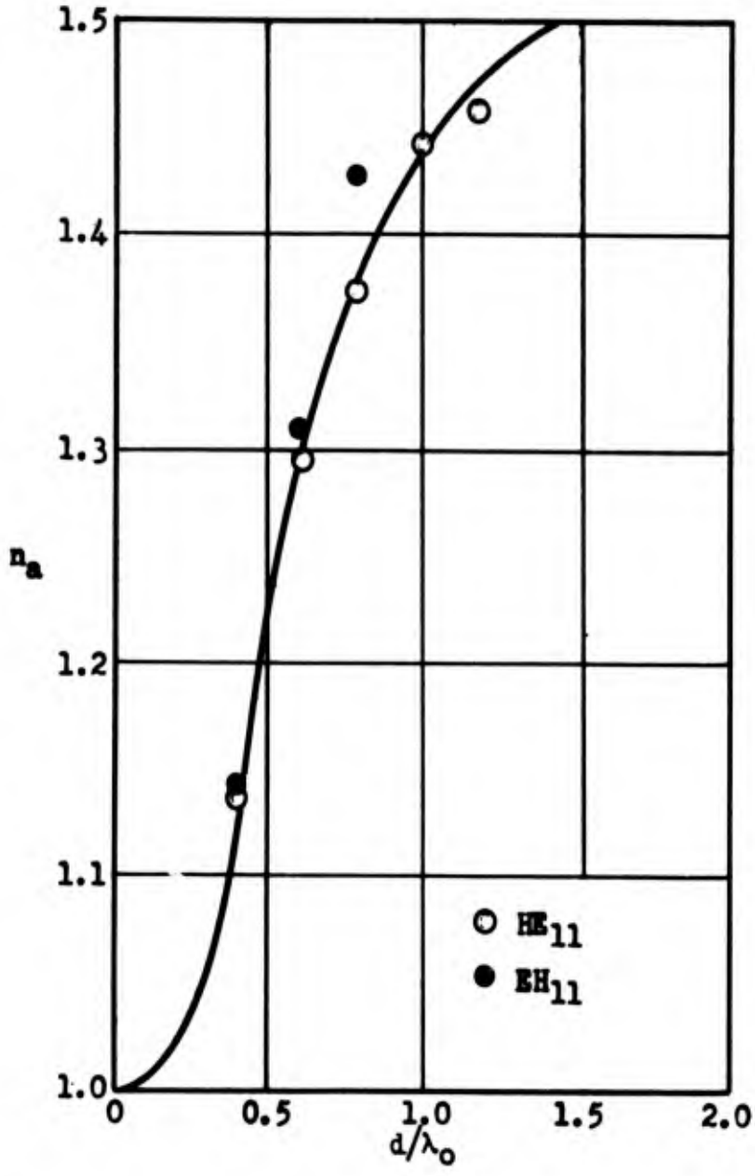

Modes: HE_{11} and EH_{11} Index of Refraction = 1.60 ± .01

Probe Method Material: Lucite

$n_a = \lambda_o/\lambda_g$ = Wavelength in air/wavelength on guide

Solid curves are Experimental.

Fig. 2.13

THE DEPENDENCE OF THE APPARENT INDEX OF REFRACTION, n_a, ON THE DIAMETER OF A DIELECTRIC WAVEGUIDE.

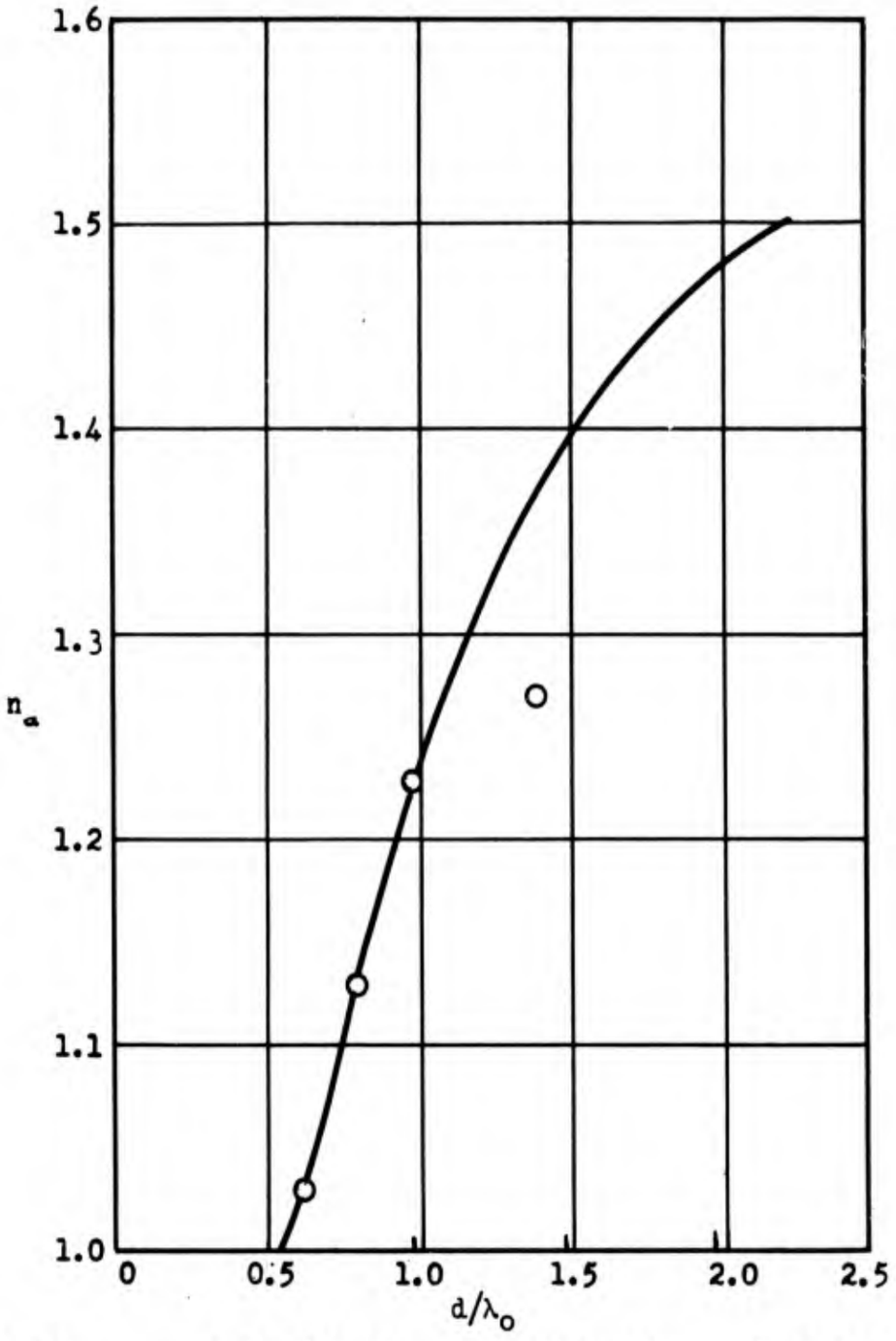

Mode: TE_{01} Probe Method d: diameter Material: Lucite

Apparent Index of Refraction, $n_a = \lambda_o/\lambda_g$ λ_o = wavelength in air

Index of Refraction = 1.6 λ_g = wavelength on guide

Solid curve is experimental.

Fig. 2.14

THE DEPENDENCE OF THE APPARENT INDEX OF REFRACTION, n_a, ON THE DIAMETER OF A DIELECTRIC WAVEGUIDE.

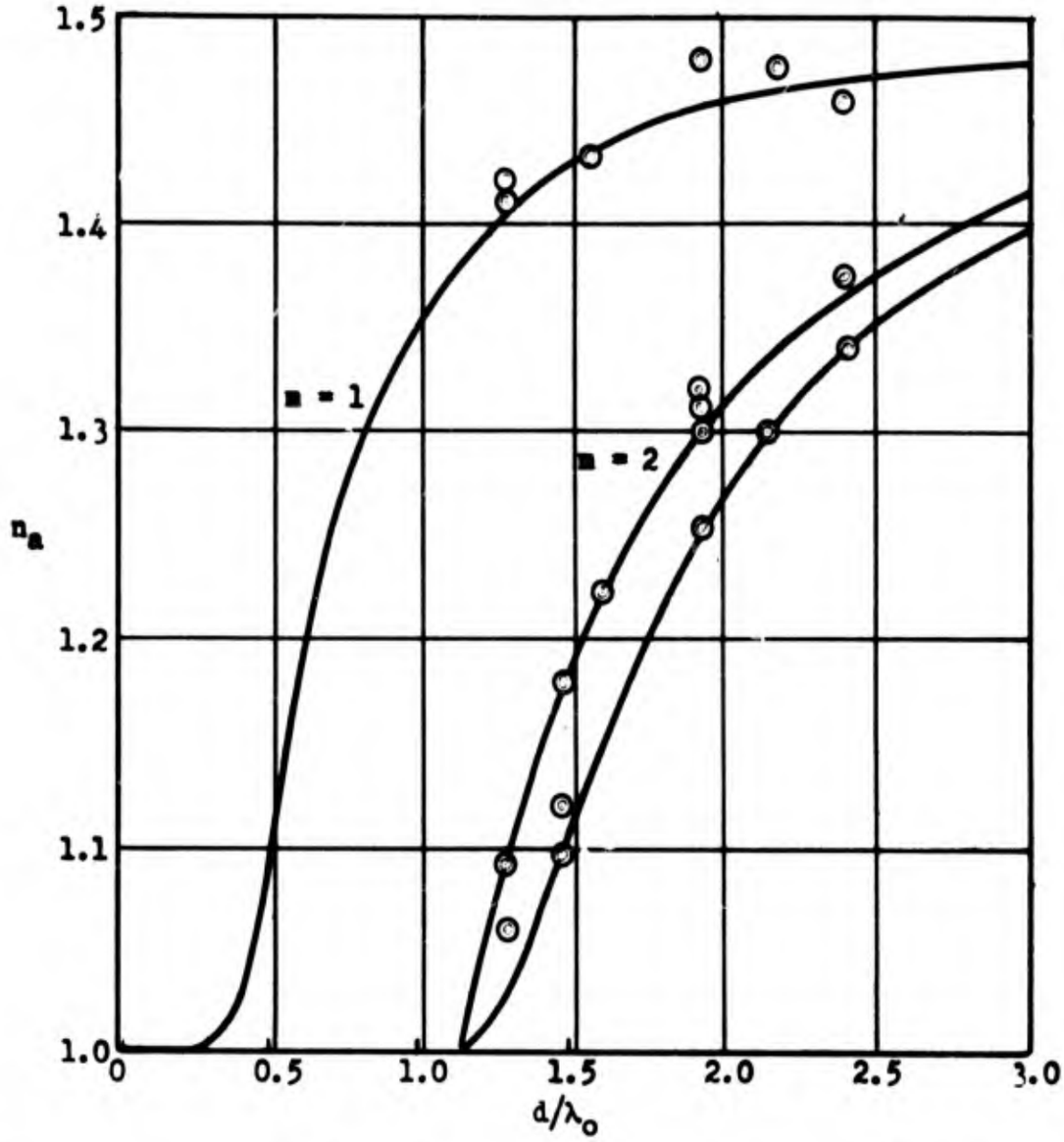

Mode: HE_{1m} Resonator Method d: diameter Material: Paraffin

λ_o = wavelength in air λ_g = wavelength on guide

Apparent Index of Refraction, $n_a = \lambda_o/\lambda_g$

Solid curves are theoretical.

Index of Refraction = 1.5

Fig. 2.15

THE DEPENDENCE OF THE APPARENT INDEX OF REFRACTION, n_a, ON THE DIAMETER OF A DIELECTRIC WAVEGUIDE.

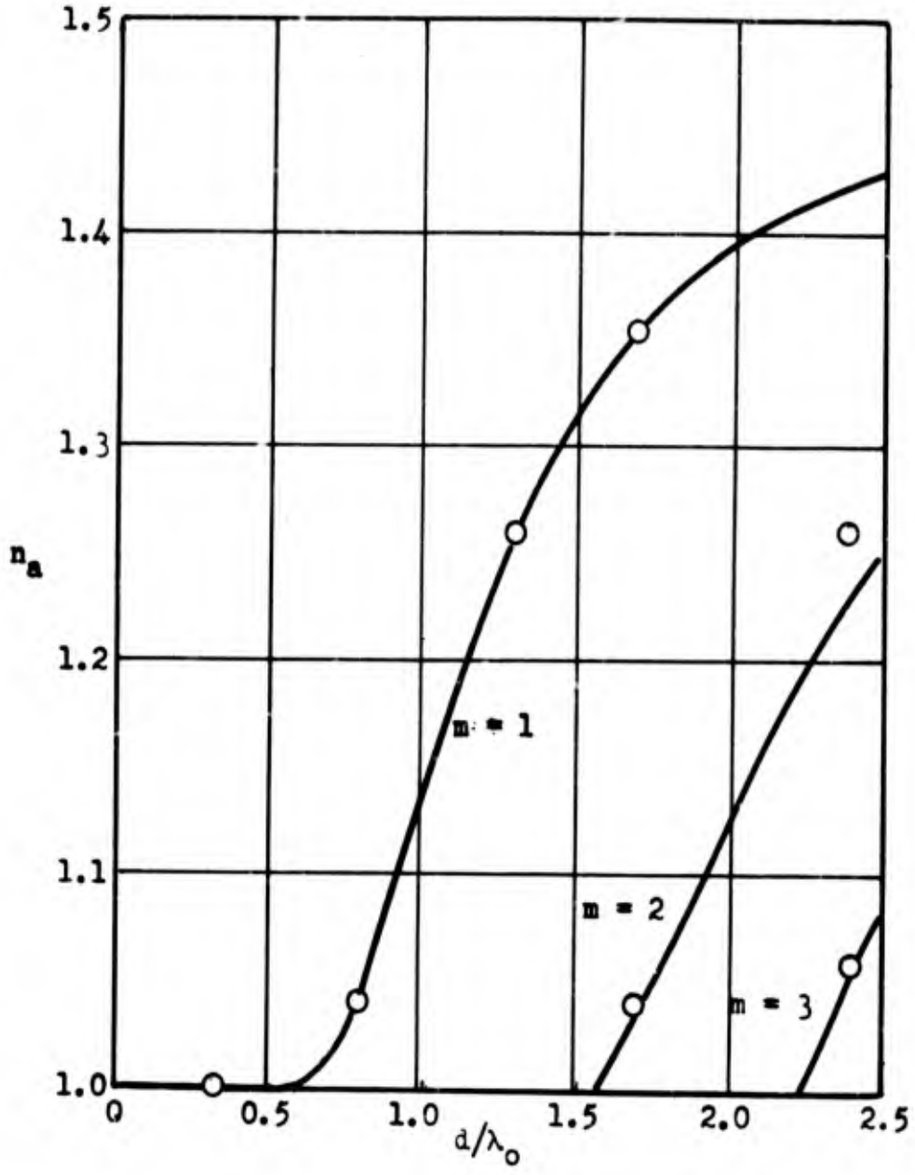

Modes: TM_{Om} Index of Refraction = 1.5
Probe Method Material: Nujol in Polystyrene tubes
$n_a = \lambda_o/\lambda_g$ = Wavelength in air/wavelength on the guide.

Solid curves are theoretical (Horton).

Fig. 2.16

THE DEPENDENCE OF THE APPARENT INDEX OF REFRACTION, n_a, ON THE DIAMETER OF THE DIELECTRIC WAVEGUIDE.

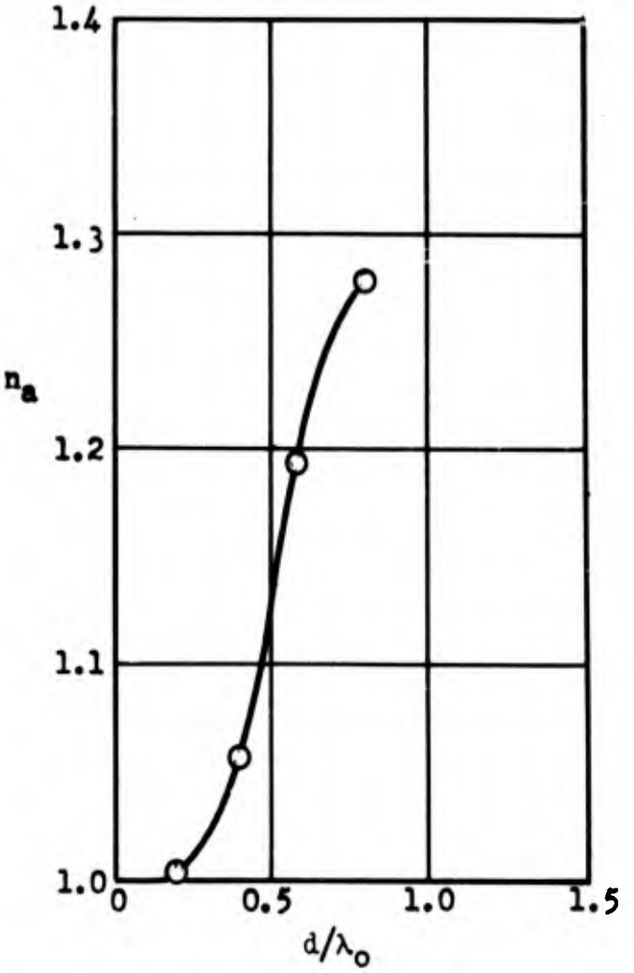

Mode: HE_{11} Index of Refraction = 1.5

Probe Method Material: Nujol in Polystyrene Tubes

$n_a = \lambda_o/\lambda_g$ = wavelength in air/wavelength on guide

Solid curve is Theoretical (Horton).

Fig. 2.17

THE DEPENDENCE OF THE APPARENT INDEX OF REFRACTION, n_a, ON THE DIAMETER OF THE DIELECTRIC WAVEGUIDE.

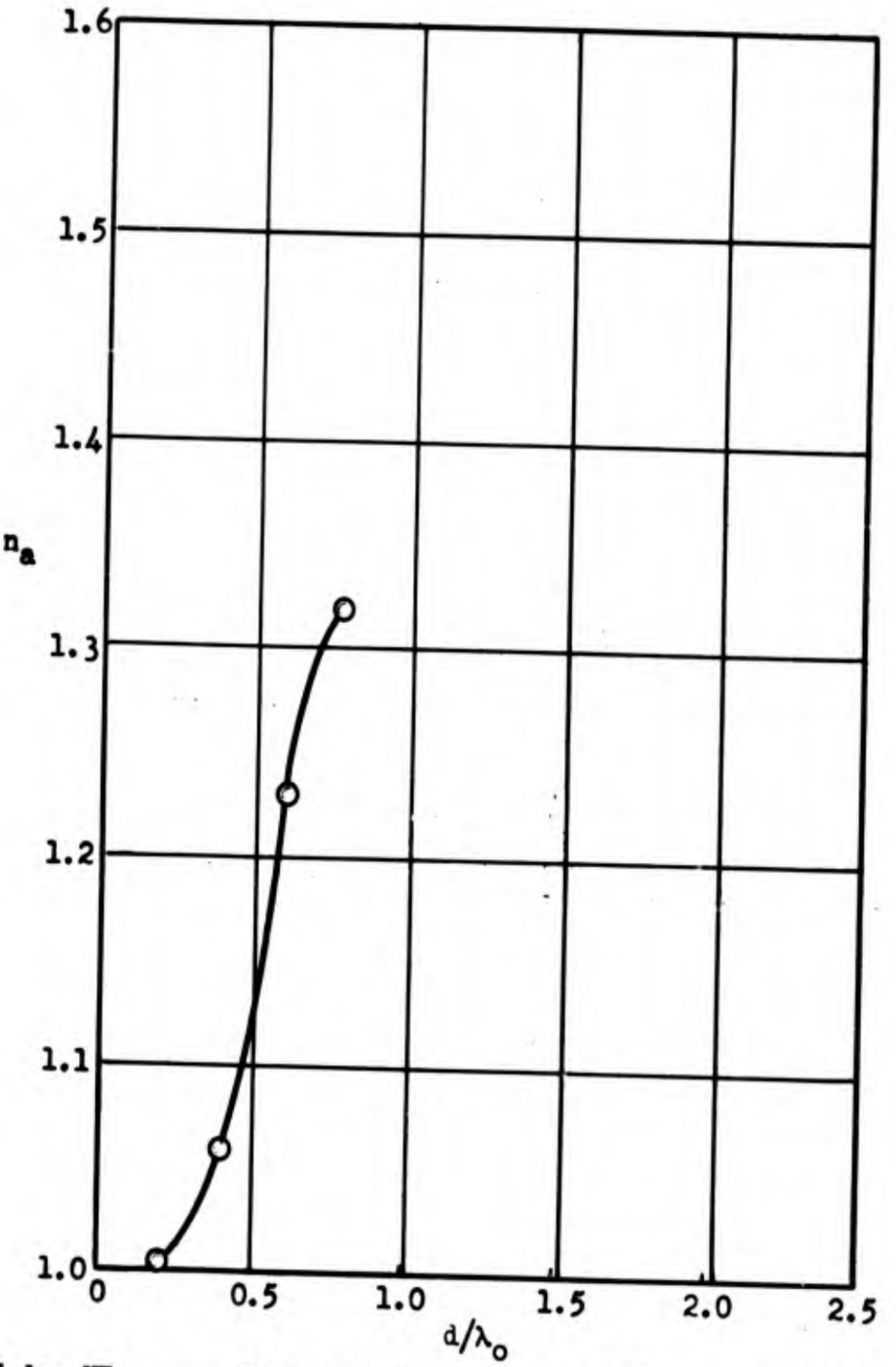

Mode: HE_{11} Index of Refraction = 1.6 Method: Probe

Apparent Index of Refraction, $n_a = \lambda_o/\lambda_g$ d: diameter

λ_o = wavelength in air λ_g = wavelength on guide

Material: Dioxane in thin-walled Polystyrene tubes

Solid curve is experimental.

Fig. 2.18

THE DEPENDENCE OF THE APPARENT INDEX OF REFRACTION ON THE DIAMETER OF A DIELECTRIC WAVEGUIDE.

Also, the determination of the peaks and nulls of the modulation envelope are arbitrary over a fairly wide range. It is felt that the data of Figure 2.15 verifies the existence of the two branches of the HE_{12} mode. The errors could easily be due to inhomogeneity of the paraffin which was first cast into the approximate size and then machined as accurately as possible. Figure 2.13 shows experimental data of n_a for lucite rods excited from a TE_{11} exciter and also from a TM_{11} exciter. For the small diameter rods, propagating only one mode it appears that the n_a is the same for the waves excited from either exciter. Based only on this small amount of data, it seems that the EH mode is the same as the HE mode.

2. General Field Configurations on the Dielectric Rods. The apparent index of refraction for the dielectric rods excited in the TM_{0m} and HE_{1m} modes could be determined by the measurement of the radial component of the electric field as a function of the axial distance z. Likewise, the apparent index of refraction for rods excited in the TE_{0m} mode could be determined from measurements of the angular component of the electric field as a function of the distance z. Figures 2.19 and 2.21 are typical of the measured field on rods $.870\lambda_o$ in diameter excited in the TM_{01} and HE_{11} mode, respectively. This size rod will only support the lowest TM_{0m} mode and hence the standing wave pattern is uniform. The same rod, excited in the HE_{11} mode can support the HE_{11} mode and is approximately the critical diameter for the HE_{12} modes. The latter modes are probably the cause of the slight modulation. Figure 2.22 is a graph of the electric field on the surface of a rod $1.84\lambda_o$ in diameter excited in the TM_{01} mode. The modulation

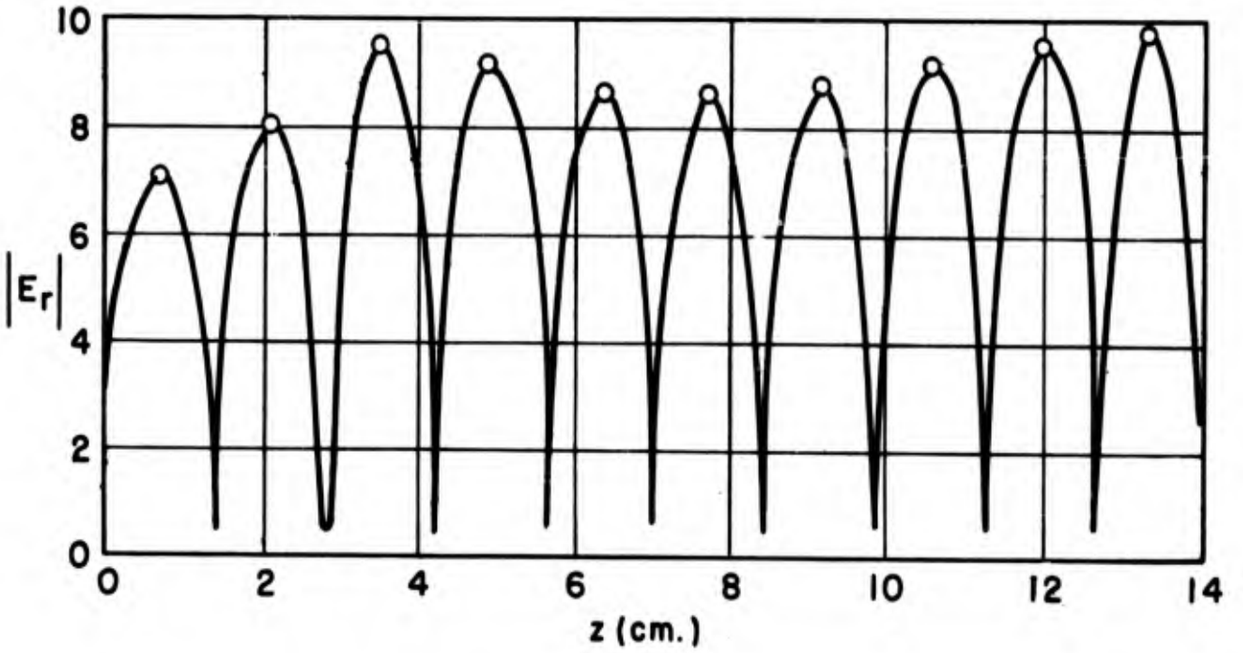

Mode: TM_{01} $d = .870\lambda_o$ $\lambda_o = 3.20$ cm.
Material: Polystyrene Dielectric Constant = 2.56

Fig. 2.19

RADIAL COMPONENT OF THE ELECTRIC FIELD VERSUS AXIAL DISTANCE, z.

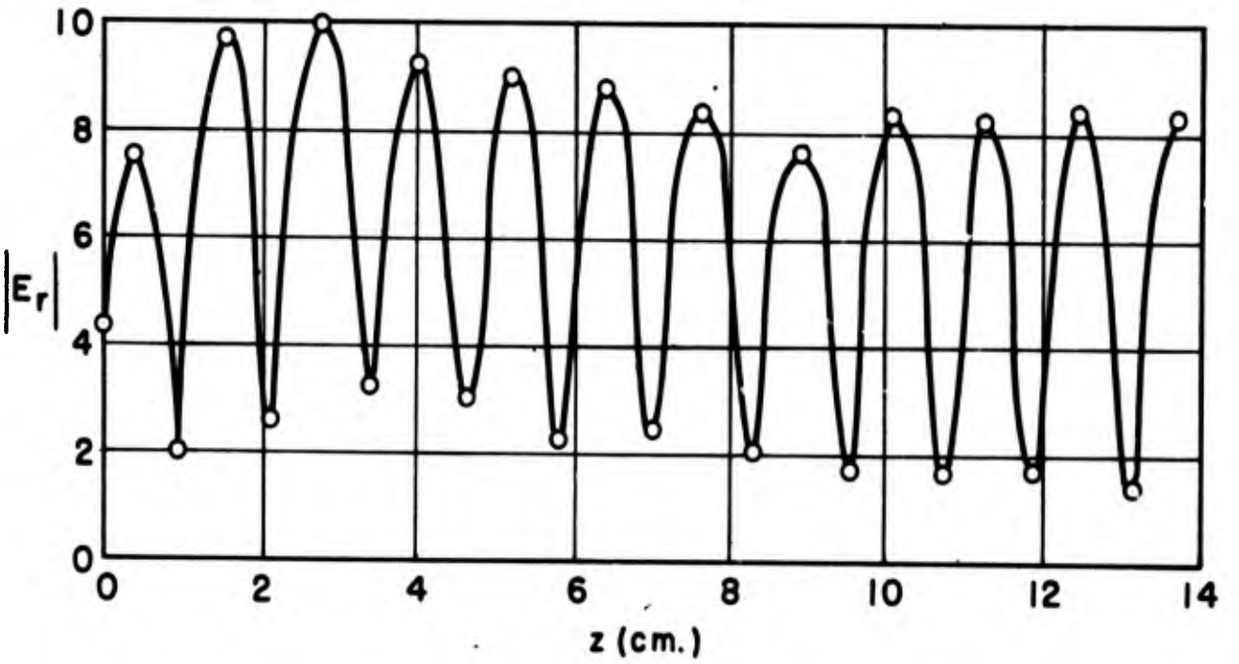

Mode: HE_{11} $d = .596\lambda_o$ $\lambda_o = 3.20$ cm.
Material: Lucite Dielectric Constant = 2.56 $\phi = 0°$

Fig. 2.20

RADIAL COMPONENT OF THE ELECTRIC FIELD VERSUS AXIAL DISTANCE, z.

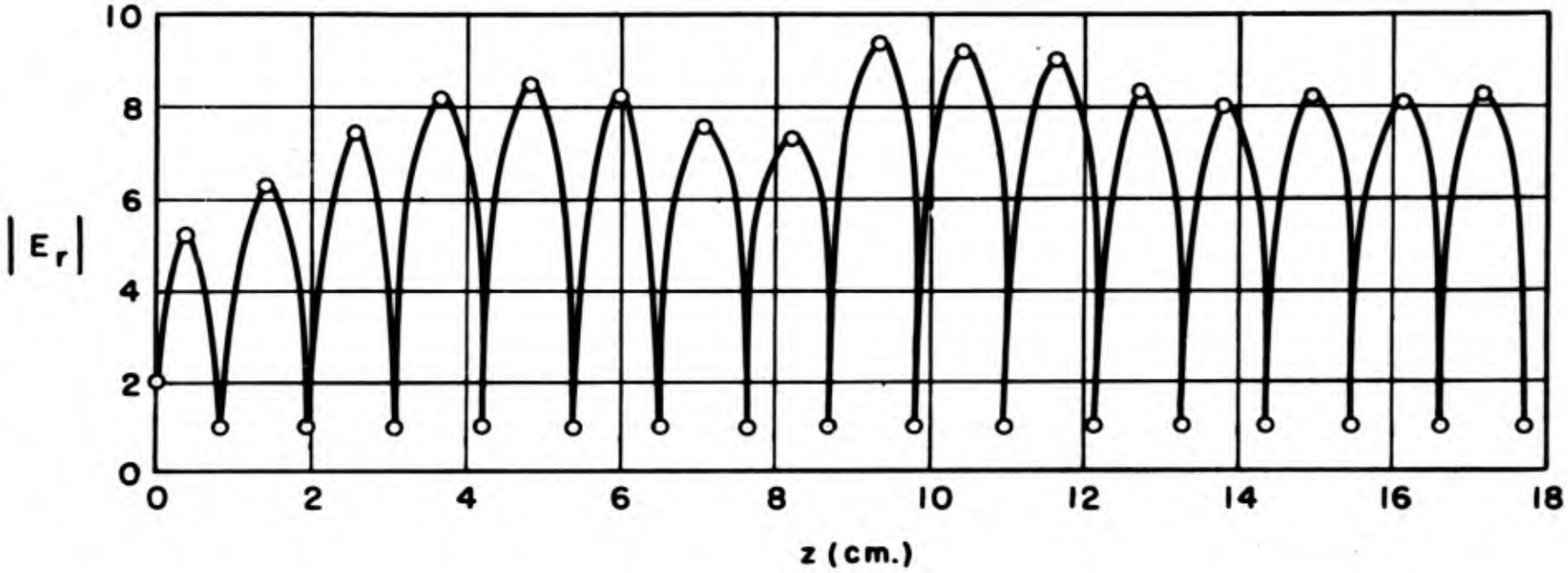

Mode : HE_{11}. Material : Polystyrene. Diameter : .870 λ_0.

λ_g = 2.255 cm. n_a = 1.42 $\phi = 0^\circ$ λ_0 = 3.20 cm.

Fig. 2.21 — Radial Component Of The Electric Field As A Function Of z.

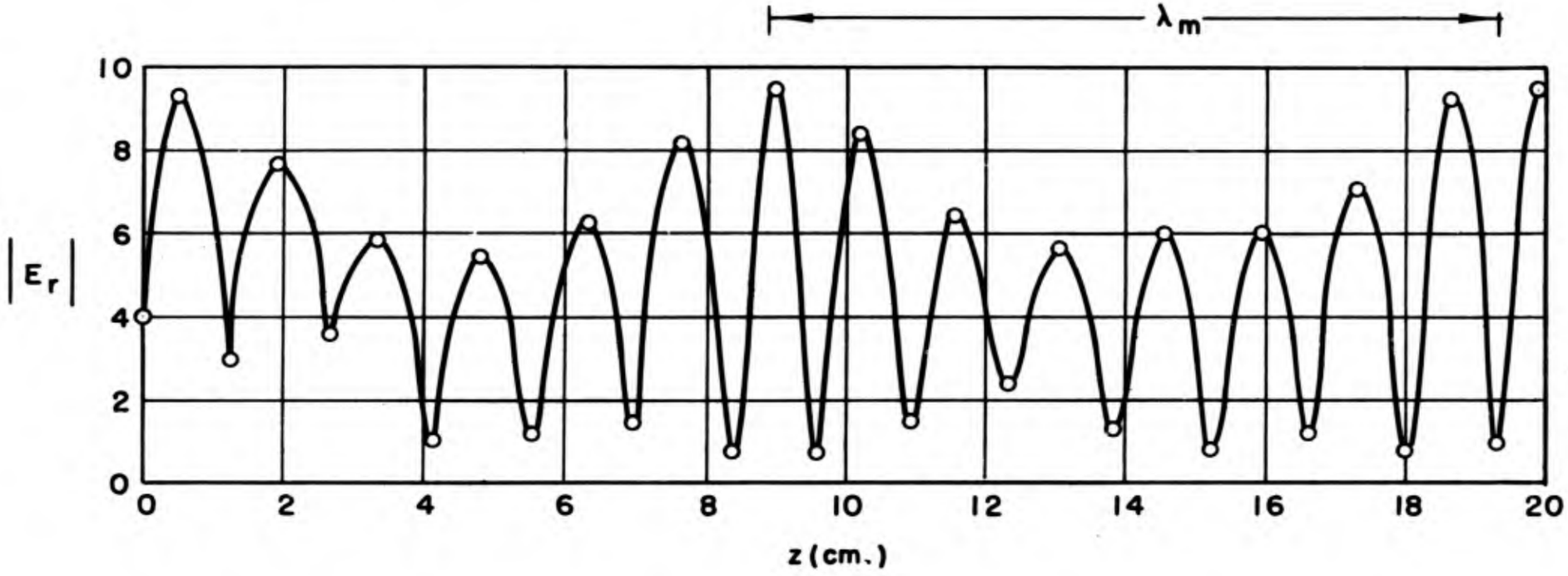

Mode : $TM_{01} - TM_{02}$. Material: Textolite Diameter : $2\frac{5}{16}$".

λ_o = 3.20 cm. $\overline{\lambda}_{g1}$ = 2.79 $\overline{n}_{a1}$ = 1.15 λ_m = 11.1 cm.

$\phi = 0°$ n_{a2} = 1.44

Fig. 2.22 – Radial Component Of The Electric Field As A Function Of z.

envelope, due to the TM_{01} and TM_{02} modes combining, is very distinct, and the variation of the individual λ_g can be seen. Figure 2.20 shows a graph of the radial component of the electric field on a rod $.595\lambda_o$ in diameter, excited in the HE_{11} mode. In this case the standing wave pattern is uniform because the diameter of the rod is only large enough to support propagation of the dominant mode.

All of the measurements described above were made as functions of the axial distance z. Other measurements were made which indicate the behavior of the electric field as a function of radial distance, r. With the solid rods it is, of course, impossible to measure the fields inside the rod. However, measurements could be made of the fields across the flat face of the ends of the rods. These measurements were made on the rods that were used as antennas. The probe was oriented to be parallel to the electric field at all times. Figure 2.23 shows graphs of the radial component of the electric field as a function of radial distance for rods of several diameters excited in the TM_{01} mode. The dotted lines for the 2.4 and 1.0 d/λ_o rods are theoretical curves. The field expressions in Chapter III were used to calculate the fields. The discrepancy between the measured and the theoretical fields is due probably to several factors. In making these measurements it was necessary to have the probe and a considerable part of its transmission line in a region of comparatively strong fields. Thus the probe and transmission line undoubtedly caused appreciable distortion of the fields. The failure of E_r to vanish at the origin probably was due to induced currents on the outer conductor of the

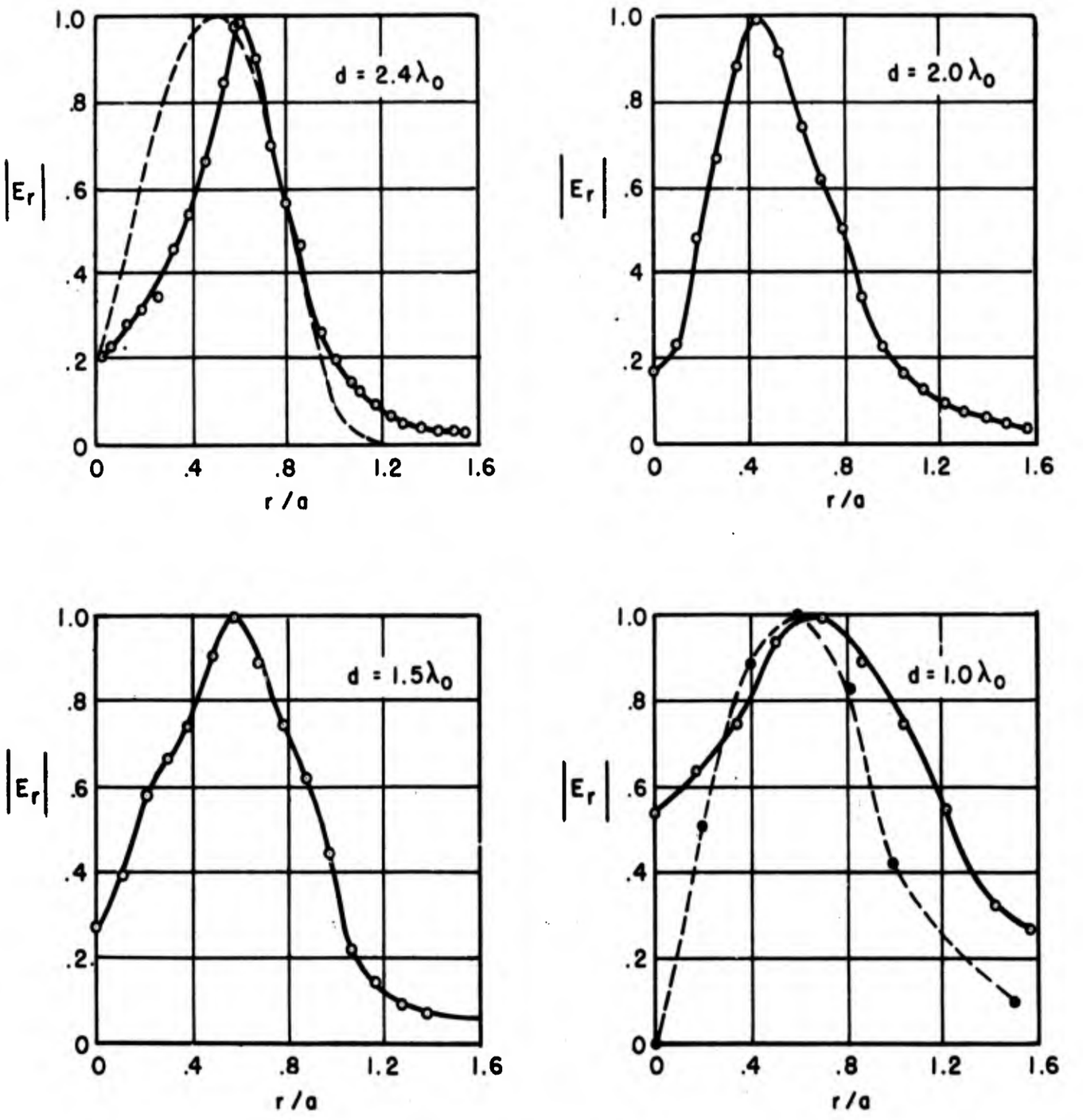

Material: Polystyrene
Mode: TM_{01}
r = radial distance

d = diameter

Index of Refraction = 1.60
a = radius
λ_o = 3.20 cm.

Fig. 2.23

RADIAL COMPONENT OF THE ELECTRIC FIELD VERSUS RADIAL DISTANCE ACROSS THE END SURFACES OF DIELECTRIC WAVEGUIDES.

transmission line. In the case of the 2.4 d/λ_o rod, the discrepancy between the calculated and measured values was due to the presence of the TM_{02} mode. The TM_{02} mode would have one change of phase in the distance from the origin to the surface of the rod. If it is assumed that the two modes were of opposite phase, then the resulting curve would be similar to that which was measured. The agreement between calculated and measured fields for the 1.0 d/λ_o rod is good considering the possible sources of errors.

The measured fields across the ends of these rods were not entirely symmetrical about the origin. This asymmetry was found to be due to the presence of the probe and not to the fields in the rod. The measured values shown in Figure 2.23 are those which were measured with the least amount of the probe transmission line in front of the rod. It is believed that these values were the most accurate.

It can be seen that the ratio of the field at the surface to the maximum value of the field is much larger for small diameter rods than for large diameter rods. This characteristic is in agreement with the theory of the dielectric waveguide, of course.

Figure 2.24 gives graphs of E_r as a function of radial distance for the same dielectric rods described above except excited in the HE_{11} mode. The measurements were made for $\varphi = 0^o$. As before, theoretical curves are plotted for the 2.4 d/λ_o and 1.0 d/λ_o rods. The sources of error are also the same. Very good agreement was obtained for the 1.0 d/λ_o rod. The other rods have considerable amounts of higher order modes which cause the lack of agreement between the calculated and measured data. In a qualitative manner it can be seen that the presence

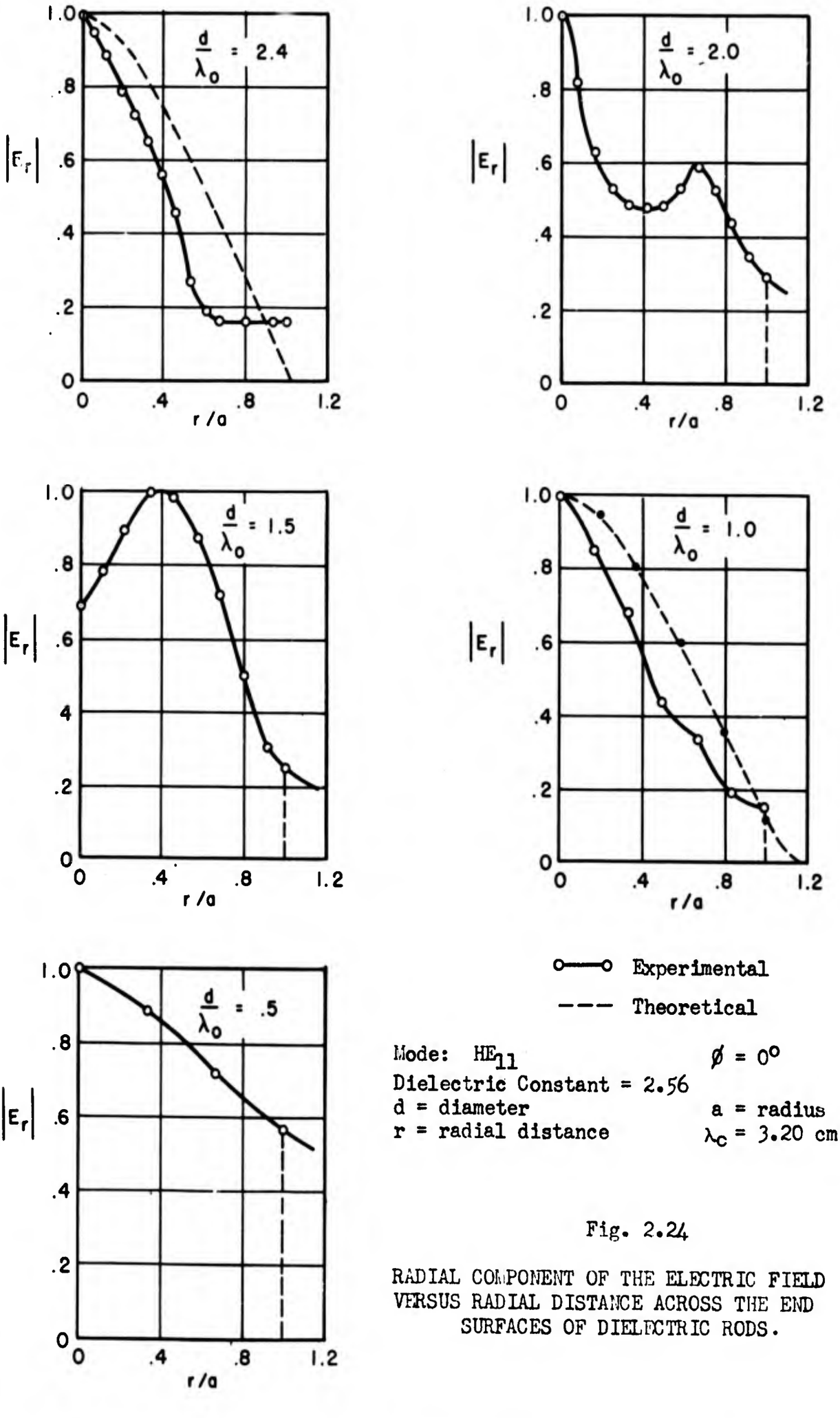

Fig. 2.24

RADIAL COMPONENT OF THE ELECTRIC FIELD VERSUS RADIAL DISTANCE ACROSS THE END SURFACES OF DIELECTRIC RODS.

of the HE_{12} mode could cause the irregularities in the 2.0 and 1.5 d/λ_o rods. In the former case the two modes would have to be of the same phase while in the latter case the two modes would have to be of opposite phase to produce the slight null at the origin.

Figure 2.25 shows graphs of the angular component of the electric field, E_φ, as a function of r with $\varphi = 90^\circ$. The rods are the same as above. The agreement between the calculated and measured values is about the same as for the radial components.

Figure 2.26 shows a graph of the angular component of the electric field across the end surface of a dielectric rod 2.125 inches in diameter excited in the TE_{01} mode. It will be noted that some asymmetry existed about the origin. It can be seen from the following discussion that the asymmetry was due to the presence of some HE_{11} mode. The lower dotted curve is a plot of the radial component of the electric field measured as a function of r. Since the TE_{01} mode does not have a radial component of the electric field, the field which was measured must have been due to the HE_{11} mode. If it had been due to the TM_{01} mode, a maximum would not have occurred at the origin. It should also be noted that the phase of the HE_{11} mode is the same across the entire cross section, while for the TE_{01} and TM_{01} modes the phase reverses at the origin. Bearing this point in mind, it is seen that a combination of HE_{11} with TE_{01} would produce an asymmetrical field. In all of the graphs of measured data, it is the absolute value which is plotted since only the absolute value was measured.

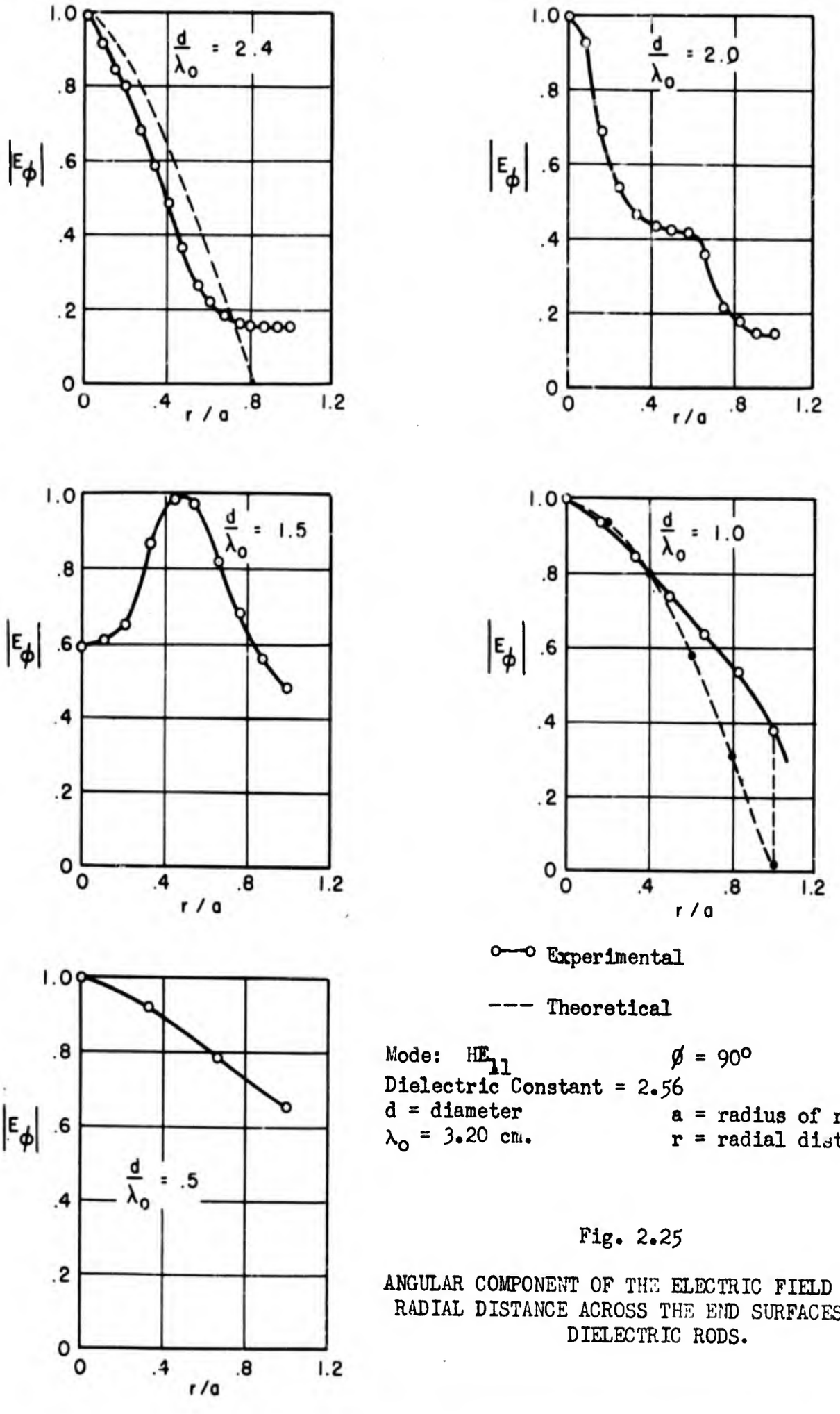

Mode: HE_{11} $\phi = 90°$
Dielectric Constant = 2.56
d = diameter a = radius of rod
λ_0 = 3.20 cm. r = radial distan

Fig. 2.25

ANGULAR COMPONENT OF THE ELECTRIC FIELD VE S
RADIAL DISTANCE ACROSS THE END SURFACES O
DIELECTRIC RODS.

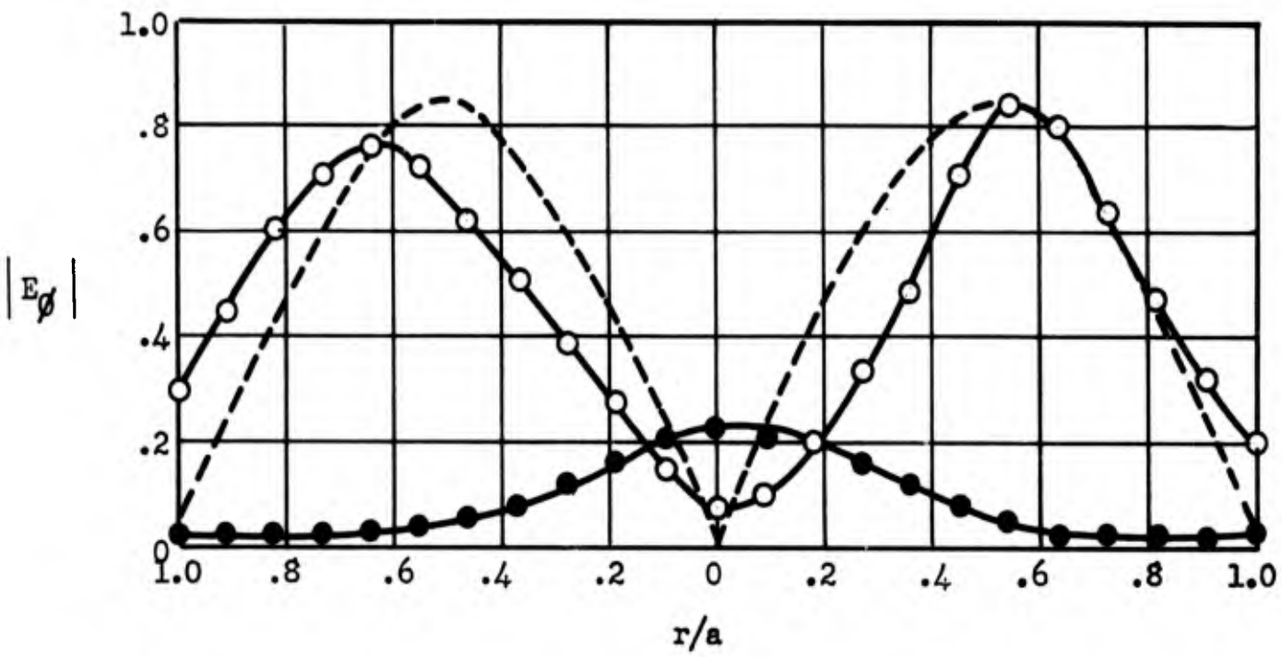

○——○ TE_{01} (Experimental)

----- TE_{01} (Theoretical)

●——● HE_{11} (Experimental)

TE_{01} Mode $\phi = 90^\circ$

$\lambda_o = 3.20$ cm a = radius of waveguide

(HE_{11} Mode was detected by measuring E_r)

Fig. 2.26 ANGULAR COMPONENT, E_ϕ, OF THE ELECTRIC FIELD AS A FUNCTION OF RADIAL DISTANCE, r, ACROSS THE END SURFACE OF A DIELECTRIC ROD.

Figure 2.27 gives graphs of the electric field components on the surface of the 2.125-inch diameter dielectric rod excited from the TM_{11} exciter. If these graphs for E_r and E_φ are compared with Figures 1.03 and 1.16 of Part One, which give graphs of the fields across the end of the TM_{11} exciter, it can be seen that the fields in the dielectric rod are considerably different from those of the metal waveguide. Furthermore, if the curves of Figure 2.27 are compared with Figures 2.24 and 2.25, it can be seen that the fields of rods excited from TE_{11} and TM_{11} exciters are very similar. Therefore, it is concluded that in dielectric rod waveguides the HE and EH modes are the same. This is in agreement with conclusions made on the apparent index of refraction measurements. The small maximum on each side of the origin for both E_φ and E_r was probably due to the transition between the fields in the metal waveguide and those in the dielectric rod not being complete. These measurements were made on a rod about twelve inches in length. If the measurements had been made on the end surface of a much longer rod, these secondary maxima might not have been present.

Figure 2.27-b shows the asymmetry due to the probe being in the field. Due to the shape of the probe, for E_φ measurements the disturbance of the field by the probe was symmetrical about the origin. But for E_r measurements, this was not the case. Figure 2.27-b is an extreme example of probe distortion.

Figure 2.27-c is included to give an idea of the field configuration as a function of the axial distance z. It should be noted that

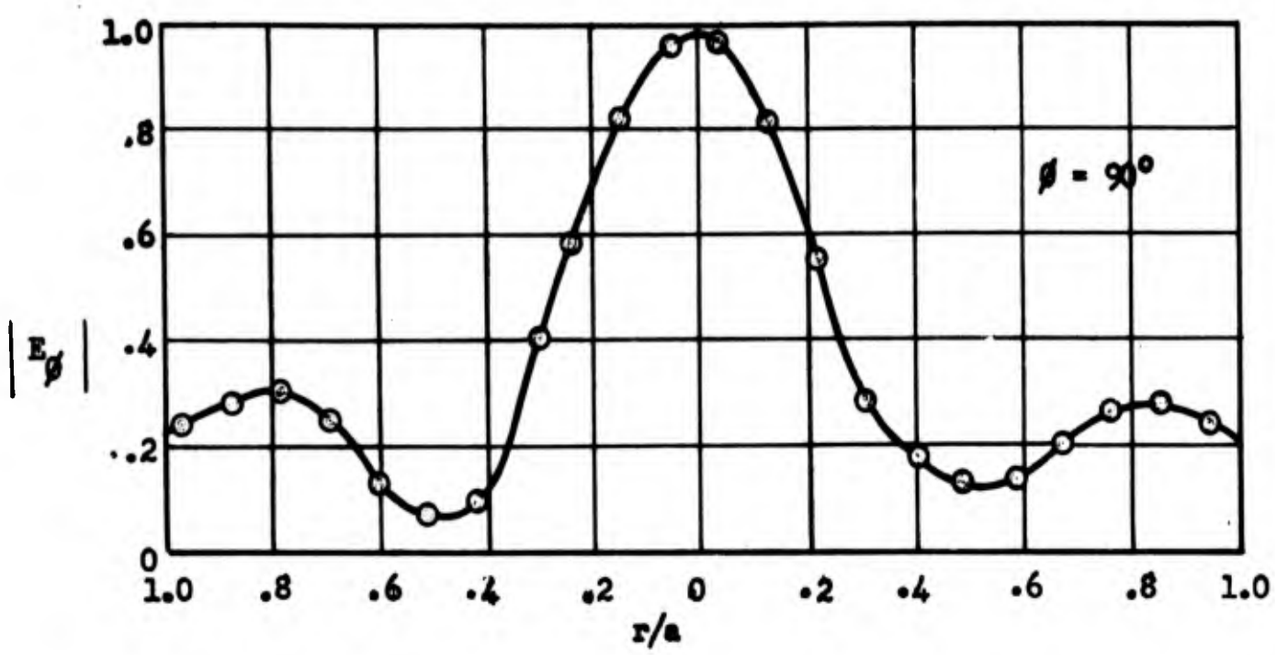

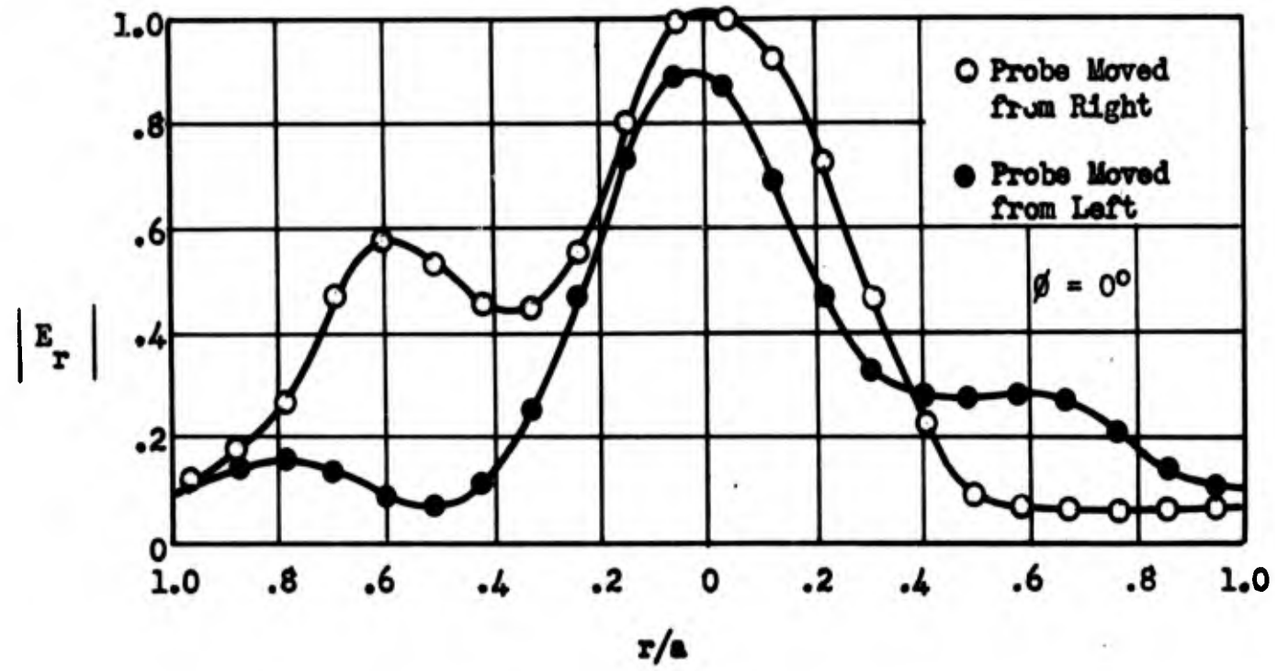

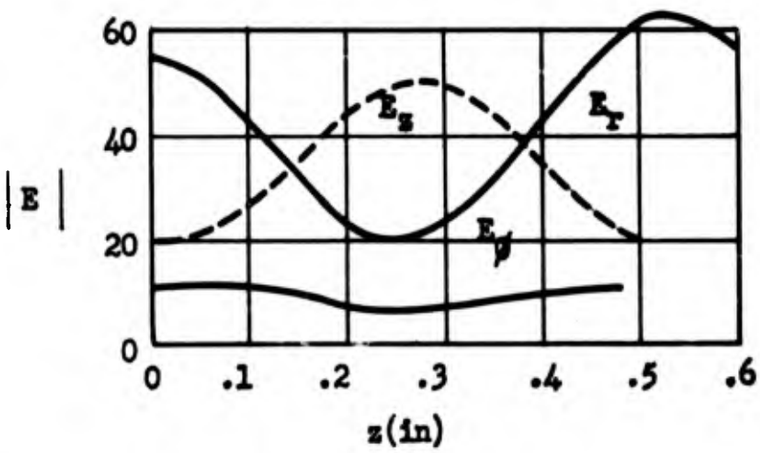

Fig. 2.27 ELECTRIC FIELD COMPONENTS ON THE SURFACE OF A DIELECTRIC WAVEGUIDE EXCITED IN THE EH_{11} (TM_{11}) MODE.

the effect of the probe in measurements of fields on the cylindrical surfaces was much less than on the end surfaces because in the former case, most of the probe is in a region of the weak field. It has been shown previously that the fields are extremely weak at a radial distance from the surface of only a fraction of a wavelength.

3. Attenuation Measurements. The attenuation of Lucite and Textolite rods was measured for HE_{11}, TM_{01}, and TE_{01} modes. The results of these measurements are shown graphically in Figures 2.28 through 2.29. The solid curves are from Wegener. Figure 2.30 shows the same data plotted in db. per ft. It is believed that the experimental data verifies Wegener's work within the accuracy of the measurements.

Figure 2.31 shows the attenuation of Nujol filled flexible vinyl tubes as a function of radius of curvature of bends. Three sizes of tubes were used. Each was two feet in length. Figure 2.32 shows the attenuation for the 9/16-inch tube as a function of differential heights of transmitter and receiver. From these measurements it is evident that slight bends may be tolerated and that the attenuation, as expected, increases sharply for small tubes.

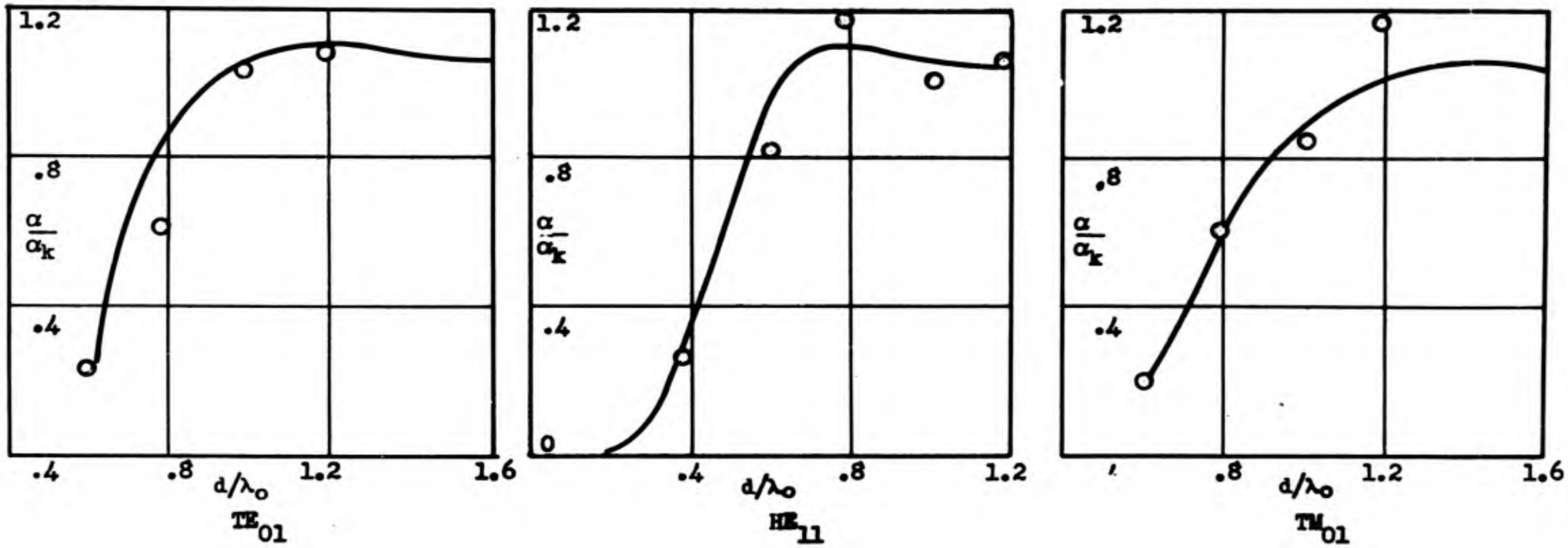

λ_o = Wavelength in Air

tan δ = .01

α = Attenuation in Rod

Material: Lucite

α_k = Dielectric Attenuation in Coaxial Cable

Fig. 2.28 THE DEPENDENCE OF ATTENUATION IN A DIELECTRIC ROD ON THE DIAMETER, d, OF THE ROD

SOLID CURVES ARE THEORETICAL VALUES

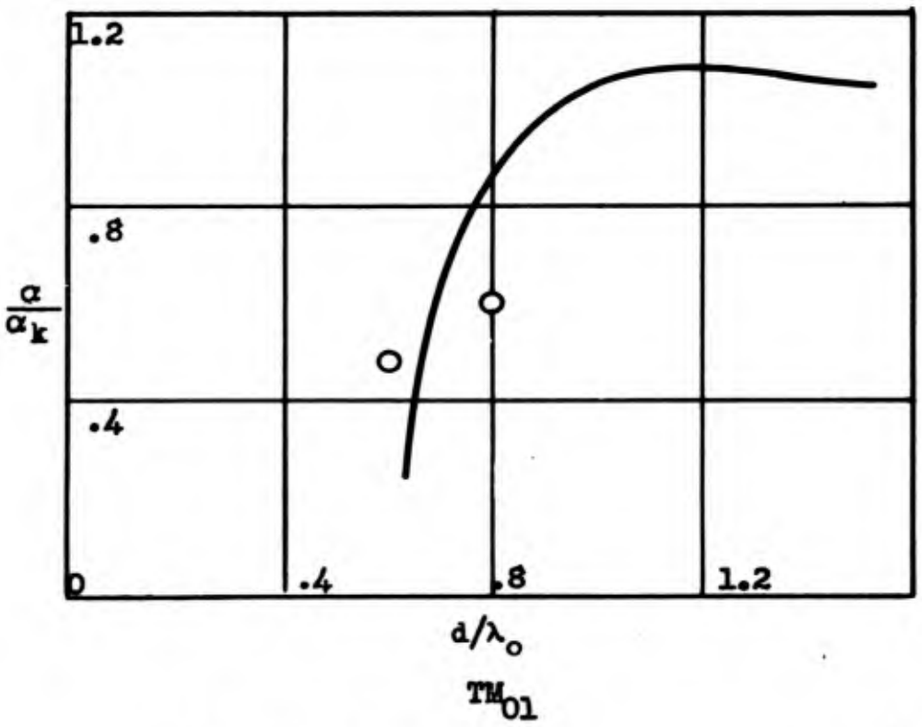

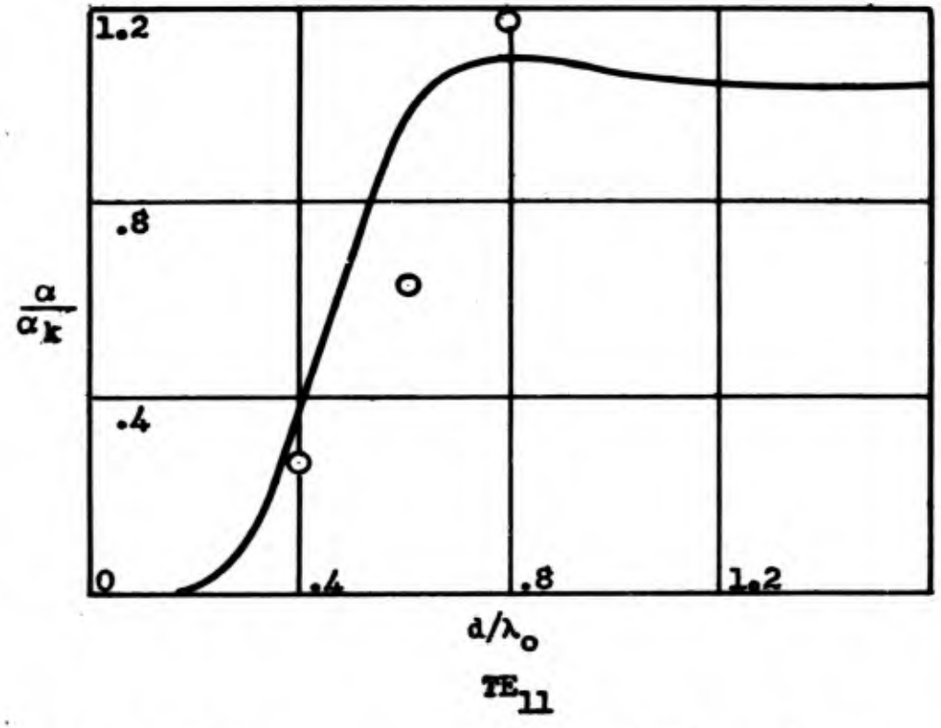

λ_o = Wavelength in Air

tan δ = .001

α = Attenuation in Rod

Material: Textolite

α_k = Dielectric Attenuation of Coaxial Cable

Fig. 2.29 THE DEPENDANCE OF ATTENUATION, α, IN A DIELECTRIC ROD ON THE DIAMETER, d, OF THE ROD
SOLID CURVES ARE THEORETICAL VALUES

Material: Lucite

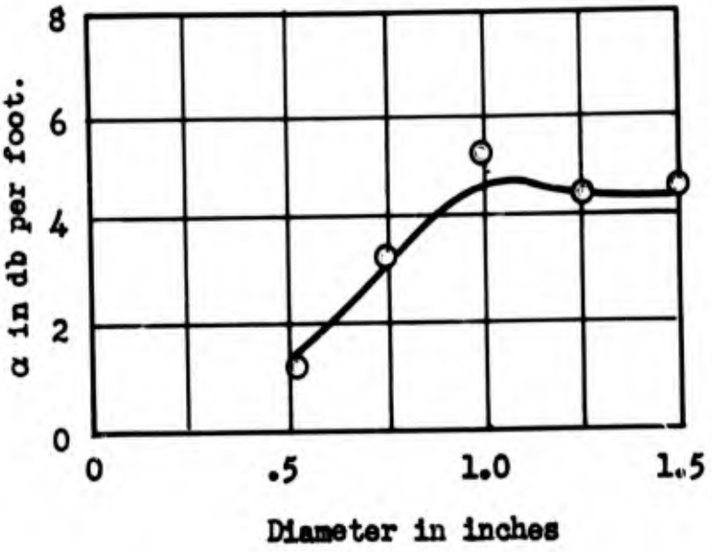

HE_{11}

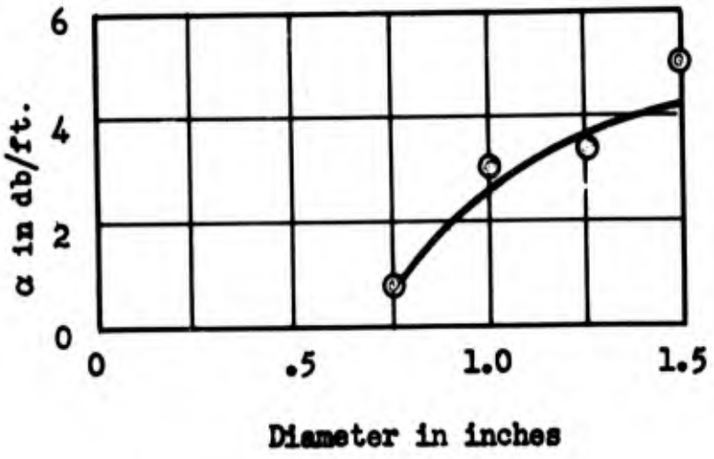

TM_{01}

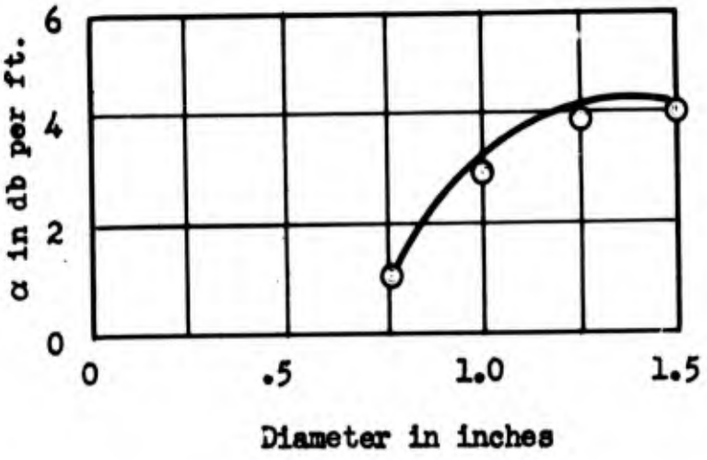

TE_{01}

Fig. 2.30 ATTENUATION IN A DIELECTRIC WAVEGUIDE AS A FUNCTION OF DIAMETER.

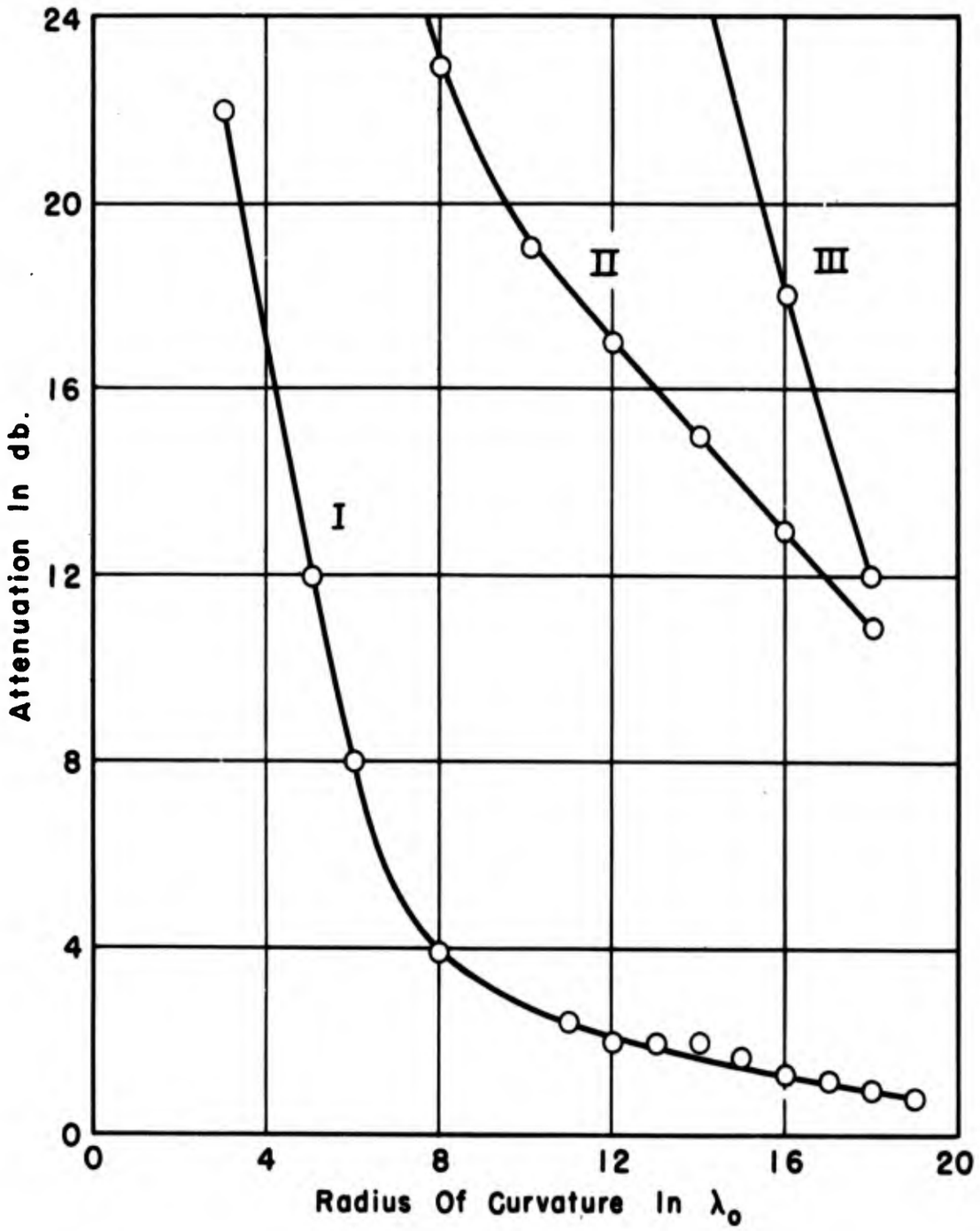

Length: 2.0 Ft. λ_0 = 3.20 cm.

Material: Vinyl Tubes Filled With Nujol.

Diameter: I. $\frac{9}{16}$" O.D.

II. $\frac{7}{16}$" O.D.

III. $\frac{9}{32}$" O.D.

Fig. 2.31 – Attenuation Of Dielectric Waveguide As A Function Of Bending.

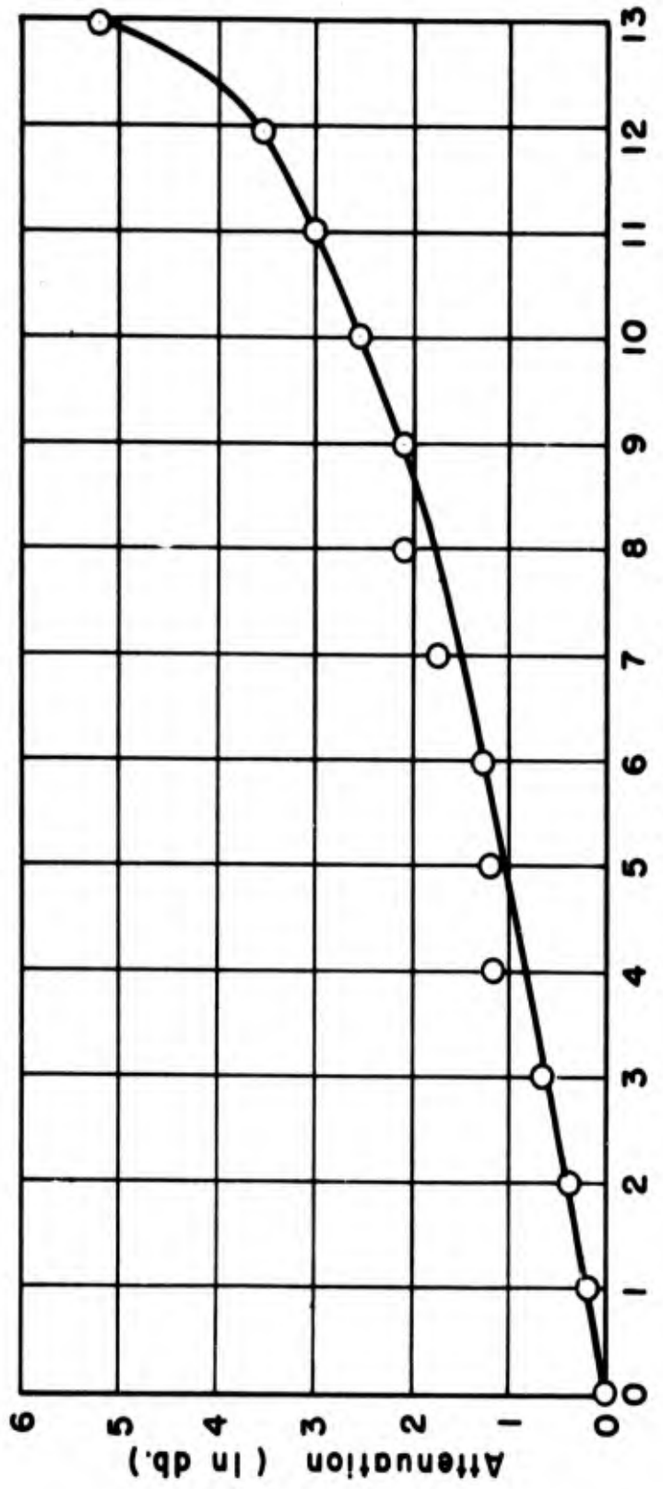

Length: 2.0 Ft. Diameter: $\frac{9}{16}$" O.D.

Material: Vinyl Tube Filled With Nujol.

Fig. 2.32 – Attenuation Of Dielectric Waveguide As A Function Of Differential Height Of Transmitter And Receiver.

CHAPTER VI

PRACTICAL ASPECT OF THE DIELECTRIC WAVEGUIDE

The dielectric waveguide has never been used as a practical means of energy transmission because the loss in the best of the dielectrics is considerably greater than in air, the dielectric used in metallic guides. The attenuation may be decreased by using small diameter rods but when this is done, losses due to bending and radiation due to nearby objects increase. However, it does appear that for rods as small as $\lambda_o/3$ in diameter, considerable bending can take place without excessive loss. Thus there may be some uses for the flexible dielectric waveguide for use as short patch cords between pieces of equipment, etc. These types of guides are extremely cheap and easy to make.

Certain types of linear particle accelerators make use of a waveguide which has a phase velocity of the order of magnitude of particles entering the system.[34] In the ordinary air-filled metal waveguide, the phase velocity is greater than the velocity of light and hence, that type of guide is not useful in accelerator applications. It is common practice to "load" the metal waveguides by means of various obstacles such as disks, etc., to reduce the phase velocity to a suitable value. It appears that the dielectric waveguide, which has a phase velocity less than that of light in a vacuum, might have some application in accelerator work. This possibility has not been investigated in this project, but certain problems are immediately evident. By using large

---

[34] Slater, J. C., "The Design of Linear Accelerators," Review of Modern Physics, 20, 473, (July 1948).

diameter rods or material of high dielectric constant, the phase velocity could be made to approach $c/\sqrt{K}$. However, under this condition, higher order modes could also be propagated. Since it seems likely that mode purity would be desirable, the problem of suppression of the higher order modes would have to be solved. The particle path could probably be a small axial hole through the waveguide. The device would then be a dielectric tube rather than a rod, but for the diameter of the hole, small compared to the rod diameter, the effect of the hole would be small. The rod could probably be gradually tapered to a smaller diameter in order to increase the phase velocity of the wave. Probably the most difficult problem would be that of supplying energy to the rod to overcome the loss of energy due to attenuation by the waveguide. Since the attenuation of the dielectric guide (for large diameters) is considerably greater than that of air-filled metallic guides, this probably represents a serious drawback to the possibility of the use of the dielectric waveguide as a particle accelerator.

It is entirely possible that combination of certain modes could be efficiently transmitted by the dielectric waveguide. However, in order to investigate this possibility systematically one would have to be able to insert controlled amounts of the various modes at the transmitter and extract these modes efficiently at the receiver. It is impossible to do this at the present time.

PART THREE

DIELECTRIC RADIATORS

BLANK PAGE

CHAPTER I

HISTORICAL SUMMARY OF WORK ON THE DIELECTRIC ROD RADIATOR

It was mentioned in the preface that one of the disadvantages of the dielectric waveguide is the fact that some radiation occurs along the rod. If the rod were infinitely long and if the free space wavelength λ_o were shorter than the critical wavelength λ_c, no radiation of energy into the surrounding medium would occur. However, for rods of finite length radiation of energy will occur. Obstructions near the rod will also cause distortion of the field with resulting radiation. This apparent disadvantage has been made use of in the so-called "Polyrod" or dielectric antenna. The expression "Polyrod" is derived from the name polystyrene, the most common material used in their construction. During World War II, both the Allies and Germany used the polyrod antenna in production models of radar equipment. In this country Bell Telephone Laboratories[1] developed an antenna array for fire control which made use of forty-two polyrod elements, arranged in three rows of fourteen each. The Germans[2] used a much smaller array, consisting of four elements arranged in a horizontal plane, in an airborne radar set. Thus it is seen that the dielectric radiator has already proven itself to be a useful, practical antenna and considerable work, both theoretical and experimental, has been done on them. This section gives a brief summary of this work.

---

[1] Friis, H. T., and Lewis, W. D., "Radar Antennas," B.S.T.J., 26, 278 and 300, 1947.

[2] Linder, W. J., "The Dielectric Rod Antenna," M.S. Thesis, University of California, Berkeley, January 1948.

Southworth,[3] at Bell Telephone Laboratories, was probably the first person to suggest the use of the dielectric waveguide as an antenna, though he did not do any work on this subject until 1941. In 1947, Mueller and Tyrrell[4] reported on the work at Bell Laboratories which had been done between 1941 and 1944. They compared the polyrod antenna to a general type of end-fire antenna array consisting of a number of isotropic radiators spaced along a transmission line. On the basis of the general end-fire array, they concluded that a sinusoidal variation of the intensity of field along the rod would reduce minor lobes and produce a narrow beam. In the case of the dielectric rod, this condition was approximated by uniformly tapering the rod for about one-half of its length, thus causing more and more of the energy to travel outside the rod. The last half of the rod was allowed to have a uniform cross section, since the radiation gradually reduced the intensity of the surface fields. They included the radiation pattern for several tapered rods of both circular and rectangular cross section of different lengths. The experimental data were only for 100° of the 360° pattern and for one plane only, although the orientation was not mentioned. The dielectric rods used had diameters of $\lambda_o/2$ or less. It should be noted that the type of analysis that they used does not include such factors as rod diameter, distribution of the fields in cross section, the vector nature of the fields or the material of the

---

[3] Southworth, G. C., U. S. Patent No. 2,206,923, Granted 9 July 1940, filed 12 September 1934.

[4] Mueller, G. E., and Tyrrell, W. R., "Polyrod Antennas," B.S.T.J., 26, 837, 1947.

rod. They also showed experimentally, that the gain decreases as the attenuation in the rod increases.

Mallach,[5] in Germany, presented a thesis in 1939 on centimeter dielectric radiators, and as far as is known, all of the work in Germany in this field, stems from his investigations. As mentioned in Part Two, Mallach made some measurements on the dielectric waveguide, but he was primarily interested in the radiation properties. Mallach's first work was an attempt to terminate the aperture of metal horn antennas with a quarter wave dielectric plate in order to obtain good impedance matching. From this work he progressed to dielectric rod and tube antennas. Mallach used small diameter rods (considerably less than λ_o) excited in the HE_{11} mode by means of a dipole antenna. Mallach developed a simple theory for the dielectric rod antenna based on the consideration that each element of the surface acted as a radiator and that the phase of the excitation of these radiators depended on the wavelength along the rod. This elementary theory is given in Chapter III because it is useful in studying some of the general properties of this type of antenna. However, this theory is inadequate and has several faults. It is assumed that a linearly polarized plane wave of constant phase and intensity cross section propagated down the rod without attenuation or reflection. The diameter of the rod is not considered except in the determination of λ_g. Furthermore, this theory is not useful except for the dominant mode. One of the most

---

[5] Mallach, Peter, "Dielectric Directional Antennas for dm and cm Waves," Air Material Command Report F-TS-2223-RE, February 1948. Translated by P. L. Harbury, Harvard University, Cambridge, Mass.

serious objections is that only small angles of diffraction are considered (that is, the spherical nature of the wave is not taken into account).

Thus, it is not useful for obtaining the lobe structure for the entire radiation field. However, for the sizes of rods used by Mallach, and for small angles of diffraction, the theory is satisfactory.

Mallach also found that by tapering the cross section of the rod, the secondary lobes and back radiation could be reduced. He also noted that an increase in the length of the rods reduced the width of the major lobe but increased the relative amplitudes of the minor lobes, which is in general agreement with other types of end-fire antennas. Mallach further contended that increasing cross section increased side lobe intensity. This last point is not verified by the present project.

Mallach's other work consisted of experiments on arrays of dielectric rods and work on dielectric tubes as antennas.

Halliday and Kiely[6] have investigated experimentally the dielectric rod antenna of circular cross section, excited in the HE_{11} mode. Most of their work was of the nature of verifying and repeating Mallach's work.

Linder[7] has made a study of the work of Mallach and Wegener and extended the theory of the dielectric rod waveguide to include rods of slight tapers. However, this extension does not appear to be useful in

---

[6] Halliday, D. F., and Kiely, D. G., "Dielectric-Rod Antennas," J. Inst. Elec. Engrs., 94, 610, 1947.

[7] Linder, op. cit.

the consideration of the tapered dielectric antenna. Linder's thesis also included some results of interrogation of German Scientists.

Wilkes[8,9,10] has considered the dielectric antenna of circular and rectangular cross section, excited in the HE_{11} mode, from the viewpoint of a lens of dimensions comparable to the wavelength. He experimentally obtained results which were in agreement with earlier work. The rods used by him were relatively small. One point of interest is that he found the apparent index of refraction to be a function of length of the rod. However, these measurements were made over a rather limited range. Wilkes also computed some radiation patterns based on analogy to metallic antenna arrays. These calculations were fairly well verified for the major lobe.

Horton and Watson[11,12] have done extensive work since 1946 on dielectric rods, primarily of rectangular cross section, excited in the dominant mode. Their work has been of both a theoretical and experimental nature. Their diffraction theory is based on certain equivalence theorems of Schelkunoff and represent the only satisfactory theory of the dielectric radiator at the present time. In brief, the

---

[8]Wilkes, Gilbert, "Wavelength Lenses," Ph.D. Dissertation, University of Paris, Sorbonne, December 5, 1946.

[9]Wilkes, Gilbert, "Wave Length Lenses," BUMBLEBEE Report No. 59, Applied Physics Laboratory, Johns Hopkins University, June 1947.

[10]Wilkes, Gilbert, "Wavelength Lenses," Proc. I.R.E., 36, 206, 1948.

[11]Watson, R. B., and Horton, C. W., "The Radiation Patterns of Dielectric Rods - Experiment and Theory," J. App. Phys., 19, 661, July 1948.

[12]Watson, R. B., and Horton, C. W., "On the Calculation of Radiation Patterns of Dielectric Rods," J. App. Phys., 19, 836, September 1948.

equivalence theorems state that the fields inside a volume can be replaced by fictitious electric and magnetic current sheets on the surface. Horton and Watson replace the wave traveling in the dielectric rod by these surface currents, from which electric and magnetic vector potentials are calculated. The fields at distant points are then determined from these vector potentials. They have obtained good agreement for rectangular rods of lengths up to $6\lambda_o$. The weak point of the theory is in estimating the fields inside the dielectric guide. They have assumed that the fields are similar to those in metallic waveguides of similar cross section.

Horton and Karal[13,14] have extended the theory to rods of circular cross section excited in the HE_{1m}, TM_{0m}, TE_{0m} modes and obtain excellent agreement with experimental patterns obtained in the present project for a number of different radiators. This theory will be discussed in more detail in Chapter III. The improvement is due to a better knowledge of the field distribution of the circular rod than for the rod of rectangular cross section.

Further investigations of the dielectric rod antenna are in progress at the present time at several institutions in this country. One particular project under the direction of G. E. Mueller[15] at Ohio State University has as a particular aim to develop a broadside

---

[13]Horton, C. W., Karal, F. C., and McKinney, C. M.,""On the Radiation Patterns of Dielectric Rods of Circular Cross Section," Paper HA6 presented at the 1950 Annual Meeting of the American Physical Society, February 1950, New York City.

[14]Horton, C. W., unpublished manuscript.

[15]Mueller, G. E., Report on Dielectric Antennas, Quarterly Report, January 1949; Quarterly Report, April 1949; Quarterly Report, July 1949; Annual Report, October 1949. Ohio State University Research Foundation, Columbus, Ohio.

dielectric antenna, that is, one whose pattern has the major lobe at right angles to the axis of the dielectric rod. They are investigating the beaded dielectric antenna for this purpose. The beaded rod consists of a rod of one dielectric constant on which beads of a higher dielectric constant are mounted.

CHAPTER II

PURPOSES OF THE PRESENT INVESTIGATION OF THE DIELECTRIC ROD RADIATOR

From the foregoing section it is evident that considerable work has already been done on dielectric antennas and consequently it is in order to explain how the present investigation extends the field of knowledge of the subject. As has been mentioned previously, all of the work on dielectric antennas has been with the dominant mode of excitation, HE_{11}. This is understandable when one realizes that the dominant mode does give maximum directivity in the forward direction, is easy to excite, and can be obtained in very pure form. The TM_{01} and TE_{01} modes are more difficult to excite, and have not been used in practical application up to the present time. However, it is believed that there are at least two practical applications for antennas with a null in the forward direction. They will be explained in more detail later.

A more important goal in this investigation was to obtain a large amount of accurate and extensive experimental data, which could be used to verify theoretical work both present and future. In order to be useful in this respect the range of the parameters should be extended as far as possible. In previous work, for instance, the lengths of the dielectric rods have been limited mostly to about $6\lambda_o$ and diameters (which were seldom varied) were less than $\lambda_o/2$. Likewise the measuring equipment has usually been of a nature that

prevented accurate recording of position and intensity of minor lobes beyond the first one or two. It is the agreement between theory and experiment for large angles of diffraction that gives a true test to the theory. In this work the diameters have been varied from $0.25\lambda_o$ to $2.4\lambda_o$, length from 2 to $10\lambda_o$, tapers in several ways, and the following modes of excitation have been used: HE_{11}, TM_{01}, TE_{01}, and EH_{11}. The nature of the measuring equipment is such that signals could be measured over a range of 50 db (10^5 power ratio) which enabled as many as 22 lobes in 180° to be recorded for some of the antennas. An attempt has been made to analyze the radiation patterns and gain measurement so that the maximum possible information could be obtained.

CHAPTER III

BRIEF THEORY OF THE DIELECTRIC RADIATOR

Certain general characteristics of the dielectric rod antenna may be observed from the elementary theory first used by Mallach. Consider a plane polarized wave traveling in a dielectric waveguide in the positive z direction, which is parallel to the axis of a dielectric rod antenna. See Figure 3.01. The field at a distant point P will be due to the energy of the wave which is radiated from all parts of the dielectrid rod. The point P is considered to be at such a distance that all radiation from the rod comes from the same direction. Now consider the point along the rod. The phase of the energy at each successive point along the rod will be delayed by the time required for the wave to travel the distance Δz. However, the phase of the radiation from the surface at each point will be advanced by the time required for the radiation to travel the distance $\Delta z \cos \theta$, over that of the previous point. Therefore, the total difference in phase between successive points is

$$\delta = \frac{2\pi}{\lambda_o} \Delta z \cos \theta - \frac{2\pi}{\lambda_g} \Delta z = \frac{2\pi \Delta z}{\lambda_o} (n_a - \cos \theta) \qquad (3.01)$$

where $n_a = \lambda_o/\lambda_g$.

The field ΔE_p due to each element of length dz, can be expressed as

$$\Delta E_p = g dz \sin 2\pi ft \qquad (3.02)$$

where g is a constant.

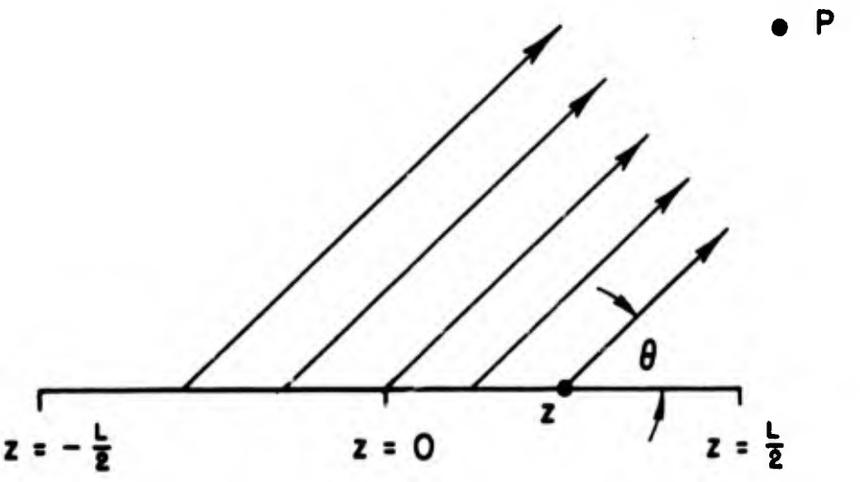

Fig. 3.01 – Notation For Antenna Theory.

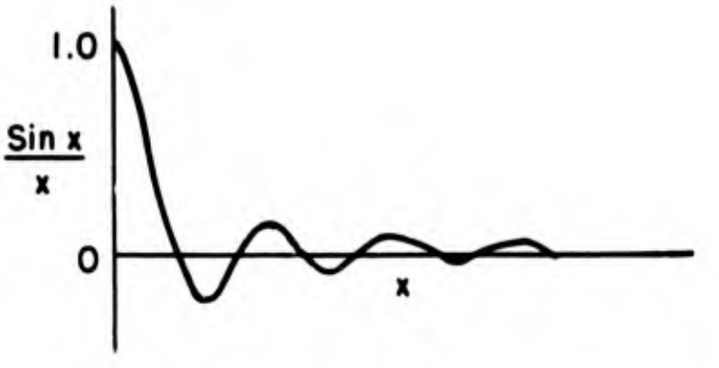

Fig. 3.02 – Graph Of $\frac{\sin x}{x}$ As A Function Of x.

The phase of the wave arriving from point z will be different from that arriving from point $z = 0$ by the angle

$$\delta = \frac{2\pi z}{\lambda_o} (n_a - \cos \theta) . \tag{3.03}$$

Then

$$\Delta E_p = g dz \sin \left[2\pi f t - \frac{2\pi z}{\lambda_o} (n_a - \cos \theta) \right] . \tag{3.04}$$

The total field E_p will be

$$E_p = \int_{-L/2}^{L/2} g \sin \left[2\pi f t - \frac{2\pi z}{\lambda_o} (n_a - \cos \theta) \right] dz. \tag{3.05}$$

Let $x = \frac{\pi L}{\lambda_o} (n_a - \cos \theta)$. (3.06)

Then

$$E_p = \int_{-L/2}^{L/2} g \sin \left(2\pi f t - \frac{2x}{L} z \right) dz \tag{3.07}$$

$$E_p = gL \frac{\sin x}{x} \sin 2\pi f t \tag{3.08}$$

Let $E = gL$, then

$$E_p = E \frac{\sin \frac{\pi L}{\lambda_o} (n_a - \cos \theta)}{\frac{\pi L}{\lambda_o} (n_a - \cos \theta)} \sin 2\pi f t \tag{3.09}$$

This is of the form $\sin x/x$ which is graphed in Figure 3.02. The function $\sin x/x$ has an absolute maximum for $x = 0$ and is zero for $x = n\pi$ where n is an integer. Secondary maxima occur between the zero points. These loops constitute the lobes of the radiation pattern. The largest lobe is the "primary" or "main" lobe and the others are "secondary" lobes. For either n_a or L/λ_o different from zero, the radiation pattern will not begin at $x = 0$, but at some larger value. Thus it can be seen that a maximum ratio of major lobe to minor lobe intensity is obtained if either $n_a = 1$ or $L/\lambda_o = 0$. For any value of n_a different from 1, the relative values of the minor lobe intensities increase as L/λ_o increases, but the angular position of the nulls decrease also. This corresponds to a narrow major lobe. Large values of L/λ_o also correspond to large limits on x (for maximum value of θ), which means that the number of lobes increase with length. The number of lobes will also increase as n_a increases.

It is evident that the above discussion is inadequate since the diameter of the rods is not even considered nor the vector properties of the wave, but it is useful for obtaining some general ideas about the dielectric antenna.

Figure 2.01 of Part Two gives the field configurations of the modes with angular symmetry. It is evident from physical considerations that for $\theta = 0$, the contribution from any element of surface will be exactly neutralized by the diametrically opposite element of surface. Therefore, the radiation in the forward direction will be zero.

It was mentioned in Chapter I of Part Three that the most accurate theory of the dielectric rod radiator available at the present time is one which is based on the equivalence theorem of Schelkunoff.[16,17] Horton[18,19,20] has applied this method to a number of different types of antennas, including the dielectric rod antenna of both rectangular and circular cross section. A brief outline of the theory as developed by Schelkunoff and extended to dielectric rods by Horton is included in the following section.

Consider a plane wave striking an aperture as shown in Figure 3.03. The line integral of the field $\vec{H}$ around the path indicated will be equal to the electric current i enclosed.

$$\ell H_{tB} - \Delta z H_n - \ell H_{tA} + \Delta z H_n = i \qquad (3.10)$$

If the aperture is free of any real currents, the line integral vanishes. However, let it be assumed that a surface current sheet of density $\vec{J}$ does lie in the plane of the aperture. The direction of $\vec{J}$ is also in the plane of the aperture. If Δz is allowed to

---

[16] Schelkunoff, S. A., "Some Equivalence Theorems of Electromagnetics and their application to radiation problems," B.S.T.J., 15, 92, January 1936.

[17] Schelkunoff, S. A., "On Diffraction and Radiation of Electromagnetic Waves," Phys. Rev., 56, 308, August 15, 1939.

[18] Horton, C. W., "On the Dielectric Rod as an Antenna," DRL-66, CM-272, July 9, 1946; "On the Dielectric Rod as an Antenna, Part II," DRL-91, CF-481, November 8, 1946.

[19] Horton, C. W., "The Theory of the Radiation Patterns of Electromagnetic Horns," BUMBLEBEE Report No. 86, May 1948.

[20] Horton, C. W., "On the Theory of the Radiation Patterns of Electromagnetic Horns of Moderate Flare Angles," Proc. I.R.E., 37, 744, July 1949.

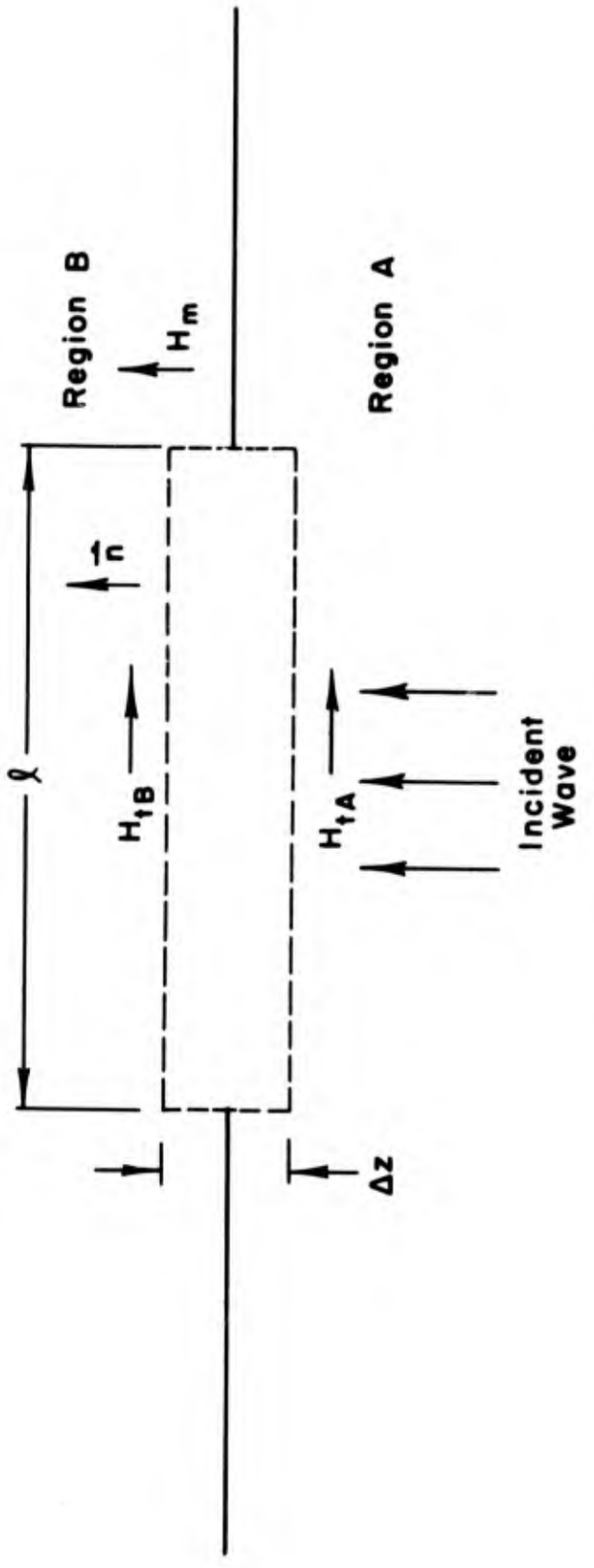

Fig. 3.03 – Diagram Of A Wave Incident On An Aperture.

approach zero, (3.10) reduces to the following expression in terms of current density:

$$H_{tB} - H_{tA} = J_t \tag{3.11}$$

Equation (3.11) may be written in the vector form of

$$\vec{J} = \vec{n} \times \vec{H}_o \tag{3.12}$$

where $\vec{H}_o$ is the total field, $\vec{J}$ is the current density which has a direction normal to $\vec{H}_o$, and $\vec{n}$ is the unit normal pointing away from the source. It is evident that, due to the direction of $\vec{n}$, this current sheet cancels the field H_{tA} but provides for a field H_{tB} on side B.

The process outlined above may be repeated for the tangential component of the electric field to obtain the analogous expression for a magnetic current density

$$\vec{M} = -\vec{n} \times \vec{E}_o \, . \tag{3.13}$$

Thus it is seen that the electric and magnetic current sheets have replaced the source in side A and these current sheets can therefore be considered as an equivalent source. It is not of importance that magnetic current sheets are not known physically, because all of the assumed current sheets are fictitious and are used only as an aid in analysis.

Vector potentials at a point in space a distance r from the source, due to these electric and magnetic current sheets may be

expressed as[21]

$$\vec{A} = \int_S \frac{\vec{J}\, e^{-jkr}}{4\pi r}\, ds \tag{3.14}$$

and

$$\vec{F} = \int_S \frac{\vec{M}\, e^{-jkr}}{4\pi r}\, ds \,. \tag{3.15}$$

$k = 2\pi/\lambda_o$ where $\vec{A}$ is the magnetic vector potential and $\vec{F}$ is the electric vector potential. It is assumed that the currents are periodic in time and therefore the factor $e^{j\omega t}$ has been omitted. These potentials $\vec{A}$ and $\vec{F}$ are retarded potentials which are solutions of the inhomogeneous wave equation. The fields $\vec{E}$ and $\vec{H}$ at the point P in space may be calculated from the following equations:

$$\vec{E} = - j\omega\mu \vec{A} + \frac{1}{j\omega\epsilon} \nabla(\nabla \cdot \vec{A}) - \nabla \times \vec{F} \tag{3.16}$$

$$\vec{H} = - j\omega\epsilon \vec{F} + \frac{1}{j\omega\mu} \nabla(\nabla \cdot \vec{F}) + \nabla \times \vec{A} \,. \tag{3.17}$$

ϵ and μ are the inductive capacities of the space.

The orientation of the dielectric rod with respect to the coordinate systems is shown in Figure 3.04. The aperture is considered to be the surface of the dielectric rod. The only component

---

[21] Stratton, J. A., Electromagnetic Theory, McGraw-Hill Book Company, New York, Chapter VIII, 1941.

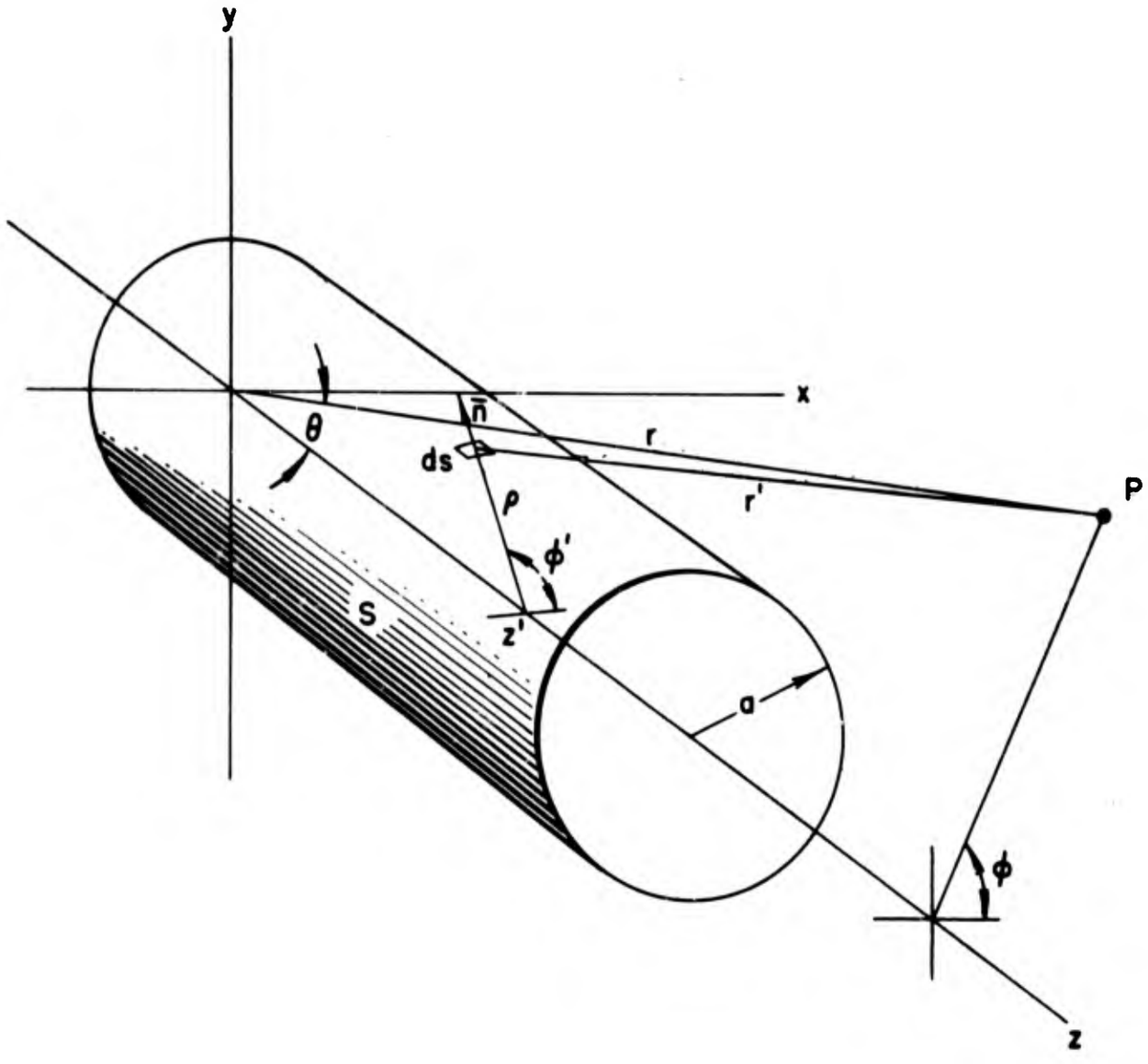

Fig. 3.04 – Coordinate Systems.

of $\vec{n}$ is n_r. Hence J and M reduce to

$$\vec{J} = \vec{n} \times \vec{H} = \vec{i}_{\varphi'} H_z + \vec{i}_z H_{\varphi'} \tag{3.18}$$

$$\vec{M} = -\vec{n} \times \vec{E} = \vec{i}_{\varphi'} E_z - \vec{i}_z E_{\varphi'} . \tag{3.19}$$

If the point P is considered to be at such a large distance from the origin, that the variable distance r' is parallel to r, then r' may be expressed as

$$r' \doteq r - a \sin\theta \cos(\varphi-\varphi') - Z' \cos\theta. \tag{3.20}$$

Also, for large r, the factor $1/r'$ may be replaced by the approximate value $1/r$. With these approximations one has

$$\vec{A} = \frac{e^{jkr}}{4\pi r} \int_S \vec{J}\, e^{-jk\left[a \sin\theta \cos(\varphi-\varphi') + Z' \cos\theta\right]} ds \tag{3.21}$$

and

$$\vec{F} = \frac{e^{jkr}}{4\pi r} \int_S \vec{M}\, e^{-jk\left[a \sin\theta \cos(\varphi-\varphi') + Z' \cos\theta\right]} ds \tag{3.22}$$

If the values of $\vec{J}$ and $\vec{M}$ from (3.18) and (3.19) are substituted into (3.21) and (3.22), the following expressions for the components of $\vec{A}$ and $\vec{F}$ are obtained:

$$A_x = \frac{e^{jkr}}{4\pi r} \int_S H_z \sin\varphi'\, e^{-jk\left[a \sin\theta \cos(\varphi-\varphi') + z' \cos\theta\right]} ds \tag{3.23}$$

$$A_y = \frac{-e^{jkr}}{4\pi r} \int_S H_z \cos\varphi' \, e^{-jk\,[a \sin\theta \cos(\varphi-\varphi') + z' \cos\theta]} \, ds \qquad (3.24)$$

$$A_z = \frac{+e^{jkr}}{4\pi r} \int_S H_{\varphi'} \, e^{-jk\,[a \sin\theta \cos(\varphi-\varphi') + z' \cos\theta]} \, ds \qquad (3.25)$$

$$F_x = \frac{-e^{jkr}}{4\pi r} \int_S E_z \sin\varphi' \, e^{-jk\,[a \sin\theta \cos(\varphi-\varphi') + z' \cos\theta]} \, ds \qquad (3.26)$$

$$F_y = \frac{e^{jkr}}{4\pi r} \int_S E_z \cos\varphi' \, e^{-jk\,[a \sin\theta \cos(\varphi-\varphi') + z' \cos\theta]} \, ds \qquad (3.27)$$

$$F_z = \frac{-e^{jkr}}{4\pi r} \int_S E_{\varphi'} \, e^{-jk\,[a \sin\theta \cos(\varphi-\varphi') + z' \cos\theta]} \, ds \qquad (3.28)$$

The vector operations of (3.16) and (3.17) may be performed to obtain

$$E_r = 0 \qquad (3.29)$$

$$E_\theta = j\omega\mu \,[A_x \cos\theta \cos\varphi + A_y \cos\theta \sin\varphi - A_z \sin\theta] - jk\,[F_x \sin\varphi - F_y \cos\varphi] \qquad (3.30)$$

$$E_\varphi = j\omega\mu \,[-A_x \sin\varphi + A_y \cos\varphi] - jk\,[F_x \cos\theta \cos\varphi + F_y \cos\theta \sin\varphi - F_z \sin\theta] \qquad (3.31)$$

In obtaining (3.29) - (3.31) all terms involving $(1/r)^2$ are neglected. Substituting (3.23) - (3.28) into (3.29) - (3.31) yields

$$E_r = 0 \tag{3.32}$$

$$E_\theta = \frac{j\omega\mu\psi}{4\pi} \int_S [H_{z'} \cos\theta \sin(\varphi'-\varphi) - H_{\varphi'} \sin\theta] \, e^{-jk[a \sin\theta \cos(\varphi-\varphi') + z' \cos\theta]} a\,d\varphi'\,dz'$$

$$+ \frac{jk\psi}{4\pi} \int_S E_{z'} \cos(\varphi'-\varphi) \, e^{-jk[a \sin\theta \cos(\varphi-\varphi') + z' \cos\theta]} a\,d\varphi'\,dz' \tag{3.33}$$

$$E_\varphi = -\frac{j\omega\mu\psi}{4\pi} \int_S H_{z'} \cos(\varphi'-\varphi) \, e^{-jk[a \sin\theta \cos(\varphi-\varphi') + z' \cos\theta]} a\,d\varphi'\,dz'$$

$$+ \frac{jk\psi}{4\pi} \int_S [E_{z'} \cos\theta \sin(\varphi'-\varphi) - E_z \sin\theta] \times e^{jk[a \sin\theta \cos(\varphi-\varphi') + z' \cos\theta]} a\,d\varphi'\,dz' \tag{3.34}$$

where

$$\psi = \frac{e^{-jkr + j\omega t}}{r}$$

It is reasonable to assume that the field components along the rod on the surface S have a transmission factor $e^{jkz'}$ in common. This is verified by measurements of field components on the surface

which indicate that very little energy is reflected from the end of the rod. The factor h is the propagation constant for waves on the rod and is given by $2\pi/\lambda_g$.

Since energy is radiated from all elements of the surface S, it is also logical to assume that the amplitudes of the fields are functions of z', represented by $w(z')$.

Strictly speaking the surface of integration should be a closed surface which would include the surface of the dielectric rod and a surface in space such that the point P would be interior to this surface. However, it is assumed that the sources are entirely within the dielectric rod and that the integral over all of the surface except that of the rod is zero. Also the integral over the end surface is neglected since its value is small compared to the integral over the cylindrical surface. Making these assumptions, the integrals in (3.33) and (3.34) may be expressed as the product of two integrals. One of these integrals is of the form

$$I_S = \frac{1}{2} \int_0^L w(z')\, e^{+j(h - k\cos\theta)z'}\, dz' . \qquad (3.35)$$

This integral will be referred to as the shading integral since it depends on the shading function $w(z')$.

It will be noted that the apparent index of refraction can be expressed in terms of h and k by

$$n_a = h/k = \lambda_o/\lambda_g .$$

Thus (3.35) may be written as

$$I_S = \frac{1}{2} \int_0^L w(z') \, e^{+j(n_a - \cos\theta)\, kz'} \, dz' \, . \qquad (3.36)$$

Mueller and Tyrrell[22] have shown that a sinusoidal shading function is useful from the standpoint of practical design. $w(z')$ can then be expressed in the form

$$w(z') = d + (1-d) \sin\left(\frac{\pi z'}{L}\right) \qquad (3.37)$$

where d is defined in Figure 3.05.

Substituting this value of $w(z')$ into (3.36) and integrating, yields

$$I_S = \frac{Ld}{2} \left[\frac{\pi}{2} \frac{(1-d)}{d} \frac{\cos x}{\left(\frac{\pi}{2}\right)^2 - x^2} + \frac{\sin x}{x} \right] e^{jx} \qquad (3.38)$$

where

$$x = (n_a - \cos\theta) \frac{kL}{2} \, . \qquad (3.39)$$

For uniform field distribution on the rod, $d = 1$, and

$$I_S = \frac{L}{2} \frac{\sin x}{x} \, e^{jx} \qquad (3.40)$$

This integral expresses the effect of the length of the rods on the field pattern. It should be noted that equation (3.40) is of the same form as (3.09).

---

[22] Mueller and Tyrrell, op. cit.

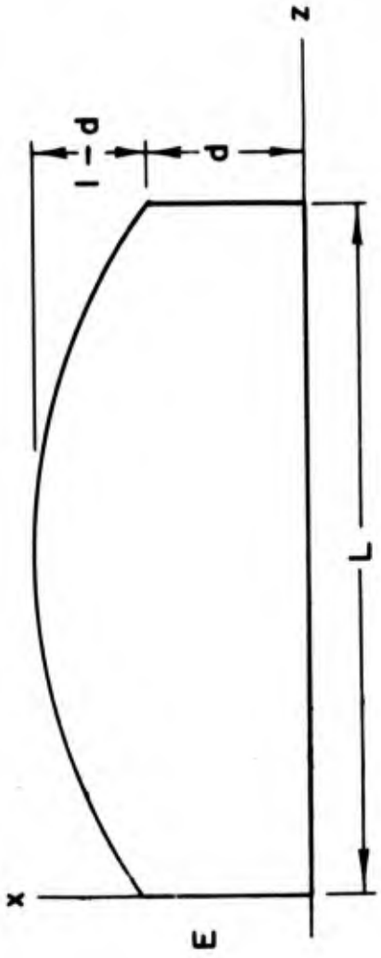

Fig. 3.05

Notation Used With The Shading Function.

It was mentioned that the integrals of (3.33) and (3.34) could be expressed as the product of two integrals, one of which was of the form of (3.35). The other integral may be evaluated if use is made of the formulas

$$I_1 = \frac{1}{2\pi}\int_0^{2\pi} e^{-jz \sin\theta \cos(\varphi-\varphi')}\, d\varphi' = J_0(z) \tag{3.41}$$

$$I_2 = \frac{1}{2\pi}\int_0^{2\pi} \sin(\varphi'-\varphi)\, e^{-jz\cos(\varphi'-\varphi)}\, d\varphi' = 0 \tag{3.42}$$

$$I_3 = \frac{1}{2\pi}\int_0^{2\pi} \cos(\varphi'-\varphi)\, e^{-jz\cos(\varphi'-\varphi)}\, d\varphi' = J_1(z)\,. \tag{3.43}$$

In order to obtain expressions for the radiation field of a dielectric rod excited in the TM_{0m} mode, use is made of equations (2.45) through (2.49) of Part Two. The notation is changed to agree with Figure 3.04.

$$E_\rho = \frac{h}{\omega\epsilon_1} H_{\varphi'} \tag{3.44}$$

$$E_{z'} = \frac{jp}{\omega\epsilon_1 b} J_0\left(p\,\frac{\rho}{b}\right) e^{-jhz' + j\omega t} \tag{3.45}$$

$$H_{\varphi'} = J_1\left(p\,\frac{\rho}{b}\right) e^{-jhz' + j\omega t} \tag{3.46}$$

$$E_{\varphi'} = H_\rho = H_{z'} = 0. \tag{3.47}$$

As before

$$p = \frac{\pi d}{\lambda_o} \sqrt{n^2 - n_a^2} \quad .$$

The radius of the cylinder over which the integration is performed is expressed as b instead of a, the radius of the rod, because it was found that agreement between theory and experiment could be obtained only if b were made less than a.

When equations (3.44) through (3.46) are inserted into equations (3.33) and (3.34), the following expressions for the field components are obtained:

$$E_r = 0 \tag{3.48}$$

$$E_\theta = - ja\omega\mu_2 J_1(p \tfrac{\rho}{b}) \left[J_0(k\, a \sin\theta) \sin\theta - \frac{1}{\omega\mu_2} \frac{k_2 p}{\omega\epsilon_1 b} \frac{J_0(p \frac{\rho}{b})}{J_1(p \frac{\rho}{b})} J_1(k\, a \sin\theta) \right] I_S \Psi \tag{3.49}$$

$$E_\varphi = 0. \tag{3.50}$$

In the measurement of antenna patterns the distance r is held constant while θ is varied. The quantity which is measured is the relative value of the time average of E_θ^2. Therefore for comparison with experimental data, the expression E_θ may be written as

$$E_\theta = 20 \log \left\{ \left| J_0(k\, a \sin\theta) \sin\theta - \frac{1}{\omega\mu_2} \frac{k_2 p}{\omega\epsilon_1 b} \frac{J_0(p \frac{\rho}{b})}{J(p \frac{\rho}{b})} J_1(k\, a \sin\theta) \right| \cdot \left| I_S \right| \right\} \tag{3.51}$$

$$E_\theta = 20 \log \left| I \right| + 20 \log \left| I_S \right| \qquad (3.52)$$

It may be noted that the factor $\frac{k_2 p}{\omega^2 \mu_2 \epsilon_1 b} \frac{J_0(p \frac{\rho}{b})}{J_1(p \frac{\rho}{b})}$ is equivalent to the peak amplitude of E_z, divided by the peak amplitude of H_φ, and the impedance of the space exterior to the rod.

CHAPTER IV

MEASUREMENT OF ANTENNA CHARACTERISTICS

1. Radiation Characteristics. The characteristics of an antenna or radiating system which are of primary interest are: (1) gain, (2) effective area or absorption cross section, (3) power distribution and requirements, (4) phase distribution, (5) impedance and bandwidth, and (6) polarization. The equipment and techniques used to obtain the information are discussed in this chapter.

Measurements of radiated electromagnetic energy may be made either in the Fresnel (or near) zone or in the Fraunhofer (or far) zone, The transition from one zone to the other is gradual but a point in space is generally considered to be in the far zone if the energy from each element of the aperture of the source arriving at this point in space essentially comes from the same direction. That is, a plane wave front arrives at the receiver. However, if the energy from each element of the aperture of the source appears to arrive from a different direction, the point is said to be in the Fresnel zone. By stating certain limits on the accuracy of measurements, a definite boundary between zones may be defined. Consider the receivers and transmitter shown in Figure 3.06, separated by the distance R. D is the maximum dimension of the receiving antenna.

$$\frac{R}{R + X} = \cos \theta \qquad (3.53)$$

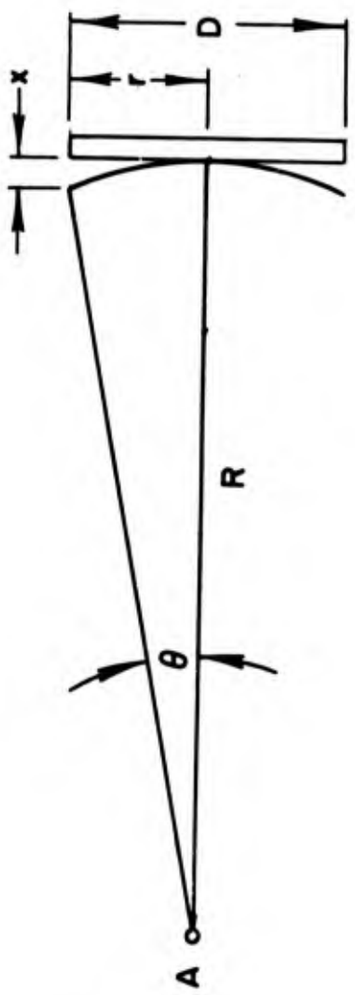

Fig. 3.06 – Diagram Indicating Phase Error Due To A Spherical Wave.

where X is the difference in distance between the center and edge of the receiving antenna.

(3.53) may be rewritten as

$$X = R (\sec \theta - 1) \tag{3.54}$$

or in terms of the phase error,

$$\Phi = \frac{2\pi R}{\lambda_o} (\sec \theta - 1). \tag{3.55}$$

For small values of θ, using only the first two terms of the series expansion, (3.55) becomes

$$\Phi \doteq \frac{2\pi R}{\lambda_o} \left[1 - 1 + \frac{1}{2} \frac{r}{R}^2 \cdot \cdot \cdot \cdot \right] \doteq \frac{\pi r^2}{\lambda_o R} \tag{3.56}$$

or

$$\Phi \doteq \frac{\pi D^2}{4\lambda_o R} . \tag{3.57}$$

It has been found from experiments that the maximum allowable value of phase error was approximately $\lambda_o/8$. Substituting this value for Φ in equation (3.57) yields

$$R = \frac{(D^2)}{\lambda_o} \tag{3.58}$$

as the boundary between the near and far zones. Since normally the receiving and transmitting antennas in radio circuits will be widely separated, the far zone radiation is of the most importance.

The gain of an antenna is a measure of its effectiveness in concentrating power. There are several special definitions of gain, but the most universal is "absolute gain" which is the ratio of peak

intensity of the given antenna to the intensity of an isotropic radiator when both are radiating the same total power, or

$$G = \frac{P}{P_o} \tag{3.59}$$

where P is the power flow per unit area and P_o is the power flow per unit area if all of the area were radiated energy uniformly.

The effective area is defined as

$$A = \frac{P_R}{P'} \tag{3.60}$$

where P_R is the received power at the antenna and P' is the power per unit area in the incident wave. It can be shown[23] that the effective area and gain are related by

$$G = \frac{4\pi A}{\lambda_o^2} \tag{3.61}$$

Since a true isotropic radiator is not available, other means must be used to determine the absolute gain. Several methods have been developed and the one used in this work will be described briefly.[24,25] The reciprocity method of gain determination has become widely used in the past several years.[26] This method makes use of the reciprocal property of antennas. Consider a radio circuit consisting of a transmitting antenna A and a receiving antenna B. Using equations

---

[23] Slater, J. C., Microwave Transmission, McGraw-Hill Book Co., New York, p. 258, 1942.

[24] Silver, S., Microwave Antenna Theory and Design, Radiation Laboratory Series, McGraw-Hill Book Co., New York, 12, 1949.

[25] Montgomery, C. G., Technique of Microwave Measurements, Radiation Laboratory Series, McGraw-Hill Book Co., New York, 11, 1947.

[26] Watson, R. B., and McKinney, C. M., "Gains and Effective Areas of Horn Antennas," J. App. Phys., 19, 871, October 1948.

(3.59), (3.60), and (3.61), the following relation is obtained

$$P_R = PA_B = \frac{P_T G_A A_B}{4\pi R^2} = \frac{P_T G_A G_B \lambda_o^2}{16\pi^2 R^2} \tag{3.62}$$

where R is the distance separating antennas A and B. Replace the terms P_R by P_B and P_T by P_A in order that all of the subscripts will refer to particular antennas. Then

$$P_B = P_A \frac{G_A G_B \lambda_o^2}{16\pi^2 R^2} \quad . \tag{3.63}$$

Now replace antenna B with a third antenna C. Denote the received power of C by P_C. Then

$$P_C = \frac{P_A G_A G_C \lambda_o^2}{16\pi^2 R^2} \quad . \tag{3.64}$$

Now replace the transmitting antenna A with antenna B. Antenna C will receive a different power now, which is denoted by P'_C. The power transmitted by antenna B is denoted by P'_B. Then

$$P'_C = P'_B \frac{G_B G_C \lambda_o^2}{16\pi^2 R^2} \quad . \tag{3.65}$$

Use equations (3.63), (3.64), and (3.65) to eliminate G_B and G_A. Then

$$G_C = \frac{4\pi R}{\lambda} \left(\frac{P_C P'_C}{P_B P'_B} \right)^{\frac{1}{2}} \quad . \tag{3.66}$$

Equation (3.66) gives the gain of antenna C in terms of power level at the transmitter and receiver and is independent of the gain of the auxiliary antennas A and B.

Intensity distribution patterns show the relative amounts of power passing through unit solid angle over the surface of an arbitrar sphere whose center is the aperture of the radiating system. Characteristics of the radiation pattern are determined by the dimensions of the aperture and the distribution of illumination and phase over the aperture.

To obtain a complete knowledge of intensity distribution, a test probe or antenna would have to be moved over the entire surface of a sphere about the antenna under test. However, it is usually considered sufficient to measure the intensity only in two planes; one passing through the antenna and lying in the plane of the electric vector of the field and the other passing through the antenna and lyin in the plane of the magnetic vector. These two planes are called the E-plane and H-plane respectively. The patterns in these two planes are usually sufficient to show the nature of the radiation pattern. If the radiation is rotationly symmetrical, one plane is sufficient.

To obtain a radiation pattern the receiving antenna is oriented so that its polarization coincides with that of the transmitting antenna. The receiving antenna must always remain a constant distance from the radiating antenna and must always be directed toward it so as to subtend a constant solid angle. Either of the two antennas can be rotated about the axis through the center of the aperture of the antenna under test. It is a matter of convenience which one is moved,

but if the separation between antennas is large, it is, of course, more convenient to rotate the antenna under test. It is easy to determine the axis of rotation for horn antennas, dipoles, etc., but not for linear end-fire arrays such as dielectric rods. However, phase measurements may be made and the center of phase (or center of rotation) may be determined. However, if the separation of antennas is sufficiently large so that an essentially plane wave arrives at the antenna, the axis of rotation is not critical. Radiation patterns made under this condition are known as secondary patterns[27] and are used for all types of measurements except in case of sources used to illuminate other arrays such as parabolic reflectors. Only secondary patterns were measured for the dielectric antennas used in this project.

Due to the reciprocal properties of antennas, the antenna under test may be used either as transmitter or receiver.

Intensity patterns should be made under free space conditions. That is, the antenna under test should be isolated from other objects and materials as far as possible. It has been mentioned that the error in phase front arriving at the antenna under test should not exceed $\lambda_o/8$. This requirement is met if measurements are made in the far zone only. That is

$$R \equiv \frac{D^2}{\lambda_o} \tag{3.67}$$

Using this requirement, the difference in power levels over the different parts of the antenna, due to the spherical divergence of

---

[27] Silver, op. cit., p. 574.

the wave, may be calculated. For a spherical aperture, the ratio of the power received from a spherical wave, to that received from a plane wave, in given by[28]

$$\frac{P_S}{P_P} = \frac{\left|\int r \cos\varphi \, dr\right|^2 + \left|\int r \sin\varphi \, dr\right|^2}{\left|\int r \, dr\right|^2} \quad . \tag{3.68}$$

For the edge of the apertures (D/2, from center), this ratio is approximately

$$\frac{P_S}{P_P} \doteq 1 - \frac{1}{12}\left(\frac{\pi}{4}\frac{D^2}{\lambda R}\right) \tag{3.69}$$

For the minimum separation distance

$$R = \frac{D^2}{\lambda} \tag{3.70}$$

which reduces to

$$\frac{P_S}{P_P} \doteq 1 - \frac{\pi^2}{12.16} \doteq 0.95 \quad . \tag{3.71}$$

For a non-circular antenna, with a maximum linear dimension of D, the power loss is less than that calculated above. Also, if the illumination is "tapered" so that the power radiated at the edge is less than that elsewhere, the power loss is again diminished.

---

[28] Montgomery, op. cit., p. 902.

The power requirements for the antenna system are readily calculated, using equation (3.62).

$$\frac{P_R}{P_T} = \frac{G_T G_R \lambda_o^2}{16\pi^2 R^2} \quad . \tag{3.72}$$

This equation gives the power loss due to radiation and should be calculated using the lowest gain antenna that will be tested, together with the antenna which will be used with the antenna under test. To the power requirements calculated from equation (3.72) must be added power losses in transmission lines connecting the antennas to the signal sources and receiver. This power requirement is based on the maximum gain of the antenna under test. To this power requirement, must be added the differential power level between the maximum gain of the antenna and the level of the weakest signal which it is desired to measure. A differential power level of 50 db is sufficient to measure in good detail the minor lobes of most radiation patterns.

In general, it is necessary to know the load impedance presented by an antenna in order that it may be properly matched to the transmission line. Actually only the normalized impedance is desired, that is, the ratio of the load impedance to the line impedance. This information can be obtained from measurements of the standing wave ratio on the transmission line due to reflection from the load, and the location of a null or minimum on the transmission line with respect to the antenna.[29] If the impedance is known, a proper matching device may be

[29] Montgomery, op. cit., Chapter 8.

designed for the load. Unfortunately such matching usually must be done by experiment because of the difficulty in deciding from which point of the antenna the distance to the null on the transmission line should be measured. In the work of this project, except for gain measurements, impedance matching was not important and consequently it was simpler to match the antenna with an adjustable probe transformer for the gain measurements.

Bandwidth of dielectric antennas, or the change in impedance as a function of frequency, is not of great importance since it has been demonstrated[30] that the bandwidth of dielectric rod antennas is limited, not by the antenna itself, but by the metallic feeding line used to excite the antenna.

Polarization of a plane wave may be determined by orienting a test antenna for either maximum or minimum received signal strength. From a knowledge of the test antenna, the polarization of the wave may be determined.

2. Apparatus. The apparatus used in this project to measure the radiation properties of antennas will now be described and it will be shown that the arrangement of equipment satisfies the requirements described in this chapter.

Figure 3.07 shows a block diagram of the arrangement of the equipment. The power source was a transmitter using a type 723 A/B

---

[30] Mueller and Tyrrell, op. cit.

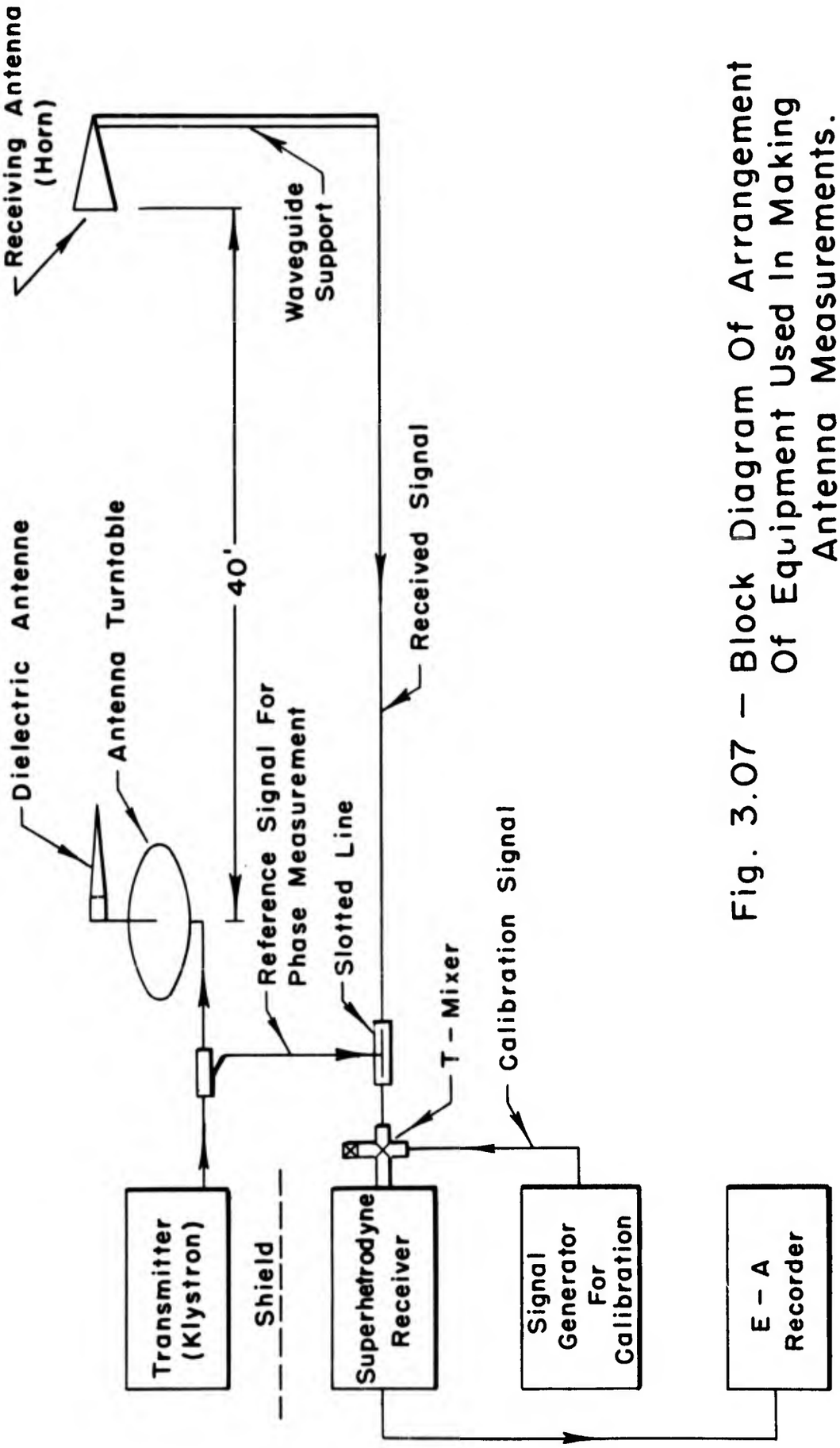

Fig. 3.07 – Block Diagram Of Arrangement Of Equipment Used In Making Antenna Measurements.

Reflex Klyston tube as the oscillator.* The transmitter had a peak power output of approximately 5 watts and an average power of 0.01 watt. The output was in the form of 2000 one-microsecond pulses per second. The frequency was adjusted to 9375 mcps or a wavelength of 3.20 cm. The receiver which was used was of the superheterodyne type. It was designed by Radiation Laboratory of Massachusetts Institute of Technology. The output of the receiver was proportional to the logarithm of the input power; that is, the output was approximately linear in db.

The output of the receiver was calibrated more accurately by means of the calibrated attenuator whic is an integral part of the type TS-13 signal generator. The TS-13 signal generator was operated at the same pulse repetition frequency and the same pulse width as the beacon transmitter. This was essential for accurate calibration. The output signal from the receiver was applied to an Esterline-Angus recorder, type AW. The recorded pattern was of the usual "curved" rectilinear type. The turntable, by means of which the antenna being tested was rotated, is shown in Figure 3.08.** It was mounted on ball bearings and was driven by a synchronous motor. This motor, with a speed of 1800 RPM was coupled to the turntable through suitable reduction gears. A turntable speed of one degree per second was found to be satisfactory for most antenna patterns when used with the

---

*The power supply for the transmitter was designed and constructed by Mr. Alfred Davis of the Defense Research Laboratory, The University of Texas.

**The turntable was designed by Mr. C. C. Johnson of the Defense Research Laboratory, The University of Texas.

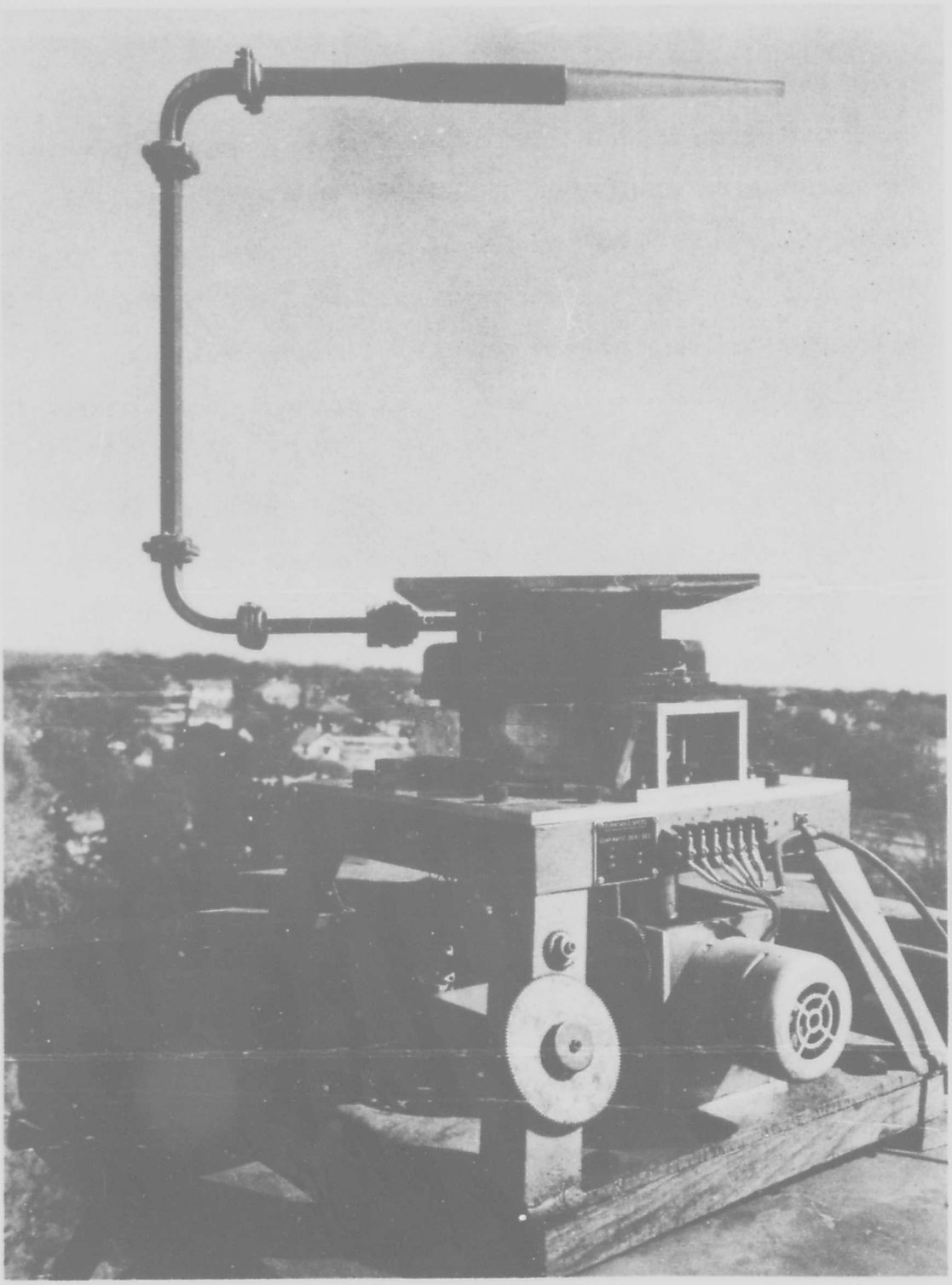

Figure 3.08
Antenna Turntable And Typical
Dielectric Rod Antenna

Esterline-Angus recorder. The antenna being tested was supported only by a section of 1-inch by 1/2-inch waveguide which transmitted the energy from the transmitter to the antenna. The antenna was mounted at least $10\lambda_o$ above the turntable. The turntable itself was mounted on a platform which was 12 feet above the roof of the building on the top of which the measurements were made.. In all of the measurements the antenna being tested was used as the transmitting antenna. The receiving antenna was a conical horn with a gain of 80. This antenna was supported also only by a 1-inch by 1/2-inch waveguide. By using supports of relatively small cross section, the diffraction due to the supports was minimized. The transmitting and receiving antennas were separated by 40 feet or approximately 385 wavelengths.

By means of equation (3.57) the error in phase at the extremity of the longest antenna used may be calculated.

$$\Phi = \frac{\pi D^2}{4\lambda R} = \frac{\pi \times 100}{4 \times 385} = 0.202 \text{ radian} = \frac{\lambda_o}{20.8} \qquad (3.73)$$

which is well within the tolerable limit, even for the longest antenna used.

The error in the intensity of power at the extreme end of the longest antenna may be calculated from equation (3.69),

$$\frac{P_S}{P_P} \doteq 1 - \frac{1}{12}\left(\frac{\pi D^2}{4\lambda R}\right) = 0.983 \qquad (3.74)$$

which is also well within acceptable limits, especially in the case

of end-fire arrays of the dielectric rod type, in which very little radiation takes place at the extreme end.

The power requirements of the system may be calculated from equation (3.62).

$$\frac{P_R}{P_T} = \frac{G_T G_R \lambda_o^2}{16\pi^2 R^2} \quad . \tag{3.75}$$

The gain of the receiving antenna was found to be 80 while the lowest gain of the dielectric rod antennas was approximately 15 db. or 31. Substituting these values into (3.75) yields

$$\frac{P_R}{P_T} = 132 = 21 \text{ db.} \tag{3.76}$$

To this figure should be added 14 db. due to loss in transmission lines and 50 db. which is the range of power levels which are desired. The total power requirements are then seen to be approximately 70 db. or a power ratio of 10^7. Since the transmitter has an average power output of 10^{-2} watts and the receiver has a sensitivity of 10^{-14} watts, it is seen that this combination of receiver, transmitter, and antennas is acceptable.

The apparatus for the measurement of gain was the same as that shown in Figure 3.07. To conserve time, the gain of a pyramidal horn antenna of the type AT-48 was determined accurately by the reciprocity method and then the gains of the dielectric antennas were determined in terms of this horn antenna. The calibration of gain measurements

was made by means of the attenuator in the TS-13 signal generator. Antenna gain measurements were made using the HE_{11} mode only.

The horn used as the receiving antenna had an aperture diameter of $3.6\lambda_o$. This aperture corresponded to a subtended angle of 0.5^o, which means that the error in pattern resolution was not greater than 0.5^o, which was within the accuracy desired.

It was mentioned earlier in this chapter that phase measurements were not of great importance in the present project. However, the equipment for phase measurements was constructed and is included in the block diagram of Figure 3.05. The phase of the received signal was compared with the phase of a reference signal obtained directly from the transmitter. This reference signal was inserted, by means of a small probe antenna, into the waveguide which connected the receiving antenna to the receiver. A long slot was cut in the broad face of the waveguide so that the position of the insertion probe could be varied. The position and penetration of the probe were adjusted such that the power level of the reference signal was approximately the same as the received signal and at such a point as to cancel the received signal. In other words, the probe was adjusted for minimum received signal strength. If the position of this probe for a null remained fixed as the antenna was rotated, the rotation was about an axis through the center of phase.

Several points should be mentioned in regard to phase measurements. The reference signal inserted into the waveguide radiates in both directions in the guide. In this project, the radiation toward

the receiving antenna was not serious, because the attenuation in the long coaxial and waveguide transmission line reduced reflections from the receiving antenna to a very low value. However, in other applications a serious difficulty might arise due to the reflected wave. The alternate method shown in Figure 3.09 would eliminate this difficulty. The phase shifter, which could be one of several available types, could be calibrated directly in phase shift. By means of the magic T junction, the energy from the receiver and from the transmitter could be coupled without interaction. This method has been tried and worked satisfactorily.

3. Measurements of Electric Fields on the Surfaces of Dielectric Radiators. It was desirable to know something of the field distribution on the surface of the dielectric rod radiators in order to predict and understand the radiation patterns. Figure 3.10 shows a block diagram of the equipment used for these measurements. It is essentially the same as that described in Chapter IV of Part Two, for field measurements, except no reflector is used. Thus the situation is approximately that of the antenna radiating into space. In general, the only measurements necessary were of E_r as a function of z and perhaps the field across the end face of the rods. From these measurements one can determine the apparent index of refraction, variation of intensity of feed with distance along the rod and usually the modes present. Figure 3.11 is a photograph of the apparatus.

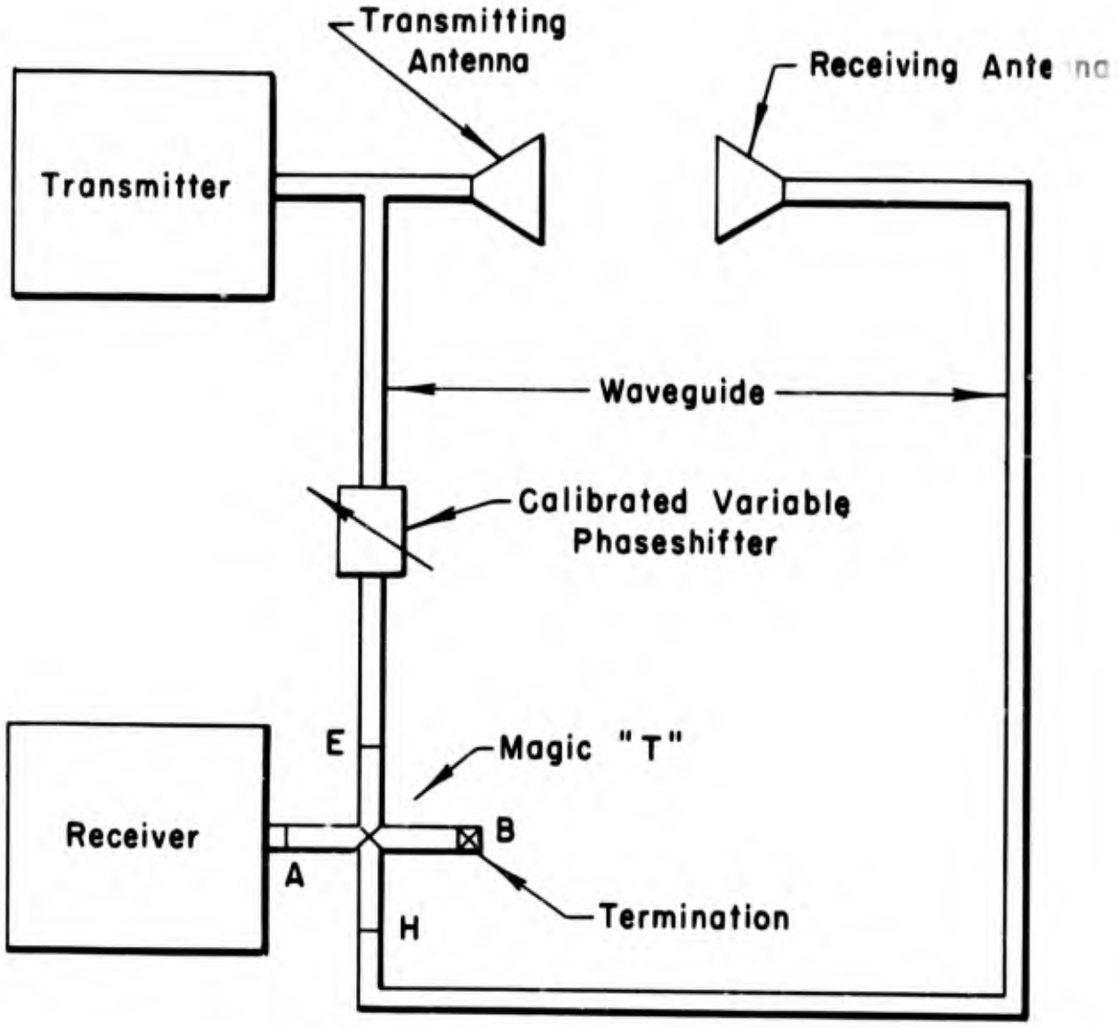

Fig. 3.09 – Block Diagram Of Phase Measuring Equipment.

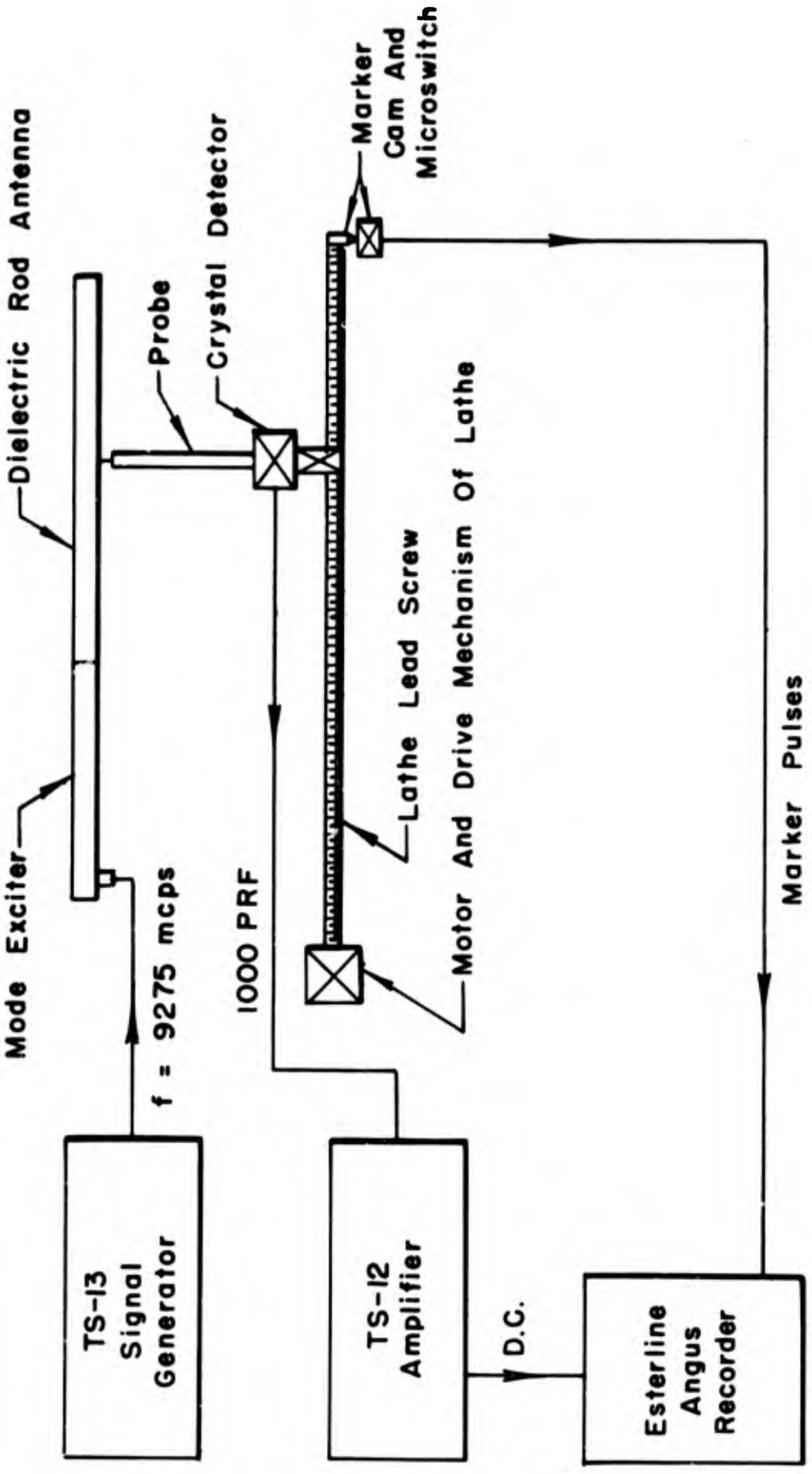

Block Diagram Of Apparatus Used To Measure Electric Fields On The Surfaces Of Dielectric Rods

Fig. 3.10

DRL - UT
DWG AE 805
CMM - CLW
1 - 13 - 50

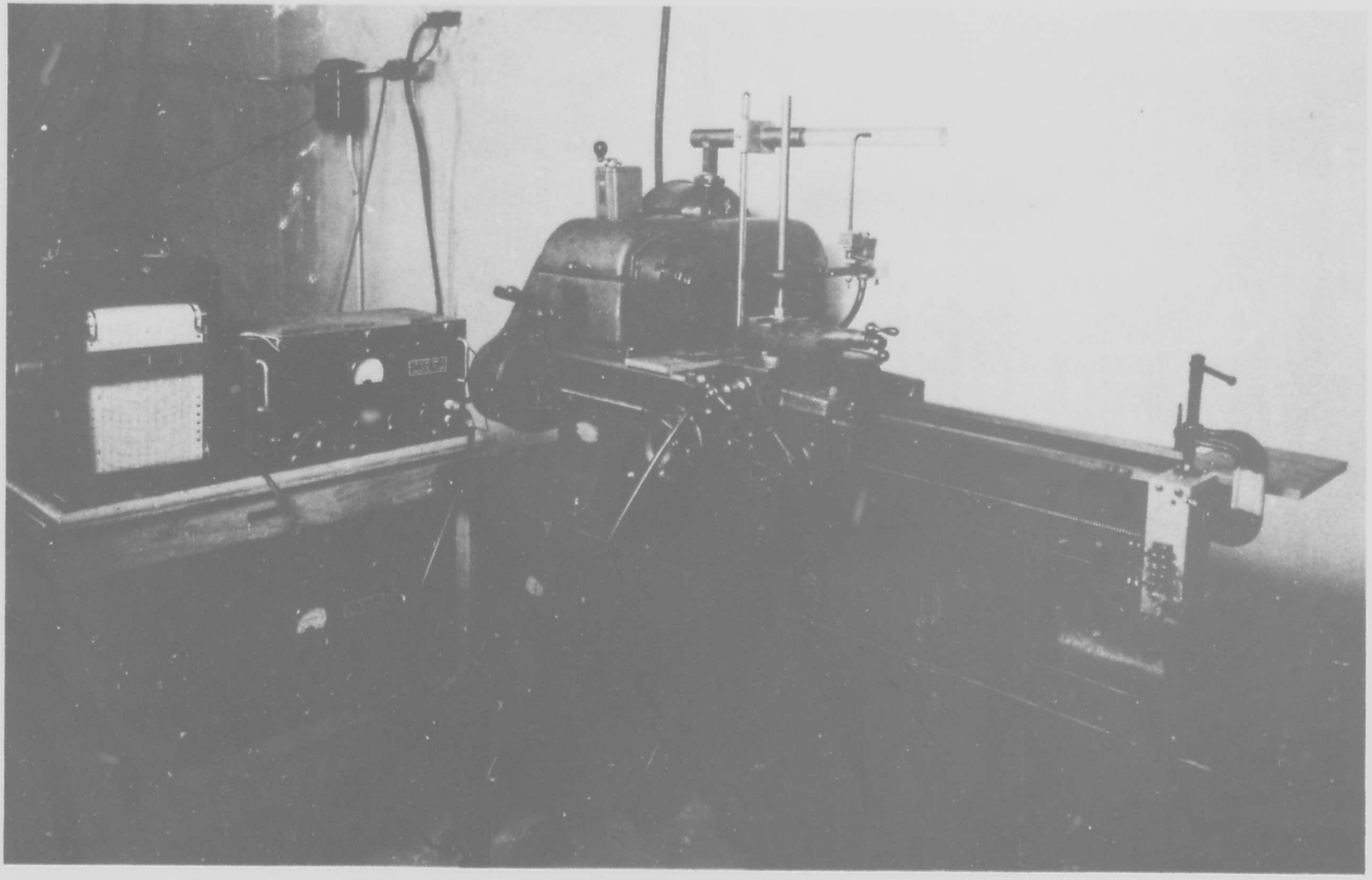

Figure 3.11
Equipment Used In The Measurement Of The Electric Field On The Surface Of A Dielectric Rod Antenna

CHAPTER V

DATA AND DISCUSSION OF MEASUREMENTS

1. Description of the Dielectric Radiators. The longitudinal sectional views of the antennas (dielectric radiators) used in this investigation are shown in Figure 3.12. The taper on the left end of each rod (3" long) and the 2" uniform section were located inside the metal waveguide which was used to excite the desired mode in the dielectric rods. The tapered section was used to suppress reflections of the wave at the interface between the air and the dielectric. This was accomplished since the effective index of refraction of the dielectric changed gradually from 1 (at the point) to the particular value of dielectric constant of the material (at the uniform diameter section). The uniform section was used both for mechanical support and alignment and to allow the wave to travel some distance in the new medium without discontinuities. The section of the rods which extended outside of the metal guide was the only part considered as the dielectric antenna. Series-F was composed of rods of uniform cross section and lengths varying from 2 to $10\lambda_o$. The material was Lucite ($K = 2.56$), and the diameter was $0.870\lambda_o$. Series-G was identical except the diameter was $0.596\lambda_o$.

The F-Series was designed primarily to be used with the TM_{01} mode since it was of sufficient diameter to support the first order radial mode but not the second. However, for the HE_{11} mode, the

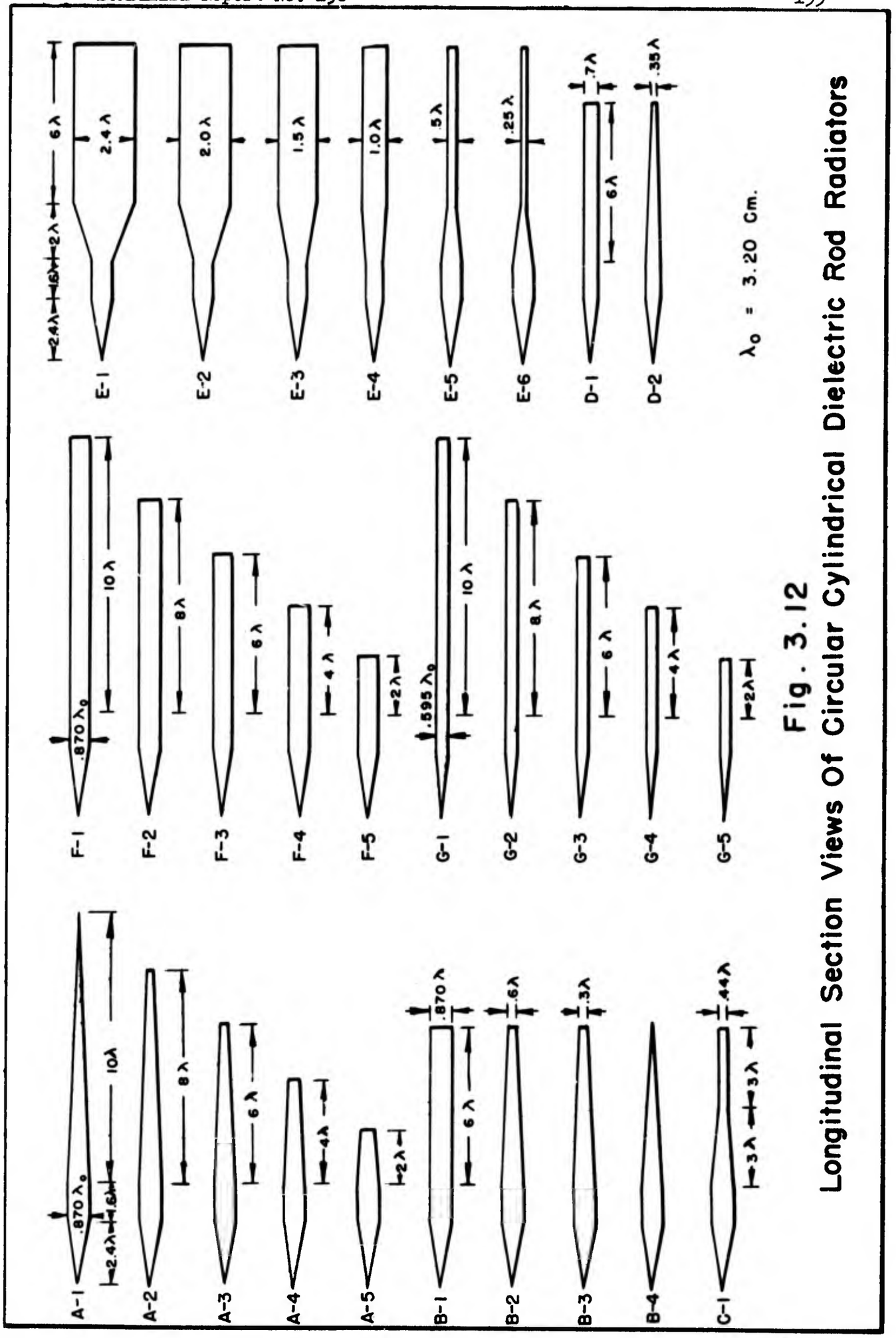

Fig. 3.12

Longitudinal Section Views Of Circular Cylindrical Dielectric Rod Radiators

DRL - UT
DWG AE 659
CMM - CLW
7 - 11 - 49

F-Series rods propagated some second order radial modes and the resulting radiation patterns were not as easy to interpret. Series-G was designed primarily for the HE_{11} mode since it was too small to propagate the second order modes. For gain measurements, a second series, identical to the F-Series was made, except the material was polystyrene, with a lower loss than Lucite. It was designated Series-H.

Series-E was designed to show a variation only in diameter ($0.25\lambda_o$ to $2.4\lambda_o$). In order to excite these rods from available metal guides, another tapered section was used which was $2\lambda_o$ long. A metal foil shield was used to prevent radiation from this tapered section. The uniform section then approximated a uniform rod extending from a metal guide. Some higher modes were excited in this transition, however. Measurements were also made with this tapered section unshielded, but it is difficult to attribute changes in the radiation pattern to variation in diameter. The material used was polystyrene. It should be noted that these particular series of antennas were not designed to be "good antennas" since no effort was made to obtain good impedance match, but they were designed so that only one parameter changed at a time. Series-A was designed to determine the effect of rod length with a constant taper. The ratio of maximum diameter to minimum diameter was also variable. Series-B should give the effect of changing the ratio d_{min}/d_{max} of maximum diameter to minimum diameter for constant length. The C-Series consisted of three rods, all of the identical shape, but constructed of different materials. The rods had a uniform taper from maximum

diameter at one end to half-maximum diameter at midpoint of the length. The other half-length was of uniform half-maximum diameter. The materials used were polystyrene, Lucite, and Bakelite.

The D-Series consisted of two rods made and tested to measure the effect of tapering on rods of smaller diameter than the B-Series.

Tapering of rods is useful for two reasons. First, the gradual changing of cross section acts as a matching transformer between the impedance of the metal waveguide (or a uniform transmission line rod) and the impedance of free space. Likewise, it has been shown by others that tapering effectively changes the amplitude of feed voltage and can thus be used to reduce side lobe intensity and reduce the beam width.

Figures 3.13 and 3.14 show the notation used in the analysis of the radiation patterns. Width of major lobe, beam width, lobe position and relative lobe intensities have been graphed as functions of length, diameter, and taper.

The dimensions of the dielectric rods given in Figure 3.12 are approximate only. Table II gives all of the dimensions of the rods to three figures.

It is in order to discuss the accuracy of the measurements of the radiation properties of the dielectric rod antennas. The following discussion is of a general nature and applies to all of the radiation measurements.

The variation in the signal level at the receiver, which was due to a combination of frequency drift of both transmitter and receiver and to changes in power level of the transmitter, was measured to be less than $\pm$ 0.5 db. over periods of time of approximately fifteen

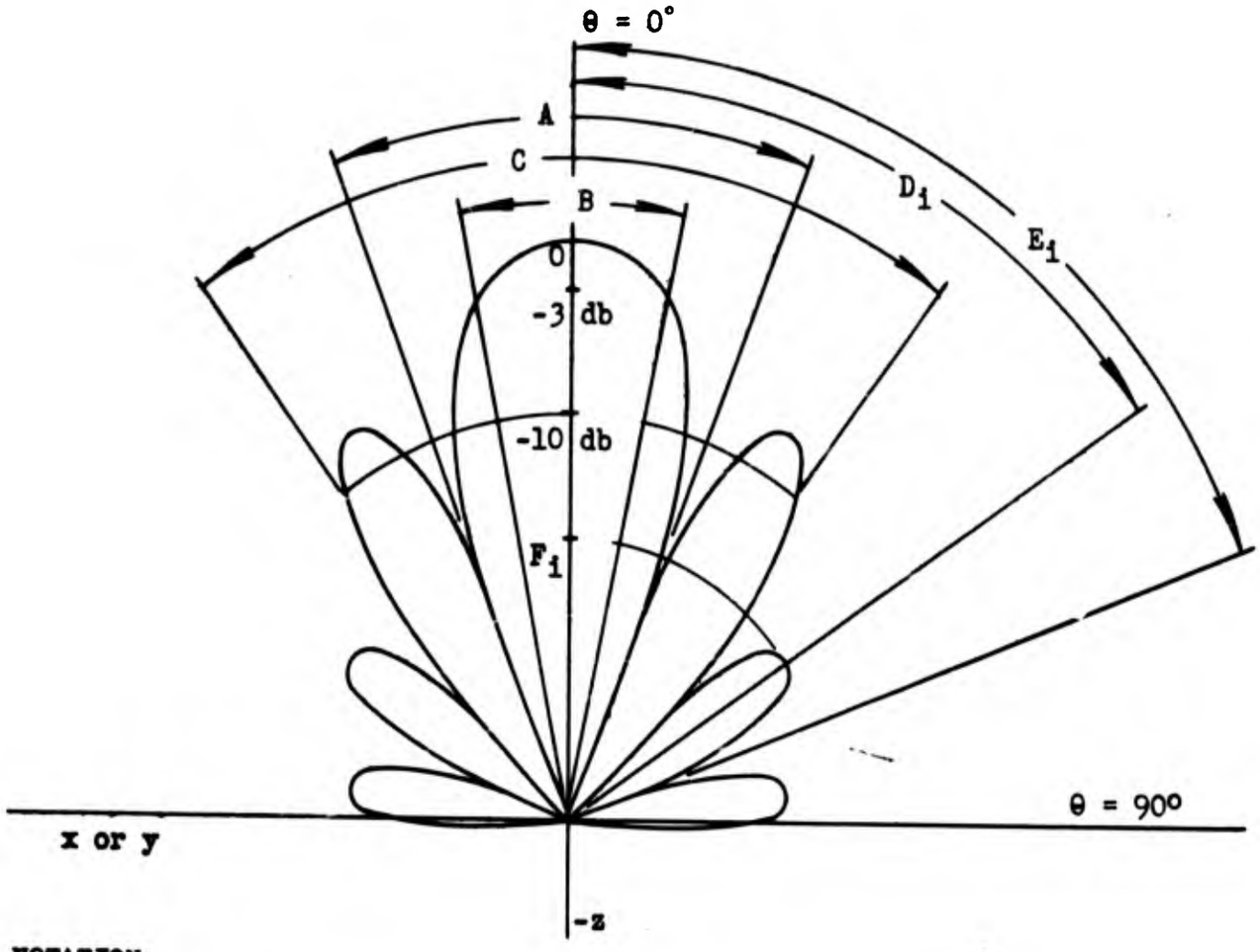

NOTATION:

A Width of major lobe in degrees.

B Half power beam width.

C Tenth power beam width.

D_i Angular position of maximum intensity of i th lobe measured in degrees from θ = 0.

E_i Angular position of the i th null measured in degrees from θ = 0.

F_i Maximum intensity of i th lobe in db. below the maximum intensity of the major lobe.

i Index with values of 1 to n where n is the number of lobes or nulls in the range of θ = 0 to θ = 180° of the radiation pattern.

Fig. 3.13 Notation Used with Radiation Patterns with Maximum Radiation in the Forward Direction

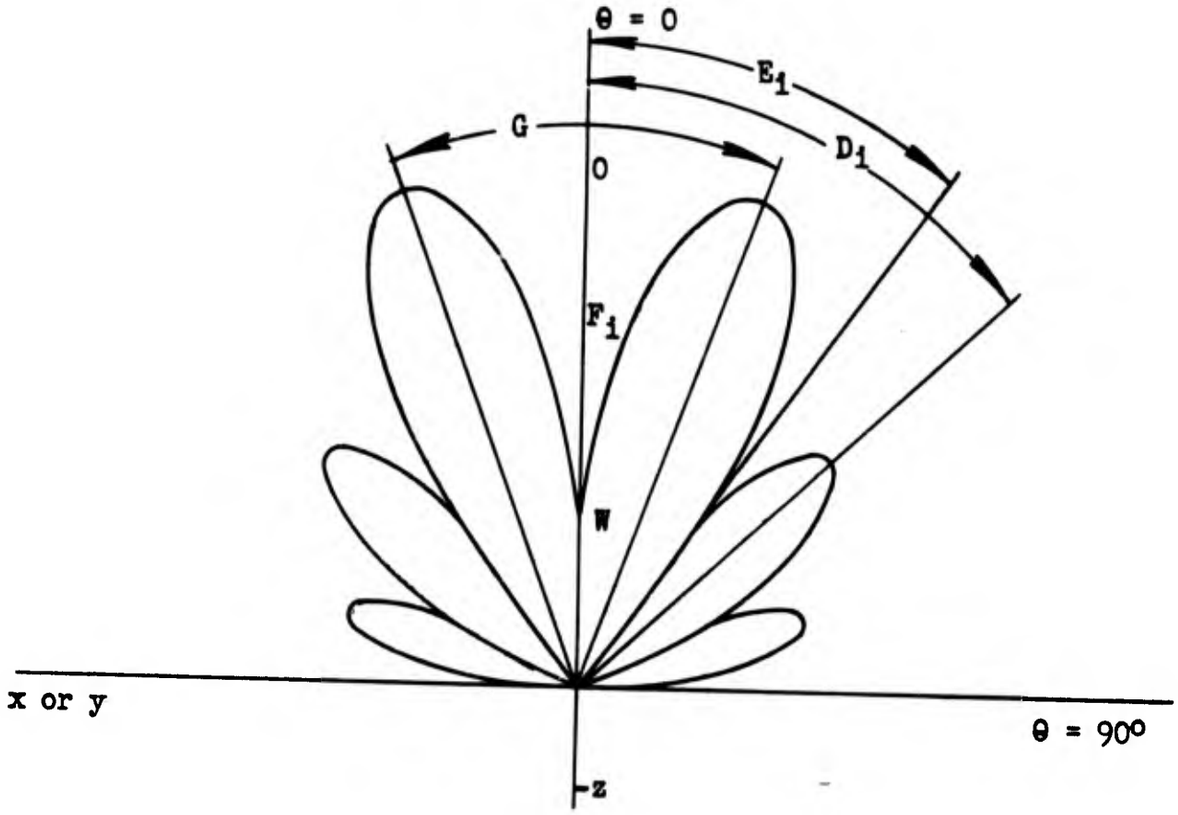

G Width of major null in degrees.

W Intensity of major null in db. below maximum intensity of the major lobes, O.

Other notation is the same as in Fig. 3.13.

Fig. 3.14

NOTATION USED WITH RADIATION PATTERNS WITH A NULL AT POSITION θ = O.

TABLE II

SPECIFICATIONS ON THE DIELECTRIC ROD ANTENNAS

λ_o = 3.20 cm

Rod	Maximum d/λ_o	Minimum d/λ_o	L/λ_o	Material	Dielectric Constant	tan δ
A-1	.870	.000	10.00	Lucite	2.56	.01
A-2	.870	.273	8.00	"	2.56	.01
A-3	.870	.409	6.00	"	2.56	.01
A-4	.870	.558	4.00	"	2.56	.01
A-5	.870	.719	2.00	"	2.56	.01
B-1	.870	.870	6.00	"	2.56	.01
B-2	.870	.595	6.00	"	2.56	.01
B-3	.870	.310	6.00	"	2.56	.01
B-4	.870	.000	6.00	"	2.56	.01
C-1	.870	.400	6.00	"	2.56	.01
C-2	.870	.400	6.00	Polystyrene	2.56	.001
C-3	.870	.400	6.00	Bakelite	4.00	.05
D-1	.696	.696	6.00	Textolite	2.50	.001
D-2	.696	.350	6.00	"	2.50	.001
E-1	2.406	2.406	6.00	Polystyrene	2.56	.001
E-2	2.009	2.009	6.00	"	2.56	.001
E-3	1.488	1.488	6.00	"	2.56	.001
E-4	.992	.992	6.00	"	2.56	.001
E-5	.496	.496	6.00	"	2.56	.001
E-6	.248	.248	6.00	"	2.56	.001
F-1	.870	.870	10.00	Lucite	2.56	.01
F-2	.870	.870	8.00	"	2.56	.01
F-3	.870	.870	6.00	"	2.56	.01
F-4	.870	.870	4.00	"	2.56	.01
F-5	.870	.870	2.00	"	2.56	.01
G-1	.598	.598	10.00	"	2.56	.01
G-2	.598	.598	8.00	"	2.56	.01
G-3	.598	.598	6.00	"	2.56	.01
G-4	.598	.598	4.00	"	2.56	.01
G-5	.598	.598	2.00	"	2.56	.01
H-1	H-Series of Rods			Polystyrene	2.56	.001
H-2	are the same shape			"	2.56	.001
H-3	as the F-Series			"	2.56	.001
H-4				"	2.56	.001
H-5				"	2.56	.001

minutes. The time required to make a complete radiation pattern was six minutes so there was probably very little error in the measurements due to the above causes. Occasionally the tuning of the receiver drifted completely out of range of the transmitter, but this always occurred very suddenly and the change in signal level was such that the error was noticed immediately.

At least two complete radiation patterns were measured for each antenna for each mode of excitation and in each plane for which data were desired. The position and intensity of each lobe was measured and an average taken of the corresponding lobes on the right and left side of the forward direction. The magnitude of the errors, which is discussed below was based on the differences in the measured values of position and intensity for the right and left lobes.

The accuracy in the calibration of the recorder was limited to $< \pm 0.5$ db. The position could be measured on the chart with an error of less than $\pm 0.5^{\circ}$.

The most accurate data were obtained on rods which were propagating only one mode. The positions of maxima could be determined most accurately on the pattern with many lobes (corresponding to long antennas) since the lobes were sharpest and most distinct in those cases. It was also found that the error was largest in the region directly back of the antenna ($\theta \doteq 180^{\circ}$).

The following figures are typical of the error in position intensity. On the G-Series excited in the HE_{11} mode, the average error in position was less than $\pm 0.25^{\circ}$ with a maximum variation

of $\pm$ 1.0°. The average error in intensity was less than $\pm$ 0.5 db. with a maximum error of $\pm$ 1.0 db. The error in position of measurement of the F-Series for both TM_{01} and HE_{11} modes was an average of $\pm$ 0.5° with a maximum error of $\pm$ 1.0°. The error in intensity was a little greater for the F-Series than for the G-Series. The average value of deviation was less than $\pm$ 0.75 db. with a maximum value of $\pm$ 2.5 db.

The E-Series antennas excited in the TM_{01} mode are typical of measurements on antenna radiating from more than one mode of excitation. The E-1 rod, with a diameter of $2.4\lambda_o$, had the maximum error with an average value of $\pm$ 1.0° in position and $\pm$ 2.0 db. in intensity. The maximum value of error was $\pm$ 2.5° and $\pm$ 4.0 db. The error in data for the smaller rods was considerably less than those for the E-1 rod.

2. Dielectric Rods Excited in the Dominant Mode (HE_{11}). As has already been mentioned, the dominant mode is used almost exclusively to excite dielectric rod antennas because of its particular type of pattern. Previous theoretical analysis, which has been amply verified by experiment, shows that the dielectric rod when excited in the dominant mode has maximum radiation in the forward direction and thus is especially suited for such applications as radar and point to point communication, which are the primary uses of microwave energy. The investigation of dielectric antennas excited in this dominant mode is primarily a verification of the work of others and an extension of range of parameters over those previously published.

The field configuration and equations of the HE_{11} mode in the dielectric waveguide have been given in Part Two. The fields are essentially the same in the dielectric rod antennas.

The rods were excited from the metallic waveguides described in Part One, and the technique and equipment used in obtaining radiation patterns, gains, etc., are described in Chapter IV of this Part. Radiation patterns were taken in the plane in which electric vector lies (E-plane) and in the plane in which the magnetic vector lies (H-plane).

The radiation intensity patterns for the F-Series for both and H planes are shown in Figure 3.15. The F-Series consists of five rods with a uniform diameter of $0.870\lambda_o$ and lengths of 2,4,6, and $10\lambda_o$. Notation is that shown in Figure 3.13. The patterns are plotted here for only $\theta = 0$ to 90^o since this is the region of primary importance. Of course, the pattern is symmetrical about $\theta =$. At least two patterns were taken of each antenna for each plane. The patterns shown and data taken from them are the average of two or four values, two right and two left. If there were any significant differences in successive patterns for the same antenna, more data were taken in order to reduce error. The linear db. scale used here (or logarithm of power) makes the secondary lobes appear unusually large but does allow more detail of secondary lobes than is usually shown in radiation patterns.

The total number of lobes in the radiation pattern are shown in Figure 3.16. It is seen from this Figure that the number of lobes is a linear function of rod length. The total width of the major lobe (angle between first nulls) as a function of length is shown in Figure 3.17. It is seen that the width decreases with increasing length but the rate of increase is less for longer lengths. Any

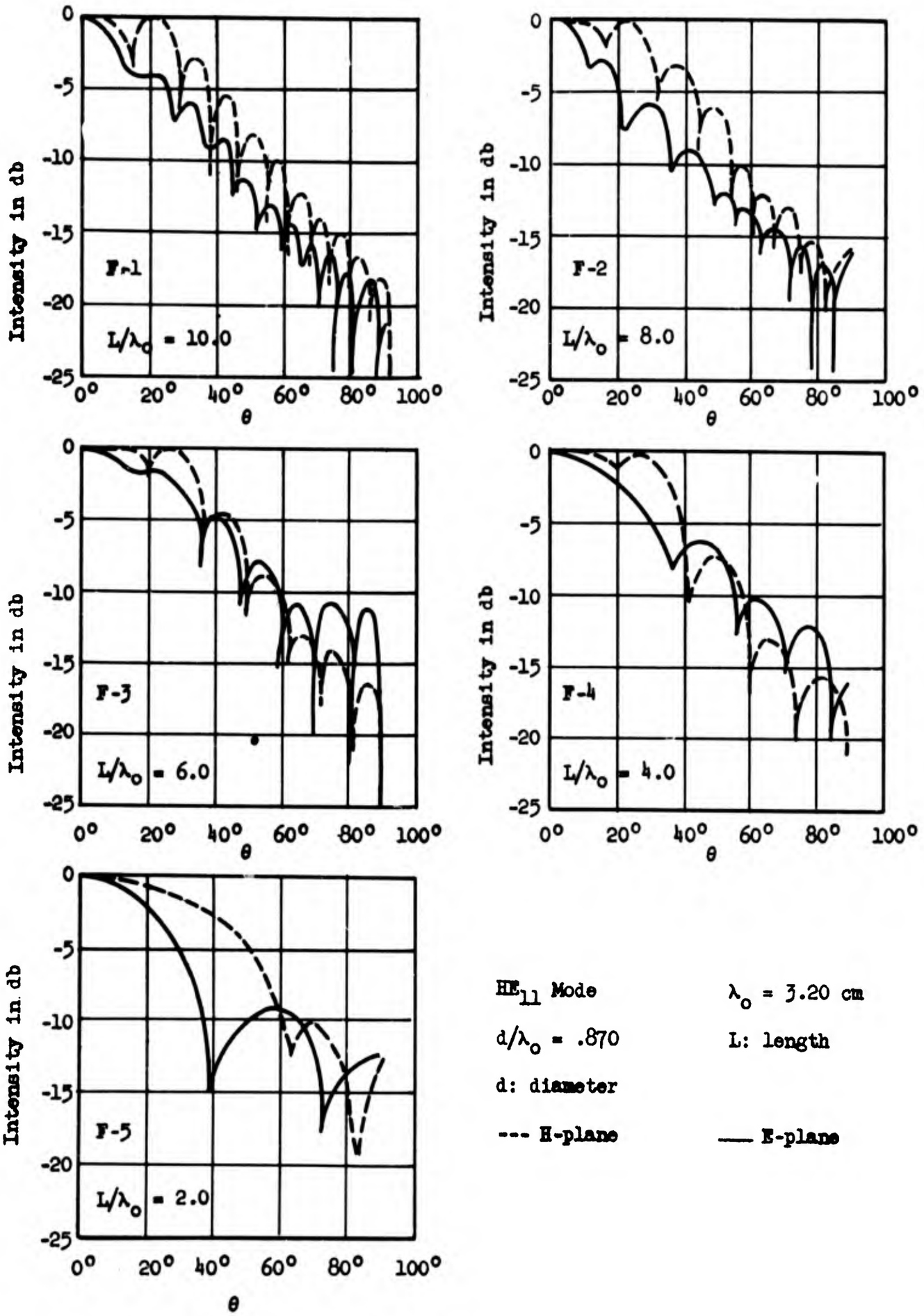

Fig. 3.15 RADIATION PATTERNS FOR THE F-SERIES

Number of Lobes in 360° of Radiation Pattern versus Length of Dielectric Rods.

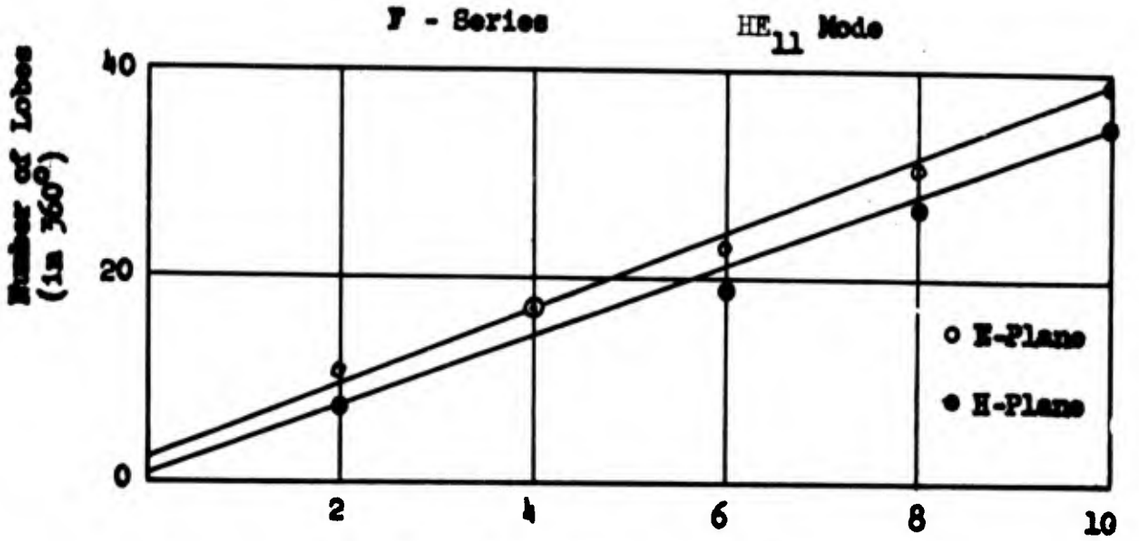

Fig. 3.16

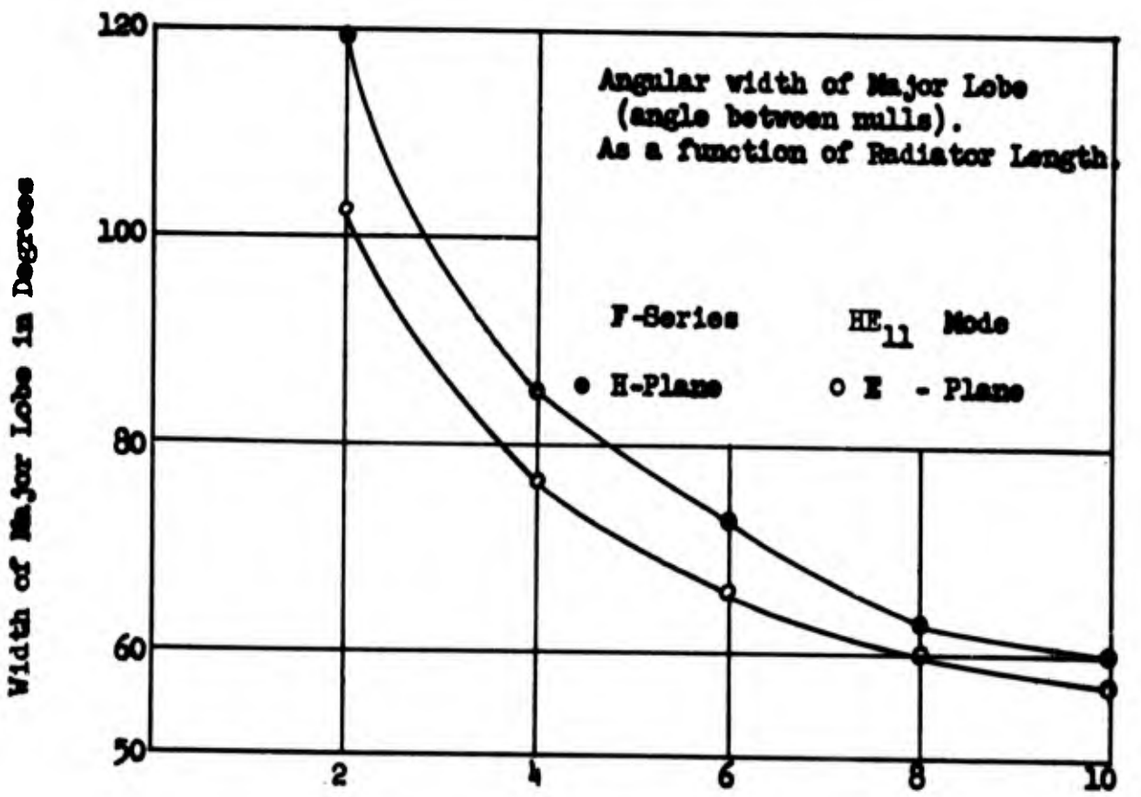

Fig. 3.17

DRL - UT
DWG AE 663
CMM -
7-5-49

increase in length greater than $10\lambda_0$ would have little effect on beam width. A more common means of rating antennas is the width of the major lobes between points at which the power is one-half the maximum. A graph of this half power (-3 db.) beam width vs. length is shown in Figure 3.18. As in Figure 3.17, it is seen that increasing length past $6\lambda_0$ would have little effect. Recently, due to radio systems having wide ranges of power sensitivity, it has become common to rate antennas in terms of 10 db. beam width. This is shown in Figure 3.19. The curves are not drawn as continuous functions because, for the longer antennas, more than one lobe are included in the 10 db. beam width and thus a continuous curve would not show the true evolution of beam width. The angular positions of the maxima of the lobes of the radiation pattern are shown in Figures 3.20 and 3.21 for the E and H plane respectively. The position of lobe number 1 (or primary lobe) is omitted since it is at zero degree for all of the rods. It appears from these figures that the position of a lobe maximum shifts gradually with change in length. Intensities of lobe maxima, relative to the maximum of the major lobe, as a function of length for E and H planes are shown in Figures 3.22 and 3.23. It is seen that the relative intensity of the minor lobes increases with length, which agrees with linear end-fire array theory. This increase is, in general, undesirable because it tends to offset the advantage of narrow beam width obtained with increasing length. Means of improving on this situation are described later. Figure 3.24 is a plot of E_r as a function of axial distance z along the $6\lambda_0$ rod. In view of the discussion in Part Two, this clearly indicates the presence of the

Fig. 3.18 Half Power (3 db) Beam Width as a Function of Length of Dielectric Radiator.

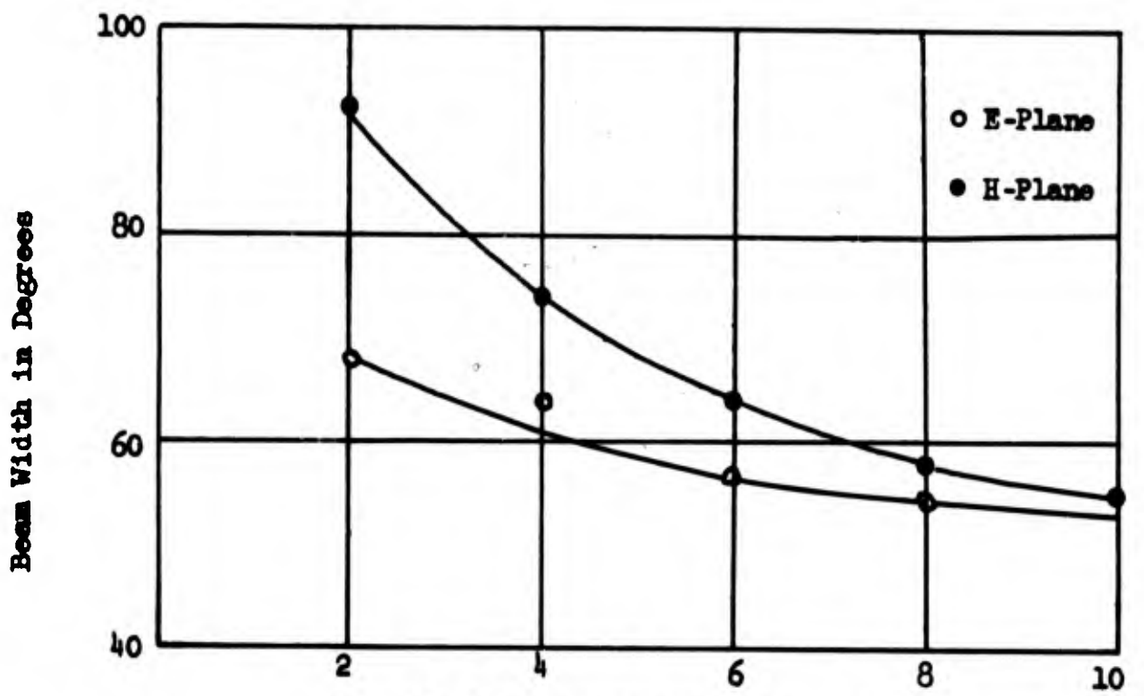

F-Series HE_{11} Mode

Fig. 3.19 10 db Beam width as a Function of Length of Dielectric Radiator

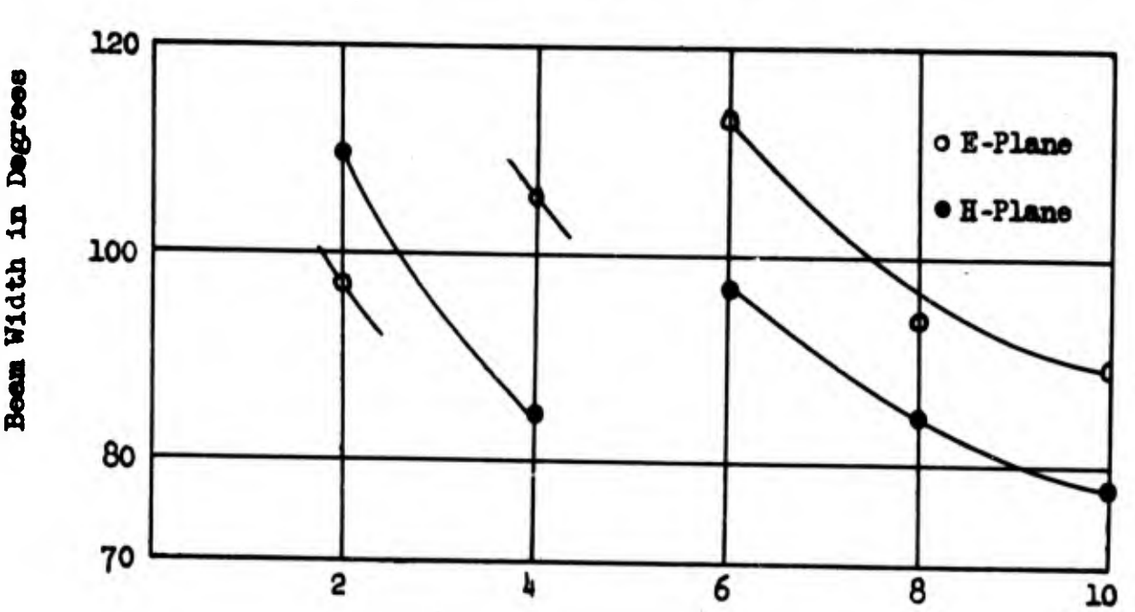

F-Series HE_{11} Mode

DRL - UT
DWG AE 664
CMM -
7 - 5 - 49

Angular Position of Maximum Lobe Intensity as a function of Length of Dielectric Radiator.

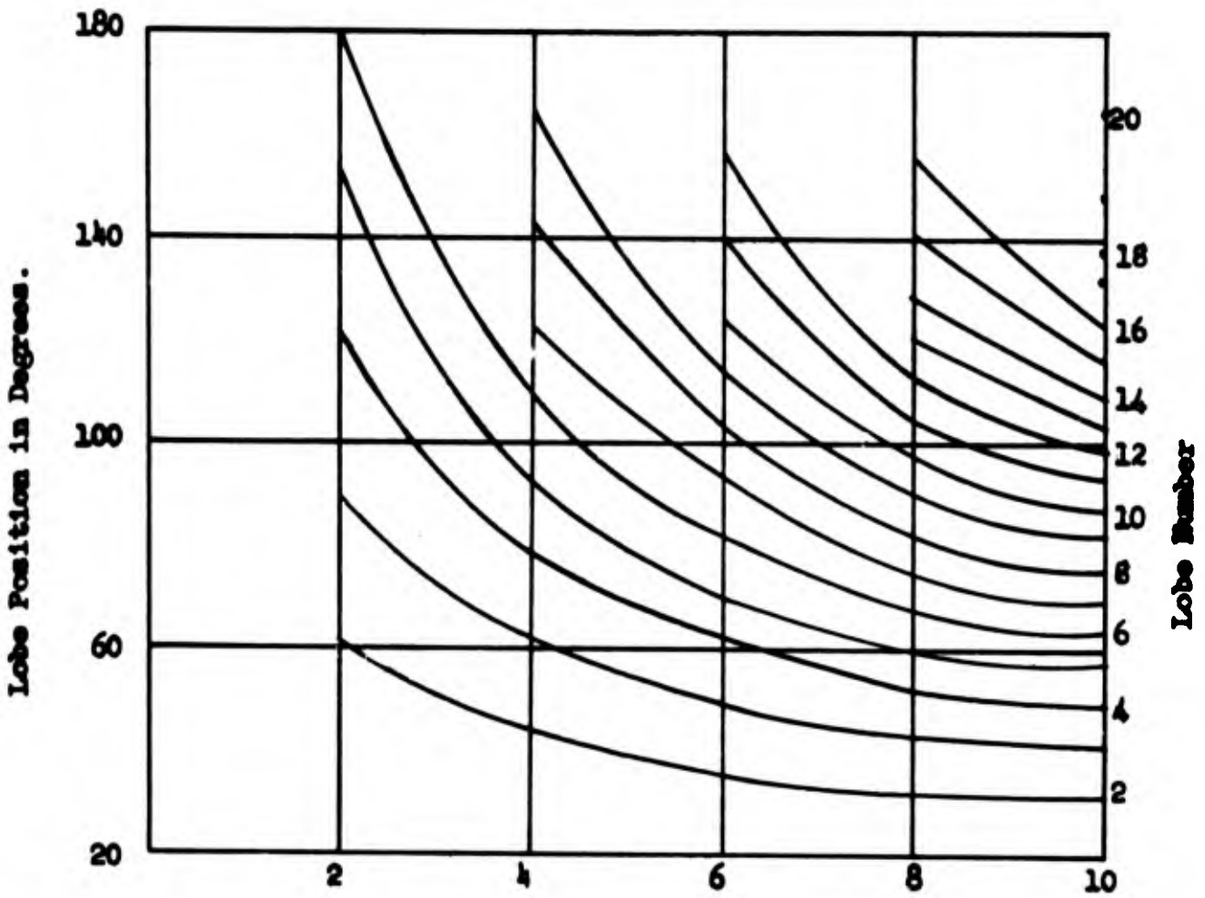

F-Series **Diameter of Rods = 1-3/32"**

HE_{11} Mode **E-Plane**

Material: Lucite

Dielectric Constant = 2.56

Fig. 3.20

DRL - UT
DWG AE 666
CMM -
7-5-9

Angular Position of Maximum Lobe Intensity as a Function of Length of Dielectric Radiator.

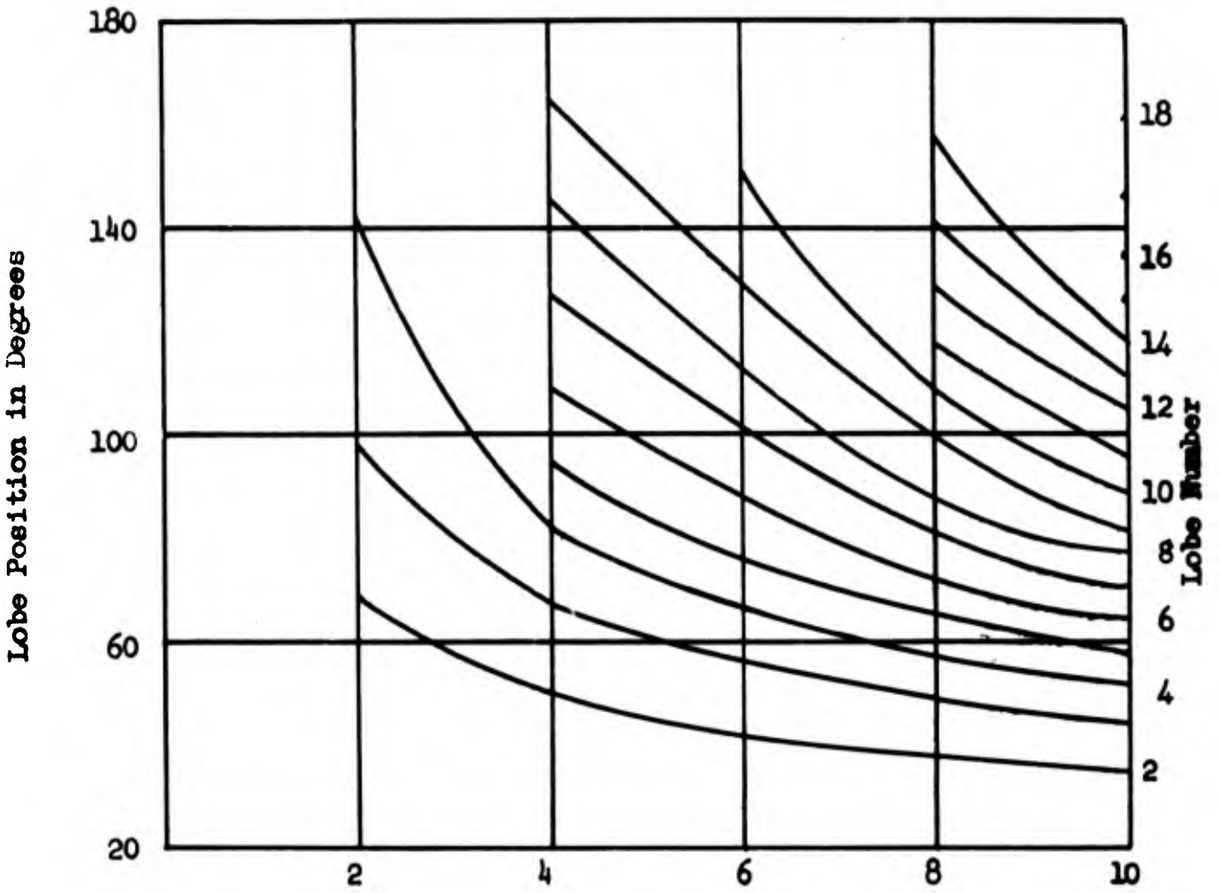

F-Series

Diameter of Rods = 1-3/32"

HE_{11} Mode

H-Plane

Material: Lucite

Dielectric Constant = 2.56

Fig. 3.21

DRL-UT
DWG AE 665
CMM-
7-5-49

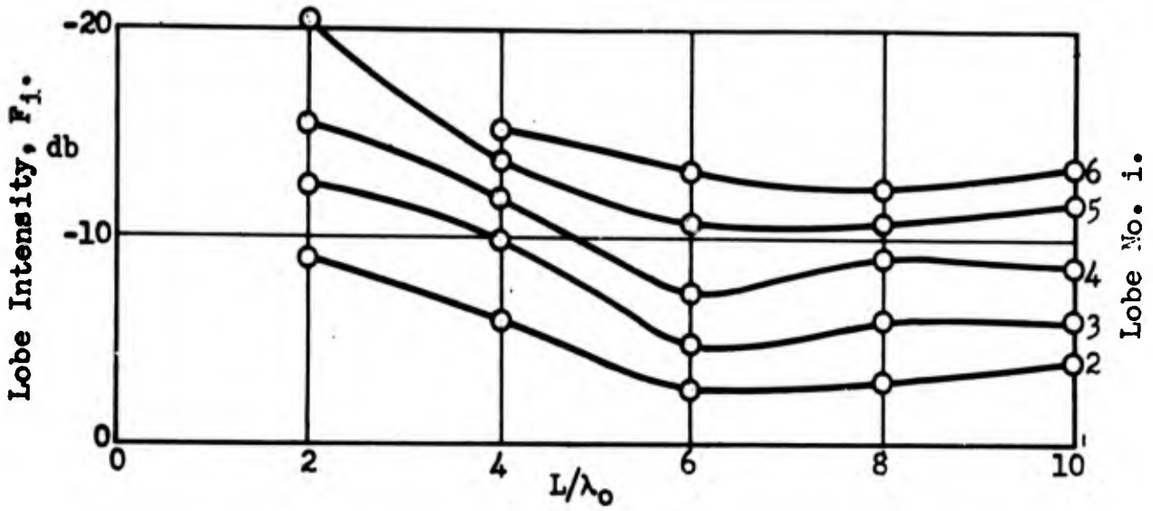

F - Series | HE_{11} Mode | E - Plane
L: Length | λ_o = 3.20 cm. | d = .870λ_o

Fig. 3.22

INTENSITY OF LOBE MAXIMA VERSUS RADIATOR LENGTH

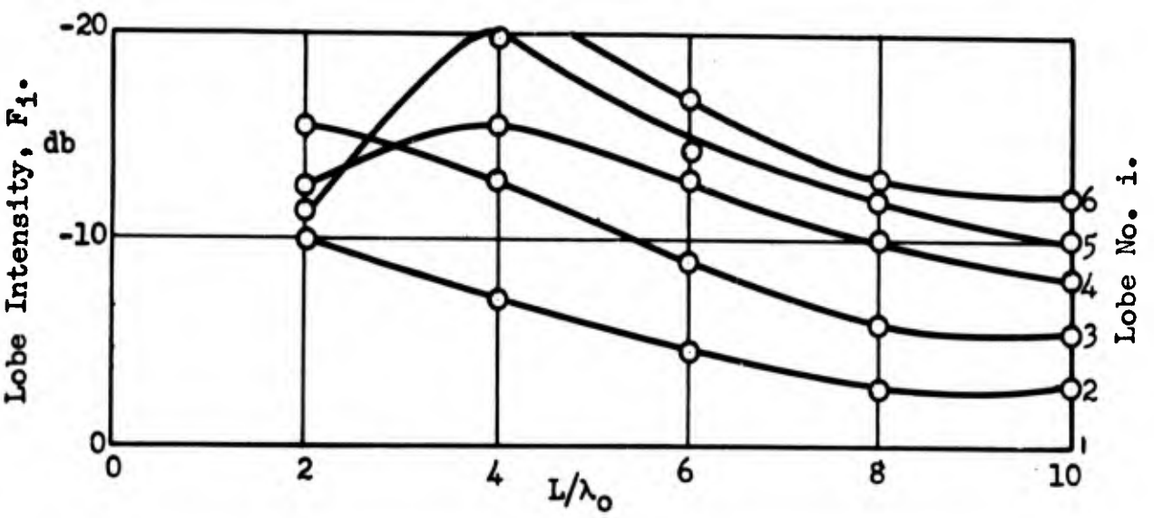

F - Series | HE_{11} Mode | H - Plane
L: Length | λ_o = 3.20 cm. | d = .870λ_o

Fig. 3.23

INTENSITY OF LOBE MAXIMA VERSUS RADIATOR LENGTH.

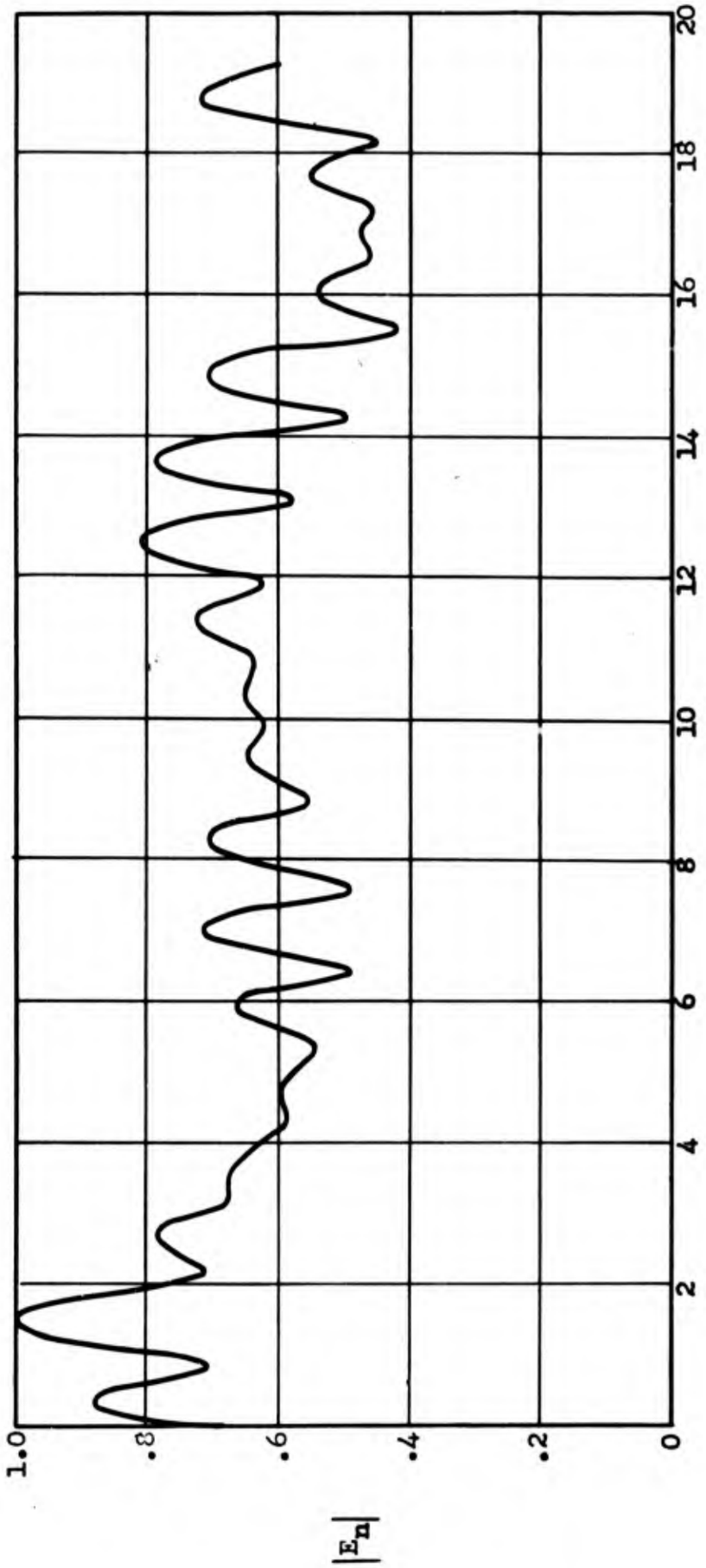

Fig. 3.24 NORMAL COMPONENT OF ELECTRIC FIELD AS A FUNCTION OF z ON THE SURFACE OF A RADIATING ROD.

HE_{12} modes. However, the dominant wavelength is that of the HE_{11} mode and apparently most of the energy is of this mode. It is apparent that very little energy is reflected from the end of the rod which verifies the assumption that most of the energy is due to a traveling wave.

The G-Series of rods are identical with F-Series except for smaller diameter. They have a diameter of 0.75-inch or $0.595\lambda_o$ when used on 3.2 cm. wavelengths which will not support the HE_{12} modes. Characteristic curves for these antennas are shown in Figures 3.25 through 3.31. The G-Series rods are of the order of diameter of rods used in most published work. The general characteristics are the same as for the larger size rods. However, in the measurement of gain, which is included later, it is clear that the larger diameter rods have the greater gain as well as other advantages.

Figure 3.31 shows the field measured along the surface of G-1. The standing wave pattern is much more uniform than in the case of the F-Series. It will be noticed that the surface field intensity increases immediately upon emerging from the metal waveguide. The increase in intensity is typical and to be expected, since the field lines just beyond the end of the metal guide extend into the outer region and naturally increase the measured field intensity. The period of transition appears to be a few wavelengths.

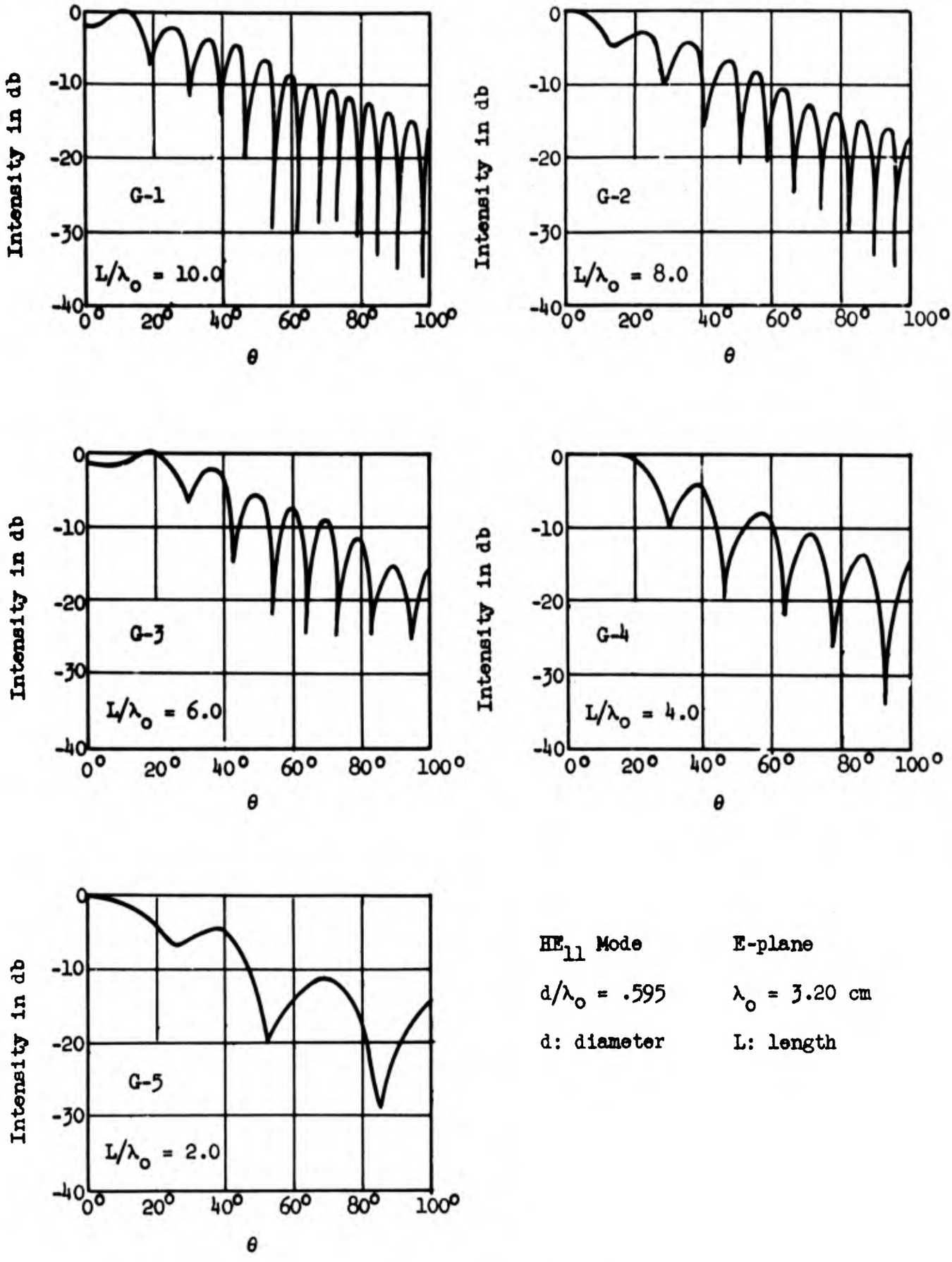

HE_{11} Mode E-plane

d/λ_o = .595 λ_o = 3.20 cm

d: diameter L: length

Fig. 3.25 RADIATION PATTERNS OF G-SERIES

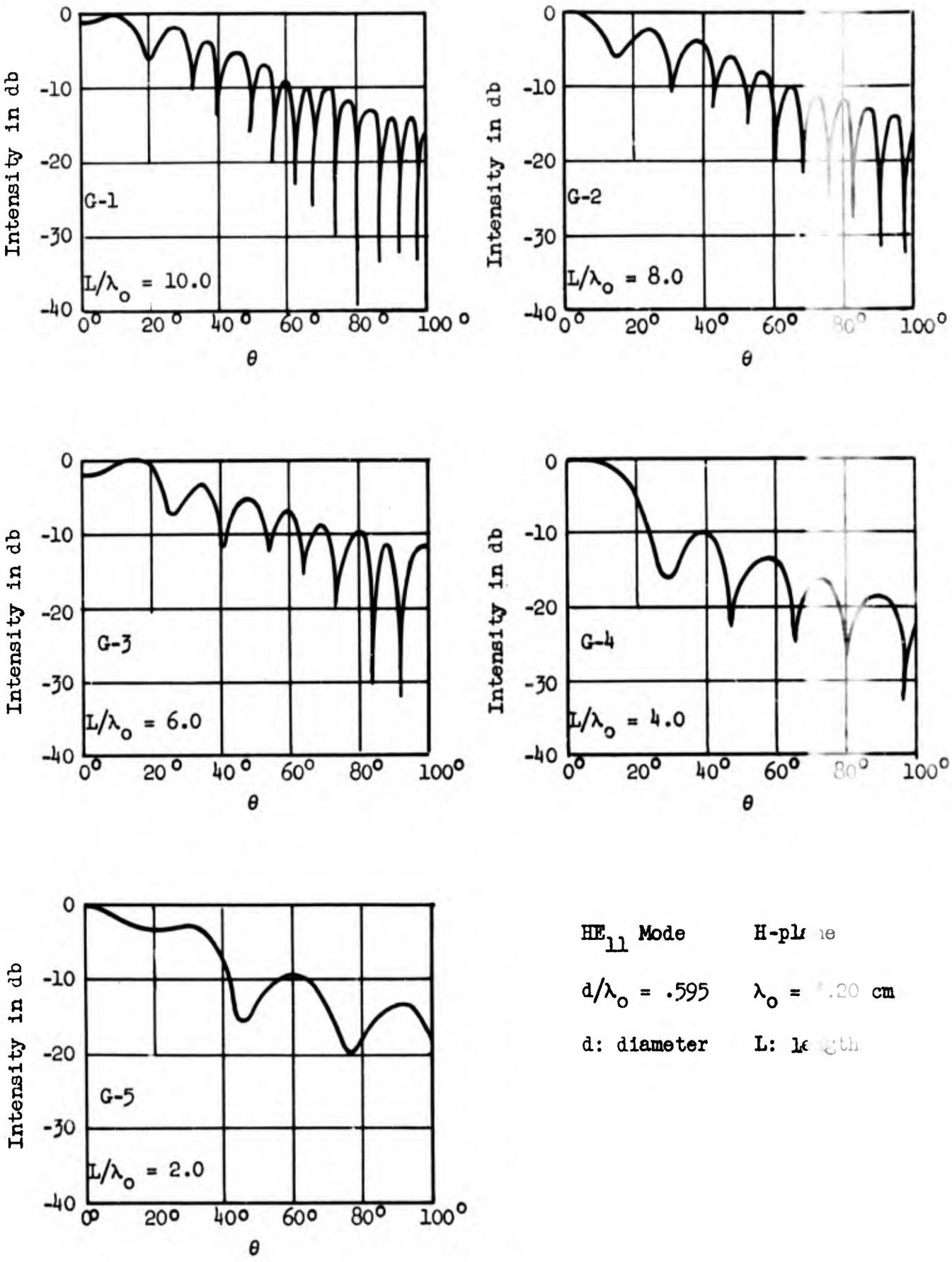

Fig. 3.26 RADIATION PATTERNS FOR THE G-SERIES

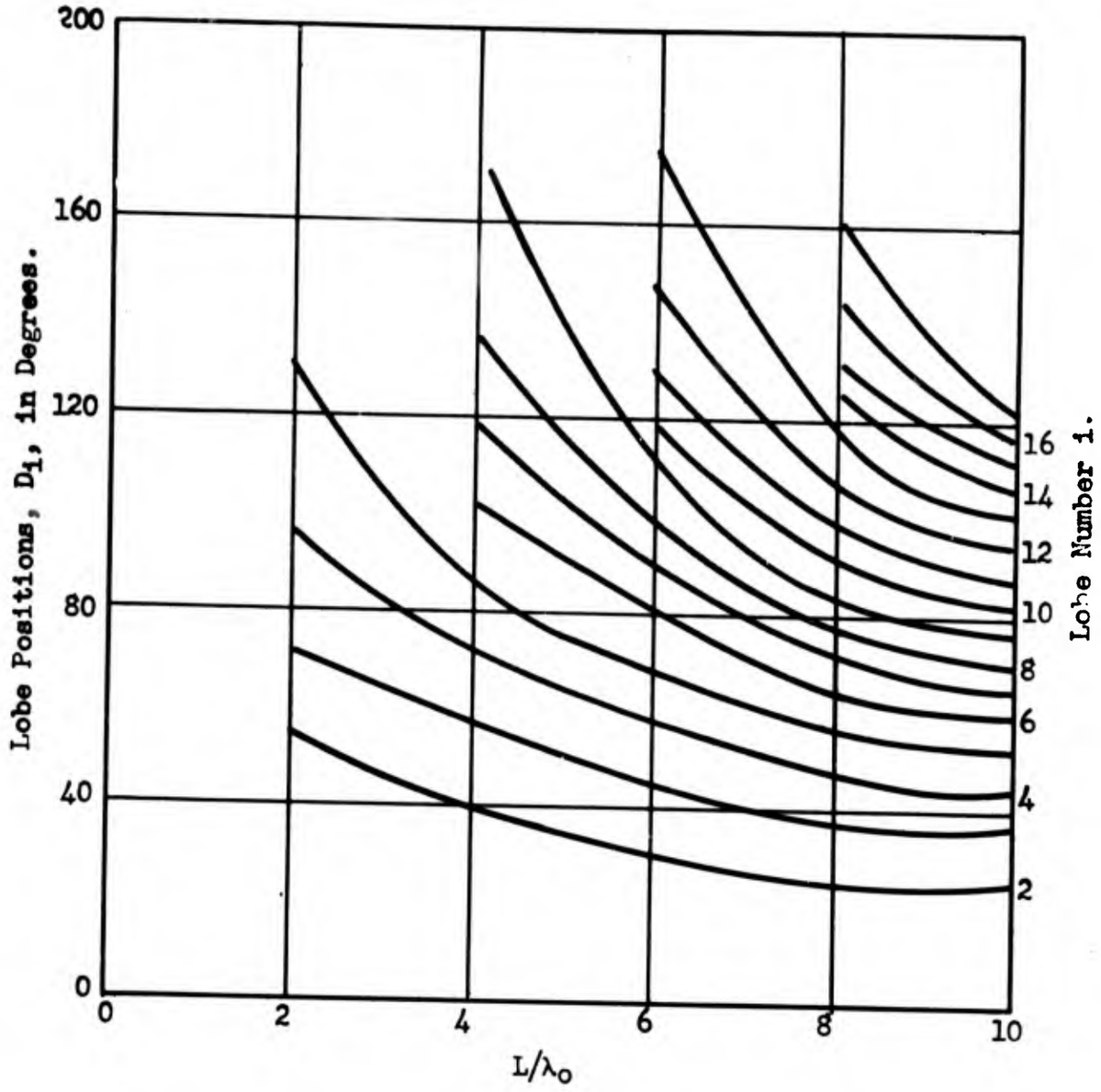

G - Series E- Plane HE_{11} Mode

λ_o = 3.20 cm d/λ_o = 5.95 K = 2.56

L: length d: diameter

Fig. 3.27

ANGULAR POSITION OF MAXIMUM LOBE INTENSITY AS A FUNCTION OF THE LENGTH OF THE DIELECTRIC ROD ANTENNA.

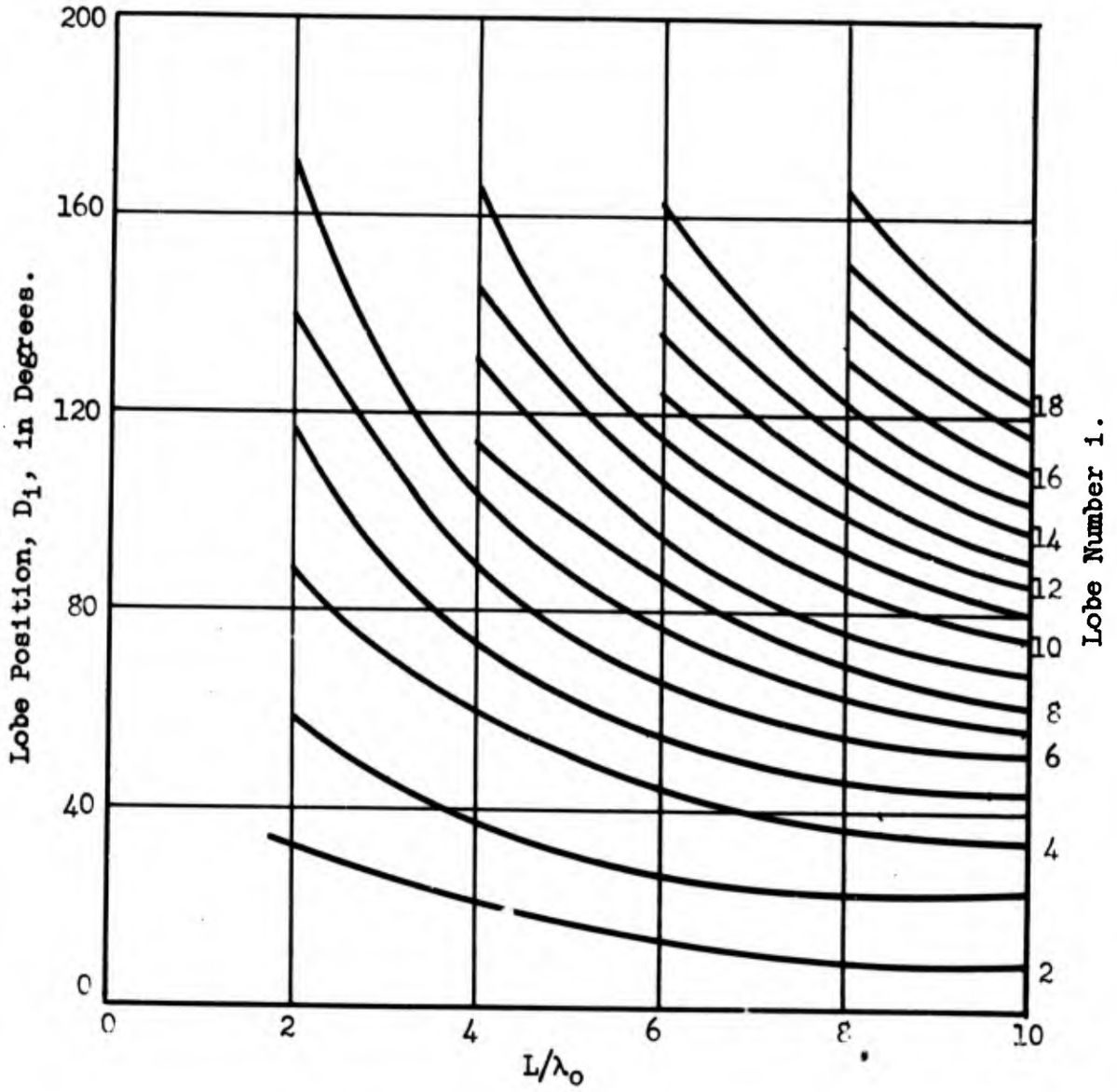

G - Series H - Plane HE_{11} Mode

λ_o = 3.20 cm d/λ_o = 5.95 K = 2.56

L: length d: diameter

Fig. 3.28

ANGULAR POSITION OF MAXIMUM LOBE INTENSITY AS A FUNCTION OF THE LENGTH OF THE DIELECTRIC ROD ANTENNA.

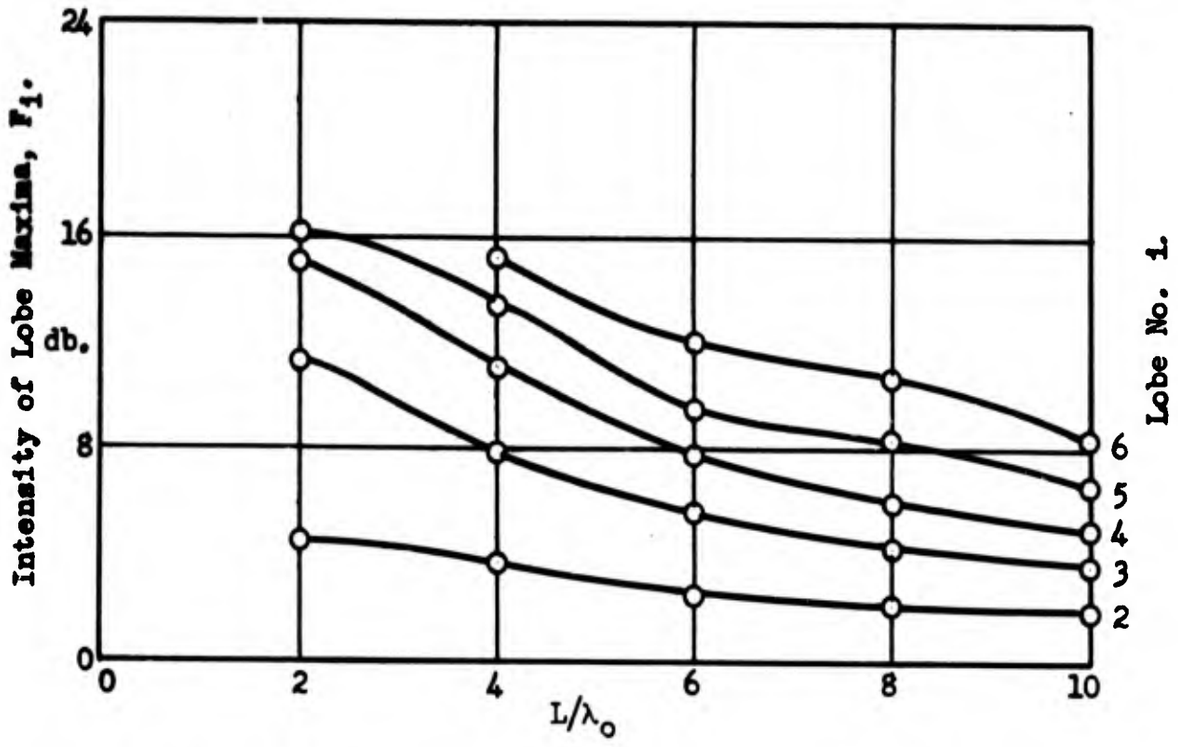

HE_{11} Mode G-Series E - Plane

λ_o = 3.20 cm

Fig. 3.29

INTENSITY OF LOBE MAXIMA AS A FUNCTION OF THE LENGTH OF THE DIELECTRIC ROD ANTENNA.

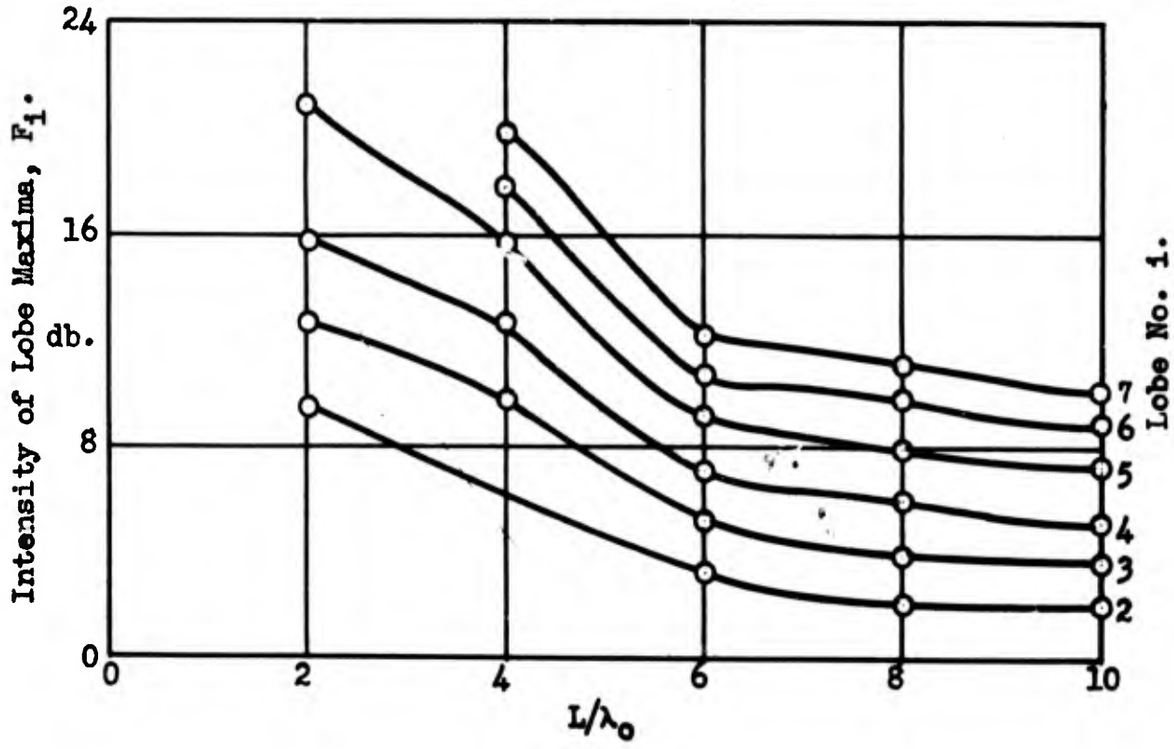

HE_{11} Mode G - Series H - Plane

λ_o = 3.20 cm

Fig. 3.30

INTENSITY OF LOBE MAXIMA AS A FUNCTION OF THE LENGTH OF THE DIELECTRIC ROD ANTENNA.

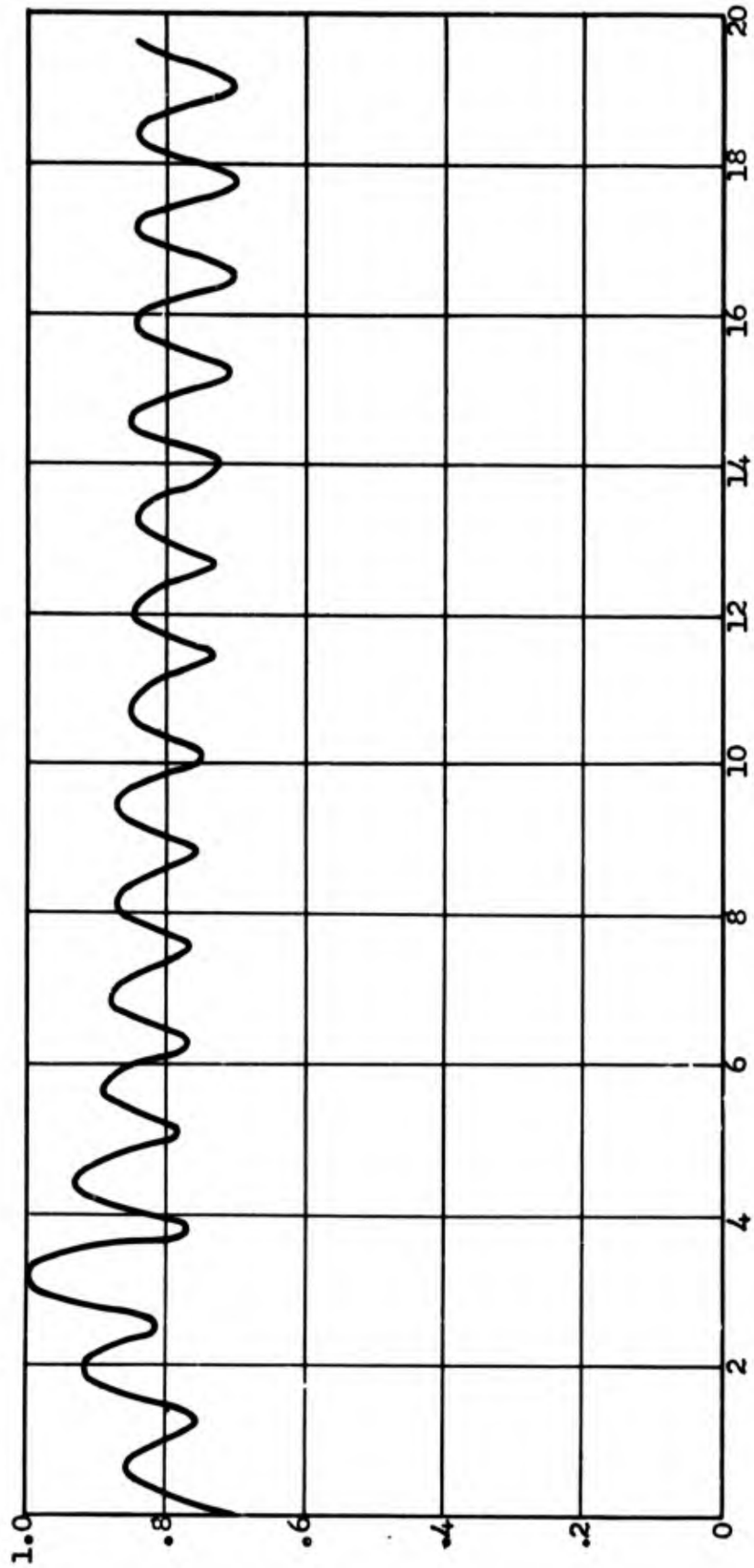

Fig. 3.31 NORMAL COMPONENT OF THE ELECTRIC FIELD AS A FUNCTION OF z, ON THE SURFACE OF A RADIATING ROD.

The E-Series antennas show the effect of varying the diameter of the dielectric rods. The general characteristics are shown in Figures 3.32 through 3.37. The number of lobes and their positions are essentially independent of rod diameter. Any variation could easily be due to the shielded taper feeding the rods. The primary difference is in the secondary lobe intensities. The data indicate that secondary lobes decrease as diameter increases up to diameter of $2\lambda_o$ and then increase. However, since only one rod greater than $2\lambda_o$ in diameter was tested, this result is inconclusive. However, it does appear that larger diameters definitely reduce secondary lobes. Therefore, it would seem that diameters considerably larger than those normally used would be satisfactory or even desirable. However, with the larger diameter, higher order modes are present and it is impossible to credit the attenuation of minor lobes to either the increase in diameter or to the presence of higher modes alone. This point is discussed in more detail later.

Envelopes of the lobe patterns are shown in Figure 3.36 for the E-plane. This Figure shows at a glance the general nature of the radiation patterns. As in the H-plane, E-2 appears to have the best minor lobe attenuation.

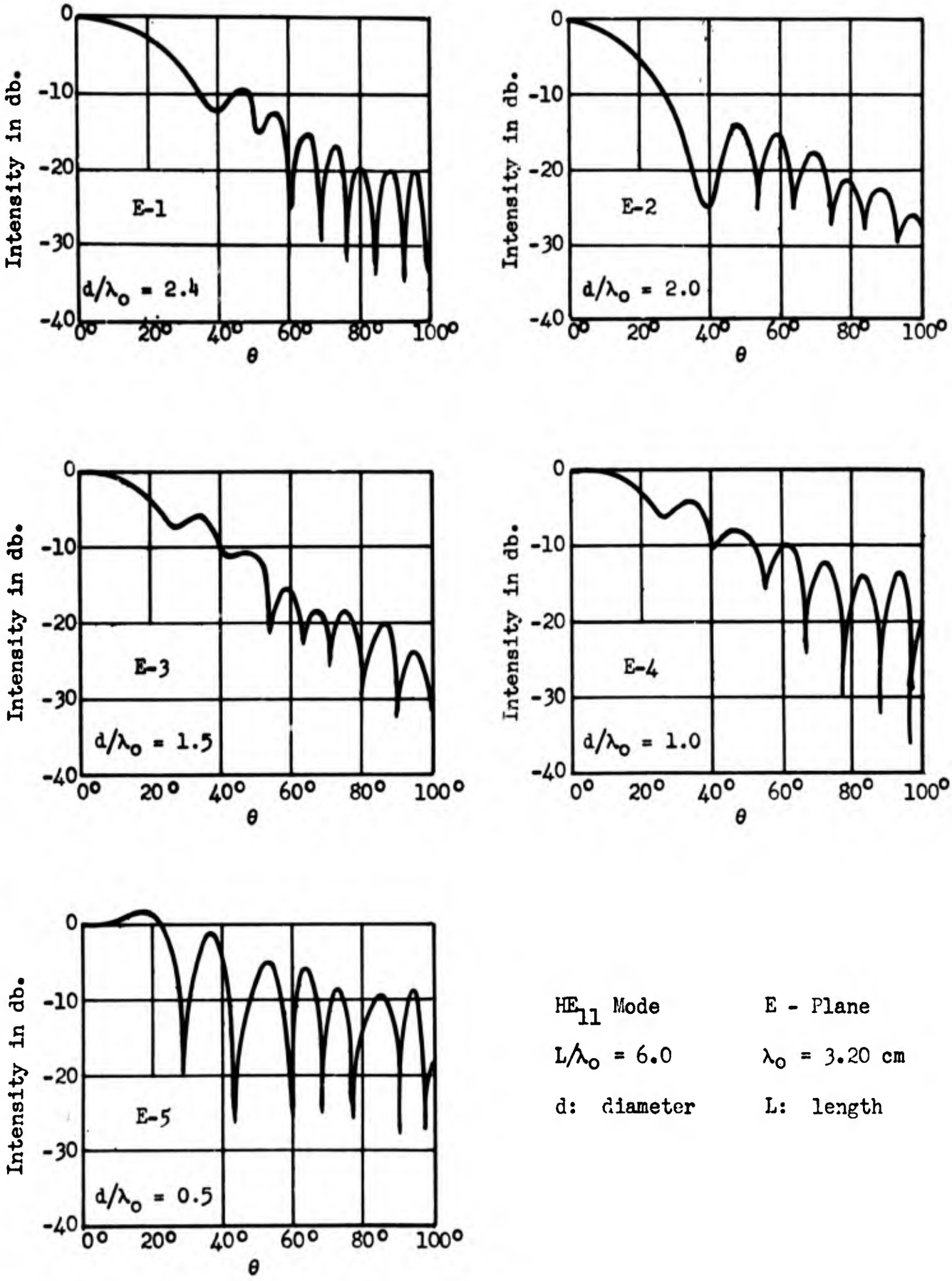

HE_{11} Mode — E - Plane

L/λ_o = 6.0 — λ_o = 3.20 cm

d: diameter — L: length

Fig. 3.32 RADIATION PATTERNS FOR THE E - SERIES

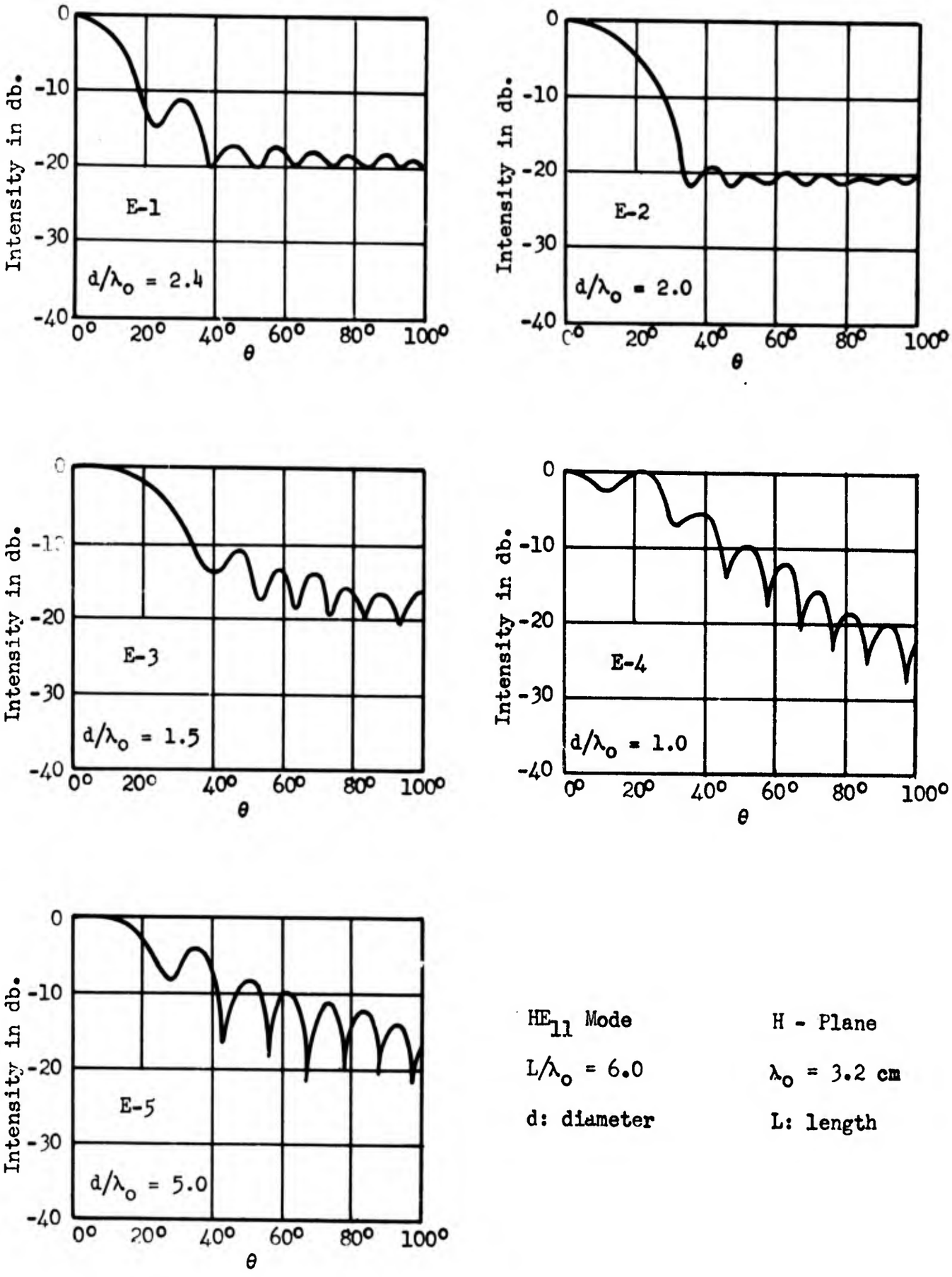

HE_{11} Mode — H - Plane

$L/\lambda_o = 6.0$ — $\lambda_o = 3.2$ cm

d: diameter — L: length

Fig. 3.33 RADIATION PATTERNS FOR E-SERIES.

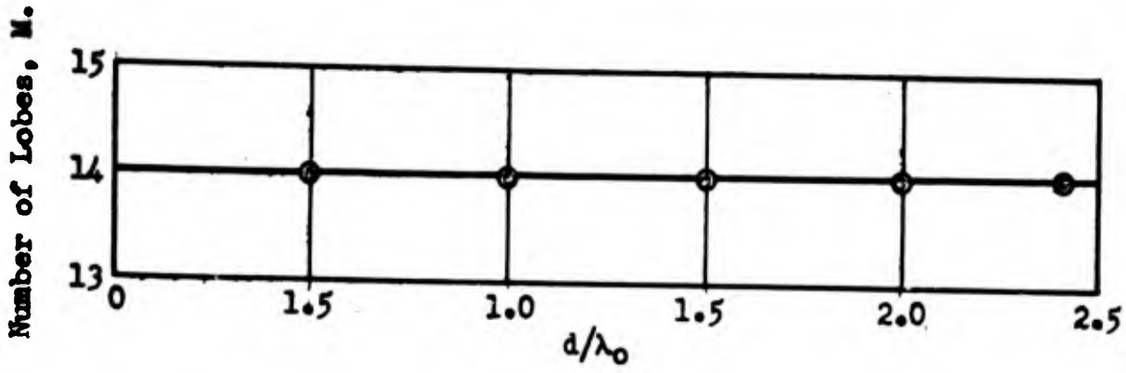

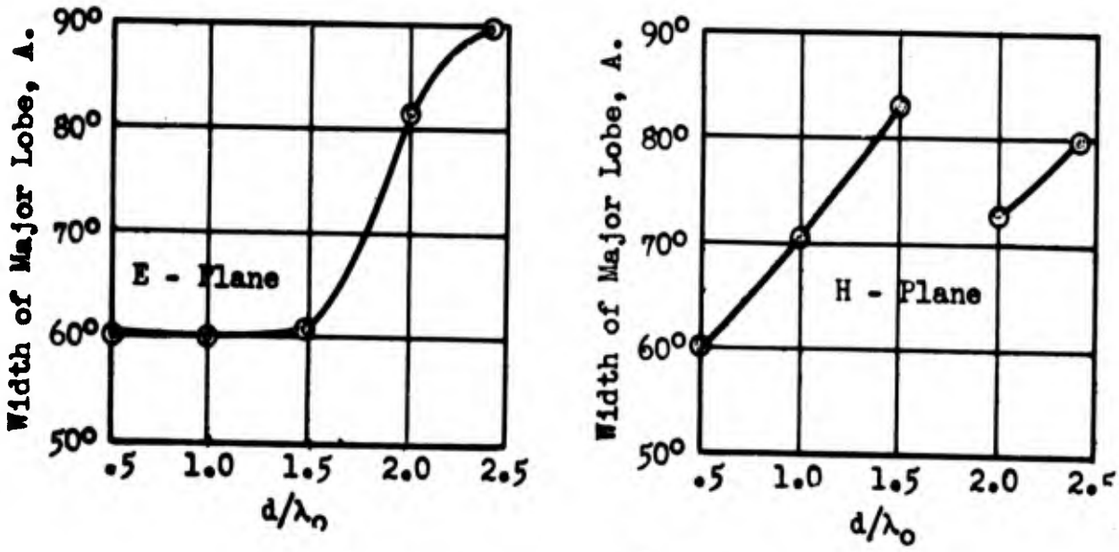

HE_{11} Mode
$L/\lambda_o = 6.0$
L: length

E- and H- Planes
$\lambda_o = 3.20$ cm
d: diameter

Fig. 3.34

CHARACTERISTICS OF THE E-SERIES OF DIELECTRIC ROD ANTENNAS.

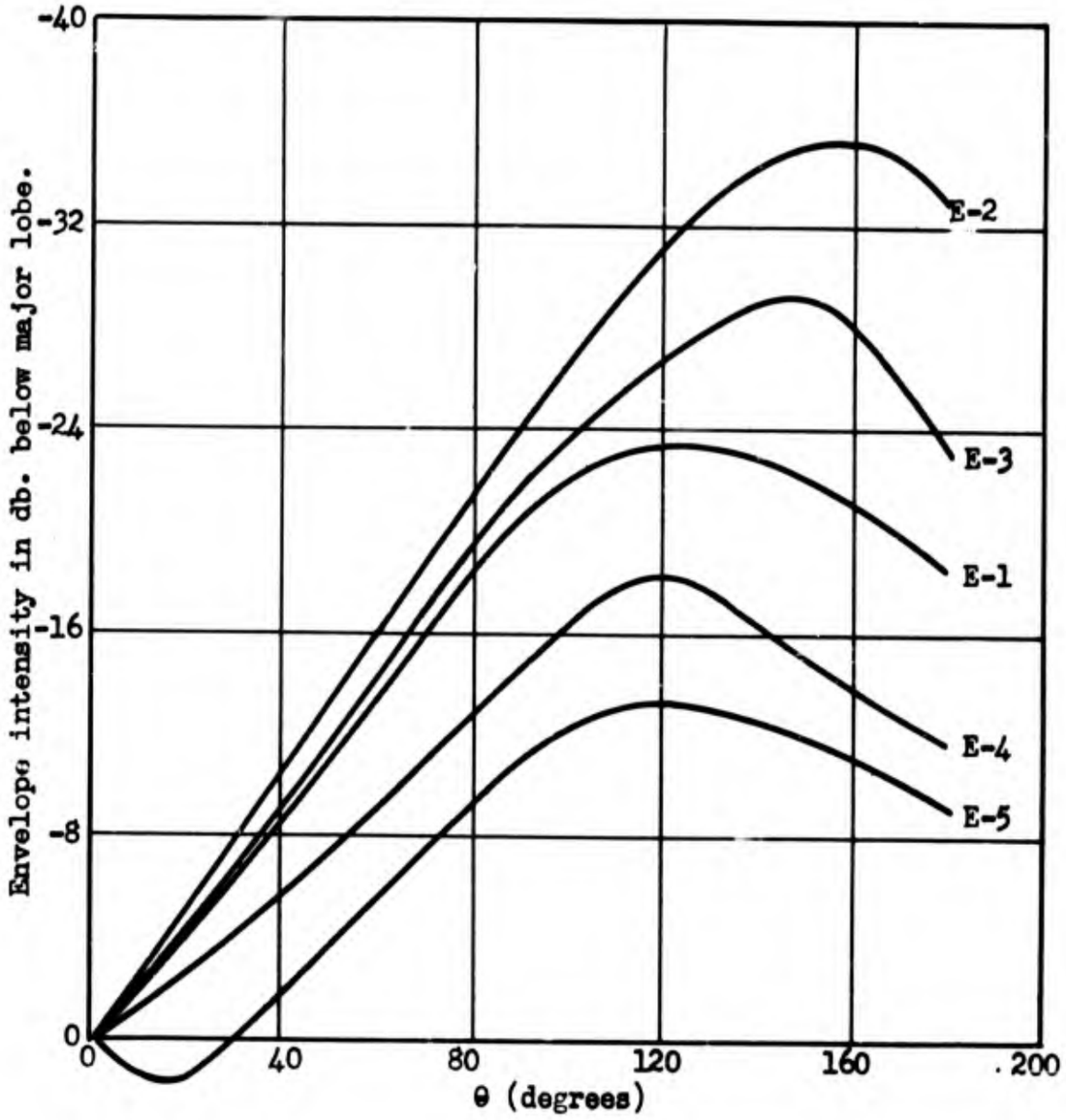

E - Series HE_{11} Mode

$L/\lambda_o = 6.0$ $K = 2.56$ $\lambda_o = 3.20$ cm

Fig. 3.35

ENVELOPE OF THE INTENSITIES OF RADIATION PATTERNS AS A FUNCTION OF THE DIAMETER OF DIELECTRIC ROD ANTENNAS.

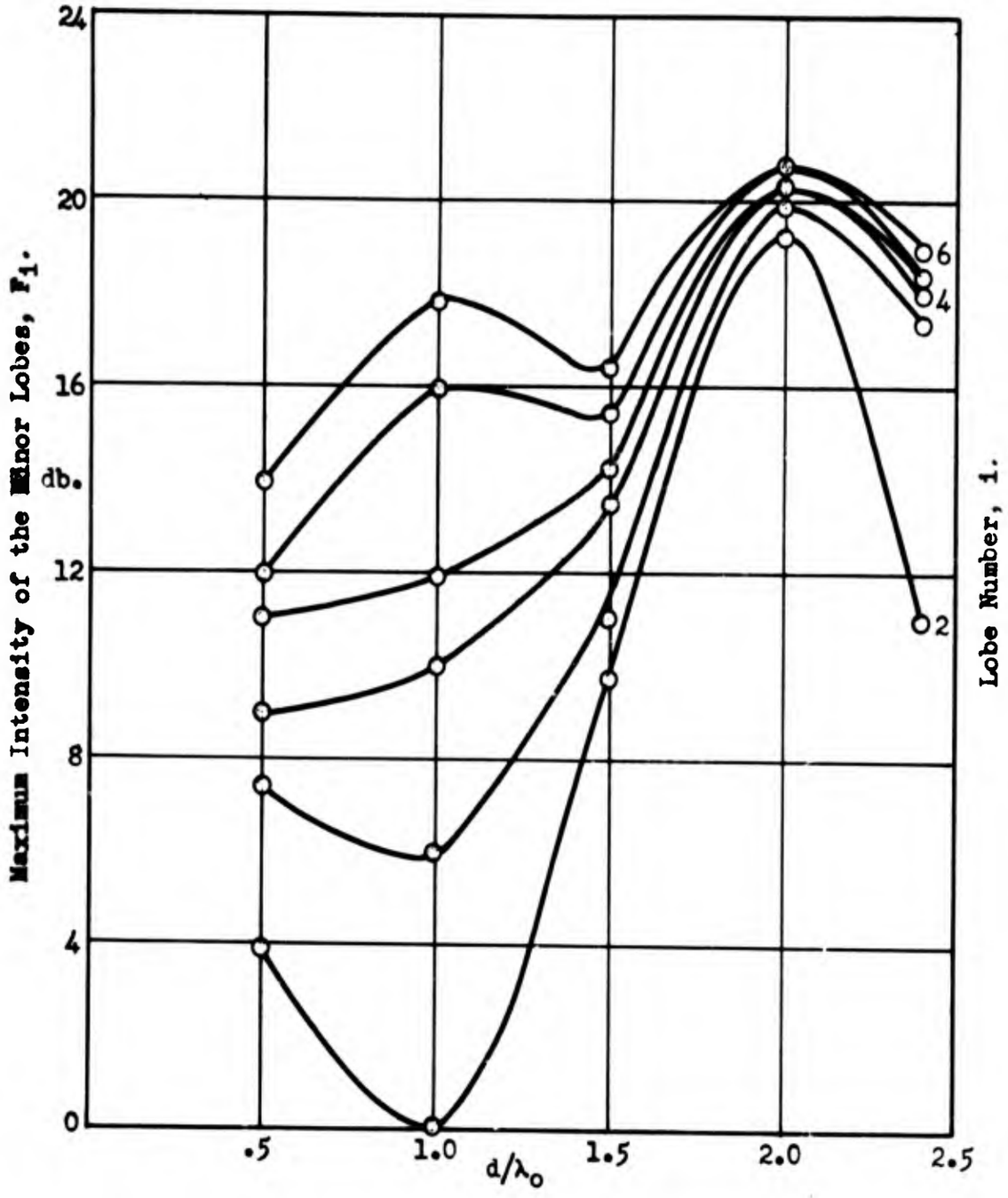

E-Series HE_{11} Mode H-Plane

$L/\lambda_o = 6.0$ $\lambda_o = 3.20$ cm K = 2.56

d: diameter L: length

Fig. 3.36

MAXIMUM INTENSITY OF THE MINOR LOBES AS A FUNCTION OF THE DIAMETER OF DIELECTRIC ROD ANTENNAS.

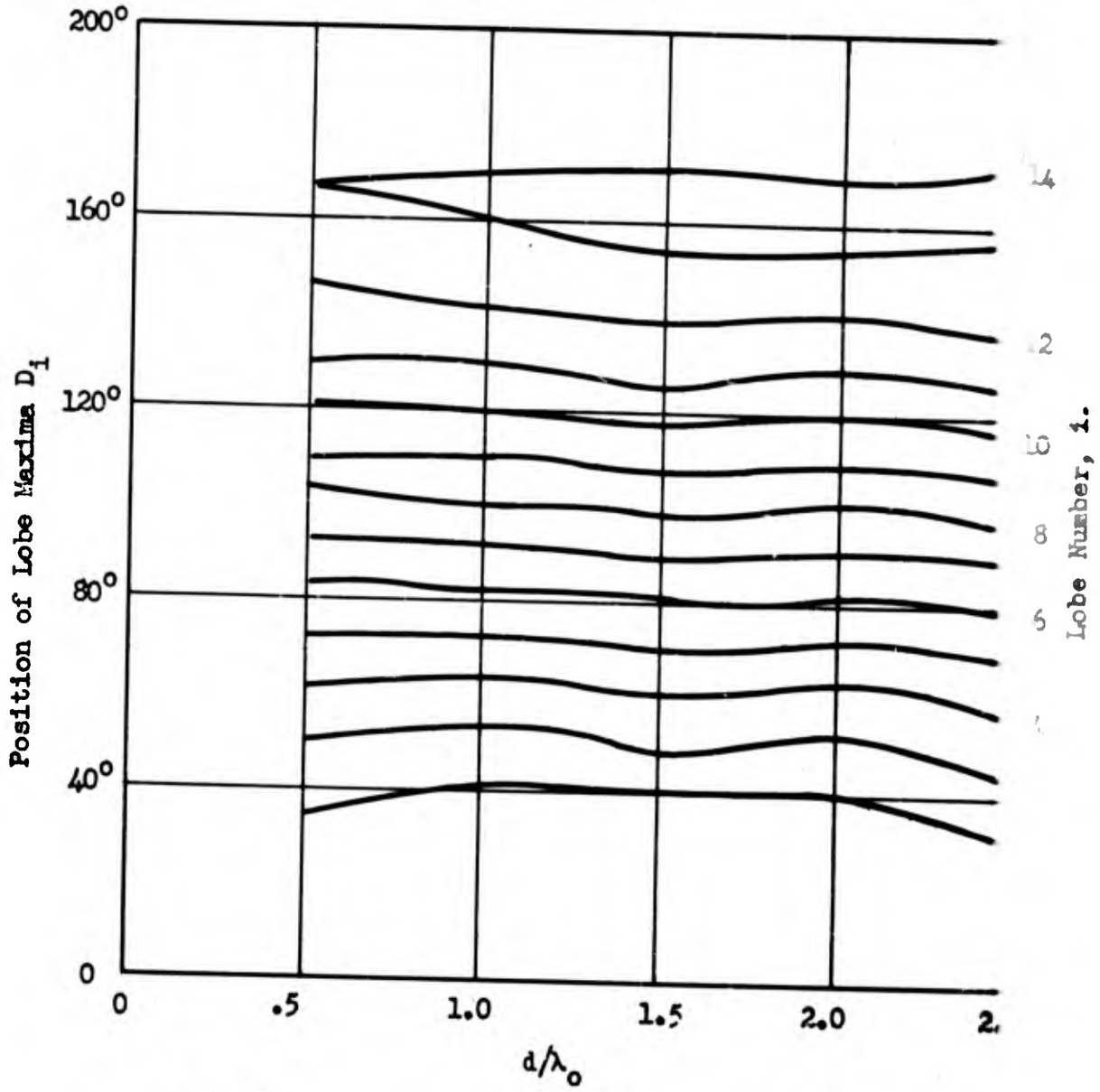

Fig. 3.37 ANGULAR POSITION OF THE LOBE MAXIMA AS A FUNCTION OF THE DIAMETER OF DIELECTRIC ROD ANTENNAS.

As has been mentioned, the dielectric rods may be tapered in diameter in order to achieve impedance matching and also reduce minor lobe intensity. The A-Series rods vary in length from $10\lambda_o$ to $2\lambda_o$ while the taper angle remains constant. Figures 3.38 through 3.44 show characteristics of this series for the E and H planes. The number of lobes does not increase linearly with length past $6\lambda_o$. This non-linearity is undoubtedly due to the fact that with the taper, most of the energy has been radiated before it reaches the end of the longer rods, and thus the end of the rods has little effect on the pattern. The beam width and width of major lobe are also not greatly affected by increasing the length past $6\lambda_o$. However, the minor lobes seem to be attenuated greatly by the increase in length. This attenuation of minor lobes is best explained by reference to Figures 3.42 through 3.44, which give the normal component of the field E_n as a function of z for the A-Series. As mentioned in Chapter I of this Part, a sinusoidal variation of intensity of feed along the rod gives maximum attenuation of the secondary lobes. For the rods of lengths $2\lambda_o$ to $6\lambda_o$, the intensity of feed seems to increase with increasing z but for the $10\lambda_o$ rods, the effect of radiation losses begins to be felt and the intensity begins to assume a sinusoidal variation. The field pattern for the $8\lambda_o$ rod is omitted in order to conserve space, but it did begin to indicate a tapering of field intensity. The $10\ \lambda_o$ rod most nearly approaches the

condition of sinusoidal feed and it also has maximum minor lobe attenuation. Therefore, it appears to be advantageous to continue the taper to a point, but this conclusion is not in complete agreement with the findings of other workers.

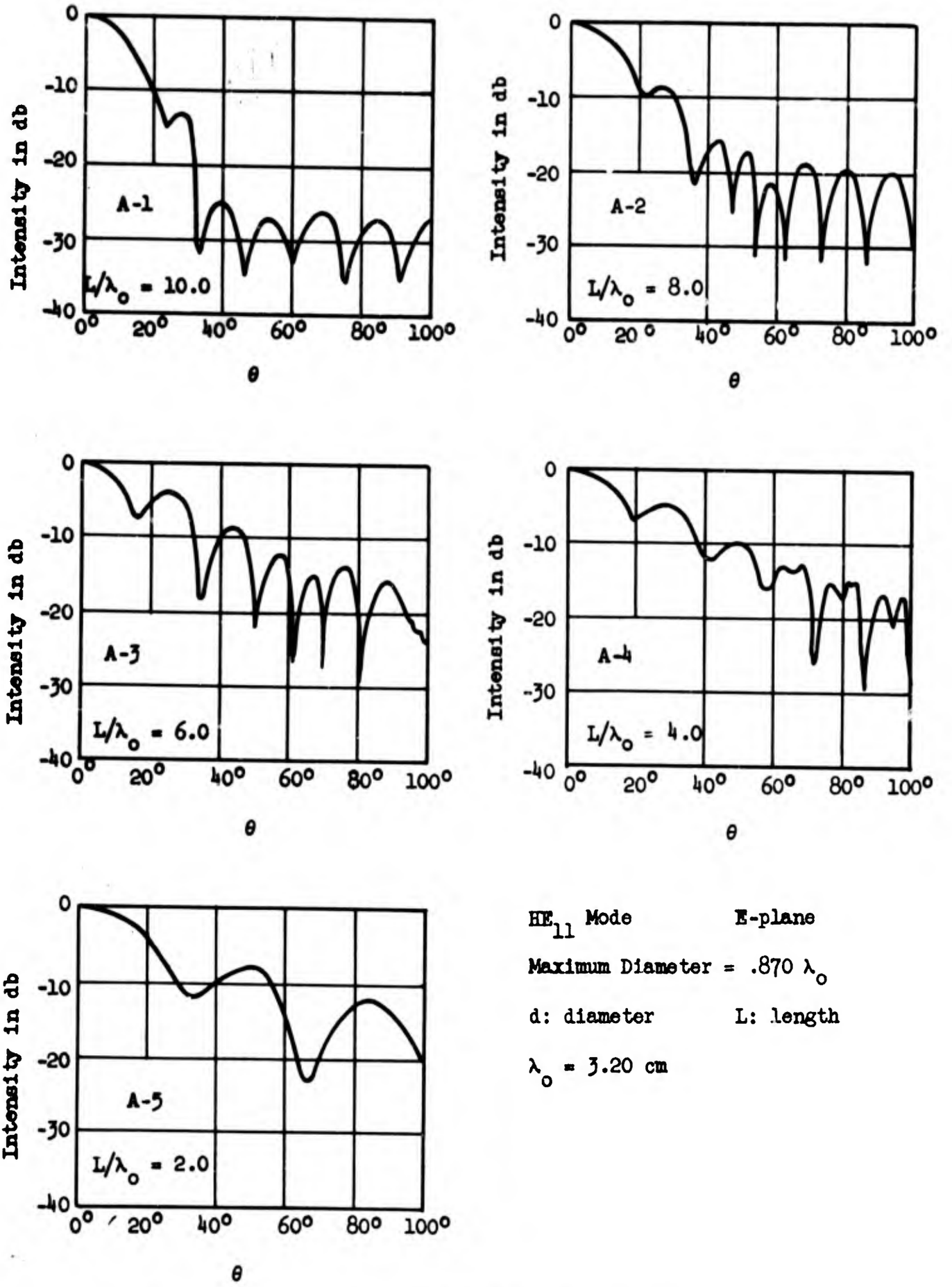

HE_{11} Mode E-plane

Maximum Diameter = .870 λ_o

d: diameter L: length

λ_o = 3.20 cm

Fig. 3.38 RADIATION PATTERNS FOR THE A-SERIES

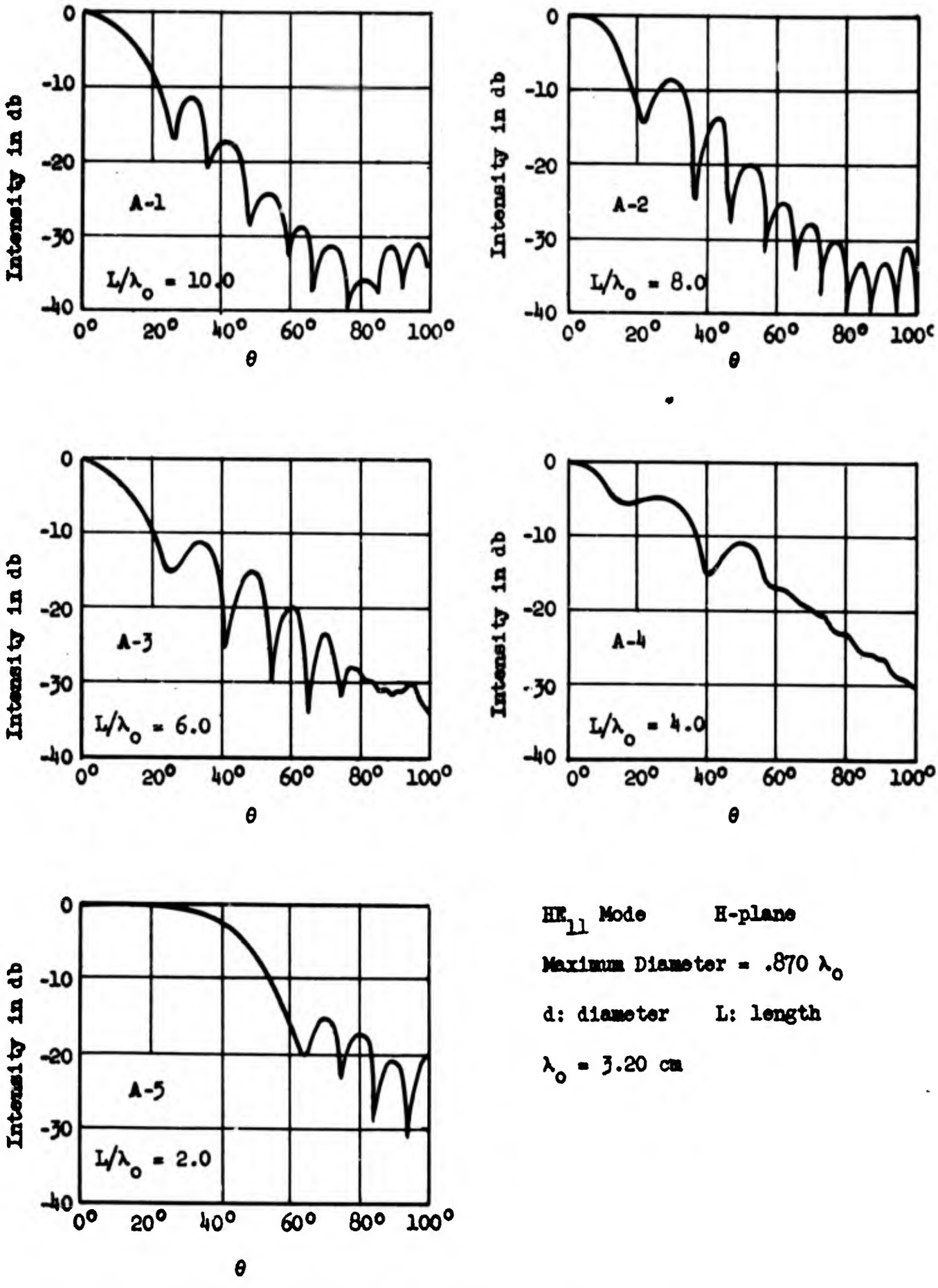

HE_{11} Mode H-plane

Maximum Diameter = .870 λ_o

d: diameter L: length

λ_o = 3.20 cm

Fig. 3.39 RADIATION PATTERNS FOR THE A-SERIES

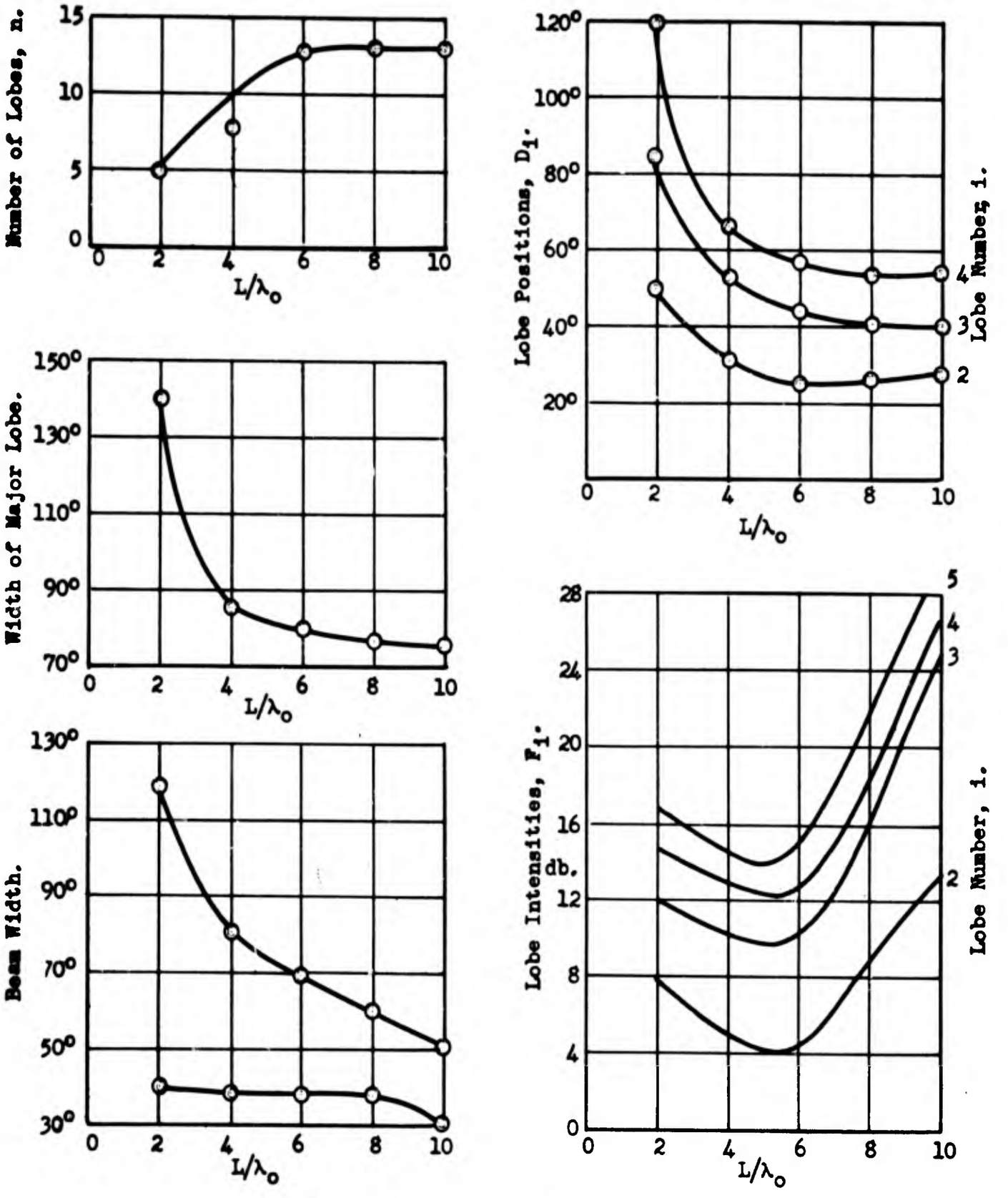

HE_{11} Mode E - Plane λ_o = 3.20 cm

Fig. 3.40

CHARACTERISTICS OF THE A-SERIES OF DIELECTRIC ROD ANTENNAS.

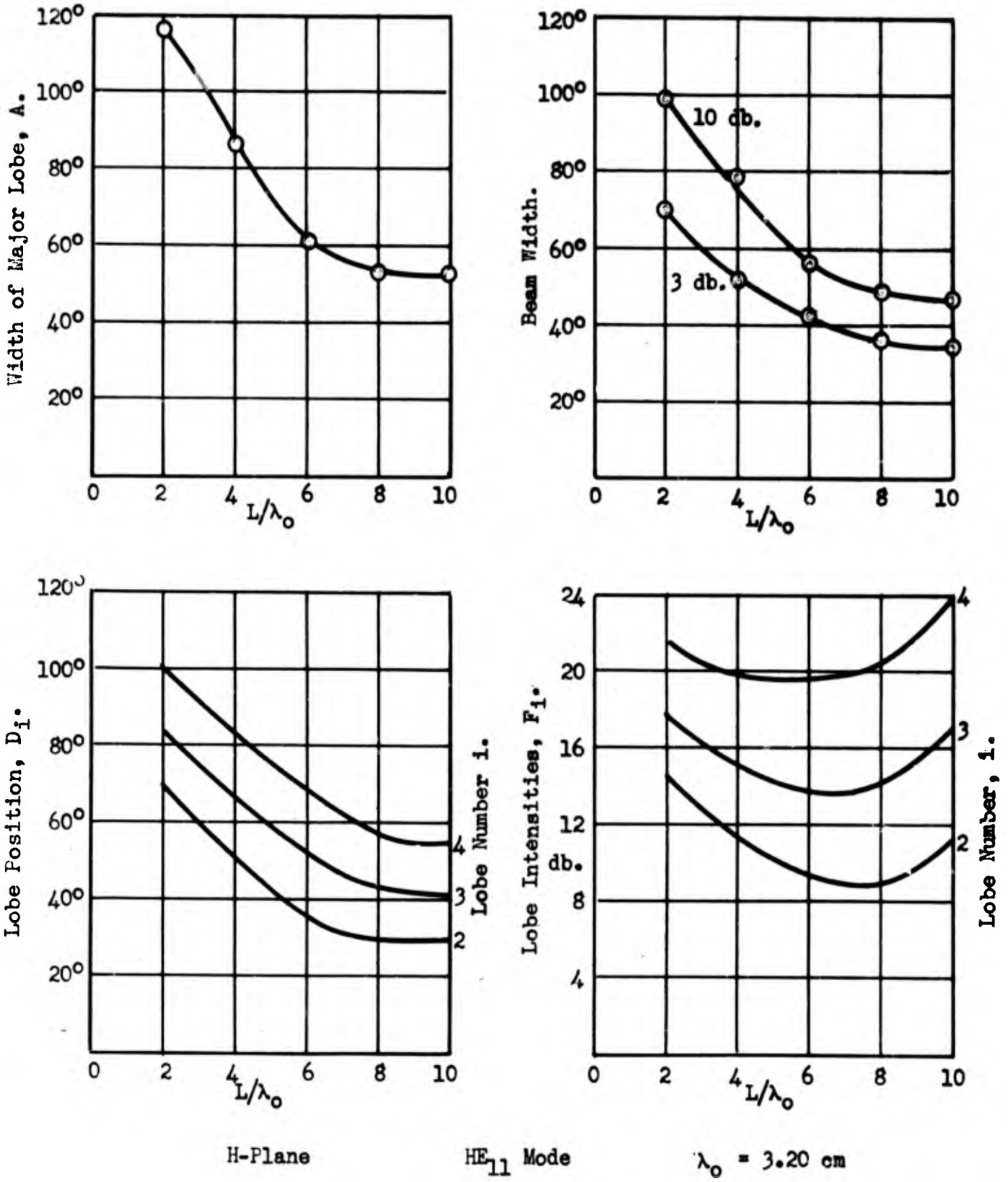

Fig. 3.41

CHARACTERISTICS OF THE A-SERIES OF DIELECTRIC ROD ANTENNAS.

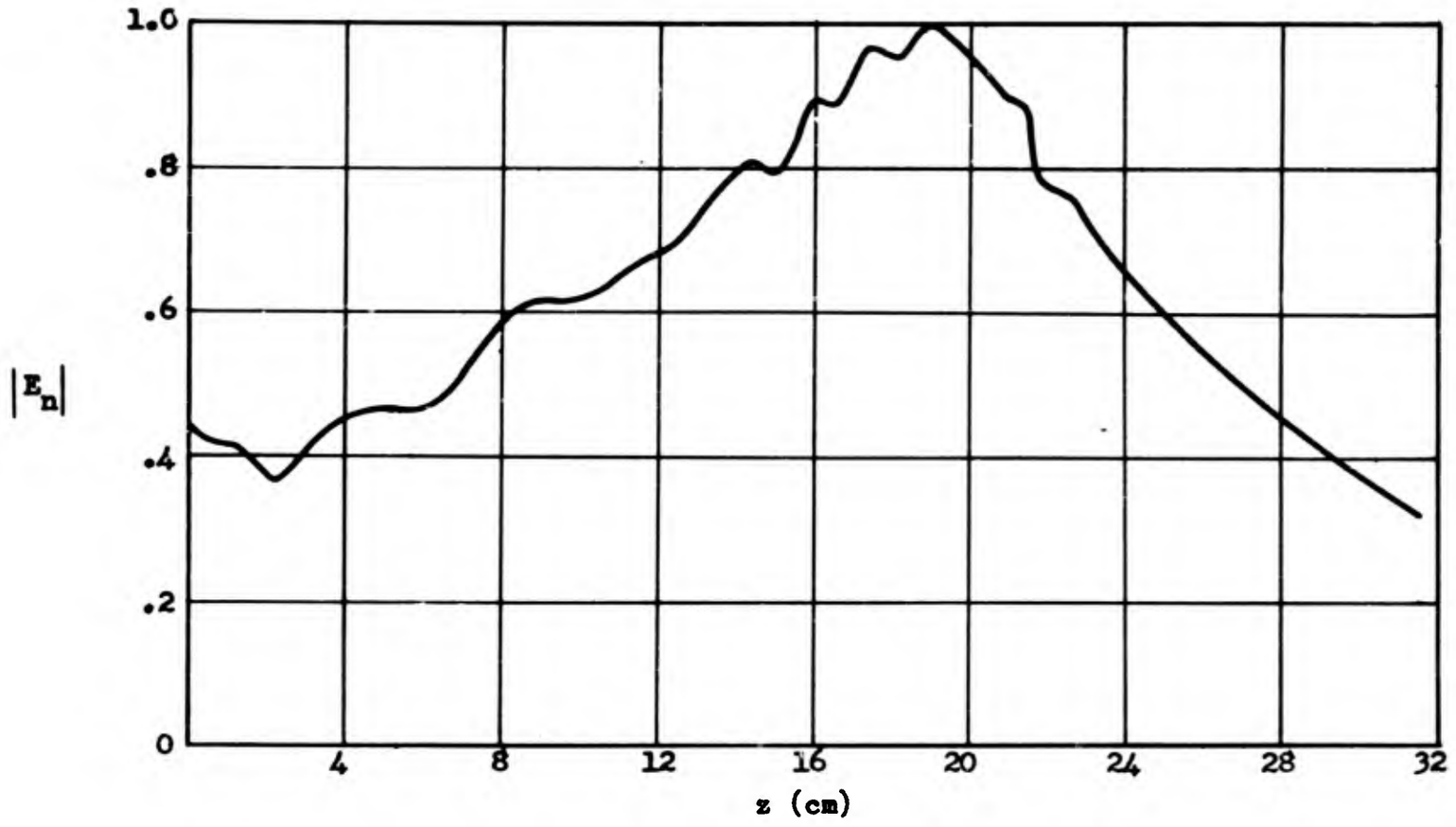

Antenna: A-1 Mode: HE_{11} $L/\lambda_o = 10.0$ $\phi = 0^o$

Antenna excited at point z== 0.

Fig. 3.42 NORMAL COMPONENT OF THE ELECTRIC FIELD AS A FUNCTION OF z, ON THE SURFACT OF A RADIATING ROD.

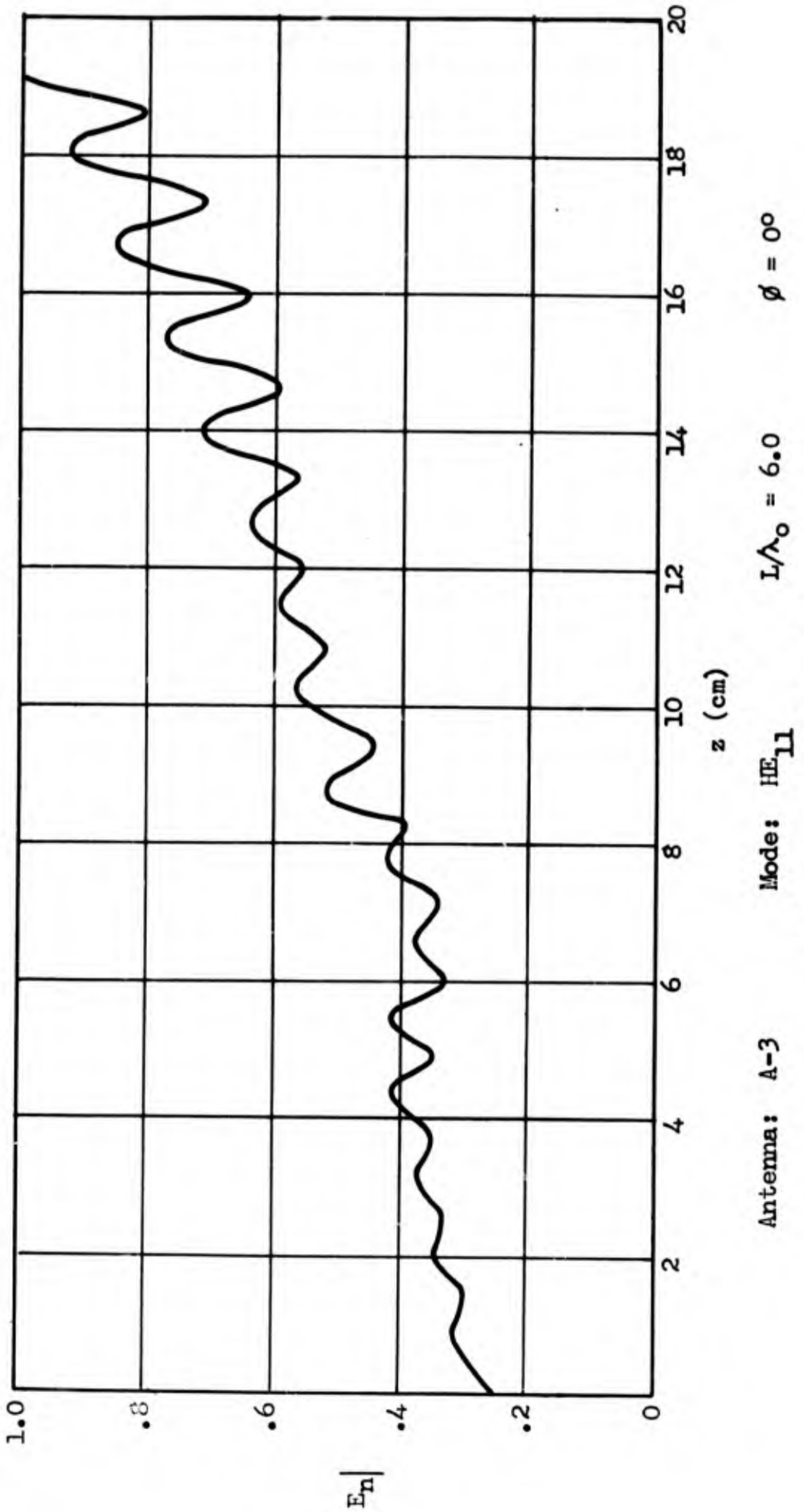

Fig. 3.43 NORMAL COMPONENT OF THE ELECTRIC FIELD AS A FUNCTION OF z, ON SURFACE OF RADIATING ROD.

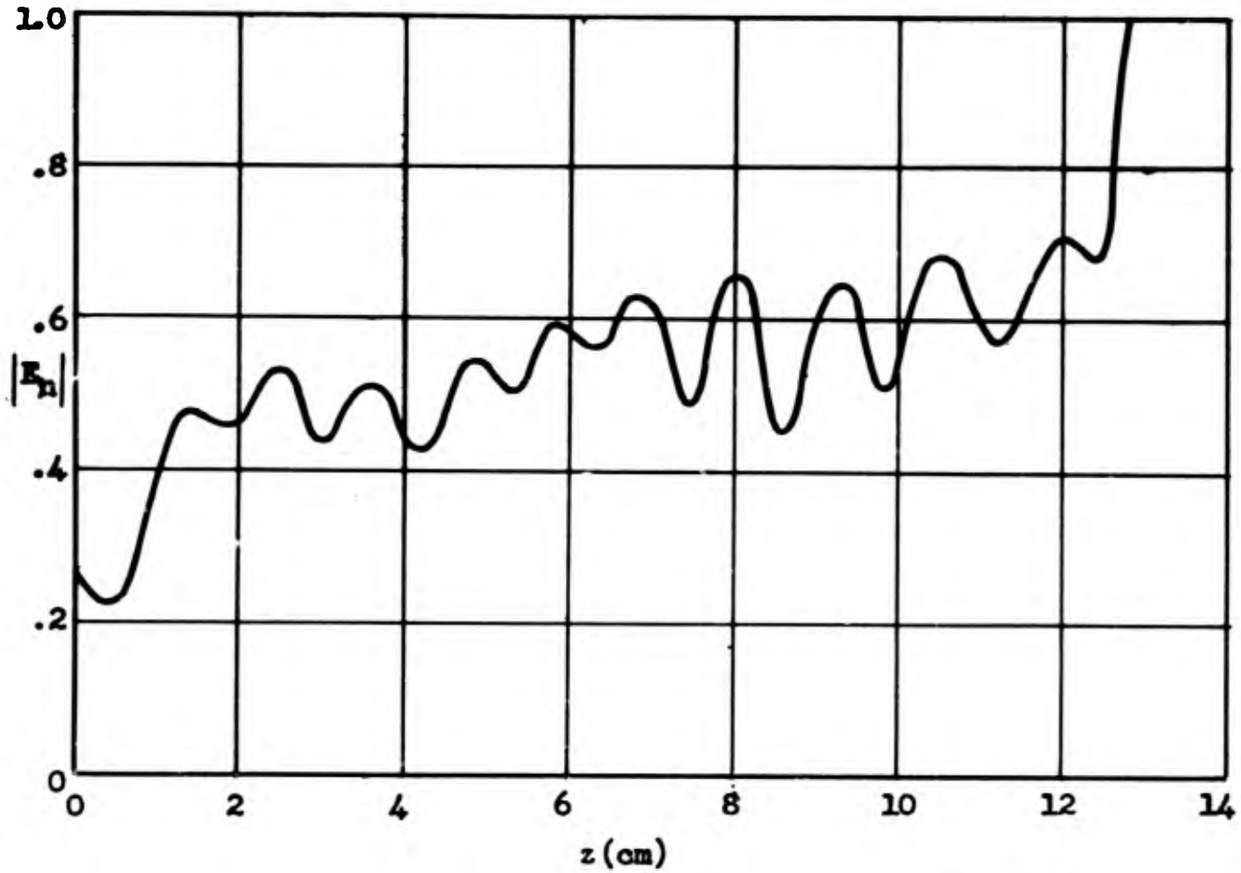

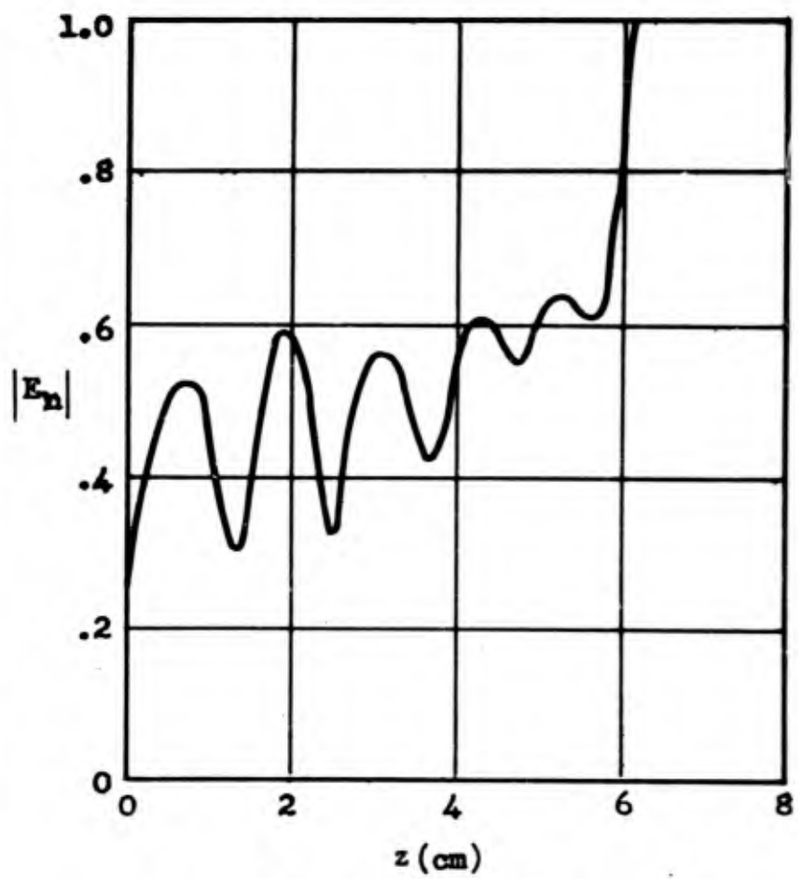

Antenna: A-4 $L/\lambda_o = 4.0$ Antenna: A-5 $L/\lambda_o = 2.0$

HE_{11} Mode $\phi = 0^o$ $\lambda_o = 3.20$ cm Maximum diameter = 8.70 λ_o

(Antennas excited at points z = 0)

Fig. 3.44 NORMAL COMPONENTS OF THE ELECTRIC FIELDS AS A FUNCTION OF AXIAL DISTANCE, z, ON THE SURFACES OF DIELECTRIC ROD ANTENNAS.

The B-Series of dielectric rods are of constant length ($6\lambda_o$) but the ratio of d_{min}/d_{max} varies from 0 to 1. The characteristics of this series are shown in Figures 3.45 through 3.50. The outstanding effect of tapering the rods is to decrease the minor lobe intensity. From the E-plane measurements it appears that using a ratio less than 1/3 has no effect on lobe attenuation, but this limit is not indicated by the H-plane measurements. The width of the major lobe appears to be a maximum in the neighborhood of $d_{min}/d_{max} = 2/3$.

Figures 3.48 through 3.50 show the normal component of the electric field plotted as a function of distance z. It is seen that the nearest approach to a sinusoidal feed is that of B-4, with a ratio of d_{min}/d_{max} of zero. This radiator also gives the maximum attenuation of secondary lobes. As in the case of the A-Series, it appears worthwhile to continue the taper of a rod to a point.

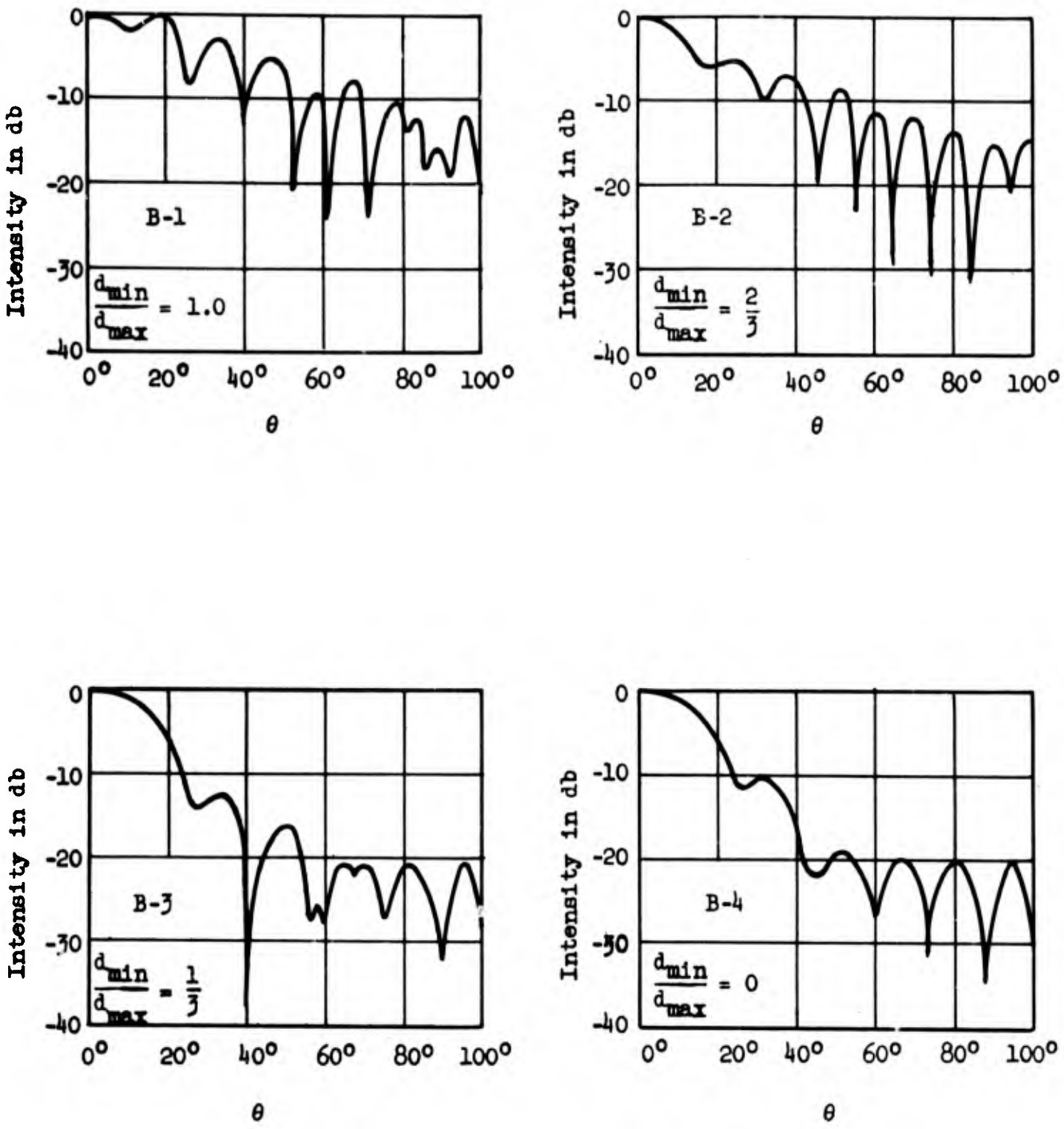

HE_{11} Mode E-Plane

$d_{max}/\lambda_o = .870$ $L/\lambda_o = 6.0$ $\lambda_o = 3.20$ cm

d_{max} = maximum diameter d_{min} = minimum diameter

Fig. 3.45 RADIATION PATTERNS OF THE B-SERIES

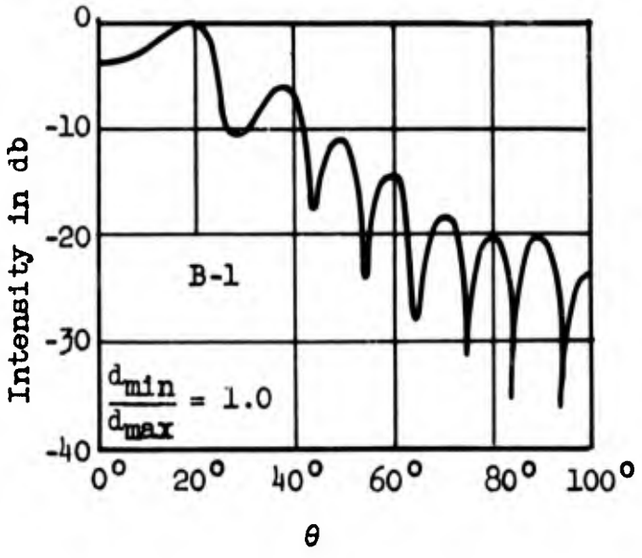

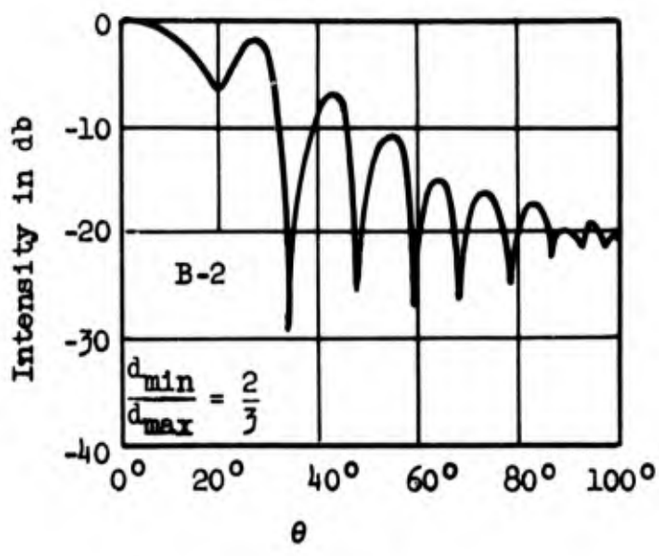

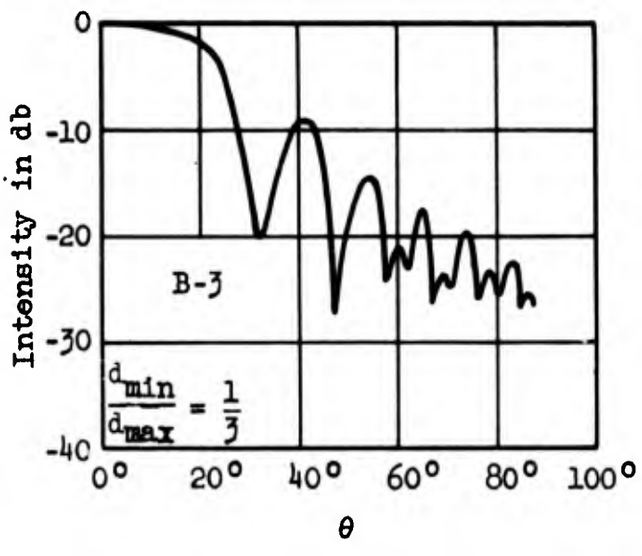

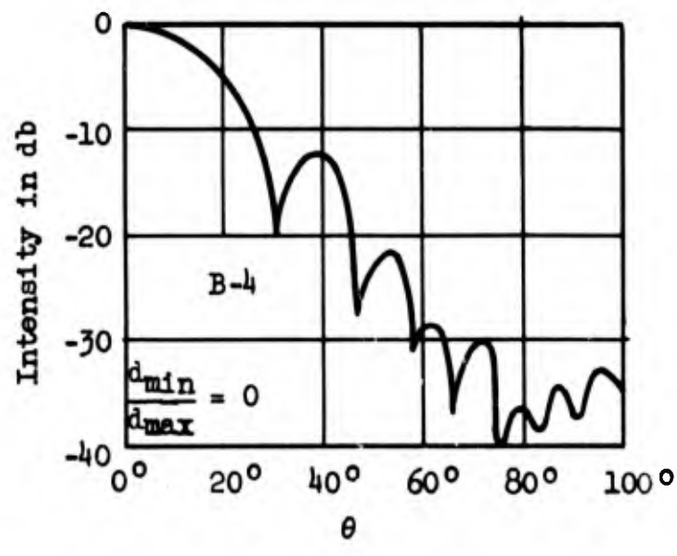

HE_{11} Mode H-Plane

$d_{max}/\lambda_o = .870$ $L/\lambda_o = 6.0$ $\lambda_o = 3.20$ cm

d_{max} = maximum diameter d_{min} = minimum diameter

Fig. 3.46 RADIATION PATTERNS OF THE B-SERIES

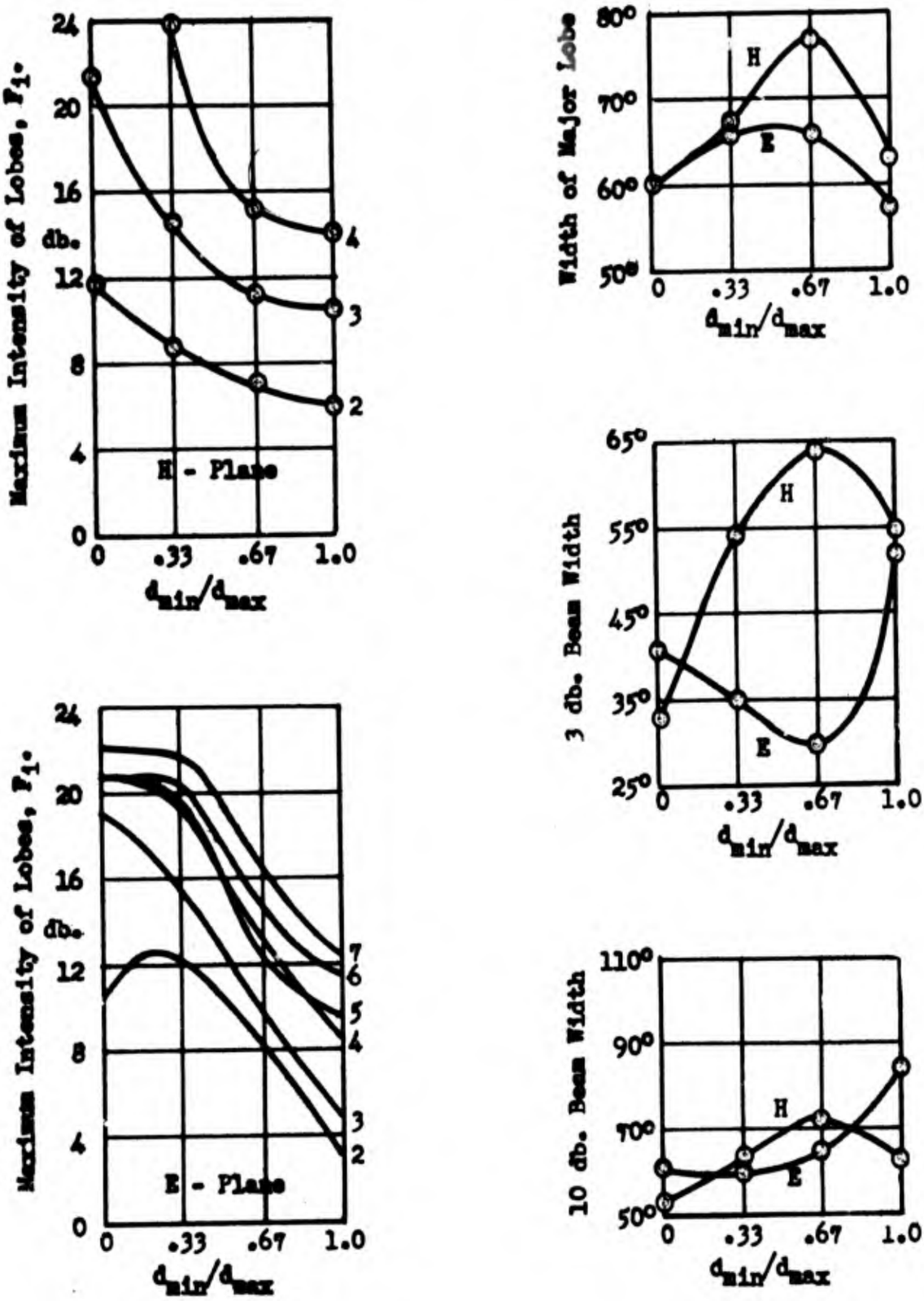

HE_{11} Mode E- and H- Planes $L/\lambda_0 = 6.0$

L: length d: diameter $\lambda_0 = 3.20$ cm

d_{min} = minimum diameter d_{max} = maximum diameter

Fig. 3.47

CHARACTERISTICS OF THE B-SERIES OF DIELECTRIC ROD ANTENNAS.

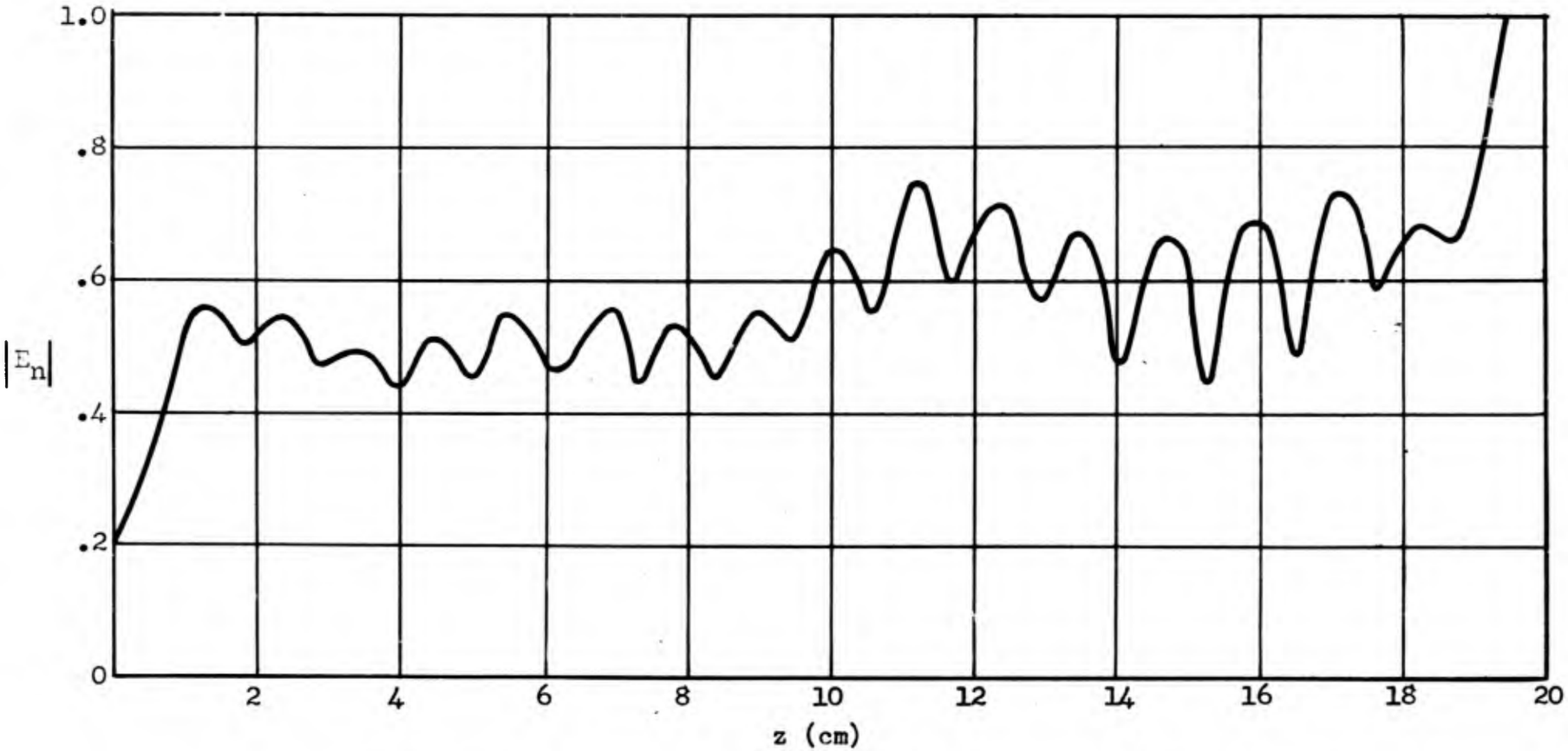

Antenna: B-2
$L/\lambda_o = 6.0$

$d_{max} = .870\lambda_o$
$d_{min}/d_{max} = 2/3$

Mode: HE_{11}
$\phi = 0^o$

Antenna excited at point z = 0.

Fig. 3.48 NORMAL COMPONENT OF THE ELECTRIC FIELD AS A FUNCTION OF z, ON THE SURFACE OF A RADIATING ROD.

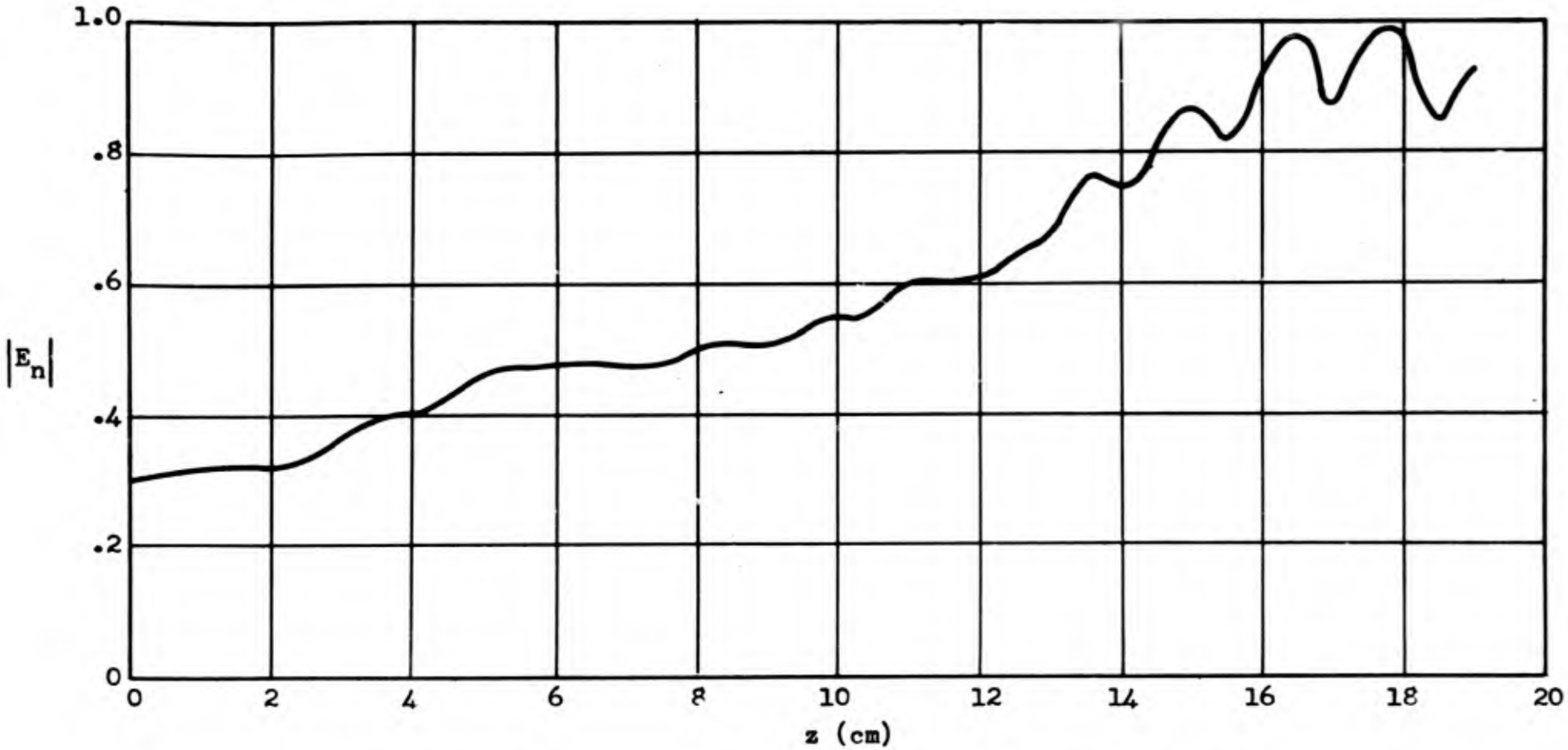

Antenna: B-3 $d_{max} = .870\lambda_o$ Mode: HE_{11}

$L/\lambda_o = 6.0$ $d_{min}/d_{max} = 1/3$ $\phi = 0^o$

Antenna excited at the point z = 0.

Fig. 3.49 NORMAL COMPONENT OF THE ELECTRIC FIELD AS A FUNCTION OF z, ON THE SURFACE OF A RADIATING ROD.

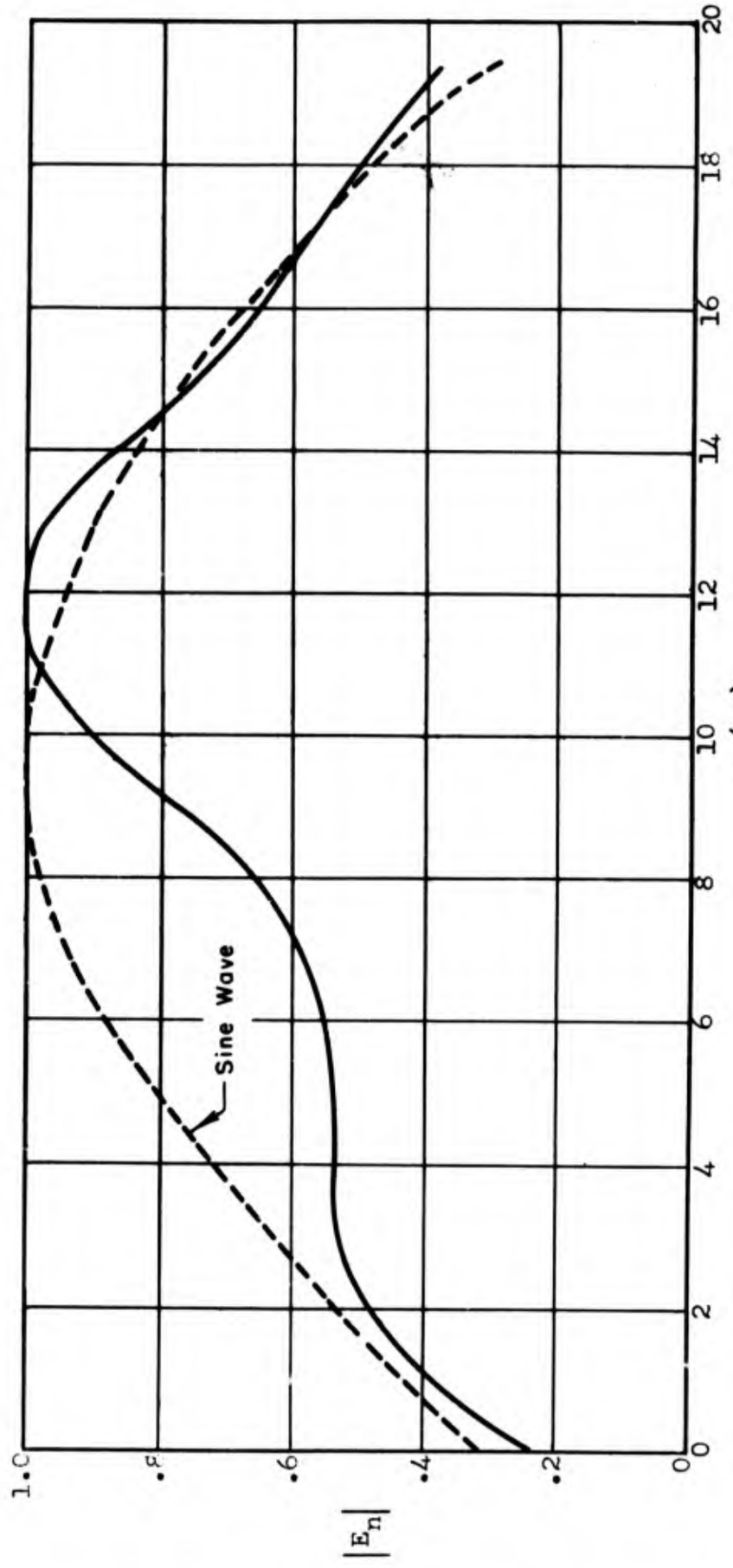

Fig. 3.50 NORMAL COMPONENT OF THE ELECTRIC FIELD AS A FUNCTION OF z, ON THE SURFACE OF A RADIATING ROD.

Figure 3.51 is the radiation pattern of antenna C-1, which is the type used by Mueller and Tyrrell[31] except of larger diameter. For the first half length of the rod, the cross section tapers uniformly to one half of maximum diameter, while the second half has a uniform cross section. The radiation pattern is similar to that of B-4, which tapered to a point, although for the H-plane it does not appear to be as good from the standpoint of minor lobe attenuation. Figure 3.52 shows the normal component of the electric field as a function of axial distance. Only the first half length appears to approach the sinusoidal field distribution. This is in agreement with the field distribution of the B-Series.

Figures 3.53 and 3.54 are the radiation patterns of rods D-1 and D-2. D-1 is $0.695\lambda_o$ in diameter and of uniform cross section. D-2 tapers uniformly to the point of $d_{min}/d_{max} = 0.5$. Both are $6\lambda_o$ long. The attenuation of minor lobes due to tapering is clearly indicated.

[31] Mueller and Tyrrell, op. cit.

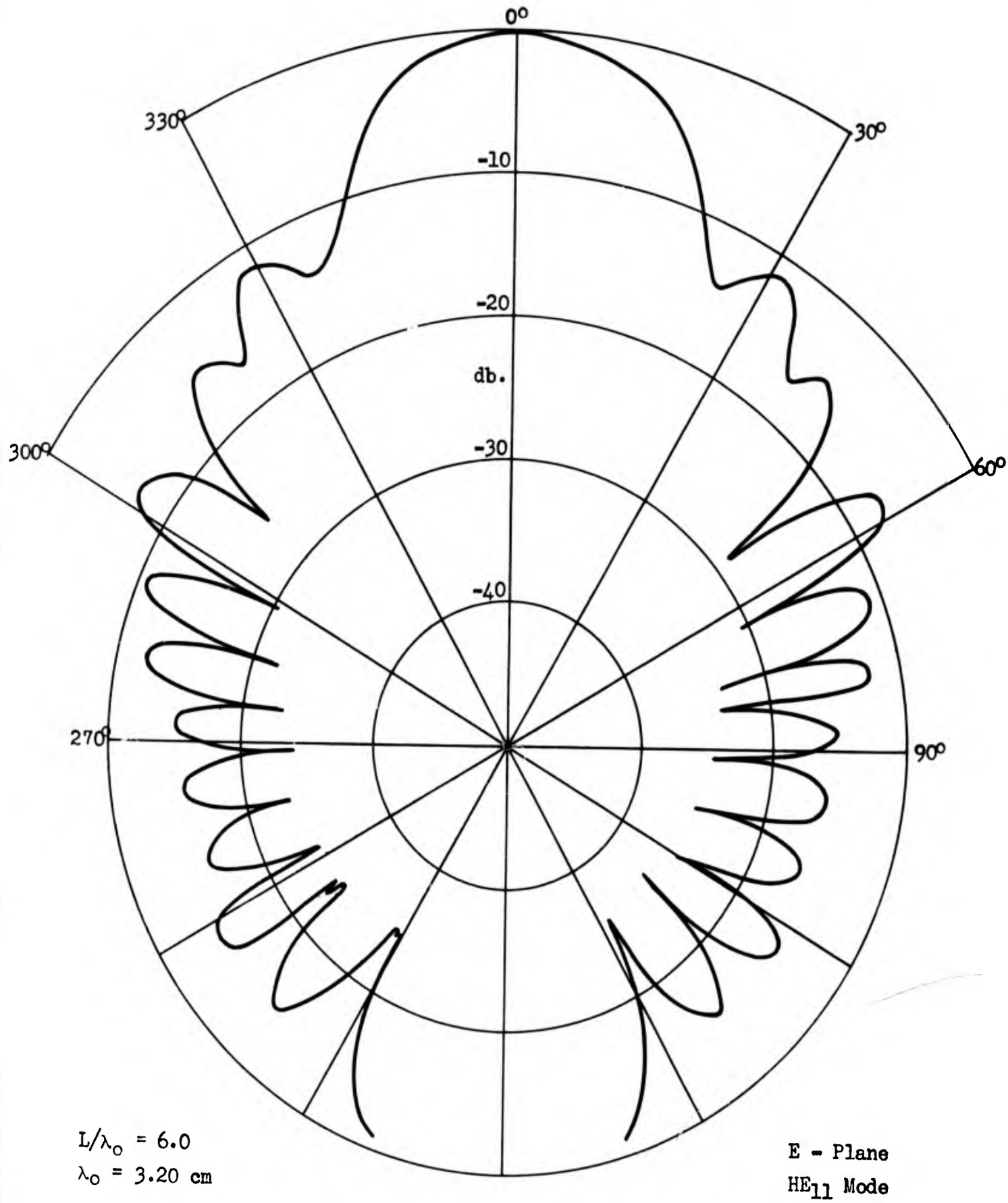

Fig. 3.51

RADIATION PATTERN OF THE ROD C-1.

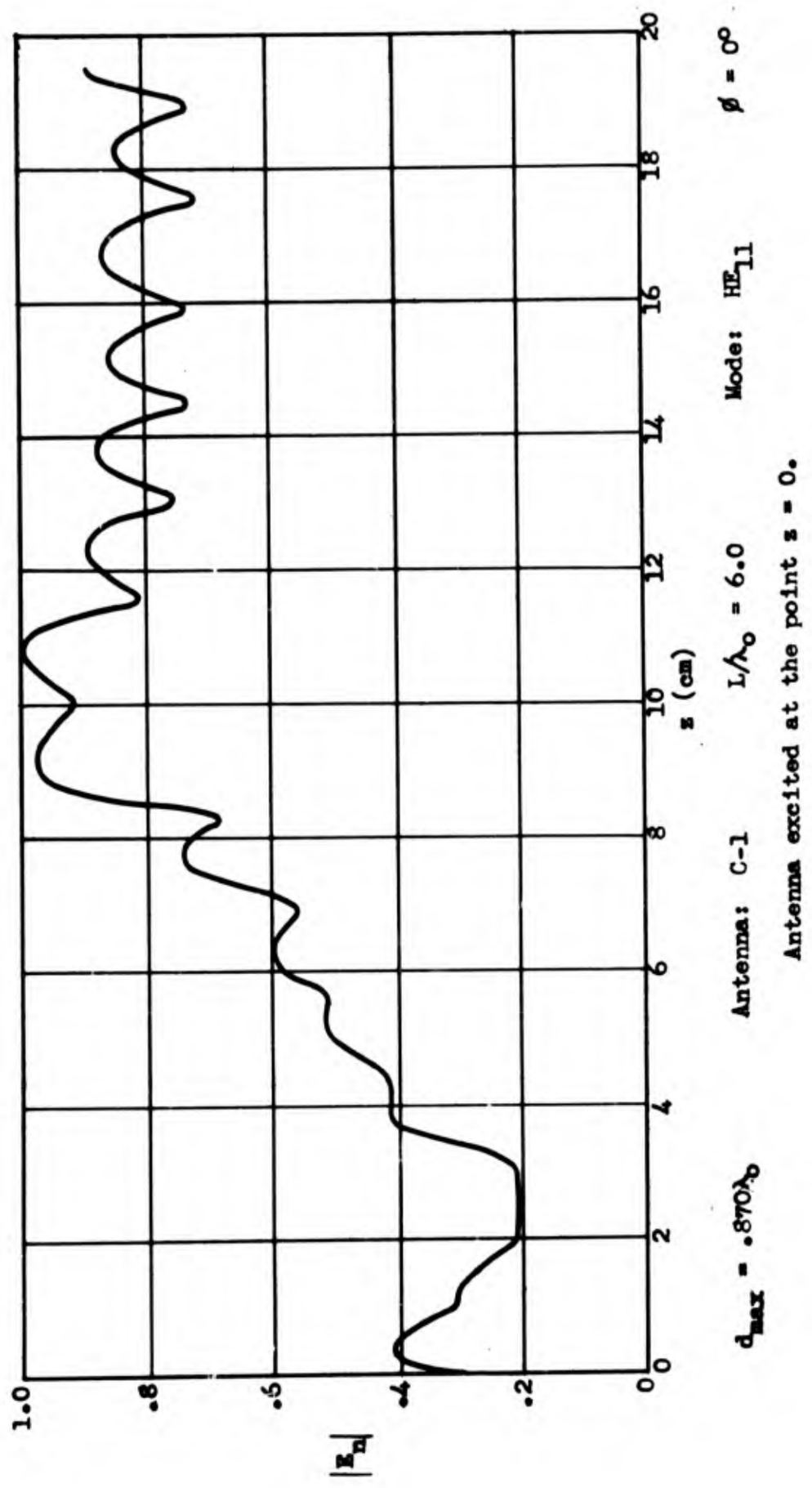

Fig. 3.52 NORMAL COMPONENT OF THE ELECTRIC FIELD AS A FUNCTION OF z, ON THE SURFACE OF A RADIATING ROD.

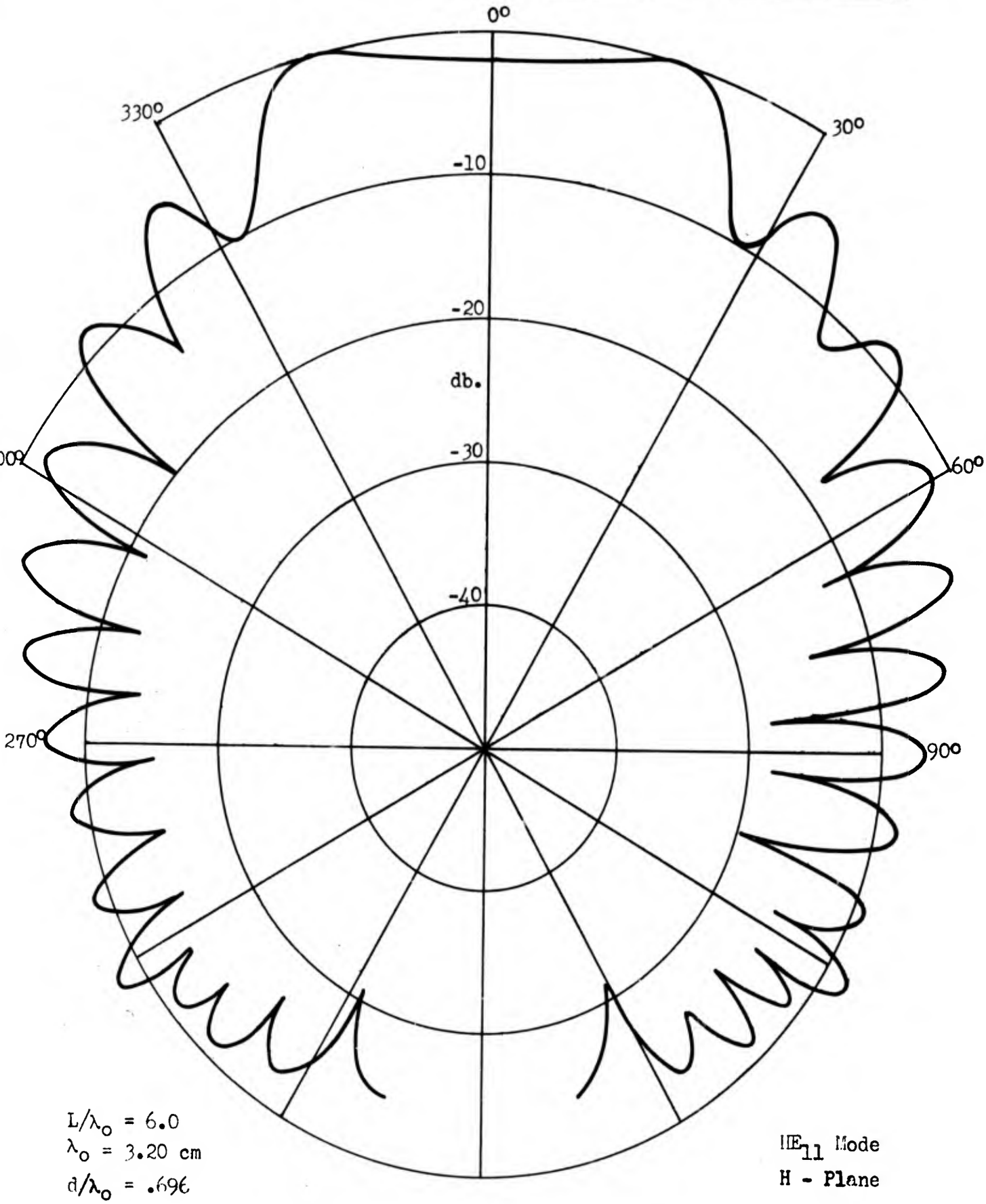

$L/\lambda_o = 6.0$
$\lambda_o = 3.20$ cm
$d/\lambda_o = .696$

HE_{11} Mode
H - Plane

Fig. 3.53

RADIATION PATTERN OF ROD D-1.

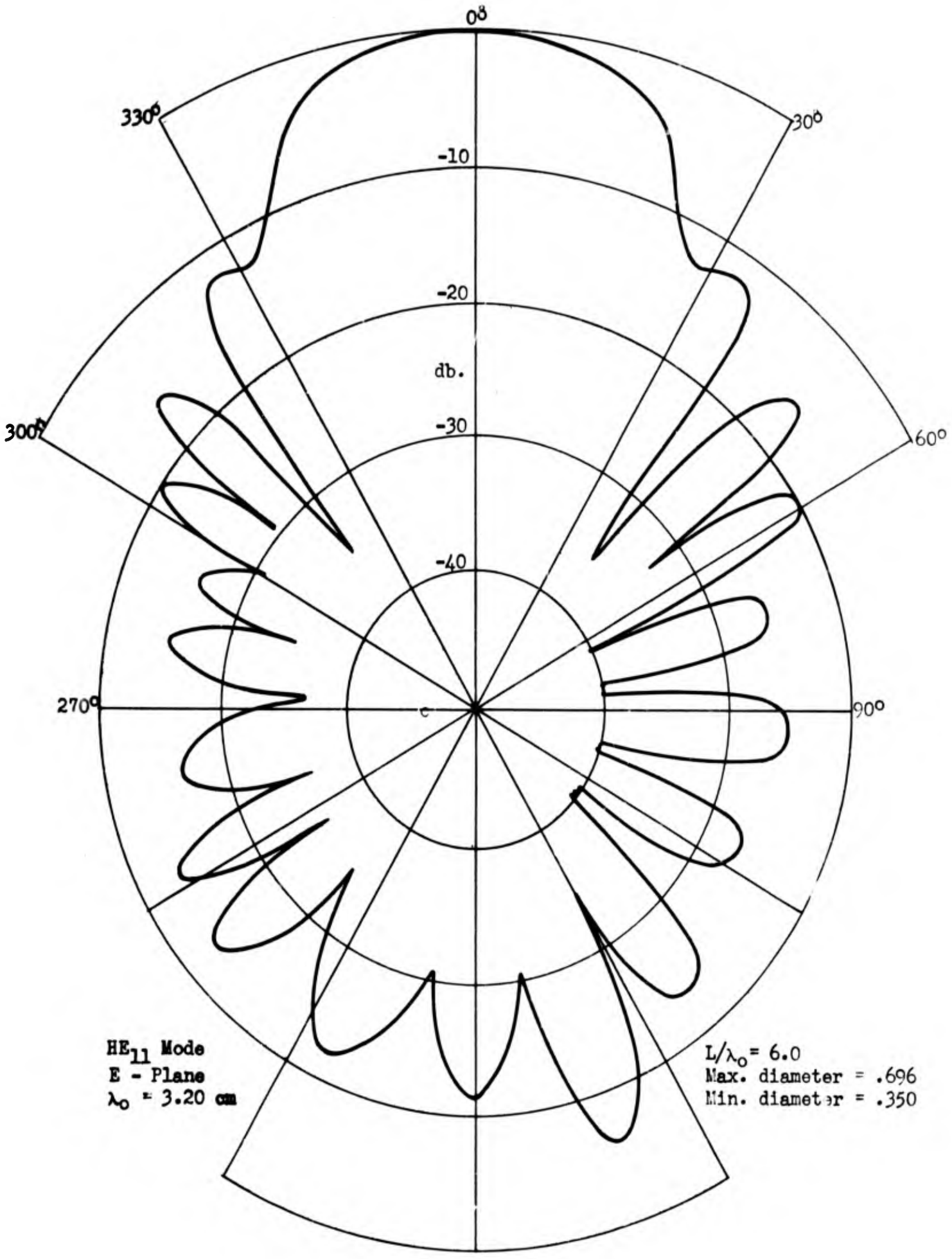

Fig. 3.54 RADIATION PATTERN OF THE ROD D-2.

The radiation pattern of an antenna does not tell the complete story of an antenna's performance by any means. If the antenna is used as a directive device, the gain is of equal importance. Figure 3.55 shows the gains of the various antennas just described. From Figure 3.55-a, it appears that the gain increases with increasin length, although not uniformly. From the trend of the curve for the H-Series, it seems that lengths greater than $L/\lambda_o = 10$ are not warrented and only a 6 db. gain occurs in increasing L/λ_o from 2 to 10. It is readily apparent why low loss dielectrics must also be used since the gain of the F-Series is considerably below that of the H-Series. It will be remembered that the F-Series consisted of rods of constant cross section but of different lengths, constructed of Lucite with a loss tangent of approximately 0.01. The H-Series rods were of identical shape but constructed of polystyrene with a loss tangent of approximately 0.001. Thus the F-Series would have more attenuation than the H-Series. The slope of the F-Series is less tha that of the H-Series, clearly indicating the loss due to attenuation within the rod itself. Figure 3.55-b indicates sizeable increases in gain due to increase in diameter. Since other workers have recommend the use of small diameter rods, it is in order to discuss this point. It is well-known that, within limits, the gain of an antenna is propo tional to its effective area, and that for such antennas as horns, etc the effective area is proportional to the geometrical area of the aper e. Now consider the E-Series in which the length is constant but the dia r varies. The rods are effectively fed by metal horns or waveguides wh area increases with the diameter of the dielectric rod. Therefore, t intensity of energy feeding the rods increases for increasing diamete

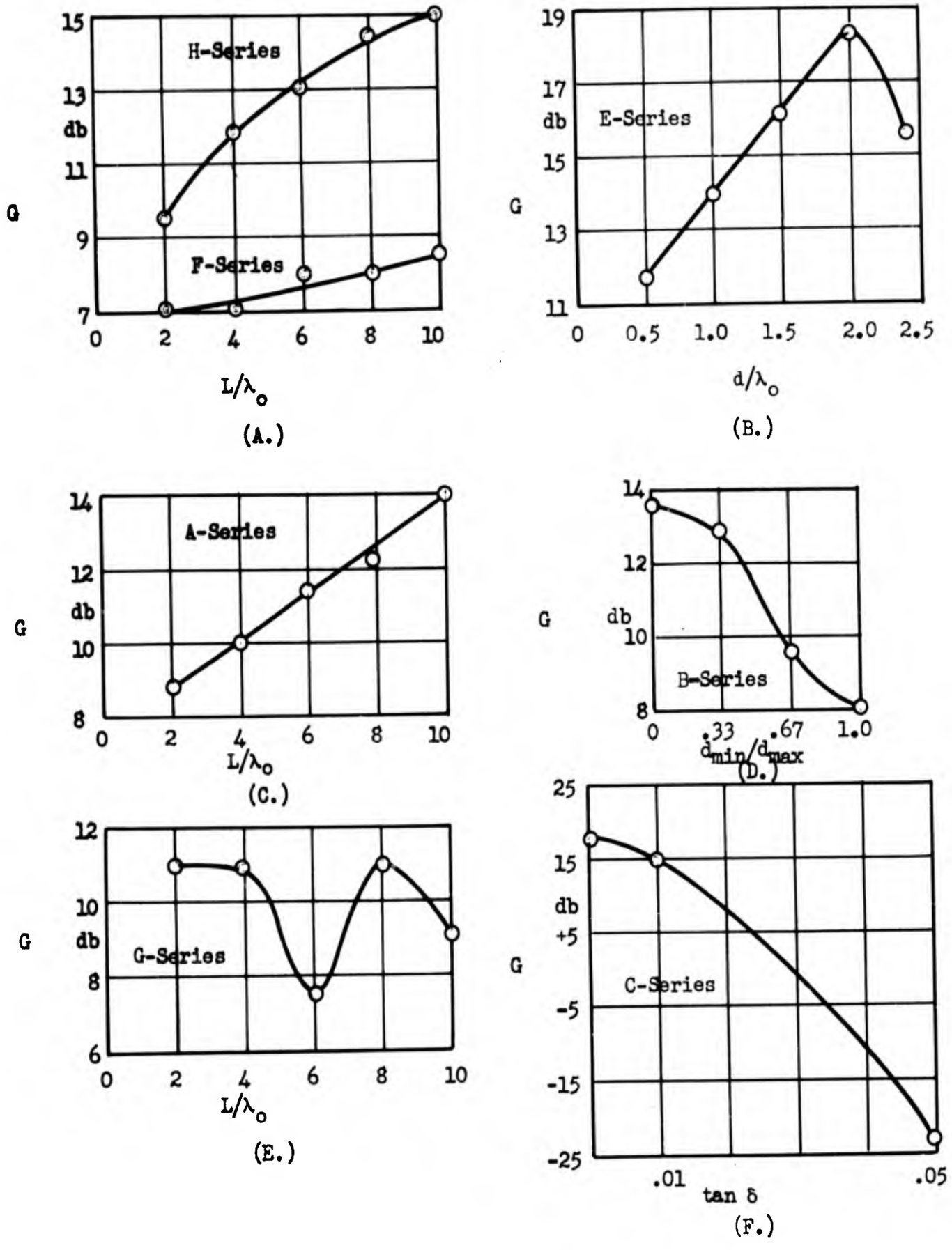

Fig. 3.55 ABSOLUTE GAIN OF THE DIELECTRIC ROD ANTENNAS.

This is another way of saying that the mode is excited more strongly in large rods than in small rods. While it is true that the gain can be increased by decreasing n_a (which would correspond to decreasing the diameter), it appears that this advantage is overshadowed by the increase in gain due to improvement in exciting the mode. Of course, for a given size rod, n_a can be decreased by using a material of lower dielectric constant. Wilkes[32] has noted this possibility and shows that the gain of antennas made from Teflon (K = 2.1) is greater than an identical one made of polystyrene (K = 2.56). However, the loss in Teflon is less than that of polystyrene by about one order and therefore, there is some doubt as to which factor the increase in gain is due. Higher gains could probably have been obtained with antennas made from thin-walled polystyrene tubes filled with paraffin or Nujol (K = 2.25).

The fact has not been considered that the increase in gain with increasing diameter might be due to the presence of the higher order modes. The higher order modes may be at least a contributing factor since, for the energy propagating in the higher modes, the n_a is small, which is desirable. However, referring again to Figure 3.55-b, it is noted that the gain decreases for diameters greater than $2\lambda_o$. While measurements were made on only one rod of diameter greater than $2\lambda_o$, it is believed that the measurements made do represent the proper trend. To understand this, again consider the case of metal horn radiators. Southworth and King[33] have shown that, for a horn excited

---

[32] Wilkes, op. cit.

[33] Southworth, G. C., and King, A. P., "Metal Horns as Directive Receivers of Ultra-short Waves," Proc. I.R.E., 27, 95, 1939.

in the dominant mode with a sinusoidal intensity variation across the throat of the horn, the gain at first increases with an increase in the flare angle of the horn and then decreases. This decrease is due to the energy distribution no longer maintaining its sinusoidal form but breaking up into other forms. This distortion of excitation might represent the case of the tapered section feeding energy to rod E-1. If such is the case, it would seem to indicate that increases in gain are due to improvements in excitation rather than to the presence of the higher modes. However, there is not sufficient data to draw definite conclusions.

Figure 3.55-c shows that for a rod of constant taper, the gain increases linearly with increasing length. Considering the knowledge of the field intensity distribution on the surface of the A-Series rods, this increase in gain is to be expected. It appears definitely worthwhile to extend the tapered rods to a point.

Figure 3.55-d shows the improvement in gain due to tapering of a rod of constant length. The maximum gain occurs for a full tapered rod or one with an approximate sinusoidal taper of field intensity. However, it should be noted that the rate of gain increase becomes less as d_{min}/d_{max} increases. If one compares the gain of B-4 and A-1 (both rods tapered to a point), it is seen that the longer rod has a slightly higher gain.

Figure 3.55-e gives the gain relationship of the G-Series. The two low points (for G-1 and G-3) are due to slight nulls in the forward direction of these rods. However, it can be seen that the loss of gain

due to attenuation within the rod probably offsets increases of gain due to increases in L/λ_o.

Figure 3.55-f shows the gain of the C-Series as function of the loss in the material. The rod C-1 is made of Lucite (tan δ = 0.01-0.001), C-2 of polystyrene (tan δ = 0.001 - 0.0001), and the C-3 rod is of laminated linen - Bakelite (tan δ = 0.05). It is clear that the gain decreases with an increase in tan δ (or power factor). Lucite probably represents the poorest dielectric that can be successfully used for dielectric antennas.

It is generally true that in the case of the end-fire antenna array, the ratio of the effective area to frontal area is greater than unity, but the ratio of the effective area to the total surface area is quite small. Graphs of the effective area as a function of geometrical area are shown in Figure 3.56. It is evident that the increase in effective area is much less than the increase in geometrical area. Fortunately, this point is not of importance in most design work.

3. $TM_{01}(E_{01})$ Mode. The TM_{01} mode is characterized by a null in the forward direction. For most applications of antennas, this null is undesirable and hence this mode has rarely been used to excite antennas. It is believed, however, that antennas with the null at the center do have some uses. Two possible applications will be discussed briefly.

To receive energy which has been radiated by an antenna excited in the TM_{01} mode, the polarization must be in the plane of r and θ, that is, the receiving antenna has to have its polarization in the plane in which the radiation pattern is measured. There are no E and H

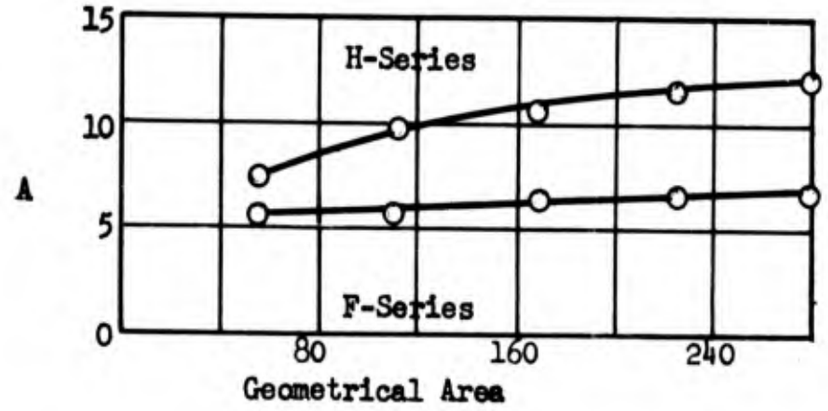

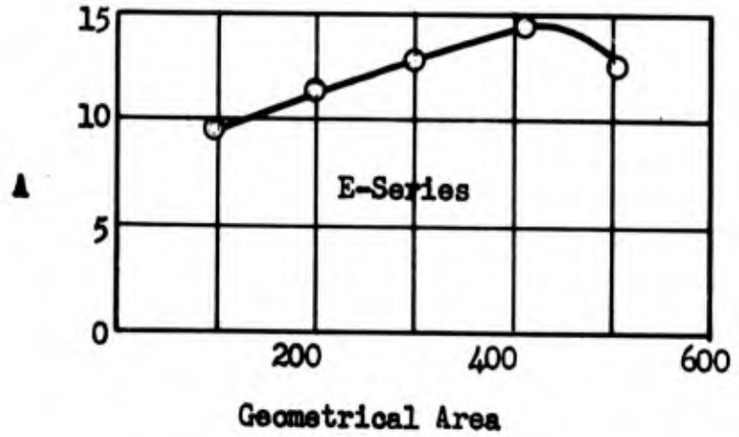

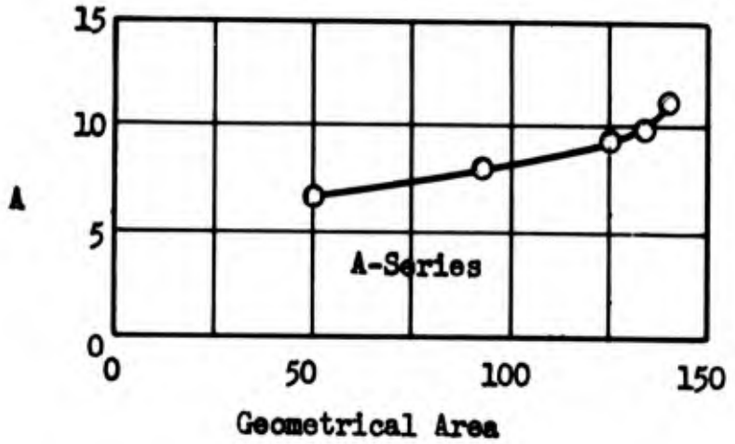

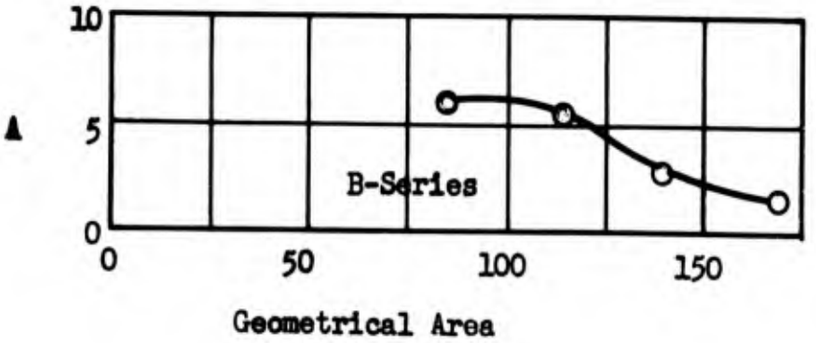

Fig. 3.56 EFFECTIVE AREA, A, AS A FUNCTION OF THE GEOMETRICAL AREA OF DIELECTRIC ROD ANTENNAS.

planes since the mode is circularly symmetric. The general type of patterns obtained with the TM_{01} wave is shown in Figure 3.57. If the antenna is pointed vertical, the radiation in a horizontal plane is omnidirectional. This type of antenna is used in types of beacons and in broadcasting. Due to the extremely small size and low cost, the dielectric rod, if properly designed might be a useful antenna in this application. For most work, the maximum radiation would be desired in the $\theta = 90^{\circ}$ plane, with the null as broad as possible and back radiation reduced as much as possible. The effect of the reflecting earth would also have to be taken into account, but it might be possible to space the antenna at such a height above the earth that the ground reflection would improve the radiation pattern. For certain types of beacons used in connection with aircraft receivers, it might be desirable to have the maximum radiation appearing at some angle less than 90°.

Another possible use of the TM_{01} type of radiation pattern is in direction finding devices. The peak of the major lobe of many antenna systems is rather broad and the angle of maximum intensity may be indefinite. Some of the experimental results in this section indicate that the central null of the TM_{01} antenna radiation can be made very sharp and, hence, a null detecting device of this kind might be an improvement over other antenna systems of similar size. For preliminary direction finding the antenna might be excited in the HE_{11} mode by some exciter such as a helix (giving circular polarization) and then switched over to the TM_{01} mode for the final determination of direction. Arrays of antennas excited in the TM_{01} mode might be

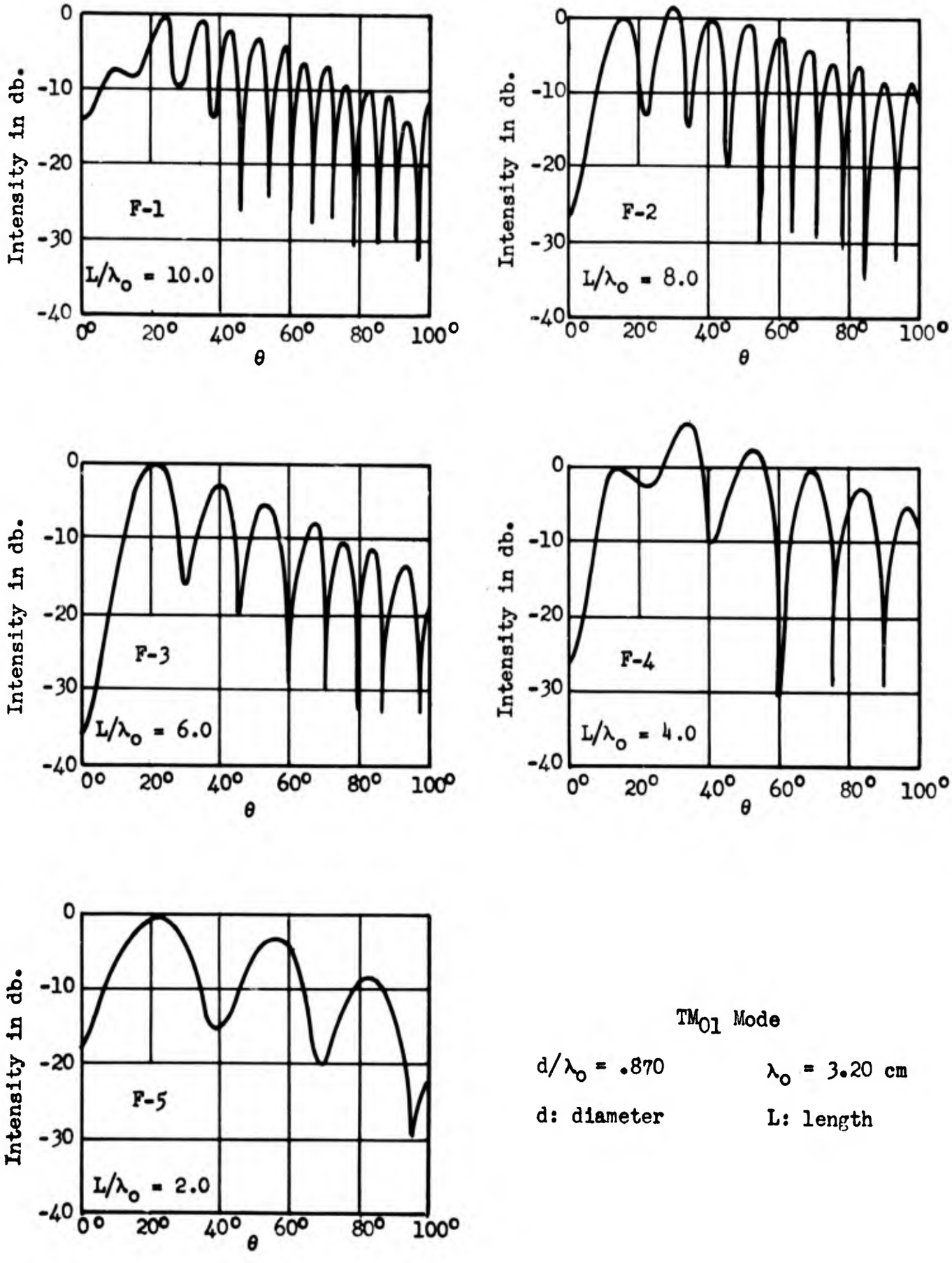

TM_{01} Mode

d/λ_o = .870 λ_o = 3.20 cm

d: diameter L: length

Fig. 3.57 RADIATION PATTERNS FOR THE F - SERIES

designed to give even sharper nulls than those of single elements. The right and left major lobes of the TM_{01} pattern are out of phase. By using the single major lobe of a HE_{11} pattern as a reference, it might be possible to obtain right-left directions.

Actually, a more important reason for investigating experimentally the radiation properties of dielectric rods excited in the TM_{01} mode was the acquisition of accurate data for checking theoretical work. Diffraction or radiation theory is a field of great interest and much activity at the present time. In most of the theoretical work, it is easier to apply the theory to antennas excited in simple modes rather than the modes of greater angular variation. Hence, it would be of value to many theoretical workers if careful and extensive experimental results were available to guide their work and to check the validity of the assumptions and approximations which are often necessary.

Characteristics of the F-Series (variation in length only) excited in TM_{01} modes are shown in Figures 3.57 through 3.59. As with the dominant mode, the number of lobes is a linear function of length. Corresponding to beamwidth of the HE_{11} mode, the width of the central null (angle between first principle maxima) and null depth (db. below maxima of main lobes) are plotted. It appears that the null width decreases with increasing length. However, there is merging of lobes as the length increases and hence, the null width is plotted as a discontinuous function of length. From theoretical consideration, the central null should go to zero signal strength. However, in practice it is variable and appears to have a maximum depth at about $L/\lambda_o = 6$.

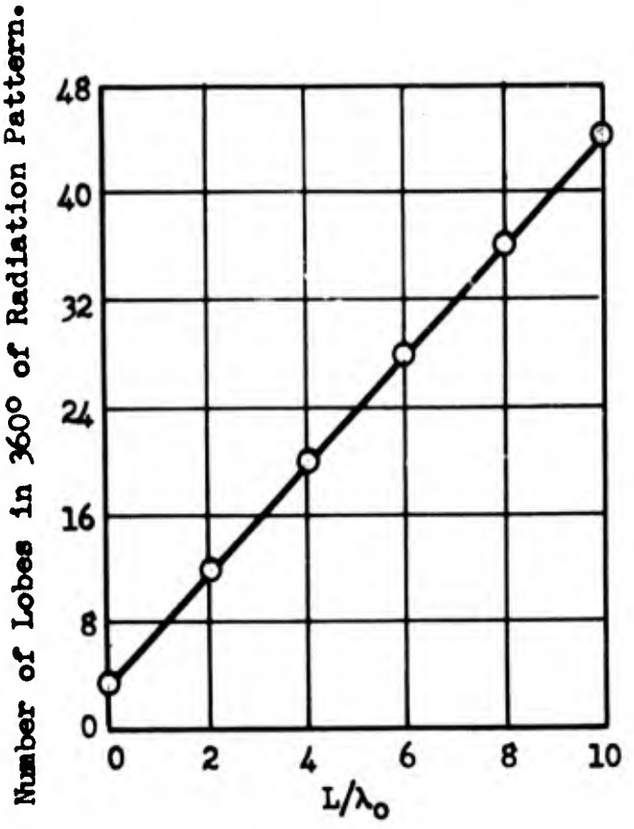

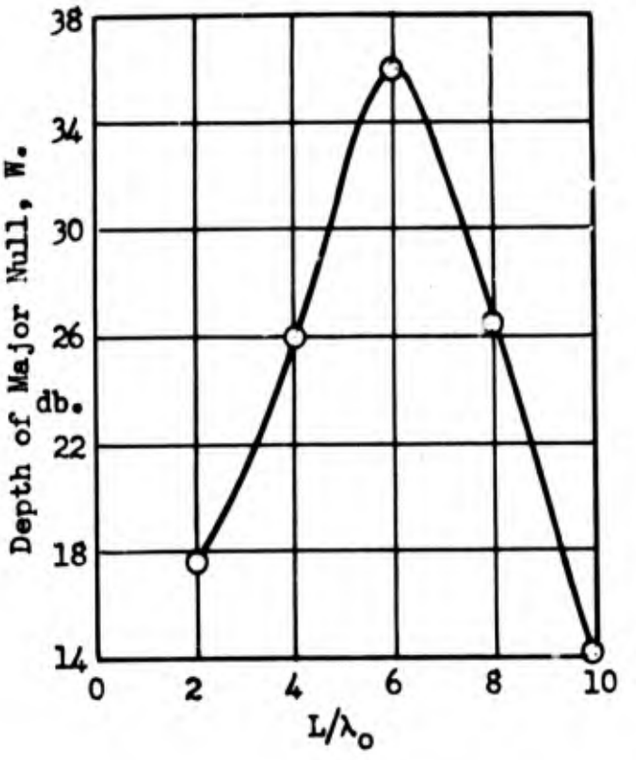

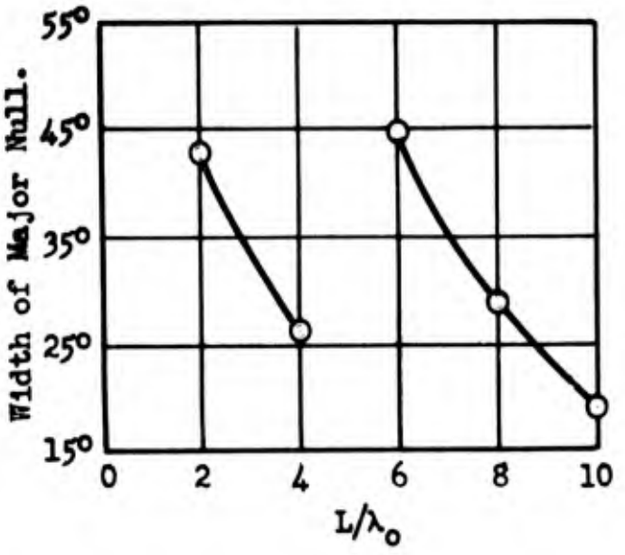

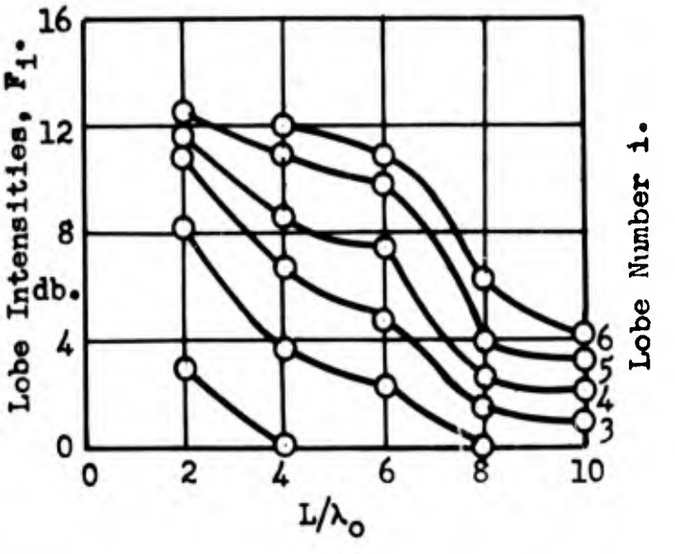

F-Series

TM_{01} Mode

Diameter of Rods = $.870\lambda_o$

Dielectric Constant = 2.56

λ_o = 3.20 cm

Fig. 3.58

CHARACTERISTICS OF THE F-SERIES OF DIELECTRIC ANTENNAS

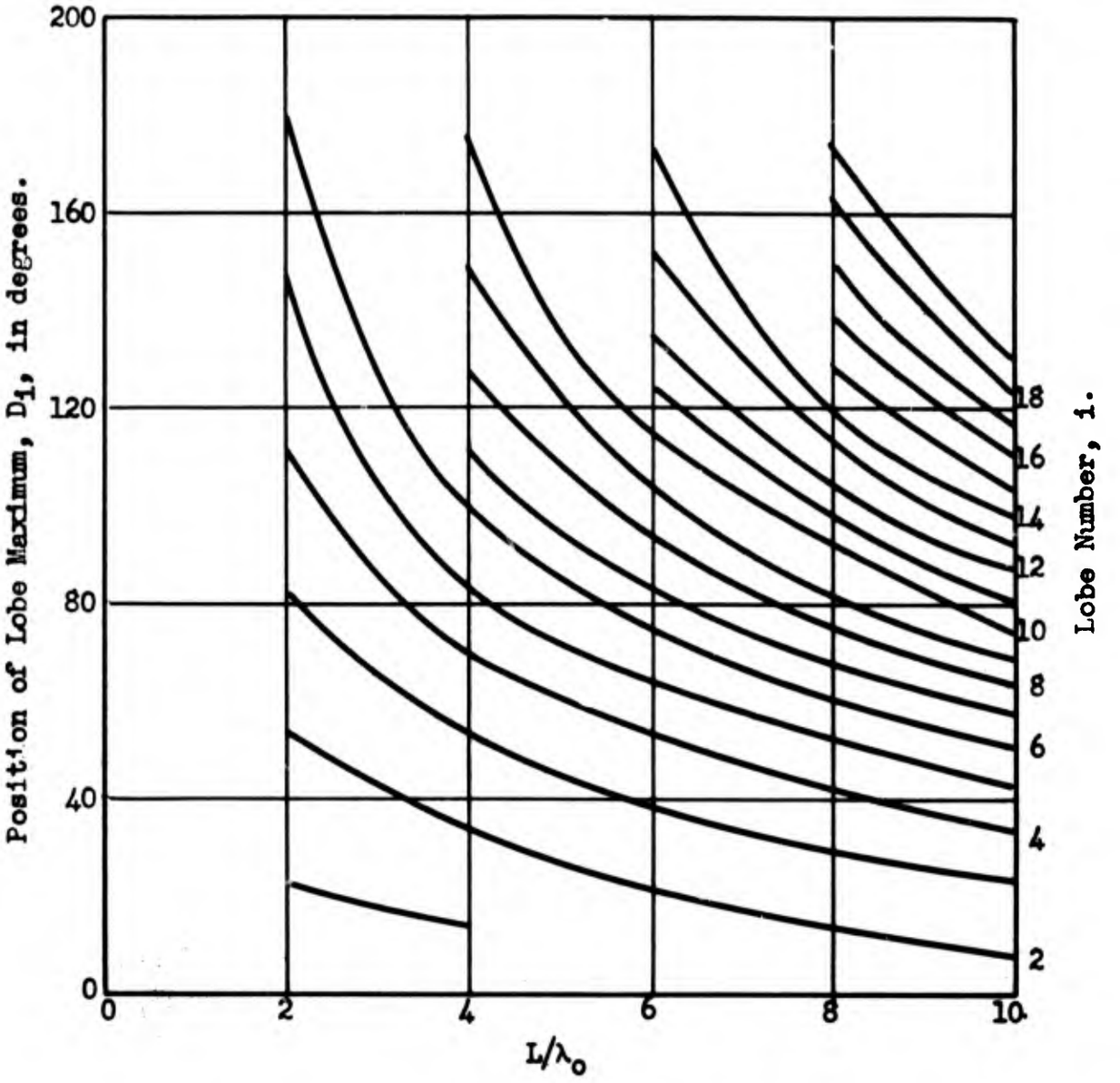

F - Series TM_{01} Mode

d/λ_o = .870 λ_o = 3.20 cm

L: length d: diameter

Dielectric Constant = 2.56

Fig. 3.59

ANGULAR POSITION OF THE MAXIMUM LOBE INTENSITIES AS A FUNCTION OF THE LENGTH OF A DIELECTRIC ROD ANTENNA.

However, it should be noted that even the most shallow null is 14db. which corresponds to a power level 4% of the maximum. The 36 db. null of the $6\lambda_0$ rod corresponds to a power level of 0.025%. The lobe positions behave similarly to the HE_{11} mode as well as do the minor lobe intensities. The loss factor of the material and the inertia of the recording system were probably the causes of the signal strength not being zero in the forward direction.

Figures 3.60 and 3.61 are polar plots of the radiation patterns for the F-Series rods of lengths $L/\lambda_0 = 10.0$ and $L/\lambda_0 = 6.0$. The theoretical patterns are plotted on the left and the experimental pattern on the right. It is seen that good agreement between theory and experiment was obtained.

Figure 3.62 is a graph of the radial component of the electric field as a function of axial distance z on the surface of a F-Series rod of length $4\lambda_0$. It can be seen that very little of the energy is reflected from the end of the rod. The lack of standing waves off the end of the rod indicate the absence of serious reflections from nearby objects. Figure 3.63 is a graph of the $\left| E_r \right|$ measured as a function of r across the end surface of a F-Series rod.

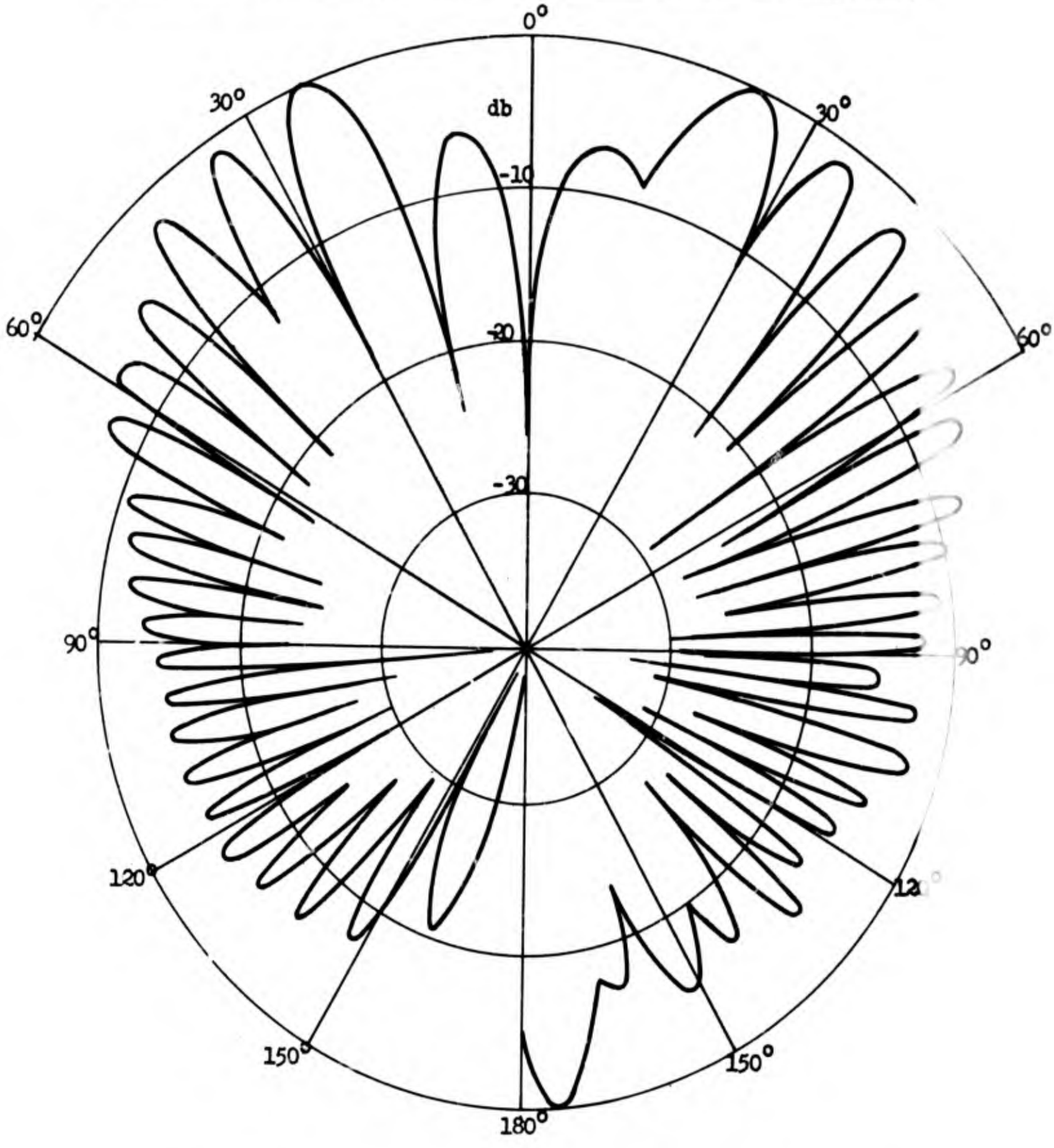

Theoretical Pattern on Left

Antenna: F-1 $L/\lambda_o = 10.0$

$\lambda_o = 3.20$ cm $n_a = 1.16$

Experimental Pattern on Right

Mode: TM_{01} $d/\lambda_o = .870$

Effective Diameter = .65d

Fig. 3.60 THEORETICAL AND EXPERIMENTAL RADIATION PATTERNS OF A DIELECTRIC ROD ANTENNA.

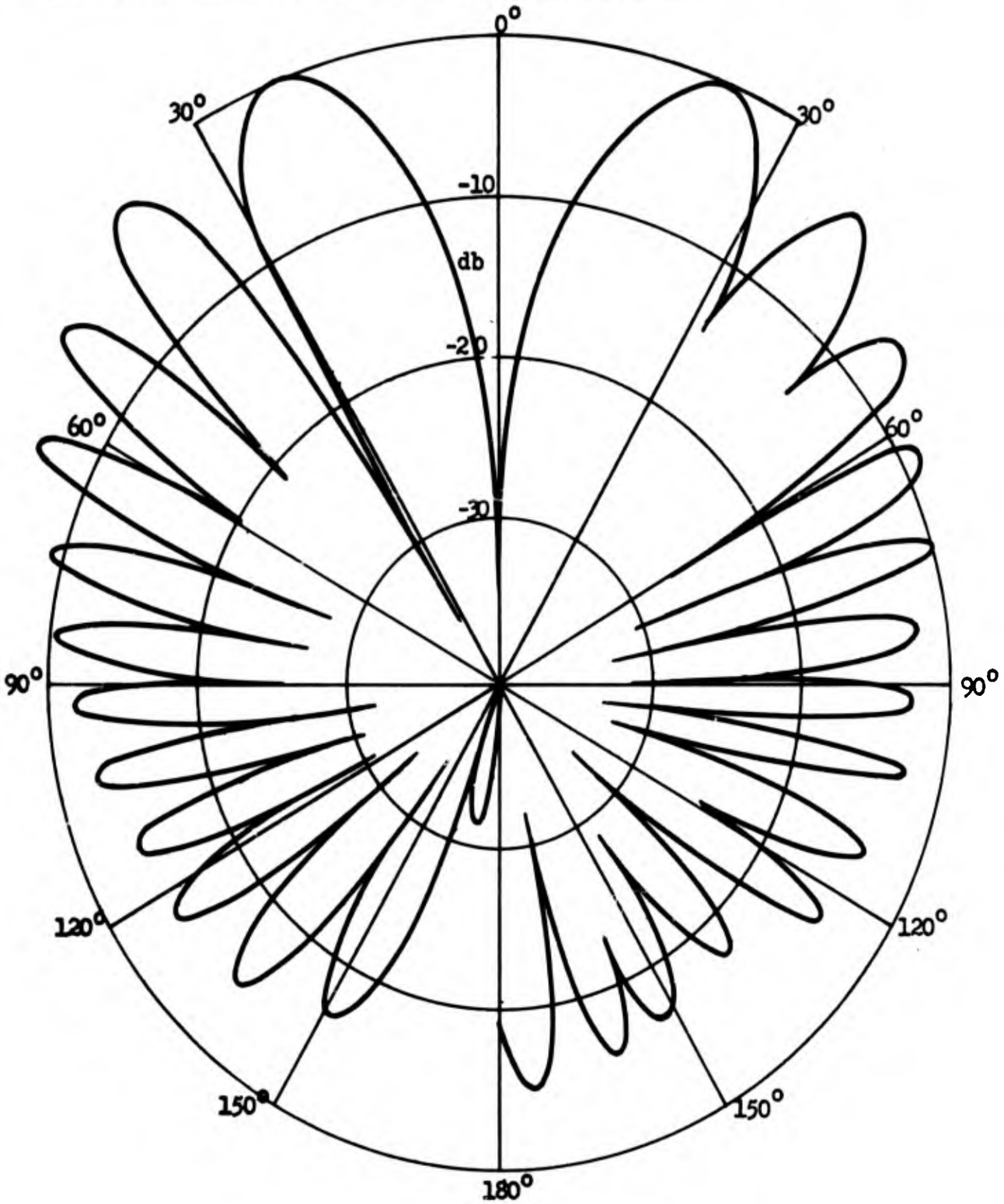

Theoretical Pattern on Left

Antenna: F-3

λ_o = 3.20 cm

L/λ_o = 6.0

n_a = 1.16

Experimental on right

Mode: TM_{01} d/λ_o = 8.70

Effective Diameter = .65d

Fig. 3.61 THEORETICAL AND EXPERIMENTAL RADIATION PATTERNS OF A DIELECTRIC ROD ANTENNA.

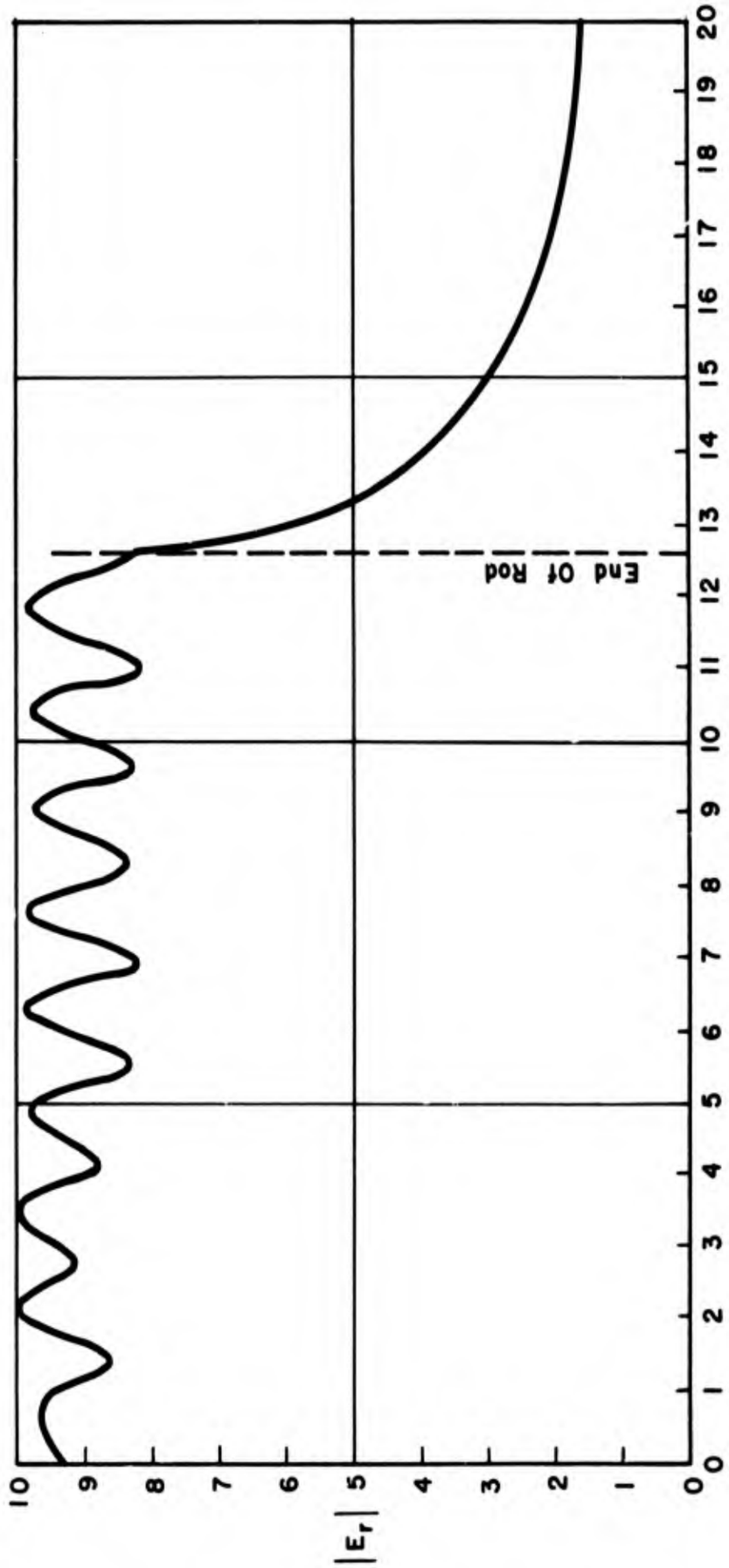

Mode: TM_{01} Diameter: $.87\lambda_o$ Length: $4\lambda_o$ Material: Lucite

Measurements Were Made At The Surface Of The Rod

Energy Is Fed To The Rod At z = 0

Fig. 3.62 Radial Component of Electric Field as a Function of Axial Length for a Dielectric Rod Radiator of Uniform Circular Cross-Section

DRL - UT
DWG AE 802
CMM - CLW
1 - 13 - 50

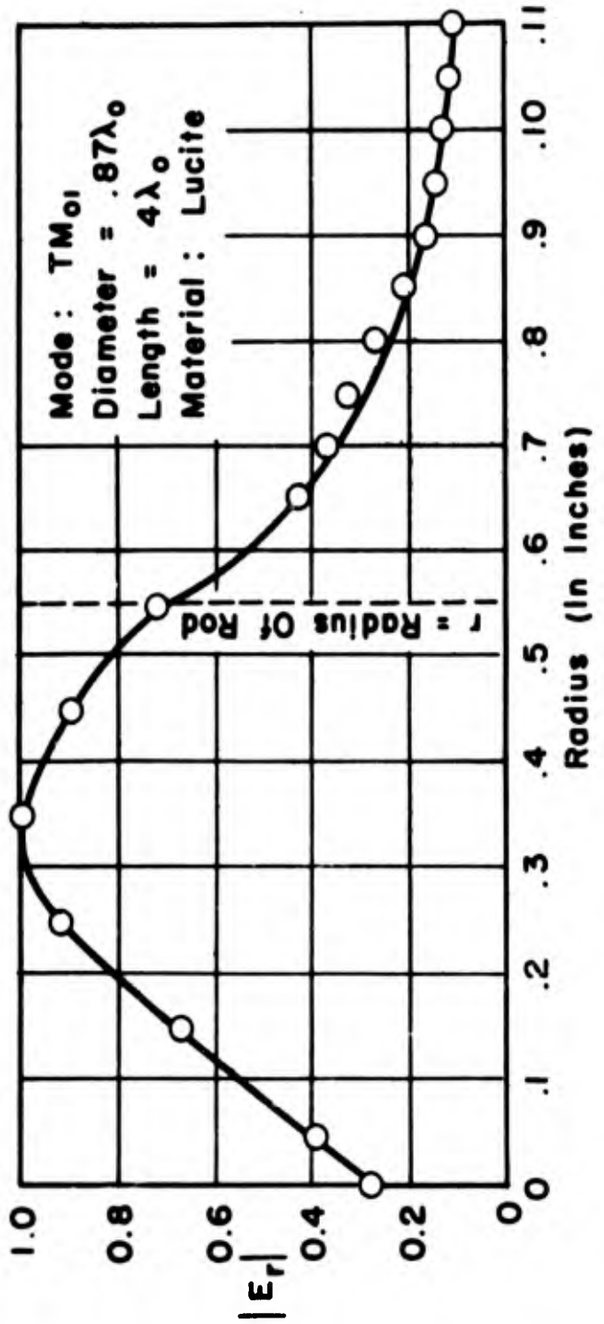

Fig. 3.63 – Radial Component Of The Electric Field As A Function Of Radial Distance, For A Dielectric Rod Radiator Of Uniform Circular Cross – Section.

The characteristics of the E-Series antennas excited in the TM_{01} mode are shown in Figures 3.64 through 3.67. It will be remembered that the E-Series rods are all of $6\lambda_o$ in length and of various diameters from $0.5\lambda_o$ to $2.4\lambda_o$. In the TM_{01} measurements the $0.5\lambda_o$ rod will not support propagation and hence, no measurements are included for it.

Lobe positions are not plotted since they are essentially independent of diameter. As was the case with the dominant mode, an increase in diameter reduced the intensity of the minor lobes. It is evident from the data given in Figure 3.65 that the depth of the central null and the width of the central null did not follow a continuous trend as the diameter increased. From these data it appears that narrow nulls are obtained with small diameter antennas but the deepest nulls would be obtained with antennas of approximately $1.5\lambda_o$ in diameter.

Figures 3.66 and 3.67 are examples of the standing wave patterns of E_r on the surfaces of two of the E-Series antennas. The pattern on the rod of diameter $1.0\lambda_o$ is reasonably uniform indicating the propagation of a single mode but the pattern of E_r on the rod $2.4\lambda_o$ in diameter clearly indicates the presence of the higher order modes.

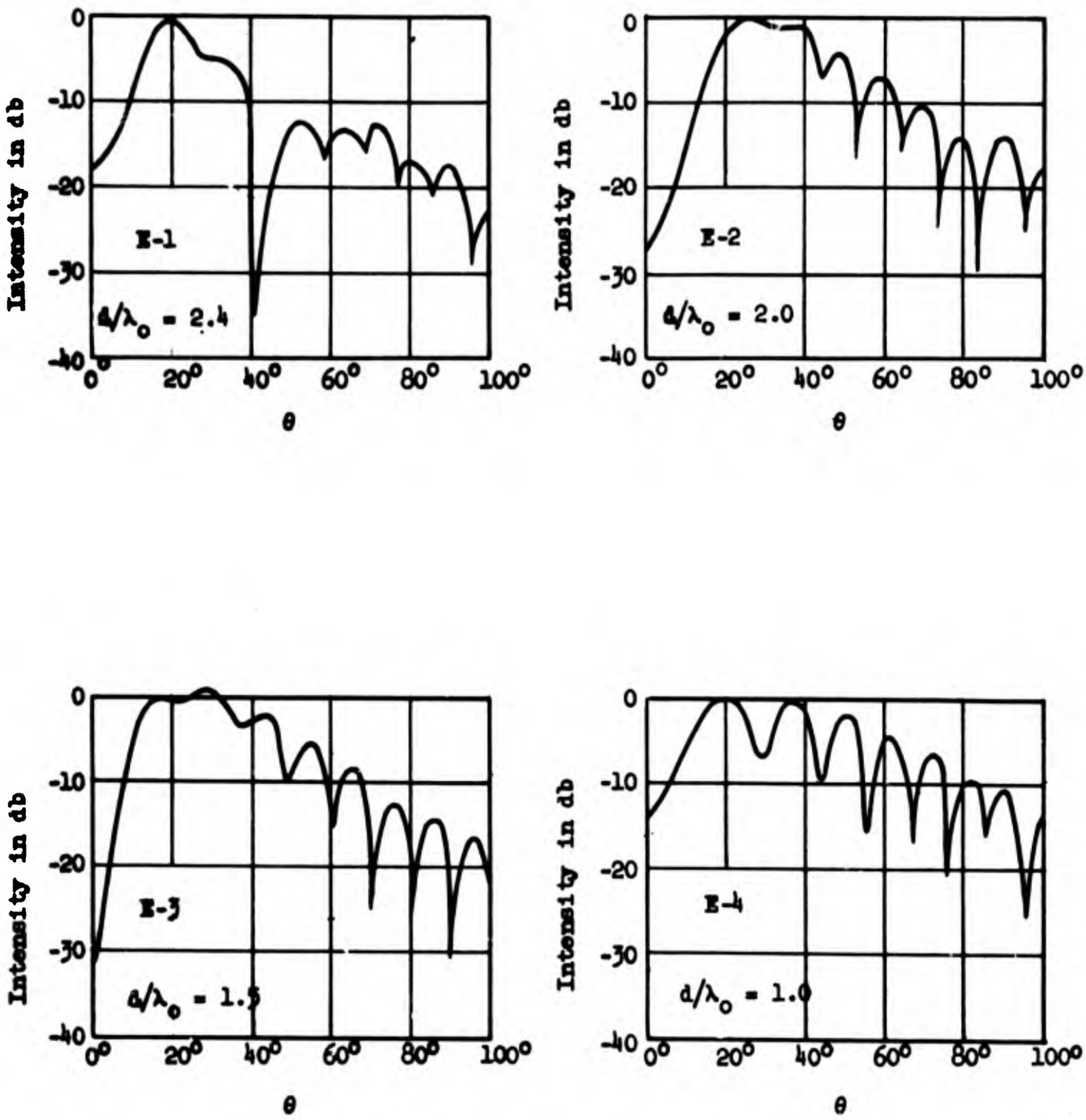

TM_{01} Mode

L/λ_o = 6.0 λ_o = 3.20 cm

L: length d: diameter

Fig. 3.64 RADIATION PATTERNS FOR THE E-SERIES

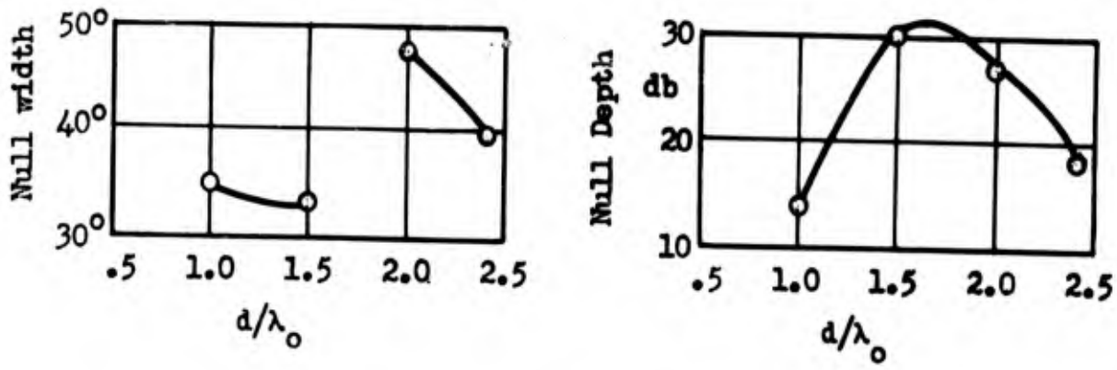

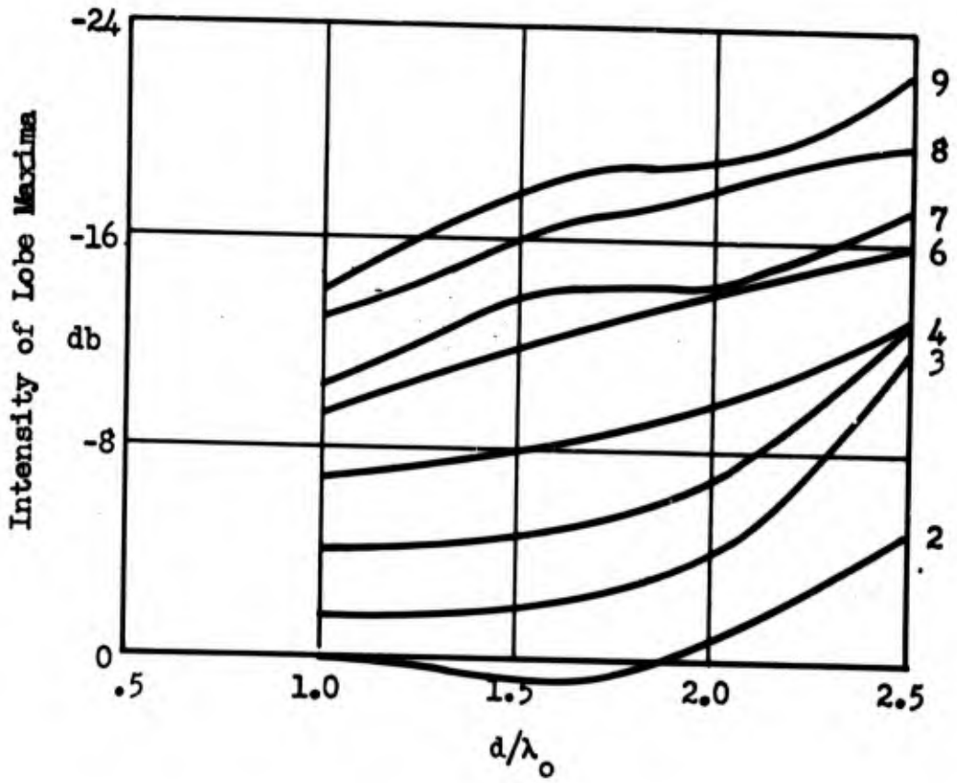

TM_{01} Mode

$L/\lambda_o = 6.0$ $\lambda_o = 3.20$ cm

Index of Refraction = 1.60

d: diameter L: length

Fig. 3.65 CHARACTERISTICS OF THE E-SERIES OF DIELECTRIC ROD ANTENNAS

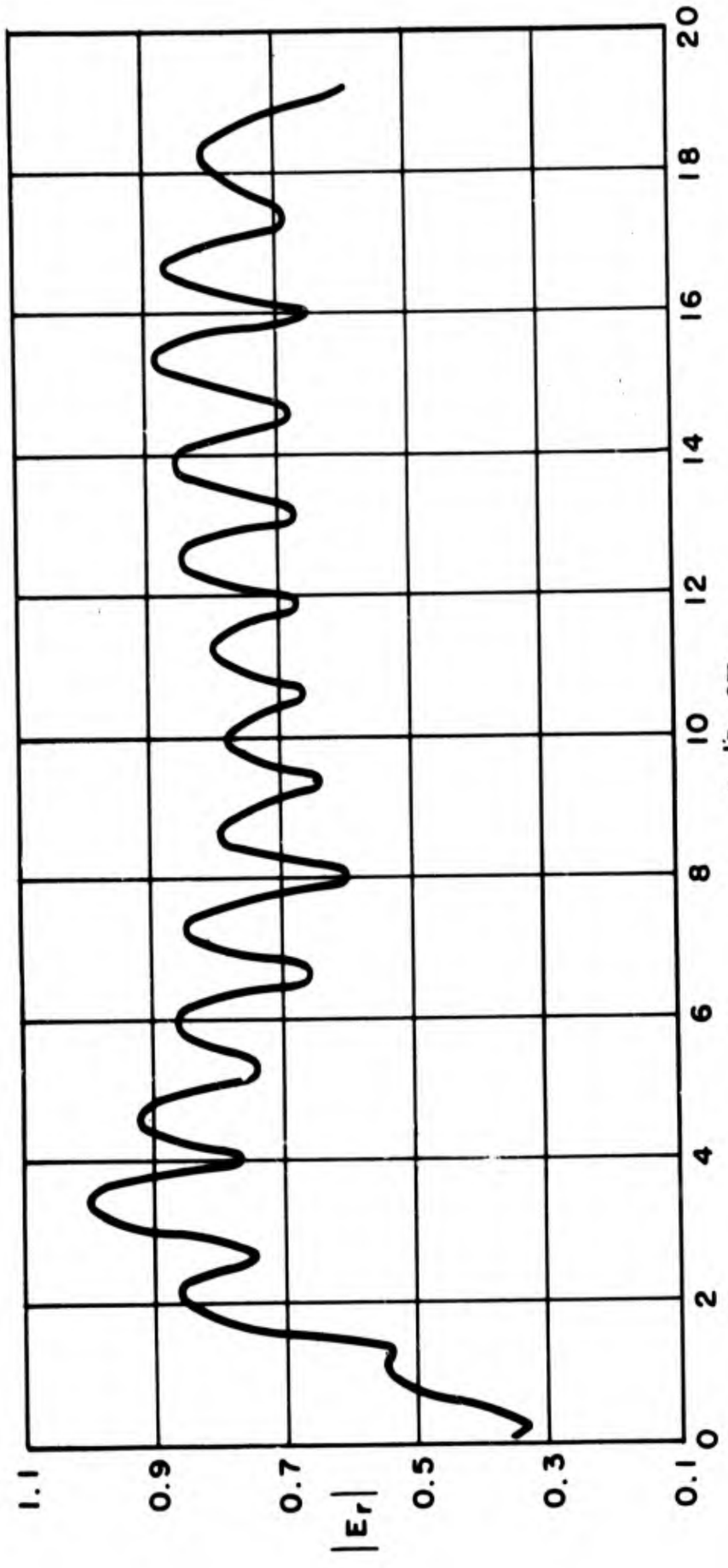

Rod: E-4 Mode: TM_{01} $L = 6\lambda_o$ $d = 1.0\lambda_o$ $n = 1.6$

Fig. 3.66 Radial Component of Electric Field on the Surface of Dielectric Rod Radiator of Circular Cross-Section as a Function of Axial Distance z.

DRL - UT
DWG AE 801
CMM - CLW
1 - 12 - 50

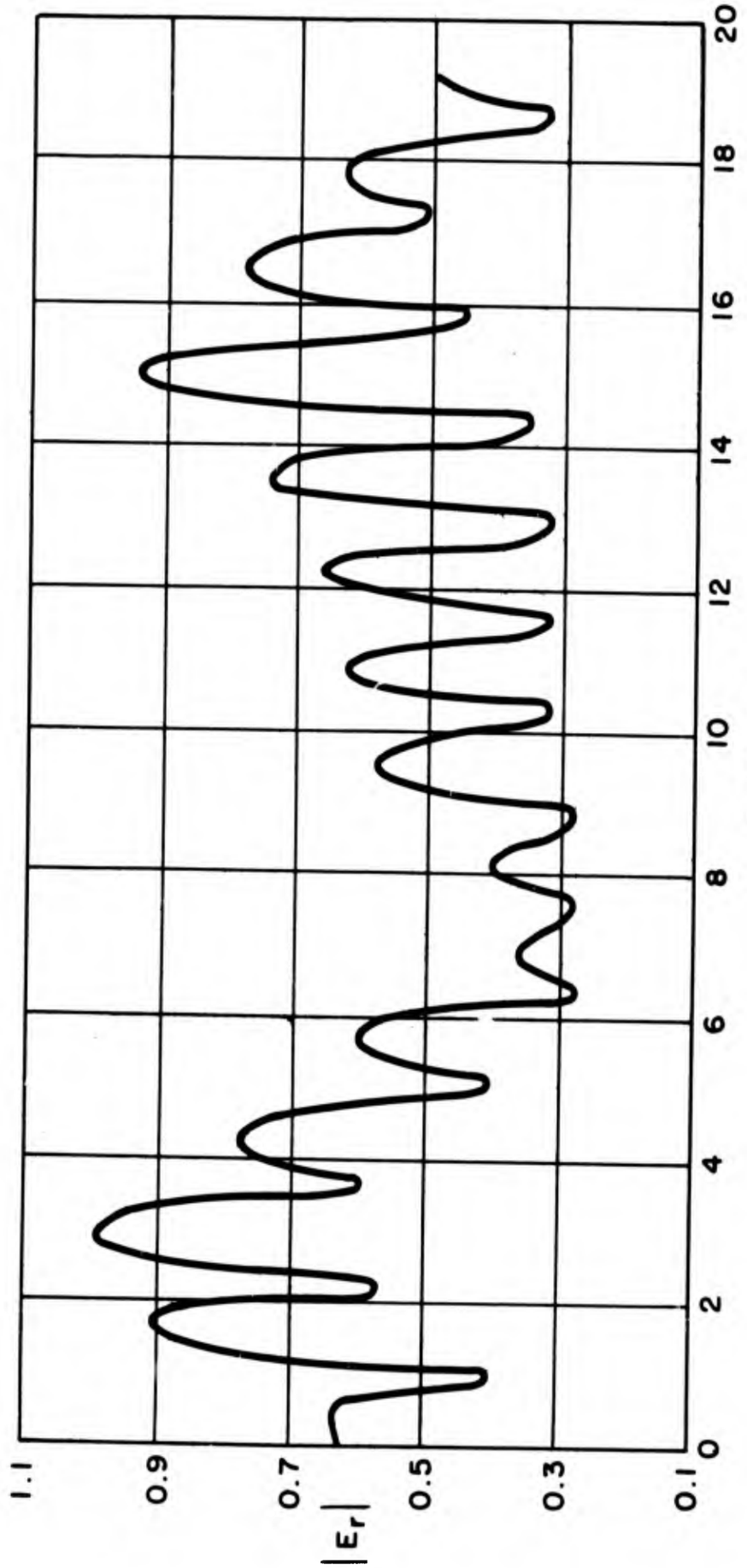

Rod : E - 1 Modes : TM_{01} and TM_{02} L : $6\lambda_o$ d : $2.4\lambda_o$ n = 1.6

Fig. 3.67 Radial Component of Electric Field on the Surface of Dielectric Rod Radiator of Circular Cross-section as a Function of Axial Distance z.

DRL - UT
DWG AE 800
CMM - CLW
1 - 12 - 50

Characteristics of the A-Series of radiators excited in the TM_{01} mode are given in Figures 3.68 through 3.72. The A-Series rods had a maximum diameter of $0.870\lambda_o$ at the point of excitation and then had a constant angle of taper to the end of the rod. The lengths were 2.0, 4.0, 6.0, 8.0, and $10.0\lambda_o$. The minimum diameter was, of course, a function of length.

The general behavior of the lobe positions, number, and intensity was essentially the same as for the same rods excited in the HE_{11} mode shown in the previous section. The null width decreased as L/λ_o increased, but the decrease was slight for lengths greater than $6\lambda_o$. Slightly sharper and deeper nulls were obtained with the F-Series but the secondary lobes were also more intense for the F-Series, which would tend to nullify that advantage.

Figures 3.70 through 3.72 show the standing wave patterns of the normal component of the electric field on the surfaces of the A-Series of rods. In Figure 3.70, it is evident that approximately the last third of length of the antenna did not support propagation. The field on the surface of rod A-3 (Figure 3.71) was approximately that of a sinusoidal distribution, which was desirable.

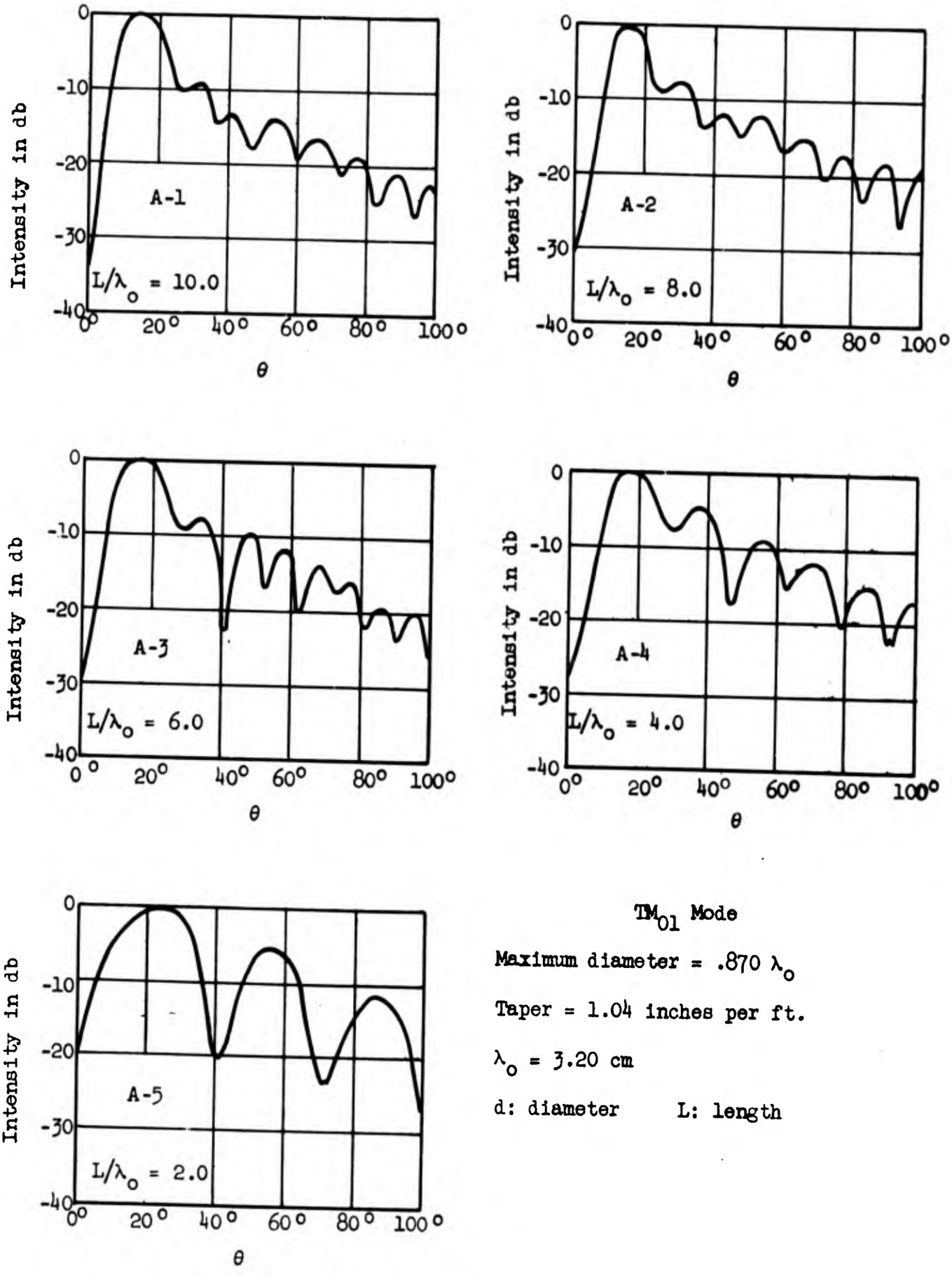

TM_{01} Mode

Maximum diameter = .870 λ_o

Taper = 1.04 inches per ft.

λ_o = 3.20 cm

d: diameter L: length

Fig. 3.68 RADIATION PATTERNS OF THE A-SERIES

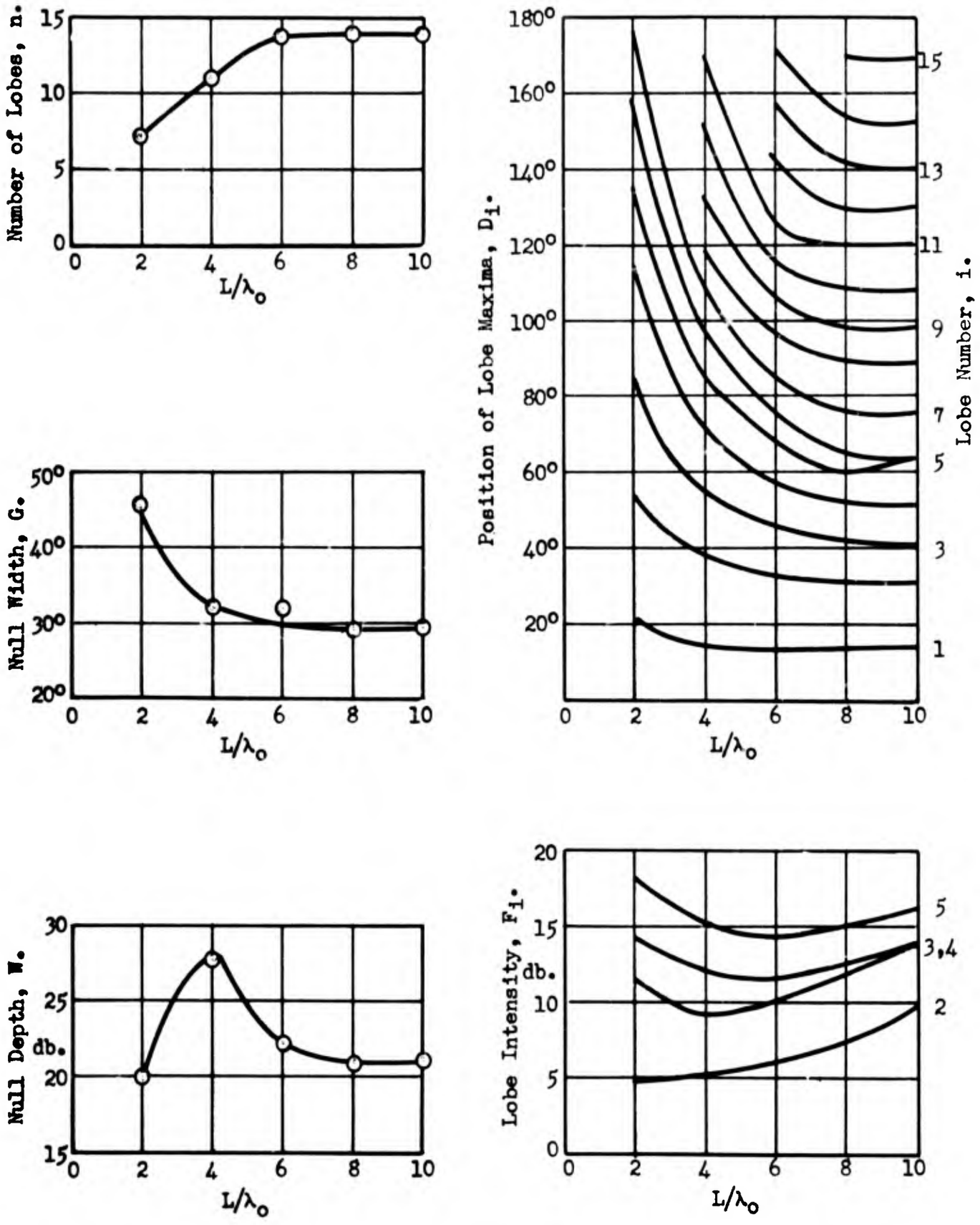

λ_o = 3.20 cm

Fig. 3.69

CHARACTERISTICS OF A-SERIES OF DIELECTRIC ANTENNAS EXCITED IN THE TM_{01} MODE.

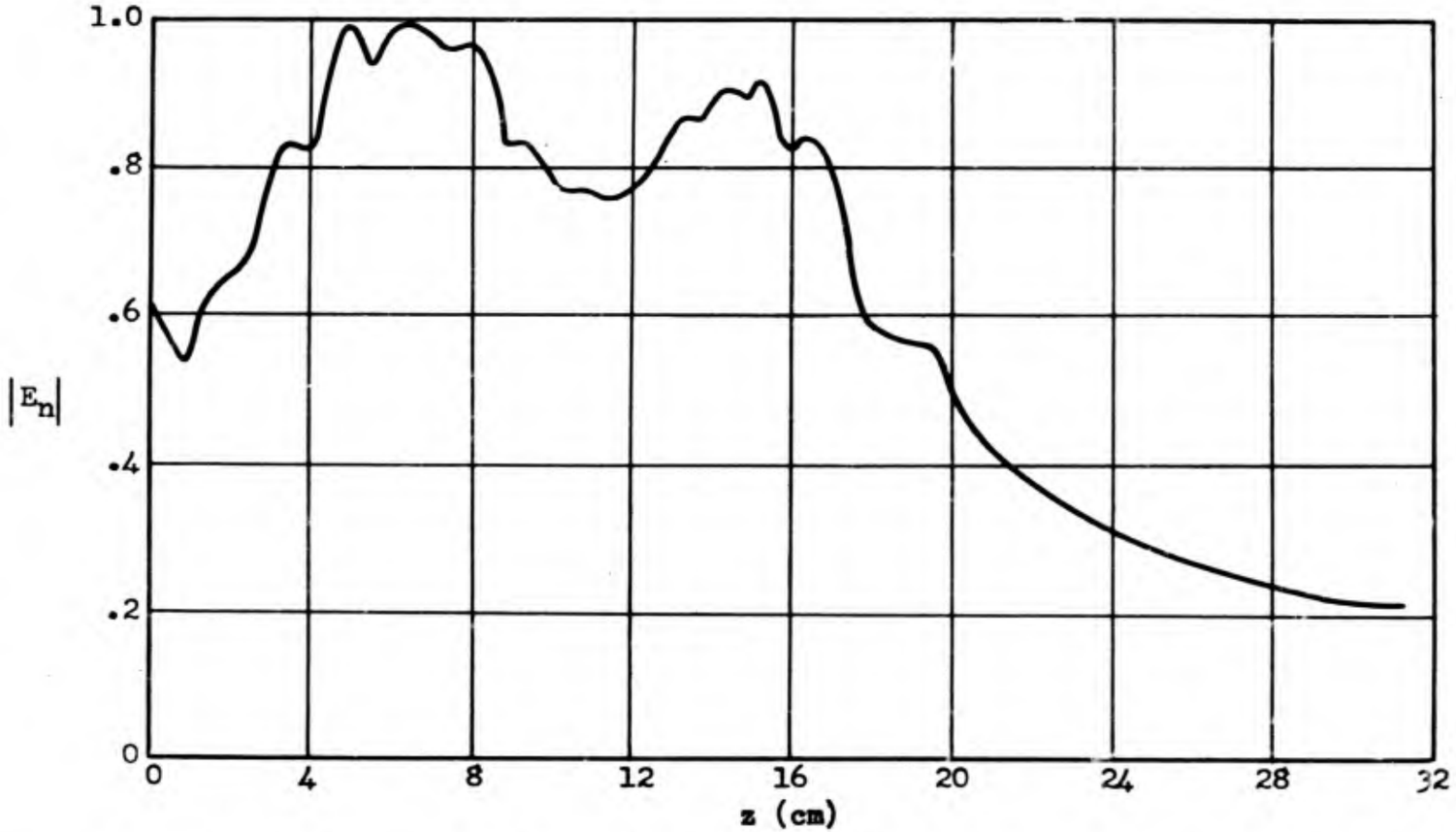

Antenna: A-1 $L/\lambda_o = 10.0$ Mode: TM_{01} $d_{max} = .870\lambda_o$

Antenna excited at the point z = 0.

Fig. 3.20 NORMAL COMPONENT OF THE ELECTRIC FIELD AS A FUNCTION OF THE AXIAL DISTANCE FROM THE SURFACE OF A CONDUCTING ROD.

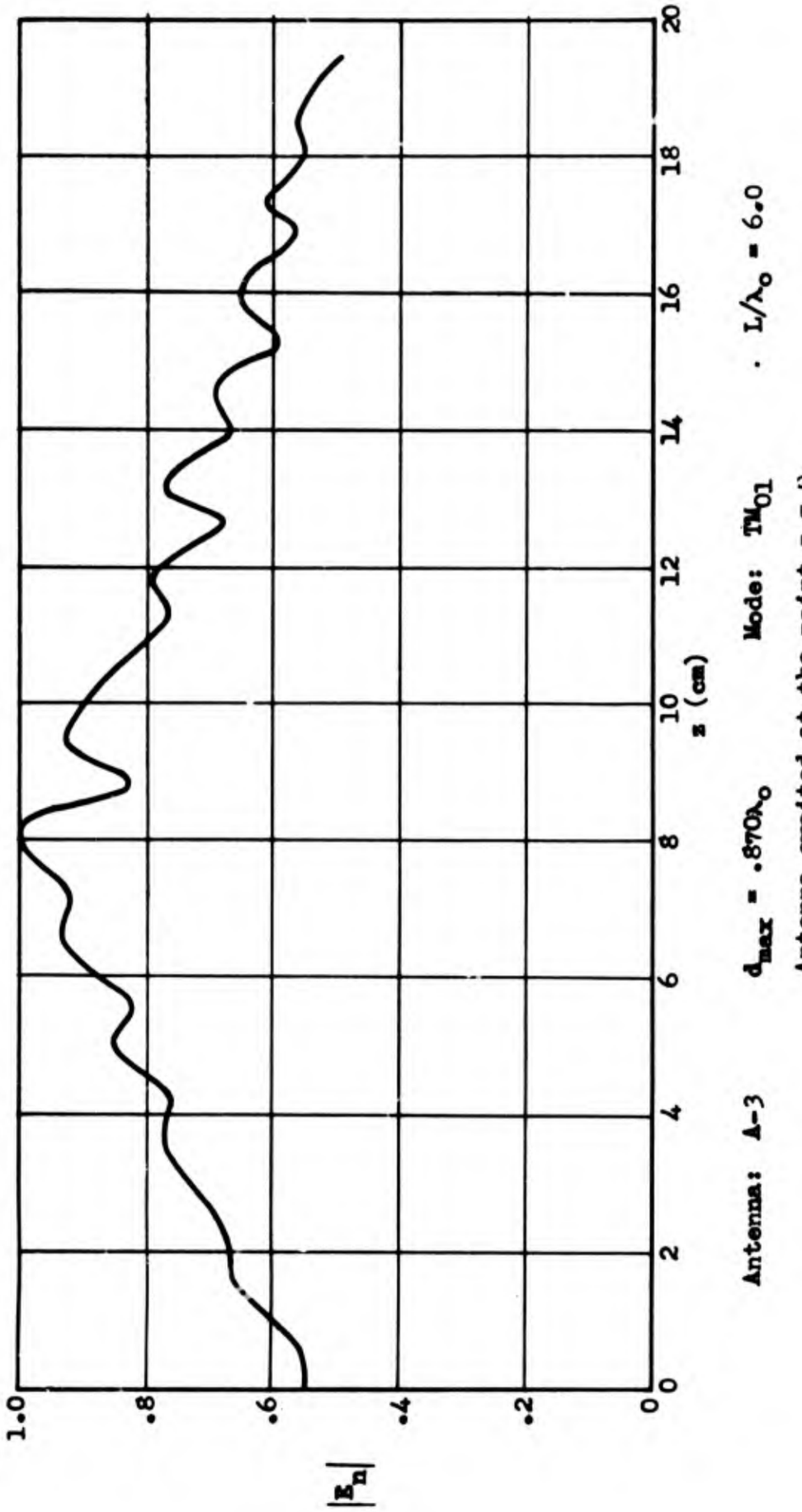

Fig. 3.71 NORMAL COMPONENT OF THE ELECTRIC FIELD AS A FUNCTION OF THE AXIAL DISTANCE z, ON THE SURFACE OF A RADIATING ROD.

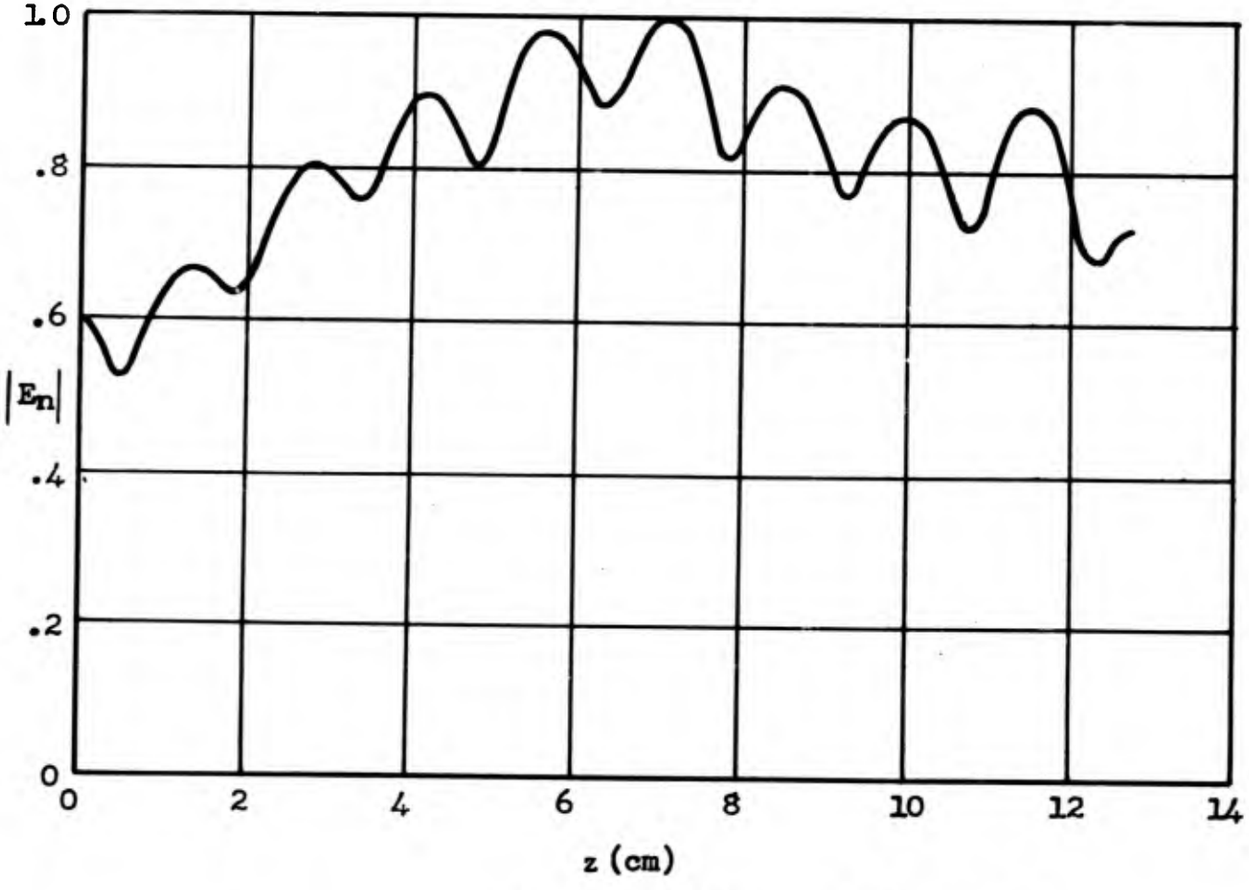

Antenna: A-4 $L/\lambda_o = 4.0$

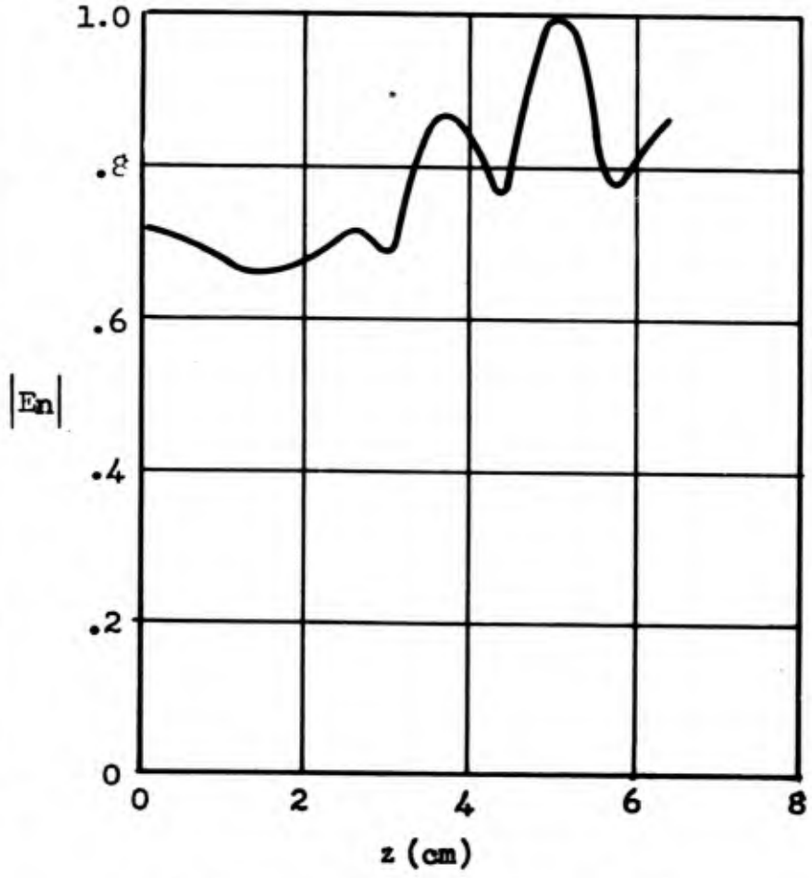

Antenna: A-4 $L/\lambda_o = 2.0$

TM_{01} Mode $\lambda_o = 3.20$ cm Maximum Diameter = .870 λ_o

(Antennas excited at points, z = 0).

Fig. 3.72 NORMAL COMPONENTS OF THE ELECTRIC FIELDS AS A FUNCTION OF AXIAL DISTANCE, z, ON THE SURFACES OF DIELECTRIC ROD ANTENNAS.

Characteristics of the B-Series of antennas excited in the TM_{01} mode are shown in Figures 3.73 through 3.77. The B-Series rods had a maximum diameter of $0.870\lambda_o$ and a length of $6.0\lambda_o$, but the rods were tapered so that the ratio of minimum diameter to maximum diameter varied from zero to one. As was the case with the rods excited in the HE_{11} mode, the attenuation of minor lobe intensity increased as the angle of taper increased.

Figures 3.75 through 3.77 show graphs of the standing wave patterns of the normal components of the electric fields on the surfaces of the B-Series. Antenna B-3 had the nearest approach to a sinusoidal distribution of energy along the rod. As was expected, a portion of the antenna B-4 near the end was of such small diameter that propagation of the wave did not occur. It will be remembered that in the case of rods excited in the HE_{11} mode, propagation of energy in the rod occurred until the diameter of the rod became zero.

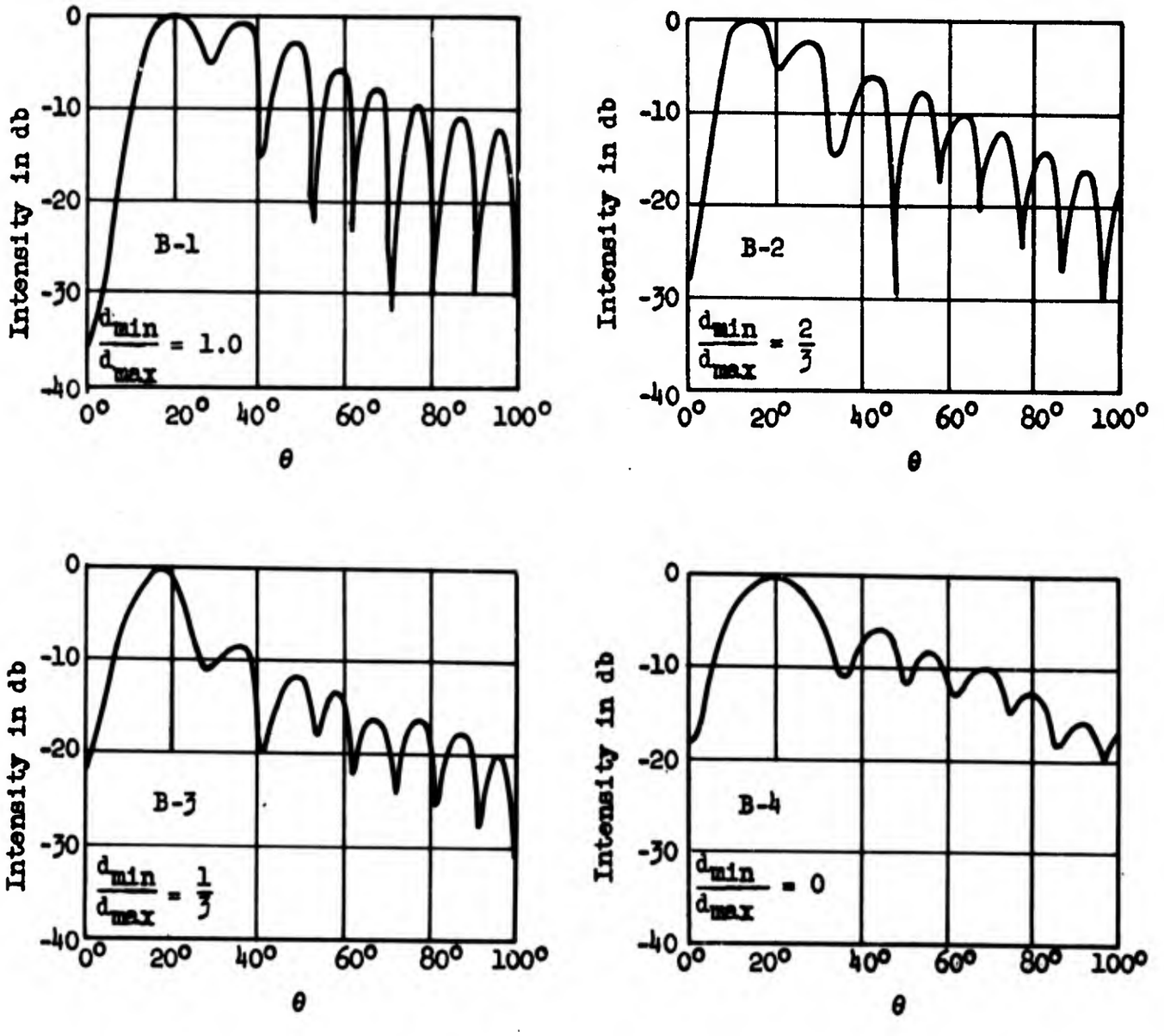

TM_{01} Mode

$d_{max} = .870\ \lambda_o$ $L/\lambda_o = 6.0$ $\lambda_o = 3.20$ cm

d_{max} = Maximum diameter d_{min} = Minimum diameter

Fig. 3.73 RADIATION PATTERNS OF THE B-SERIES

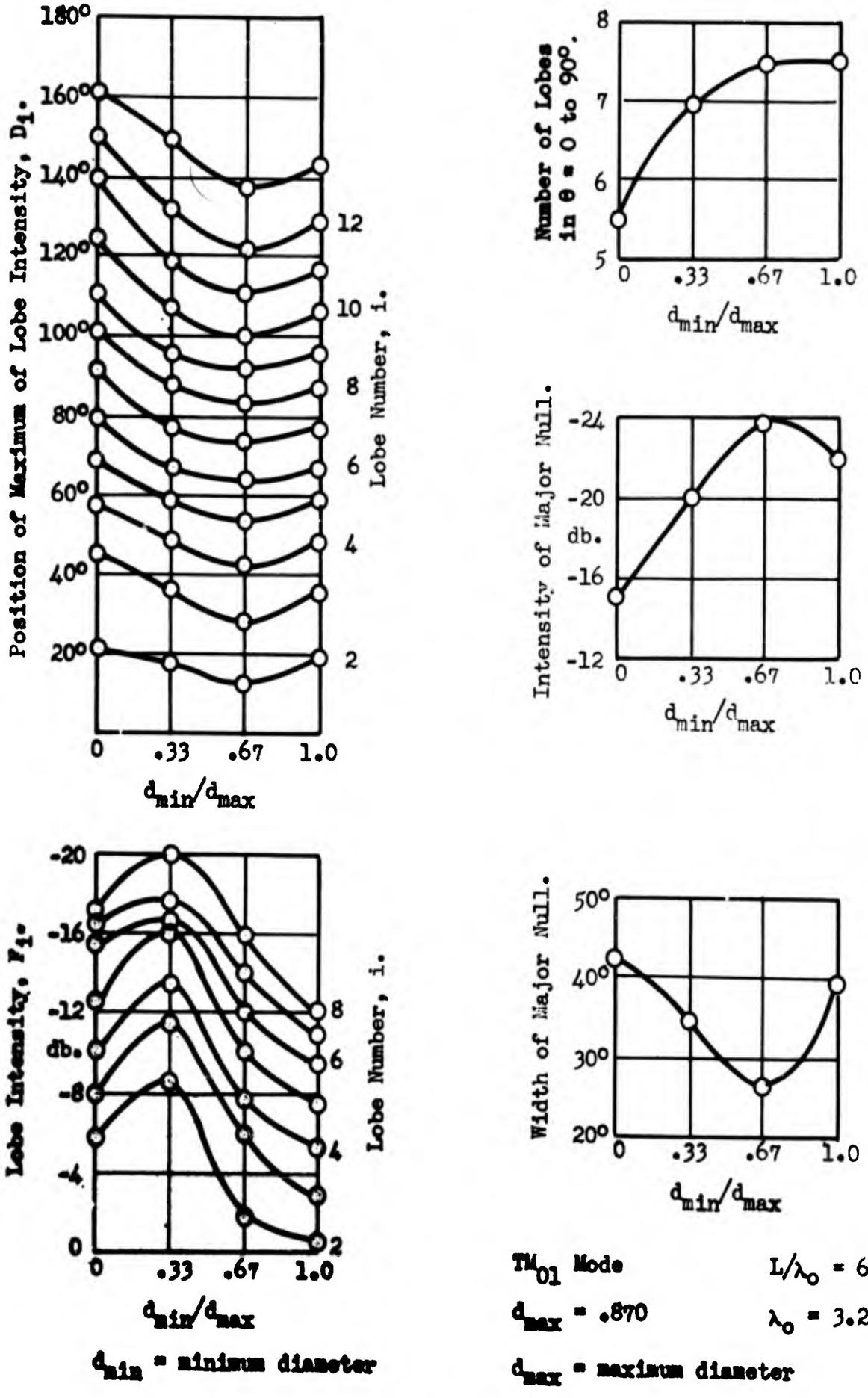

Fig. 3.74 CHARACTERISTICS OF THE E-SERIES OF DIELECTRIC ROD ANTENNAS.

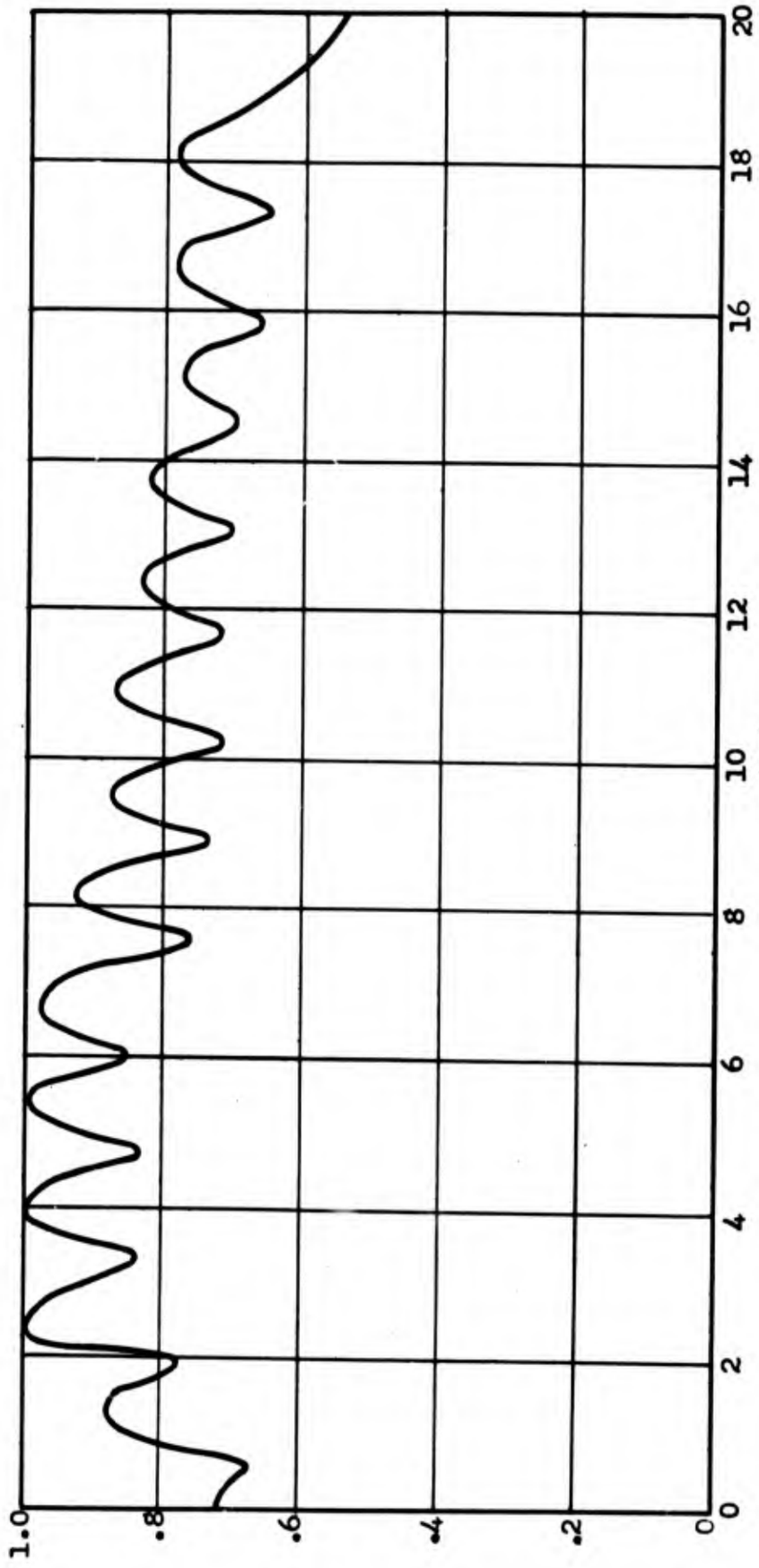

Fig. 3.75 NORMAL COMPONENT OF THE ELECTRIC FIELD AS A FUNCTION OF THE AXIAL DISTANCE z, ON THE SURFACE OF A RADIATING ROD.

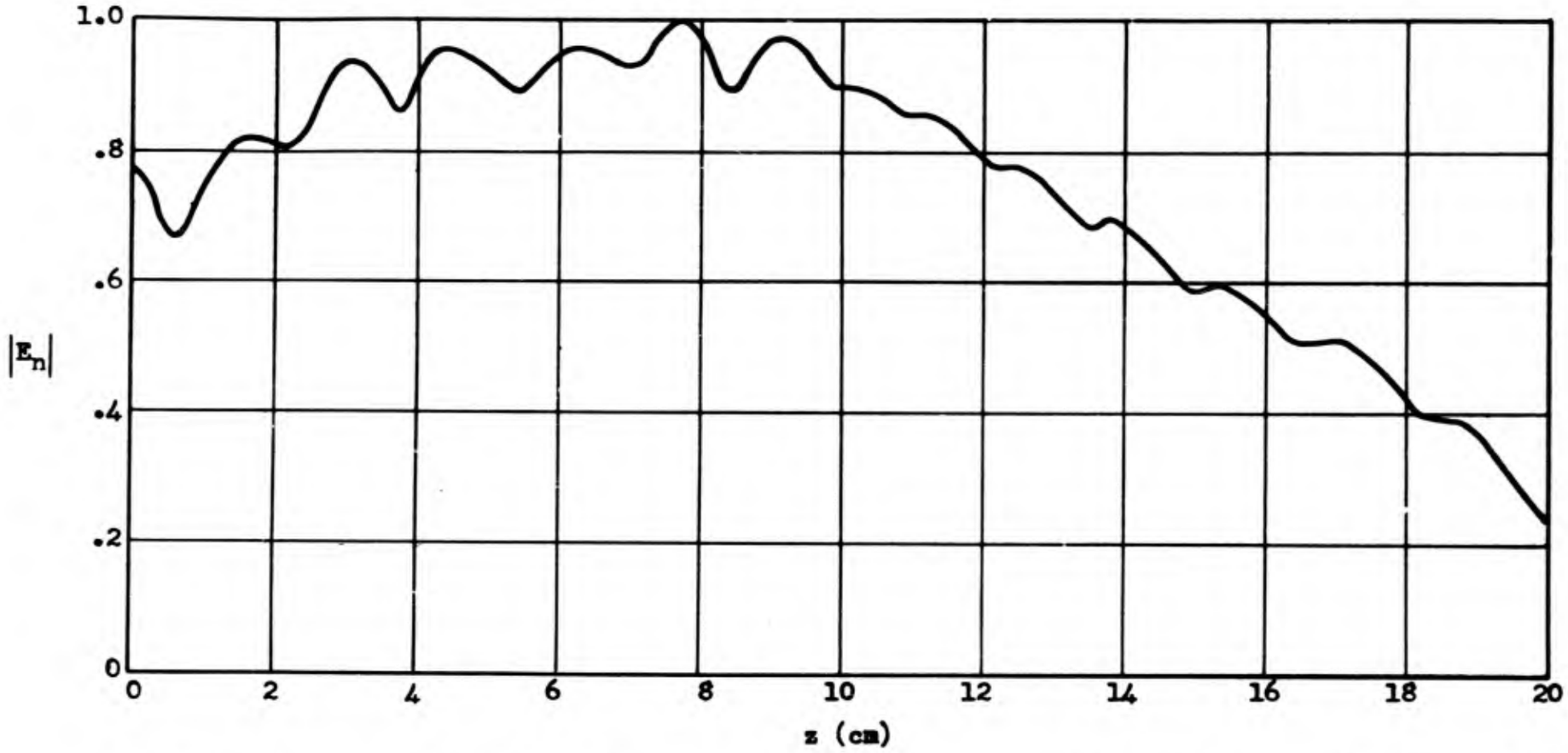

Antenna: B-3 $d_{max} = .870\lambda_o$ Mode: TM_{01} $L/\lambda_o = 6.0$ $d_{min}/d_{max} = 1/3$

Antenna excited at the point z = 0.

Fig. 3.76 NORMAL COMPONENT OF THE ELECTRIC FIELD AS A FUNCTION OF THE AXIAL DISTANCE z, ON THE SURFACE OF A RADIATING ROD.

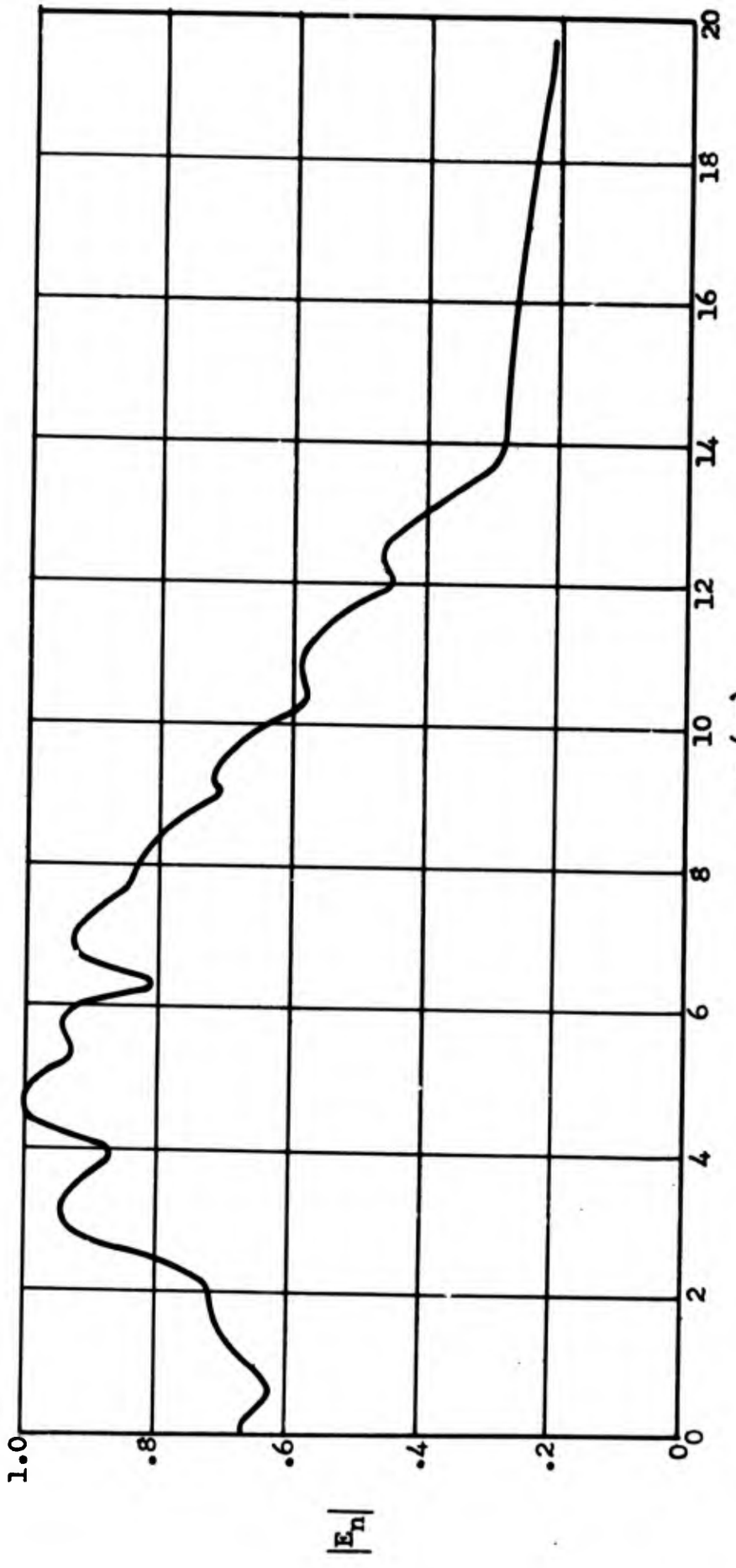

Fig. 3.77 NORMAL COMPONENT OF THE ELECTRIC FIELD AS A FUNCTION OF THE AXIAL DISTANCE z, ON THE SURFACE OF A RADIATING ROD.

4. Discussion of Radiation Patterns of the TE_{01} Mode. The experimental data obtained on radiation from dielectric rods excited in the TE_{01} mode were in general very poor. The poor data were undoubtedly due to the presence of other modes of transmission. Pains were taken to filter out other modes but the attempts were not as successful as desired.

The TE_{01} mode pattern, like the TM_{01}, has a null in the forward direction. For any practical application, the radiation patterns produced by the TE_{01} wave have no advantages over the TM_{01} wave, which is relatively easy to produce in pure form. However, in future developments, higher frequencies will undoubtedly be used and the TE_{01} wave has the unique characteristic that in metal pipes the attenuation decreases with increasing frequency. Also at the higher frequencies the necessary size of waveguide will not be impractical. Thus it appears that the TE_{01} wave might have some decided advantages in the field of transmission of energy to and from the antenna.

In order to detect TE_{01} waves, the polarization of the receiving antenna must be normal to the plane of the pattern. The radiation pattern is the same for all planes.

The F-Series patterns were so poor that they are not included. All that can be said is that the TE_{01} mode did dominate but it was impossible to determine the positions of the individual lobes with any accuracy. Some asymmetry of patterns was also present, indicating the presence of HE_{11} radiation.

The E-Series patterns were somewhat better. As would be expected from reference to other modes, increasing diameter decreases the minor

lobe intensity. However, increasing diameter tends to decrease the null depth and increase the null width, which is not in agreement with other work. The lobe envelopes and other characteristics are shown in Figure 3.78.

The envelopes of lobe intensities of the A-Series are shown in Figure 3.79. As with other modes, the lengthening of the tapered rod decreases minor lobe intensities.

The B-Series analysis, shown in Figure 3.80, indicates that increasing taper increases the depth of the central null but widens the null also.

5. Discussion of Radiation Characteristics of Dielectric Rods Excited by the TM_{11} Mode.

It was concluded in Part Two that the modes in dielectric rods excited by TE_{11} and TM_{11} modes in metal waveguides were the same. However, radiation patterns were measured of the antennas excited by the TM_{11} mode exciter and some of the results are included in this section. In order to distinguish between the modes, the mode resulting from excitation by the TM_{11} exciter will be referred to as the EH_{11} mode.

It will be noted that the fields in metal waveguides of the TE_{11} and the TM_{11} modes are considerably different. Therefore, the waves in passing from the metal waveguide to the dielectric waveguide must go through a period of transition. Bearing this in mind, one would not expect the radiation patterns of the two modes to be identical. If the radiation patterns of rods of much longer length had been measured, it

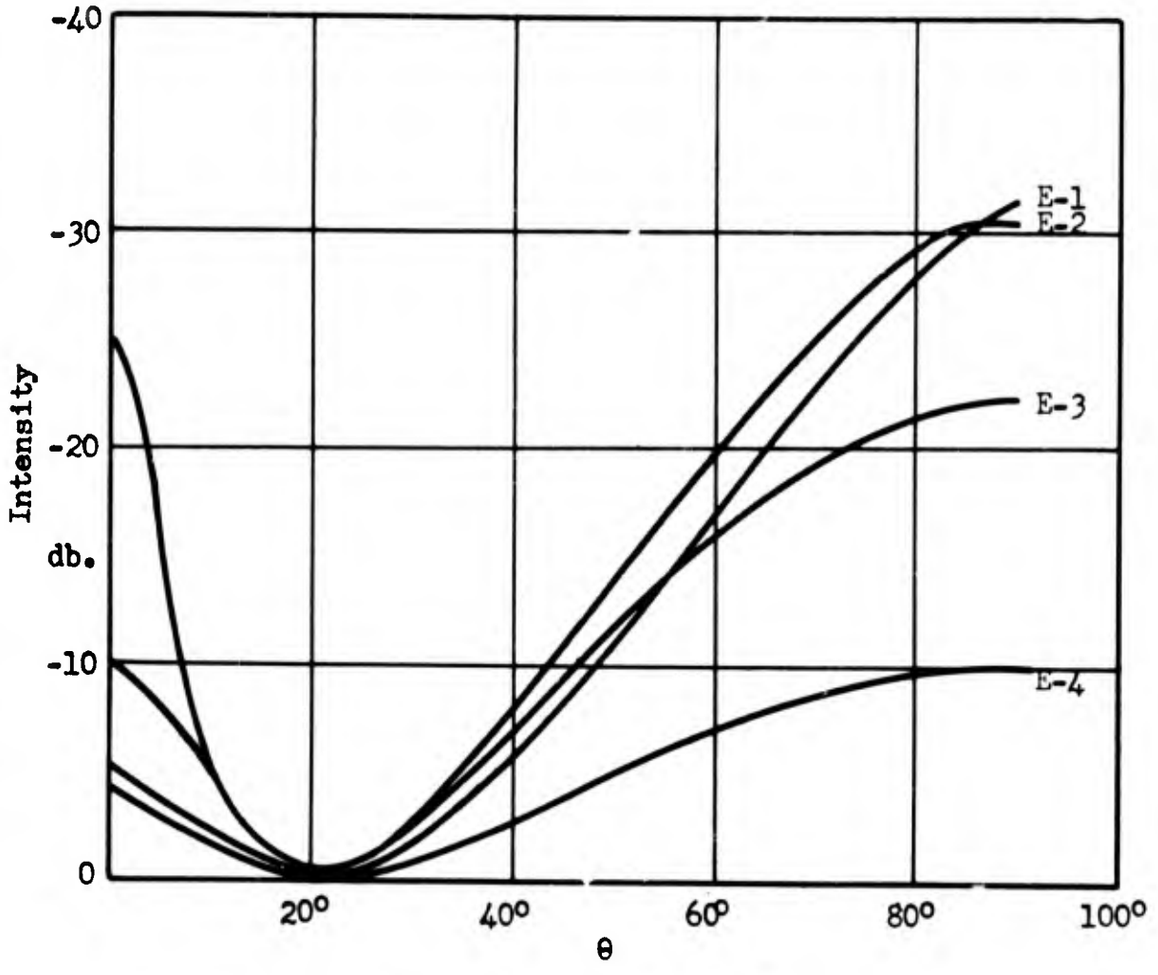

Envelope of Lobe Maxima.

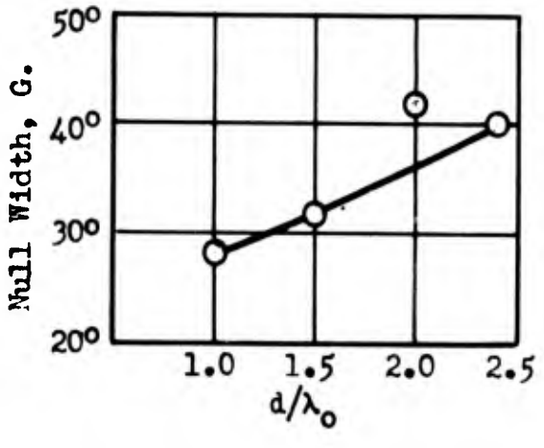

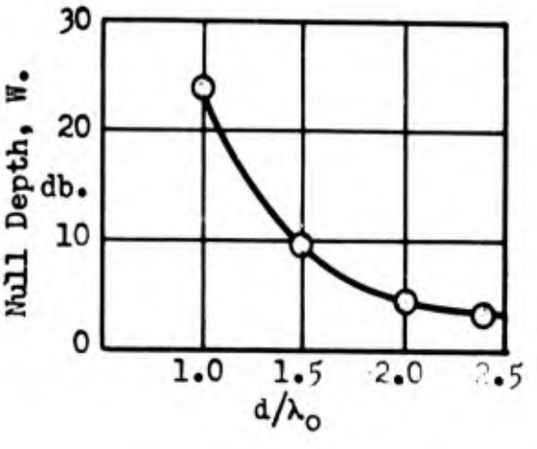

E-Series TE_{01} Mode $L/\lambda_o = 6.0$

$\lambda_o = 3.20$ cm L: length d: diameter

Fig. 3.78

CHARACTERISTICS OF E-SERIES OF DIELECTRIC ROD ANTENNAS

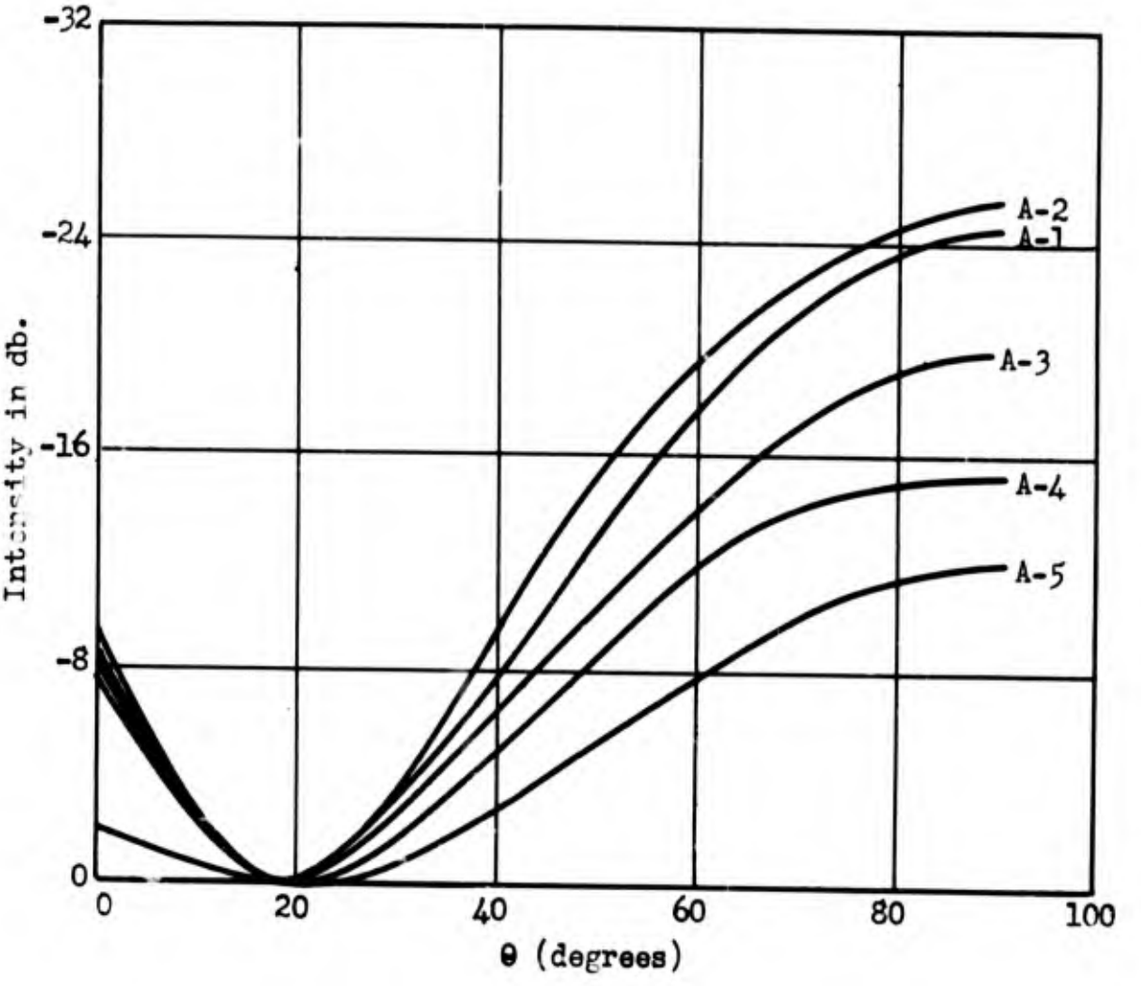

Fig. 3.79

ENVELOPE OF THE INTENSITIES OF THE LOBE MAXIMA FOR THE A-SERIES, TE_{01} MODE.

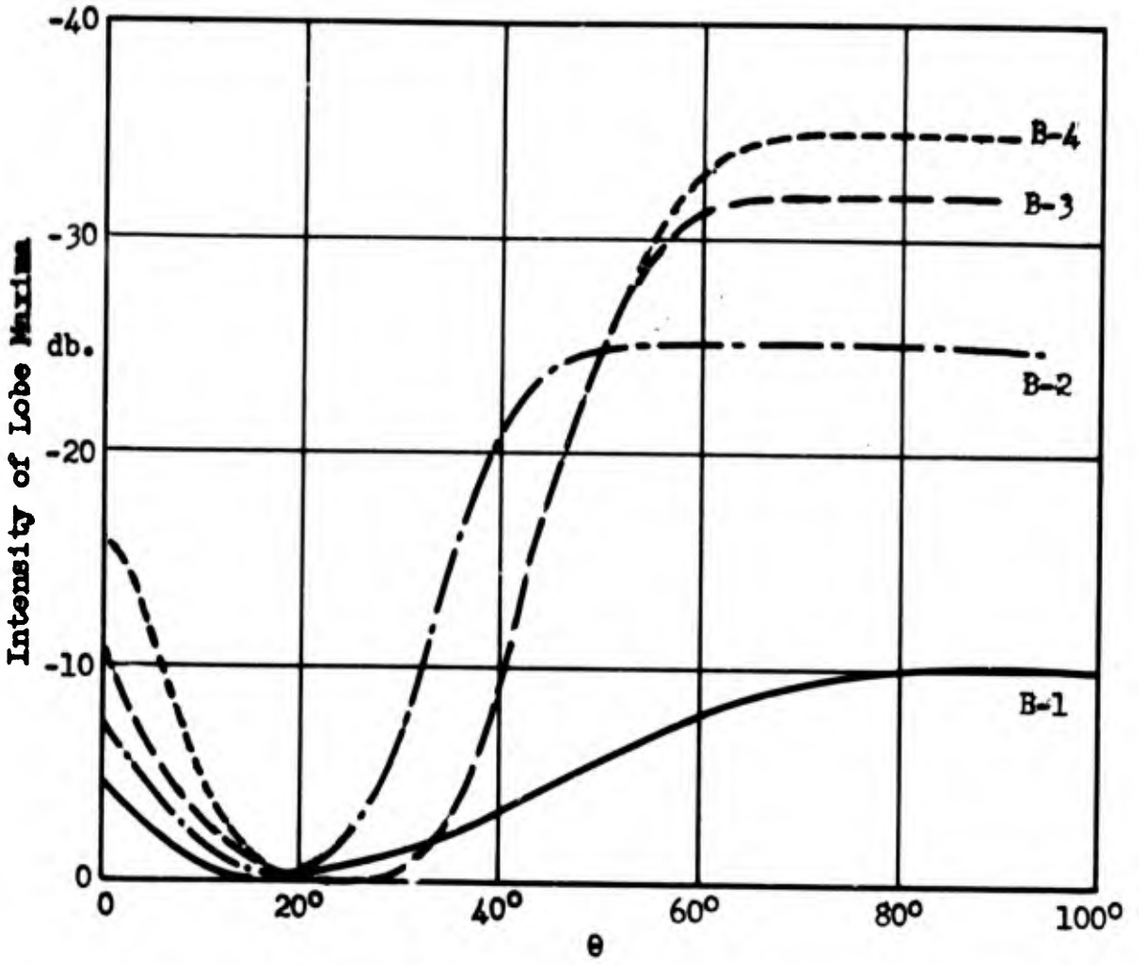

Envelope of the Radiation Patterns.

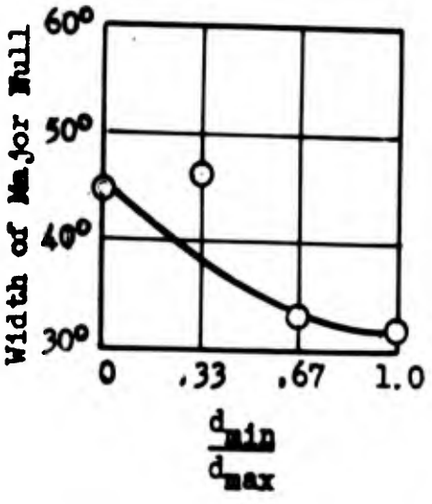

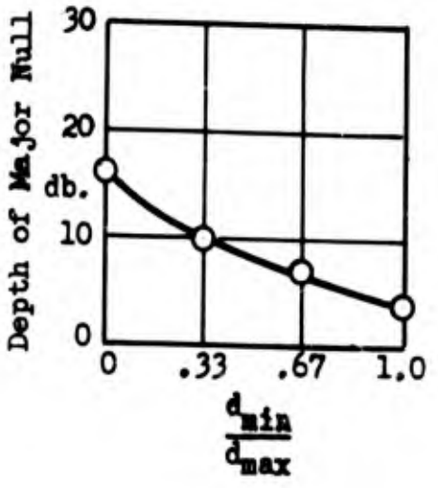

TE_{01} Mode $L/\lambda_o = 6.0$ $\lambda_o = 3.20$ cm

d_{min} = minimum diameter d_{max} = maximum diameter

Fig. 3.80

CHARACTERISTICS OF THE B-SERIES OF DIELECTRIC ROD ANTENNAS.

is entirely possible that the patterns for the two modes would be in close agreement.

Some asymmetry about the point $\theta = 0$, was noted in the patterns. This asymmetry was probably due to the presence of the TM_{01} and the TE_{01} modes. These undesired modes were undoubtedly generated in the metal waveguide since the size of metal guide which was necessary for the TM_{11} mode was also sufficiently large to support the TE_{11}, TM_{01}, and TE_{01}.

As with the HE_{11} mode, there are an infinite number of planes in which radiation measurements might be made. However, measurements were made only in the two planes corresponding to the E and H planes for the HE_{11} radiation patterns. These planes are indicated in Figure 3.81. Rotation of one of the antennas 90° resulted in cross-polarization and essentially no signal was received.

Radiation patterns for the F-Series, both E- and H-planes are shown in Figures 3.82 and 3.83. These patterns are similar to those for the same antennas excited in the HE_{11} mode. The discrepancies can probably be attributed to the transition from the metal guide to the dielectric rod.

Figures 3.84 and 3.85 give some of the characteristics of the A-Series of rods excited in the EH_{11} mode. These data are very similar to the data for the HE_{11} mode.

A considerable amount of data on antennas excited in the EH_{11} mode has been omitted in order to conserve space. However, all of the general characteristics were the same as for the same rods excited in the HE_{11} mode. The outstanding characteristic of the E-Series was that the intensity of the minor lobes was decreased as the diameter increased. This decrease in intensity agreed with the measurements made using the HE_{11} mode.

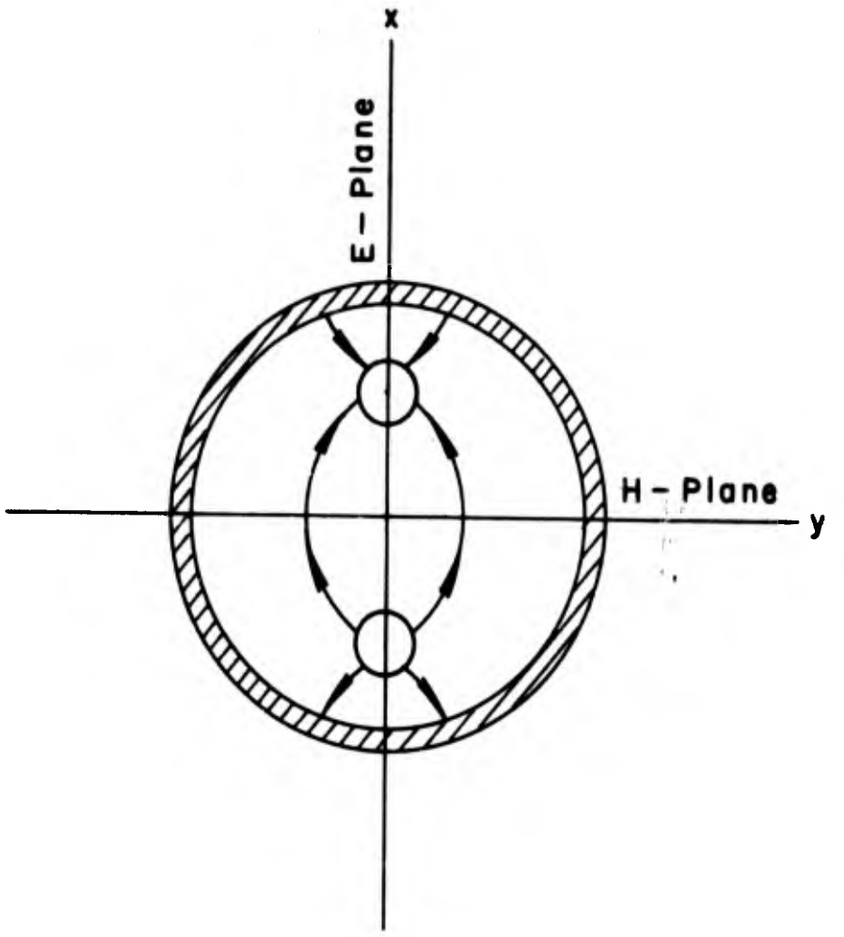

Fig. 3.81 – Orientation Of Dielectric Rods Excited In The EH_{11} Mode.

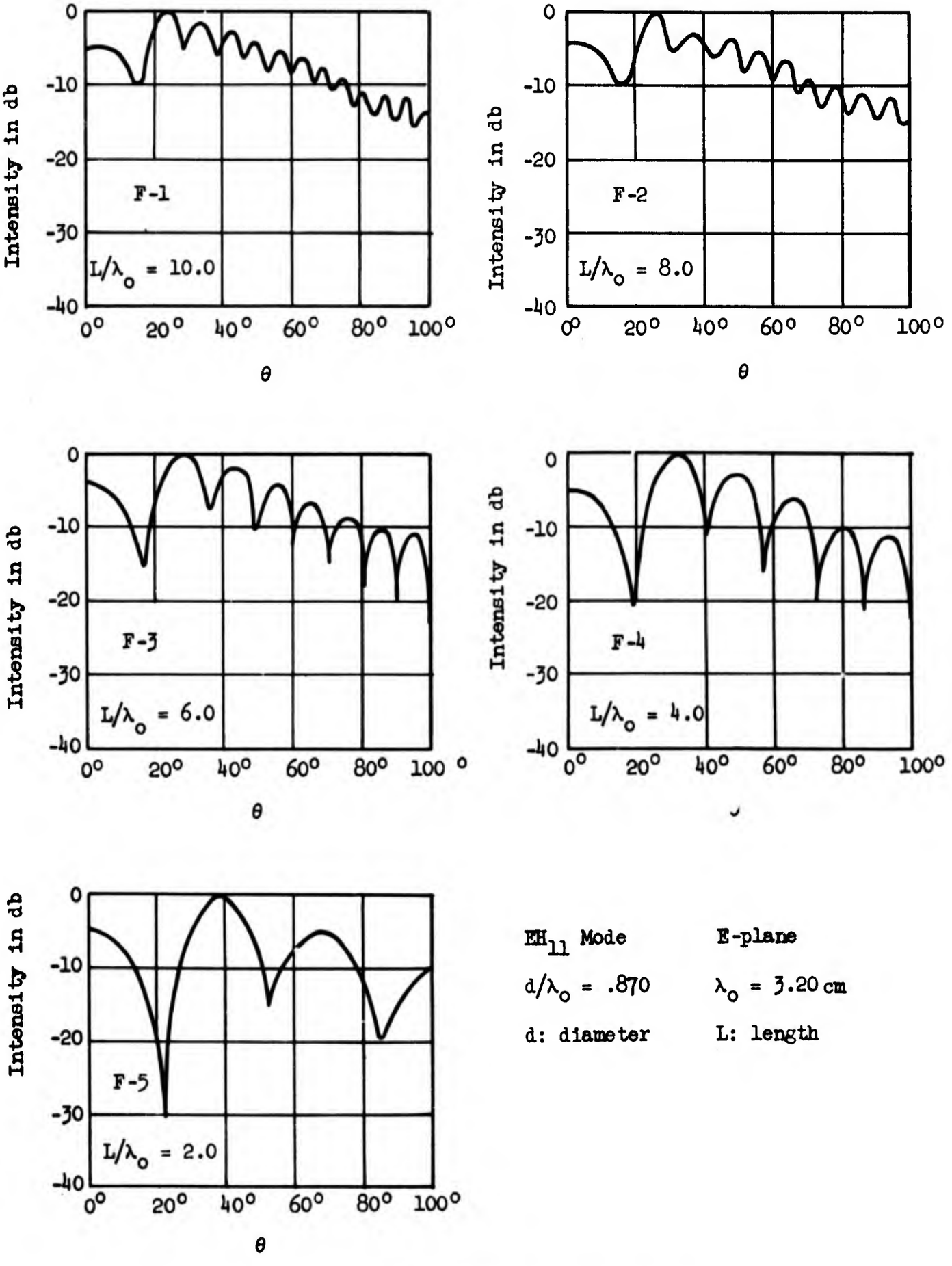

EH_{11} Mode E-plane

d/λ_o = .870 λ_o = 3.20 cm

d: diameter L: length

Fig. 3.82 RADIATION PATTERNS FOR THE F-SERIES

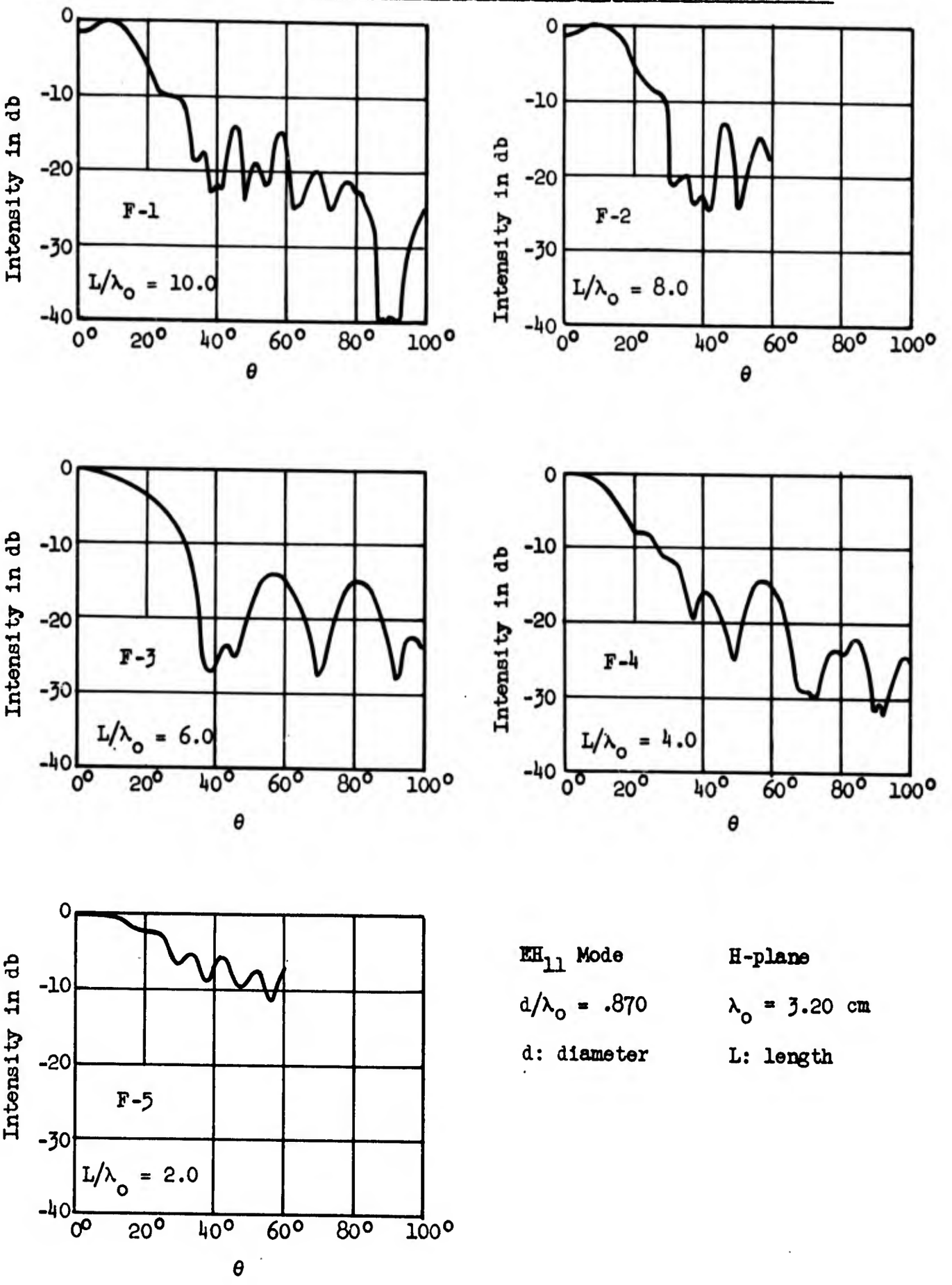

EH_{11} Mode — H-plane

d/λ_o = .870 — λ_o = 3.20 cm

d: diameter — L: length

Fig. 3.83 RADIATION PATTERNS FOR THE F-SERIES

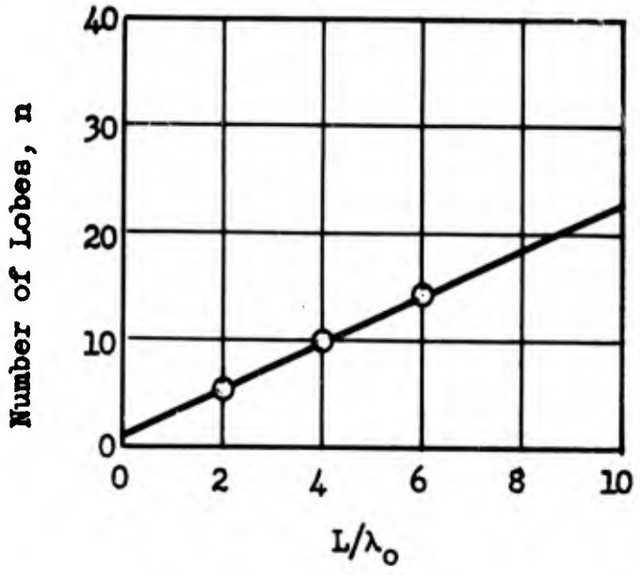

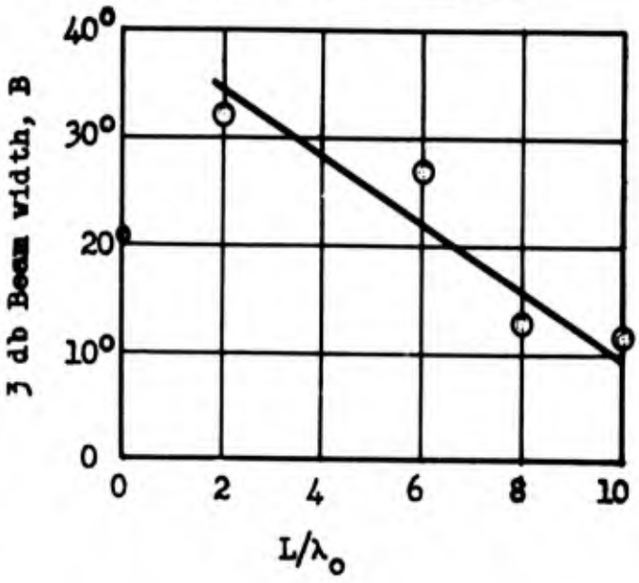

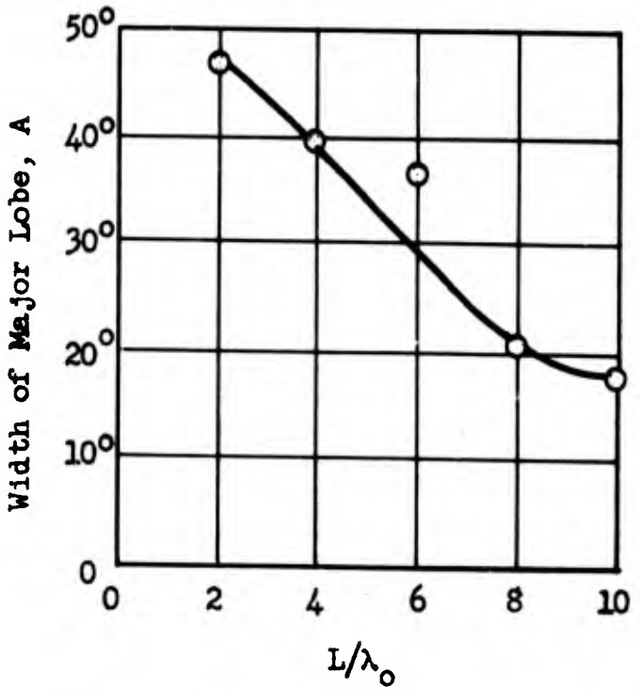

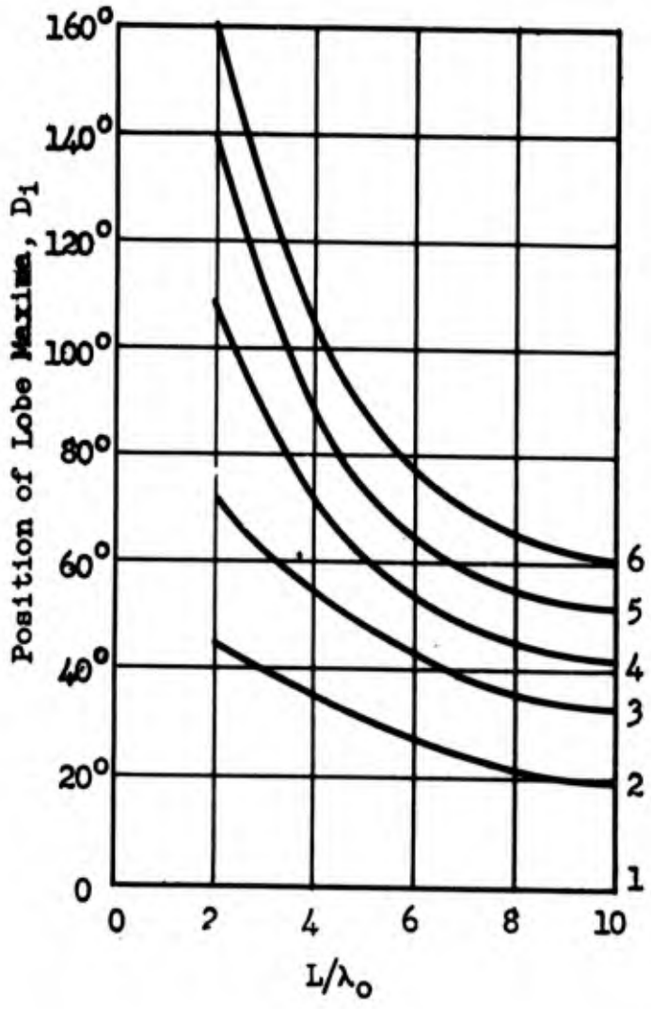

E-plane EH_{11} Mode

Maximum diameter = .870 λ_o

λ_o = 3.20 cm

Taper = 1.04 inches/ft.

Fig. 3.84 CHARACTERISTICS OF THE A-SERIES OF DIELECTRIC ROD ANTENNAS

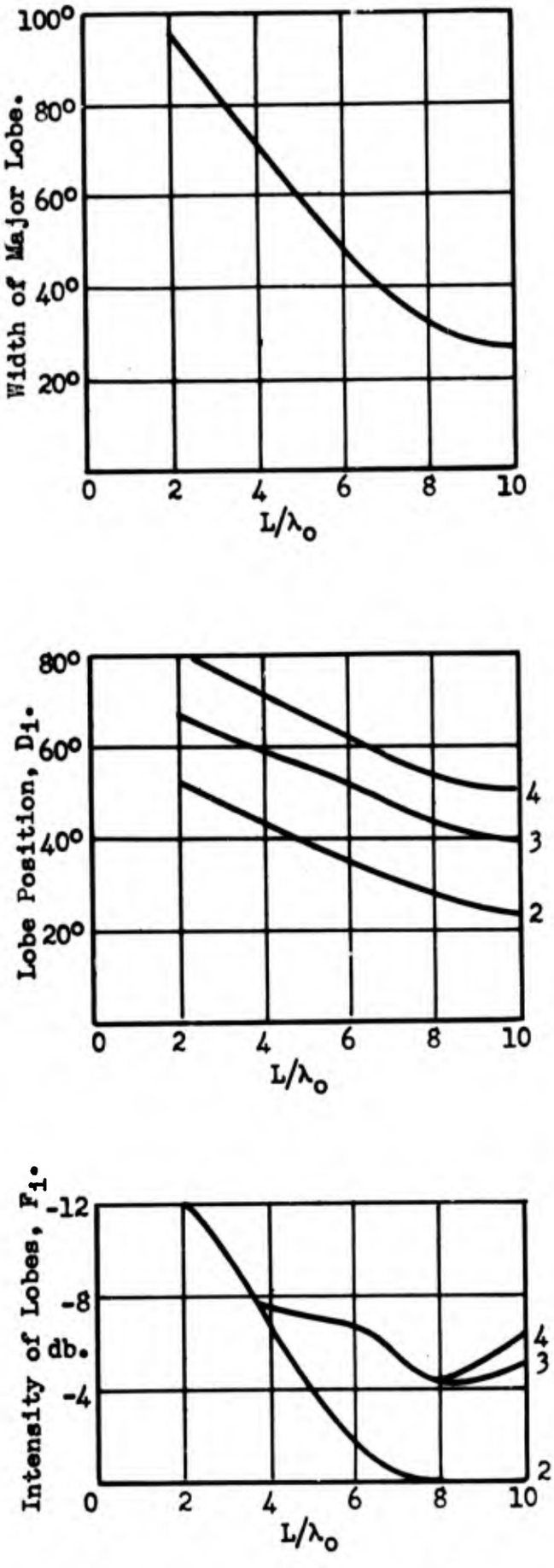

EH_{11} Mode H - Plane

L: length λ_o = 3.20 cm

Fig. 3.85 CHARACTERISTICS OF THE A-SERIES

CHAPTER VI

CONCLUSIONS

Most of the results of this investigation are in agreement with those of other workers. However, in the case of antennas excited in the HE_{11} mode, it appears that an increase in gain can be obtained by increasing the diameter considerably above the values used in previous work. It is believed that this increase in gain is due to improvement in the efficiency of exciting the wave in the dielectric waveguide. However, the addition of higher modes may have some effect on the gain measurements. Concerning the tapering of rods, it is concluded from the measurements that the directivity and gain of an antenna is a maximum for a ratio of $d_{min}/d_{max} = 0$. Most of the previous workers have contended that the latter section of a rod so tapered has no effect on the radiation properties. That may have been the case for rods which had a maximum diameter considerably less than $1.0\lambda_o$. The results of the surface field measurements show that the sinusoidal variation of intensity along the length of the rod can best be obtained by tapering the rods to a point. However, the C-type of rod gives essentially just as good a radiation pattern from the standpoint of minor lobe attenuation and gain.

The radiation patterns for dielectric rods excited in the TM_{01} mode are of the expected nature and have many of the characteristics of rods excited in the HE_{11} mode. It was seen that very sharp major nulls could be obtained which would be desirable in certain applications.

The radiation patterns of antennas excited in the TE_{01} mode were disappointing. The poor pattern definition was undoubtedly due to the presence of the HE_{11} mode.

It was concluded that the radiation patterns of antennas excited in the EH_{11} mode were essentially the same as the radiation patterns of the same antennas excited in the HE_{11} mode. The discrepancies which did exist were probably due to the transition section between the metal waveguide and the dielectric waveguide.

APPENDICES

BLANK PAGE

APPENDIX I

MEASUREMENT OF THE COMPLEX DIELECTRIC CONSTANT

The dielectric constants of the materials used in this project are accurately known to about two figures at the microwave frequencies. This accuracy is actually limited by the inhomogeneity of the material rather than by the measurement technique. However, it seemed advisable to check the values listed in available tables.[1,2,3]

If the dielectric does not have zero conductivity, the value of the electric inductive capacity, ϵ, is no longer a pure real number but is complex. It may be expressed as

$$\epsilon = \epsilon' - j\epsilon'' \tag{1}$$

or

$$\epsilon = \epsilon' (1 - j \tan \delta) = \epsilon_o K_\epsilon (1 - j \tan \delta) \tag{2}$$

where $K_\epsilon = \epsilon/\epsilon_o$ and ϵ_o = dielectric constant of a vacuum. K_ϵ is called the specific inductive capacity. However, in this thesis, the subscript has been dropped and K is referred to as the dielectric constant.

---

[1] Moreno, T., Microwave Transmission Design Data, McGraw-Hill Book Co., New York, Chapter 12, 1948.

[2] Microwave Transmission Design Data, Sperry Gyroscope Co., Great Neck, New York, Publication No. 23-80, 1944.

[3] Everhart, E. M., "Recent Dielectric Constant and Loss Tangent Measurements," MIT Radiation Laboratory Report 483-5, July 14, 1944.

For $\tan \delta = 0$, the dielectric may be considered as perfect. The angle of the complex dielectric constant is approximately the power factor of the material. It is general practice to express the dielectric constant by the two terms, K and $\tan \delta$.

Three methods were used to measure K. Two of these were at wavelength of 3.20 cm. and the third was used in the radio frequency range of 8 to 80 mcps. The reason for making measurements at frequencies other than those at which the dielectric was to be used was to ascertain that the microwave frequencies were not a part of the spectrum at which anomalous dispersion took place. If a value of K was approximately the same for several widely separated frequencies, it seemed logical to assume that no anomalous dispersion was occurring at these frequencies.

During the last war, the Radiation Laboratory at Massachusetts Institute of Technology made a thorough study of methods for determining the dielectric constant at microwave frequencies. The two methods used here are described thoroughly in the literature.[4] Therefore, the theory will be discussed only briefly.

Figure 1 shows a schematic of the phase shift method. Energy from the signal generator is divided by a magic T and passes through two sections of waveguide. One arm is arranged so that a sample of the dielectric material may be inserted. A calibrated phase shifter, capable of delaying the wave from 0 to 360°, is inserted in the

[4] Montgomery, C. G., Techniques of Microwave Measurements, MIT Radiation Laboratory Series No. 11, McGraw-Hill Book Co., New York, 1947.

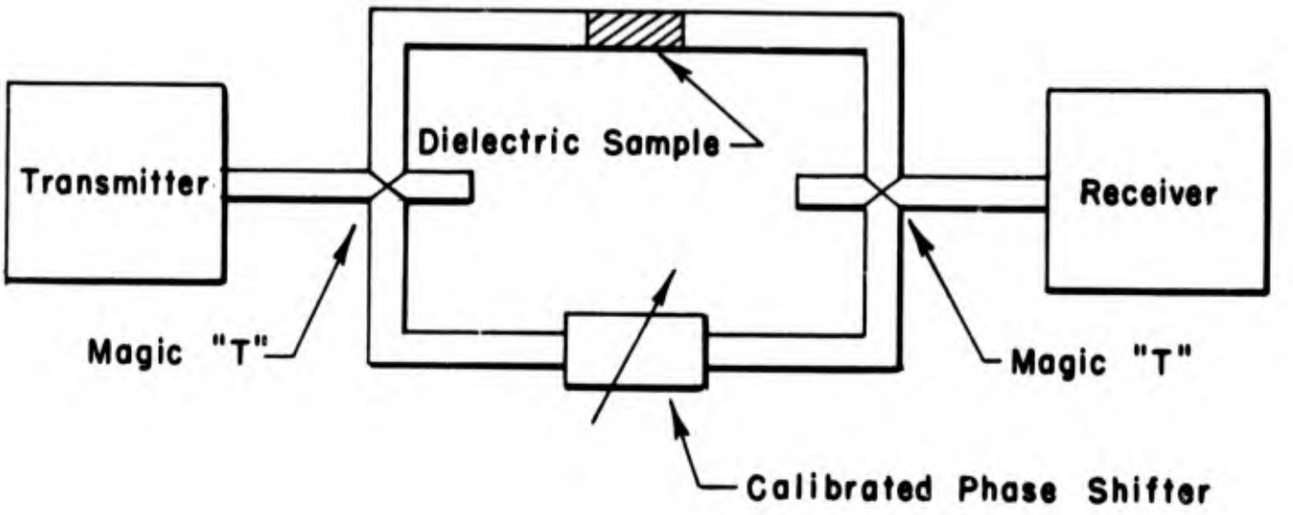

Fig. 1 — Schematic Of Phase Shift Method For Measurement Of Dielectric Constant.

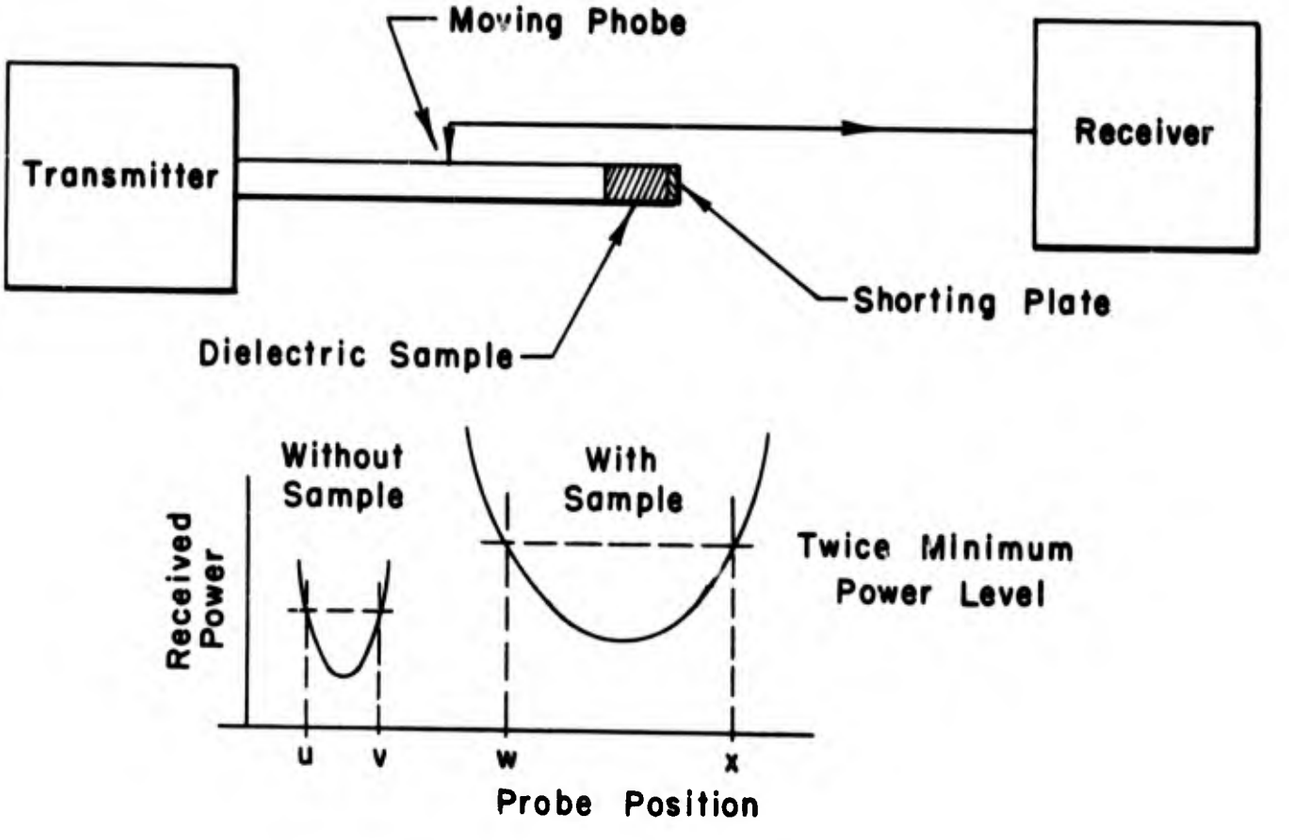

Fig. 2 — Shorted Line (Reflection) Method For Measurement Of Dielectric Constant.

second arm. The two signals are joined again by a second magic T and the sum of the two waves is detected by a crystal detector and then amplified. The procedure is as follows: first, with no sample in the guide, the phase shifter is adjusted for minimum signal which indicates that the two waves are combining 180° out of phase. Then a sample of the dielectric material, of length d, machined to fit snugly inside the waveguide, is inserted in arm number one. Again the phase shifter is adjusted for minimum signal and the change in phase shift is noted. This change in phase is equivalent to a stretching of the waveguide of distance Δ, or

$$\text{Phase shift in radians} = \frac{2\pi\Delta}{\lambda_g} . \tag{3}$$

For the air-filled guide

$$\lambda_g = \frac{\lambda_o}{\sqrt{1 - p}} \tag{4}$$

and for the dielectric filled guide

$$\lambda_{gm} = \frac{\lambda_o}{\sqrt{K - p}} \tag{5}$$

where $p = \left(\frac{\lambda_o}{\lambda_c}\right)^2$ and λ_c = cutoff frequency for the air-filled guide. This stretching is equivalent to removing in arm one, a section of the guide of length d and adding a section of length d filled with the dielectric. Or

$$\frac{2\pi\Delta}{\lambda_g} = -\frac{2\pi d}{\lambda_g} + \frac{2\pi d}{\lambda_{gm}} \tag{6}$$

$$\Delta \sqrt{1 - p} + d \sqrt{1 - p} = d \sqrt{K - p} \qquad (7)$$

Solve for K and rearrange

$$K = 1 + \left(\frac{\Delta}{d}\right)\left(2 + \frac{\Delta}{d}\right)(1 - p). \qquad (8)$$

By machining off the sample in 0.100-inch increments and repeating the measurements, a good value of K can be determined. This method does not yield the loss of the material.

The second method is known as the shorted line method and enables one to determine both K and tan δ. It is probably the best available method for solids at microwave frequencies. Figure 2 shows a block diagram of the equipment. This method is based on measuring the position of a null in a waveguide which has one end closed in order to set up a high standing wave pattern. With a sample in the end of the guide, the position of the null will be shifted. From this information, K may be determined. However, the width of the null is broader with the sample than without because of reflection from the dielectric interface and because of the passage of the wave through the dielectric. The change in width is a function of the loss in the material and hence, from these measurements tan δ may be determined. The derivation of the equations is rather lengthy and for that reason only the final equations will be given. The dielectric constant K and tan δ may be calculated from the pair of equations

$$\frac{\tan 2\pi V}{V} = \frac{\lambda_g}{d} \tan 2\pi U \qquad (9)$$

$$\tan \delta = W\left(\frac{K - p}{K}\right) \frac{4\pi \csc 4\pi U}{4\pi V \csc 4\pi V - 1} \tag{10}$$

where $U = \dfrac{(\Delta + d)}{\lambda_g}$

$V = \dfrac{d\sqrt{K - p}}{\lambda_o}$

$W = \dfrac{x - w}{\lambda_o}$

Δ = phase shift of minimum

$p = \left(\dfrac{\lambda}{\lambda_c}\right)^2$.

The procedure is to take a section of waveguide arranged for measuring the standing wave pattern in the guide. One end of the waveguide is connected to a signal generator and the other end is closed with a flat reflector plate. The position of a minimum is determined by the standing wave detector and the positions x and w are measured. These last points determine the width of the null at the points where the power level is twice that at the minimum. Then a sample of the dielectric is inserted in the guide and the new position of the null is recorded and its width measured. This width is $u - v$ and is greater than $x - w$. From these measurements K may be calculated and then $\tan \delta$. In order to determine K, a table of $\tan(2\pi V)/(2\pi V)$ is necessary. For each value of V there will be an infinite number of possible solutions. However, by making measurements on samples of various values of d, this ambiguity may be resolved. Also, the values obtained from the first method should enable one to choose the correct value of K.

Accuracy of this method is limited by the power level available at microwave frequencies. If the dielectric is of low loss, the nulls in the waveguide are very sharp and the signal level is usually only slightly above the noise level. The difficulty occurs in accurately measuring the twice-minimum power level.

Table A-I gives consolidated data for measurements by these methods for Lucite, polystyrene, and Textolite.

The resonant cavity method of measuring λ_g on dielectric rods suggests another method for measuring dielectric constant. If it is assumed that the characteristic equation is correct, it could be solved for λ_o/λ_g as a function of the dielectric constant for a given size diameter of rod and for a given mode. If small rods were used (about 0.25 inch to 0.50 inch for 3.20 cm.), the cavity has a high Q and the K may be determined to three figures. By using the HE_{11} mode and rods below cutoff for other modes, the wave should be very pure. From knowledge of λ_o and λ_g, K could be determined.

TABLE A - I

DIELECTRIC CONSTANT, K, AND LOSS FACTOR, TAN δ.

Material	K (tables)	K (phase shift)	K (shorted line)	tan δ (tables)	tan δ (shorted line)
Lucite	2.53-2.70	2.56	2.53	.016-.005	.01-.02
Textolite	2.4-2.5	2.56	2.50	.001	.001
Polystyrene	2.48-2.54	2.51	2.57	.001-.0003	.001
Paraffin	2.17-2.25	2.25		.0002-.001	
Nujol	2.25				

APPENDIX II

GLOSSARY

Symbol	Meaning	Page
$\vec{A}$	Vector potential	123
A	Effective area of an antenna	137
A	Designation of a particular antenna	137
A	Designation of a particular region	121
A	An arm of symmetry of a "Magic T"	28
A_n	Constant	46
A	Width of major lobe, in degrees	158
a	Dimension of a rectangular waveguide along x axis	5
a	Radius of a circular waveguide	5
B_n	Constant	46
B	Arm of symmetry of a "Magic T"	28
B	Designation of a particular region	121
B	Designation of a particular antenna	137
B	Half-power beam width	158
b	Dimension of a rectangular weveguide along y axis	5
C_n	Constant	46
C	Designation of a particular antenna	138
C	Tenth power beam width	158
c	Velocity of light in a vacuum	10
D	Dimension on a TE_{01} exciter	14
D_n	Constant	46

Symbol	Meaning	Page
D	Maximum linear dimension of an antenna	136
D_i	Angular position of lobe maxima	158
d	Diameter of circular waveguide	52
d	Distance between probes of a TM_{11} exciter	32
d	A function of the energy distribution of an antenna	130
d	Length of a sample of dielectric	258
ds	Element of surface	123
$\vec{E}$	Electric field vector	122
E-mode	Mode with only an electric axial component	4
E	With subscripts denotes either components of the vector field or electric components of particular waves	46
E	Arm of a "Magic T"	28
E_i	Angular position of lobe minima	158
EH	Hybrid electric wave, with and without subscripts	38
f	Frequency	10
f_c	Critical frequency	51
F_φ	$e^{jn\varphi}$	46
$\vec{F}$	Vector potential	123
F_i	Maximum intensity of i^{th} lobe	158
G	Gain	137
G	$pJ_1(p)/qH_1(q)$, a constant	57
G	Width of major null in degrees	159
g	A constant	116
$\vec{H}$	Magnetic field vector	120
H	With subscript denotes either components or the magnetic field or particular fields	46

Symbol	Meaning	Page
H	An arm of a "Magic T"	28
H-mode	Mode with only a magnetic axial component	4
$H_n^{(1)}$	Hankel function of first kind	46
HE	Hybrid mode, with and without subscripts	39
h	Propagation constant $2\pi/\lambda_g$	128
$\vec{i}$	Unit vector with or without subscripts	125
i	Electric current	120
i	Index subscript	158
I	With subscripts, refers to integral	128
$\vec{J}$	Electric current density	120
$J_n(u)$	Bessel Function of first kind of order n. A prime represents the derivative.	7
j	Square root of minus one	46
K	Dielectric constant	46
k	$\sqrt{\gamma^2 + \omega^2\mu\epsilon}$. With subscripts which refer to particular region.	46
k	$2\pi/\lambda_o$	123
L	Length of dielectric antennas	117
ℓ	A length	120
$\vec{M}$	Magnetic sheet current density	122
M	A constant	57
m	An integer	7
N	A constant	56
n	An integer	7
$\vec{n}$	Unit normal	122
n_a	Apparent index of refraction	52

Symbol	Meaning	Page
P	Point in space	124
P	Power	137
P_{cm}	Root of J	51
p	An argument of a Bessel Function	49
p	$(\lambda_o/\lambda_c)^2$	258
Q	Figure of merit of a cavity	42
q	An argument of a Hankel Function	49
r	Radial distance, in both spherical and cylindrical coordinate systems	5
R	Radius of curvature	69
R	A distance	134
S	Surface	123
S	A constant	48
S	A dimension on a TE_{10} exciter	14
T	A constant	48
TE	Transverse electric	4
TM	Transverse magnetic	4
TEM	Transverse electromagnetic	4
t	Time	46
U	$(\Delta + d)/\lambda_g$	260
U_{nm}	mth root of $J_n(U) = 0$	9
U'_{nm}	mth root of $J'_n(U) = 0$	9
u	Position along a slotted line	260
v_p	Phase velocity	10
V	$(d\sqrt{K - p})/\lambda_o$	260

Symbol	Meaning	Page
v	Position along a slotted line	260
W	$(x - w)/\lambda_g$	260
W	Intensity of major null	159
w	Position along a slotted waveguide	260
w(z')	Shading function	128
x	Cartesian coordinate	5
x	$\pi L(n_a - \cos \theta)/\lambda_o$	118
x	Position along a slotted line	260
X	Dimensionless circumference of a circular waveguide	57
X	A distance	136
y	Cartesian coordinate	5
z	Cartesian coordinate	5
z'	Cylindrical coordinate along axis of dielectric rod radiator	124
Z_o	Impedance	57
α	Attenuation constant	46
α	Phase angle between two waves	71
α_k	Attenuation constant for a coaxial cable	60
β	Phase constant	46
γ	Propagation constant	46
δ	Phase angle of a dielectric with loss	58
Δh	Increment in height	69
Δz	Increment of z	116
Δ	Phase shift	258
ϵ	Electric inductive capacity	46
ϵ_o	Electric inductive capacity of vacuum	46

Symbol	Meaning	Page
θ	Spherical coordinate	124
λ	Wavelength with and without subscripts	7
λ_o	Wavelength in a vacuum (or air)	10
λ_g	Wavelength on a waveguide	10
λ_c	Critical or cut-off wavelength	7
μ	Magnetic inductive capacity	46
μ_o	Magnetic inductive capacity of air	46
ρ	Polar coordinate	124
ρ	Argument of a Bessel Function	56
Φ	Phase angle	136
φ	Spherical coordinate	124
φ'	Polar coordinate	124
σ	Argument of a Hankel function	56
Ψ	Spherical wave function	127
ω	Angular frequency	46
∇	Gradient operator	123

BIBLIOGRAPHY

PRIMARY SOURCES

Bondi, H., and Pryce, M. H. L., "Dielectric Cylinders as Waveguides," ASE Report No. M434, British-Washington Guided Missile Committee. Admiralty Signal Establishment, Lythe Hill House, Haslemere, Surrey, August 1942.

Carson, J. R., Mead, S. P., and Schelkunoff, S. A., "Hyperfrequency Waveguides - Mathematical Theory," B.S.T.J., 15, 310, April 1936.

Chandler, C., Elsasser, W., and Iams, H., "An Investigation of Dielectric Rods as Waveguides," Digest of Paper No. 43 given at a joint meeting of the International Scientific Radio Union and the Institute of Radio Engineers, Washington, D.C., May 1948.

Chandler, C. H., "An Investigation of Dielectric Rod as a Waveguide," J. App. Phys., 20, 1188, December 1949.

Horton, C. W., "On the Dielectric Rod of Circular Cross Section," unpublished manuscript.

Horton, C. W., "On the Dielectric Rod as an Antenna," DRL-66, CM-283, 2 August 1946.

Horton, C. W., "On the Dielectric Rod as an Antenna, Part II," DRL-91, CF-481, 8 November 1946.

Linder, William J., "The Dielectric Rod Antenna," M. S. Thesis, University of California, Berkeley, 1948.

Mallach, Peter, "Dielectric Directional Antennas for dm and cm Waves," Air Materiel Command Report F-TS-2223-RE, February 1948. Translated by P. L. Harbury of Harvard University, Cambridge, Mass.

Montgomery, C. G., et al., Technique of Microwave Measurements, MIT Radiation Laboratory Series 11, McGraw-Hill Book Co., New York, 1947.

Montgomery, C. G., et al., Principles of Microwave Circuits, MIT Radiation Laboratory Series 8, McGraw-Hill Book Co., New York, 1948.

Moreno, Theodore, Microwave Transmission Design Data, McGraw-Hill Book Co., New York, 1948.

Mueller, G., and Tyrrell, W., "Polyrod Antennas," B.S.T.J., 26, 837, 1947.

Ramo, S., and Whinnery, J. R., Fields and Waves in Modern Radio, John Wiley and Sons, New York, 1944.

Ragan, G. L., Microwave Transmission Circuits, MIT Radiation Laboratory Series 9, McGraw-Hill Book Co., New York, 1948.

Sarbacher, R. I., and Edson, W. A., Hyper and Ultrahigh Frequency Engineering, John Wiley and Sons, New York, 1943.

Schelkunoff, S. A., Electromagnetic Waves, D. van Nostrand Co., Inc., New York, p. 425, 1943.

Slater, J. C., Microwave Transmission, McGraw-Hill Book Co., New York, 1942.

Southworth, G. C., "Hyperfrequency Wave Guides - General Considerations and Experimental Results," B.S.T.J., 15, 284, 1936.

Stratton, J., Electromagnetic Theory, McGraw-Hill Book Co., New York, p. 524, 1941.

Watson, R. B., and Horton, C. W., "The Radiation Patterns of Dielectric Rods - Experiment and Theory," J. App. Phys., 19, 661, 1948.

Watson, R. B., and Horton, C. W.,"On the Calculation of Radiation Patterns of Dielectric Rods," J. App. Phys., 19, 836, 1948.

Watson, R. B., "Dielectric Rod Antennas: Theory," DRL-139, CF-819, 29 October 1947.

Wegener, H., "Propagation Velocity, Wave Resistance, and Damping of Electromagnetic Waves along Dielectric Cylinders," Air Materiel Command Microfilm ZWB/FB/Re/2018, R. 8117 P 831.

Wilkes, G., "Wavelength Lenses," BUMBLEBEE Series Report No. 59, June 1947.

SECONDARY SOURCES

Abele, M., "Teoria deila propagazione di un campo elettro-magnetico lungo una guida dielettrica a sezione circolare," Atti del Congresso Internazionale della, (Radio Rome), 3, September - October, 1947.

Abele, M., "Teoria deila propagazione di un campo elettro-magnetico lungo una guida dielettrica a sezione circolare," Il Nuovo Cimento, 5, 274, 1948.

Allen, W. D., "The Coaxial to Waveguide Transformer," British Royal Society Report, G8/102, 1942.

Anonymous, "Feasibility of Dielectric Waveguides," Electronics, 19, 222, October 1946.

Astrahan, M. M., "Guided Waves on Hollow Dielectric Tubes," Ph.D. Dissertation, Department of Electrical Engineering, Northwestern University, Evanston, Ill., May 1949.

Awender, H., and Lange, O., "The Propagation of Decimetre and Centimetre Waves along Single Metallic and Dielectric Wires," Funktech Monat, 1, 5, 1938; 2, 51, 1938.

Barrow, W. L., "Transmission of Electromagnetic Waves in Hollow Tubes of Metal," Proc. I.R.E., 24, 1298, 1936.

Barrow, W. L., and Chu, L. J., "Theory of Electromagnetic Horns," Proc. I.R.E., 27, 51, 1939.

Brainerd, J. G., et al., Ultra-High-Frequency Techniques, D. van Nostrand Co., Inc., New York, 1942.

Bronwell, A. B., and Beam, R. E., Theory and Application of Microwaves, McGraw-Hill Book Co., New York, 1947.

Chu, L. J., and Barrow, W. L., "Electromagnetic Waves in Hollow Metal Tubes of Rectangular Cross Section," Proc. I.R.E., 26, 1920, 1938.

Dakin, T. W., "The Hollow Pipe Method of Measuring Dielectric Constant and Loss Factor," Westinghouse Research Laboratory Report SR-134, 25 August 1942.

Debye, P., and Hondros, O., "Elektromagnetische Wellen an dielektrischen Drahten," Ann. d. Phys., 32, 465, 1910.

Dowker, Y. N., "Dielectric Constant and Loss Tangent Computation," MIT Radiation Laboratory Report 483-19, 7 August 1945.

Droste, H. W., "Ultrahoehfrequencz - Uebertragung laengs zylindrischen Leitern und Nichtleitern," Teleg-Fernsper-Funk-und-Fernseh Tech, 27, 1938.

Elsasser, W. M., "Attenuation in a Dielectric Circular Rod," J. App. Phys, 20, 1193, 1949.

Everhart, E. M., "Recent Dielectric Constant and Loss Tangent Measurement," MIT Radiation Laboratory Report 483-5, July 1944.

Friedlander, F. G., "A Dielectric-Lens Aerial for Wide-Angle Beam Scanning," J. Inst. Elec. Engrs., 93, 658, London.

Guiton, H., "Dielectric Aerials for Centimeter Waves," Onde Electrique, 26, 459, 1946.

Halliday, D. F., and Kiely, D. G., "Dielectric Rod Aerials," J. Inst. Elec. Engrs., 94, 610, London, 1947.

Hekman, H., "Dielectric Type Antenna," Air Materiel Command Microfilm EIS/2/RE/3, R C-693 F/879.

Jakes, W., "Attenuation and Radiation Characteristics of Dielectric Tube Waveguides," Ph.D. Dissertation, Northwestern University, Evanston, Ill., 1949.

Kaspar, E., "Experimentelle Untersuchung der elektromagnetische Wellen an dielektrischen Drahten," Ann. d. Phys., 32, 353, 1938.

Kaspar, E., "Elektromagnetiske veny na dielektrickych dratech," Casopis pro Pestovani Matematiky a Fyoiky, 62, 40, 1932.

Klemt, A., "Beitrag zur Ausbreitung elektromagnetischer Wellen an dielektrischen Drahten," Funktechnische Monatshefte, 4, 122, 1939.

Liska, J., "Elecktromagneticke veny na dielektrickych trubicich," Casopis pro Pestovani Matematiky a Frysiky, 63, 97, 1934.

MacFarland, G. G., S/Ldr, "Report on Interrogation of Dr. Mallach, V.I.F.S.," CICS Evaluation Report No. 273, 30 July 1945.

Mallach, P., "Dielectric Directive Radiators," Fernmeldetich, Z., 2, 33, 1949.

Microwave Transmission Design Data, Sperry Gyroscope Company Publication No. 23-80, Great Neck, New York, 1944.

Mueller, G., Reports on Dielectric Antennas, Quarterly Report, January 1949; Quarterly Report, April 1949; Quarterly Report, July 1949; Annual Report, October 1949, Ohio State University Research Foundation, Columbus, Ohio.

Odarenko, T. M., "Report on Development Work on Radar Antennas in Germany," Field Information Agency, Technical (U.S.), Microfilm No. R-3759, F-477, Air Documents Division, T-2, AMC, Wright Field.

Lord Rayleigh, "On the Passage of Electric Waves through Tubes," Philosophical Magazine, 43, 125, 1897.

Redheffer, R. M., and Winkler, E. D., "The Measurement of Dielectric Constants in the One Centimeter Band," MIT Radiation Laboratory Report 483-15, 11 May 1945.

Richtmeyer, R., "Dielectric Resonator," J. App. Phys., 10, 391, 1939.

Ruter, H., and Schriever, O., "Elektromagnetische Wellen an dielektrischen Drahten," Schriften des Naturwissen-schaftlichen vereins fur Schlewig-Holstein, 16, 2, 1915.

Schriever, O., "Elektromagnetische Wellen an dielektrischen Drahten," Ann. d. Phys., 63, 645, 1920.

Slater, J. C., "Properties of the Coaxial-Waveguide Junction in the 725-A and 2J51 Output," Bell Telephone Laboratories Memorandum 44-180-A, November 1944.

Slevogt, K., "Uber die Fortplanzung Ultrakuryer Wellen langs eines dielektrischen Leiters," Air Materiel Command Microfilm EIS/5/PSN/15 R 216 F 368.

Slevogt, K., "On the Propagation of Ultra-Short Waves on a Dielectric Conductor," Hochfrequency and Elektroakustik, 59, 1, 1942.

Southworth, G. C., and King, A. P., "Metal Horns as Directive Receivers of Ultra Short Waves," Proc. I.R.E., 27, 95, 1939.

Southworth, G. C., "Some Fundamental Experiments with Wave Guides," Proc. I.R.E., 25, 807, 1937.

Southworth, G. C., U. S. Patent No. 2,206,923. 1940.

Watson, R. B., "Polystyrene Forms for Radar Antennas," DRL-72, CF-283, 2 August 1946.

Watson, R. B., "Antenna Design and Measurements. II," DRL-96, CF-507, 27 November 1946.

Watson, R. B., "Polystyrene Rod Antennas," DRL-200, CF-1216, 4 March 1949.

Whitmer, R., "Fields in Non-Metallic Waveguides," Proc. I.R.E., 36, 1105, 1948.

Wilkes, G., "Wavelength Lenses," Proc. I.R.E., 36, 206, 1948.

Wilkes, G., "Lens Having a Dimension of the Order of a Wavelength," Compte Rendus, 223, 1116, 1946.

Zachoval, "Elektromagnetische Wellen an dielektrischen Rohren," Ceska Akademie Ved a Umeni Prave Bulletin International, 33, 136, 1932.

Zahn, H., "Detection of Electromagnetic Waves on Dielectric Wires," Ann. d. Phys., 49, 907, 1916.

Zahn, H., "Elektrische Wellen an dielektrischen Drahten," Physikalische Zeitschrift, 16, 414, 1915.

Zinke, O., and Simon, I., "Note on Dielectric Aerials," Onde Electrique, 28, 278, 1948.

Zinke, O., "Ausgewaehlte Fragen Ueber Theorie and Technik von Antennen," Report No. F-TS-2223-RE (Translation), Air Materiel Command, Wright Field, Dayton, Ohio.

British Patent No. 420,445. December 3, 1934.